Heterogeneous Oxidation of VOCs : from fundamentals to air quality

Frederic Thevenet

N° d'ordre : 41 870

MINES Douai

Université de Lille

Habilitation à Diriger des Recherches

présentée par

Frédéric THEVENET

à l'Université de Lille 1 Sciences et Technologies

Spécialité : Physico-Chimie de l'Atmosphère

le 2 novembre 2015

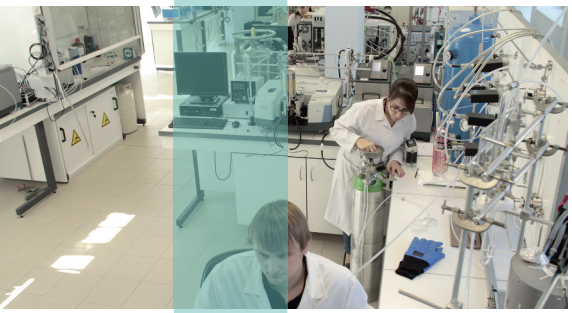

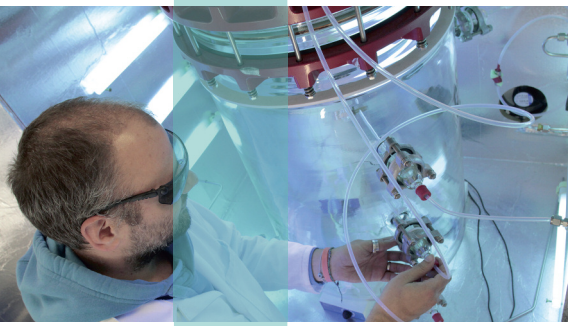

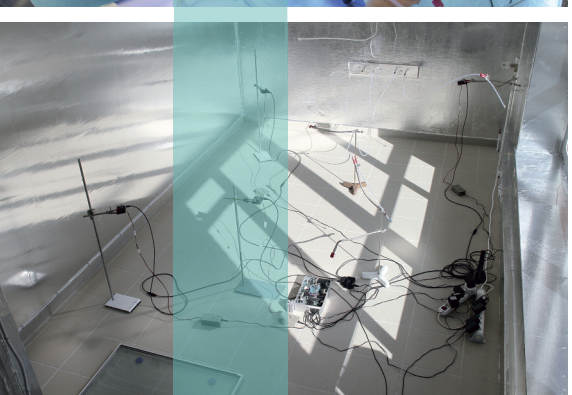

Heterogeneous oxidation of VOCs : from fundamentals to air quality

Composition du jury :

Annemie BOGAERTS	Professeur, Antwerpen Universiteit **Rapportrice**
Anne GIROIR-FENDLER	Professeur, Université Lyon-1 **Rapportrice**
Sylvie LACOMBE	DR CNRS, Université de Pau **Rapportrice**
Pascale DESGROUX	DR CNRS, Université Lille-1
Nicolas KELLER	CR CNRS, HDR, Université de Strasbourg
Nadine LOCOGE	Professeur, Ecole des Mines de Douai
Antoine ROUSSEAU	DR CNRS, Ecole Polytechnique **Garant d'HDR**

REMERCIEMENTS

Les travaux de recherches présentés dans ce mémoire sont le fruit de nombreuses collaborations et confrontations. En recherche plus qu'ailleurs rien n'est accompli *ex-nihilo*, plusieurs complices m'ont aidé à commettre ce manuscrit.

Merci aux membres du jury qui ont accepté de rapporter ce travail de synthèse. Annemie Bogaerts, illustre plasmicienne d'outre-Quiévrain, Anne Giroir-Fendler, naturellement parfaite en catalyste lyonnaise, et Sylvie Lacombe, avec qui je pressentais, à juste titre, partager rigueur et sensibilité, mais surtout une passion coupable pour les cafés sous le soleil de Californie.

Merci aux membres du jury qui ont examiné ce manuscrit avec une grande attention. Pascale Desgroux, digne présidente représentant les instances lilloises, et Nicolas Keller, dont l'absence m'a laissé face à un jury extraordinairement féminin. Nadine Locoge a commencé à examiner mes travaux bien longtemps avant l'idée même de ce manuscrit. Elle est la source d'énergie à l'origine d'une grande part de mes activités de recherche. J'admire sa force dont un jour je percerai le mystère (mais comment fait-elle… ?).

Après avoir dirigé mes travaux de thèse, Antoine Rousseau m'a fait l'honneur d'être le garant de cette HDR. Il était une évidence. Encadrer sans encadrer est son art ; un petit coup de fouet quand il faut, là où il faut, mon indépendance et mon masochisme sont comblés. Il est plus facile d'aller vite et bien dans sa carrière lorsqu'on marche dans les pas d'un modèle. Il est cher à mon cœur et il m'inspire.

Je remercie ceux que j'ai eu la chance de croiser dans les labos, et qui habitent encore mon esprit. Dominique Vouagner, Gérard Panczer et Bernard Champagnon ; Marlène Charbonnier et Maurice Romand ; Chantal Guillard, Jean-Marie Herrmann et Daniel Bianchi ; chacun a laissé à sa manière une empreinte sur mon parcours et ma personnalité.

Les doctorants (Olivier Debono, Loganathan Sivachandiran, Frédéric Batault, Christelle Barakat, Pamela Harb), comme les post-doctorants (Saravanan Chandrasekaran, Paul Gravejat, Louis Olivier, Manolis Romanias, Malak Rizk) avec qui j'ai eu la possibilité de travailler ont chacun apporté des contributions essentielles aux travaux présentés ici. Je souhaite qu'ils trouvent à travers ce manuscrit les remerciements que je leurs dois.

Je suis arrivé dans le Nord sans larmes, mais sans enthousiasme non plus. Et puis j'ai trouvé un laboratoire dans lequel brillent de nombreux soleils. Merci à Jean-Claude Gallo, dont la bienveillance m'a donné confiance, et à Patrice Coddeville qui construit chaque jour un laboratoire où il fait bon travailler. J'ai trouvé à l'Ecole des Mines de Douai non seulement des collègues mais aussi des ami(e)s. On rédige d'autant mieux que l'on peut papoter de tout et à toute heure. N'est-ce pas Nathalie Redon et Marie Verriele ? Je me suis glissé jusqu'à l'addiction dans la truculente pause de 10h30 ; mais que serais-je devenu sans ces collègues, gentiment priapiques et manifestement caféïnomanes… ?

Merci aux Lyonnais qui me regardent passer au-dessus de leurs têtes chaque lundi et vendredi, qui s'inquiètent souvent de *mon-labo-à-douai*, et qui m'offrent d'incomparables bouffées d'oxygène. Merci à ceux de ma famille qui m'apportent leur soutien et leur amour. Merci à celles et ceux qui m'aident à rendre plus facile ma drôle de vie.

Merci à Damien de m'avoir montré ce qu'est le courage.

Merci à Eric d'être là.

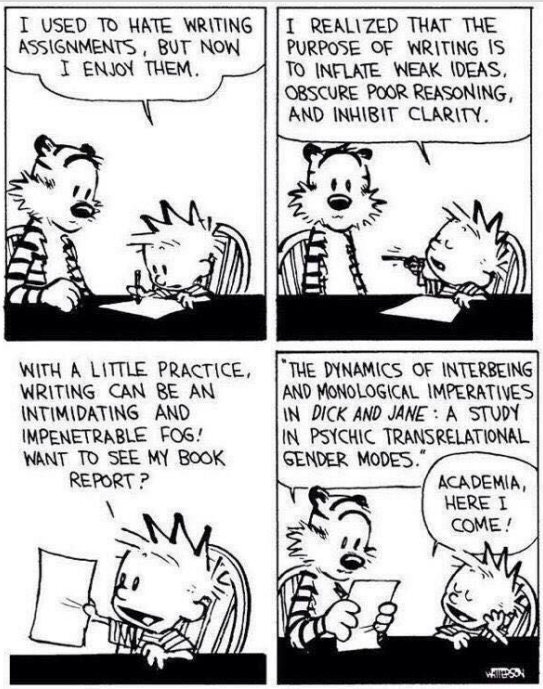

Calvin and Hobbes, Bill Waterson, *McMeel Publishing 1995*

Il fallait fuir. Mais d'abord, on ne pense pas spontanément à la fuite parce qu'on ignore qu'il existe un ailleurs. On ne sait pas que la fuite est une possibilité. On essaye dans un premier temps d'être comme les autres, et j'ai essayé d'être comme tout le monde.

En finir avec Eddy Bellegueule, Edouard Louis, *Ed. du Seuil 2014*

If it's bitter at the start,
then it's sweeter in the end.

Get together, Madonna, A. Bagge, P. Åström, S. Price, *Warner Bros Music 2005*

:P

CONTENT

Part A - BACKGROUND and CAREER

This section gives an overview of my education, research activities and teachings. First, the different steps of my professional experience are summarized to give short descriptions of my background and current position. Then, my involvements in scientific project management, student supervisions, and evaluation as well as valorization activities are detailed. Finally, complementary information about teaching and pedagogical activities, as well as administrative contributions are presented.

A-1 RESUME

Name: Frédéric THEVENET
Birth: July 12th 1979, Villefranche-sur-Saône, Rhône (69), France

Professional status: Maître Assistant / Assistant Professor at *Ecoles des Mines*
Institution : Ecole des Mines de Douai, Institut Mines-Telecom
Department : Sciences de l'Atmosphère et Génie de l'Environnement (SAGE)

✉ 941, rue Charles Bourseul
BP 10838
59508 Douai cedex, France

☎ 03 27 71 26 12
frederic.thevenet@mines-douai.fr
http://www2.mines-douai.fr/

2000-2003 **Engineer Diploma /** Material Sciences at *Institut des Sciences et Techniques de l'Ingénieur de Lyon* (Polytech'Lyon)

2002-2003 **Master of Science /** Material Sciences at *Institut National des Sciences Appliquées de Lyon* (INSA-Lyon). Research Internship / (*Université Lyon-1* & *Commissariat à l'Energie Atomique* (CEA) Marcoule): Assessment of vitrified nuclear waste stability using Eu(III) as a photoluminescent structural probe.

2003-2006 **PhD Thesis** under the supervision of C. Guillard (*Université Lyon-1*) and A. Rousseau (*Ecole Polytechnique*). Coordinated and financially supported by *Agence de l'Environnement et de la Maîtrise de l'Energie* (ADEME), in collaboration with *CIAT* and *Ahlstrom* companies, defended on September 27th 2006. Title : *Elimination et mécanismes de dégradation de l'acétylène par couplage plasma froid et photocatalyse*.

Overview of the scientific and supervision activities	➲ 5 national scientific projects ➲ 2 industrial collaborations ➲ 4 PhD supervised & 2 under current supervision ➲ 4 post-doctoral fellowships supervised & 2 under current supervision ➲ 5 Masters of Science supervised
Overview of valorization and communication	➲ 22 papers published in international peer-reviewed journals, 18 after PhD ➲ 28 orals in nat[al] and internat[al] conferences + 3 invited lectures ➲ 35 poster communications in national and international conferences ➲ 9 scientific reports ➲ 2 international patents

My research activities are based on a technical and scientific formation dealing with **material sciences** and more especially physical and chemical characterizations of materials. This background, combined with my personal interest for **environmental issues**, led me toward a PhD related to innovative **air treatment** heterogeneous process investigation and development, focused on **photocatalysis** and **non-thermal plasmas**. Further, I widened my research scope, as Post-Doc and beyond 2008 as Assistant Professor, to gas phase analytical chemistry, **adsorption** processes and **indoor air quality**. Since 2008, I initiated and developed the air treatment research axis at Ecole des Mines de Douai. This activity was not present in this laboratory before I arrived. Developments and investigations have been focused on (i) the assessment of air treatment process performances and innocuity under typical indoor air conditions, (ii) the optimization of air treatment processes coupling for both **indoor air** and **industrial effluent** issues.

A-2 ACADEMIC CAREER

Figure 1 gives a schematic representation of my academic formation and career. In the following, four summaries are proposed to describe the key issues and the main achievements of my (i) research internship, (ii) PhD, (iii) post-doc and (iv) position as Assistant Professor at Ecole des Mines.

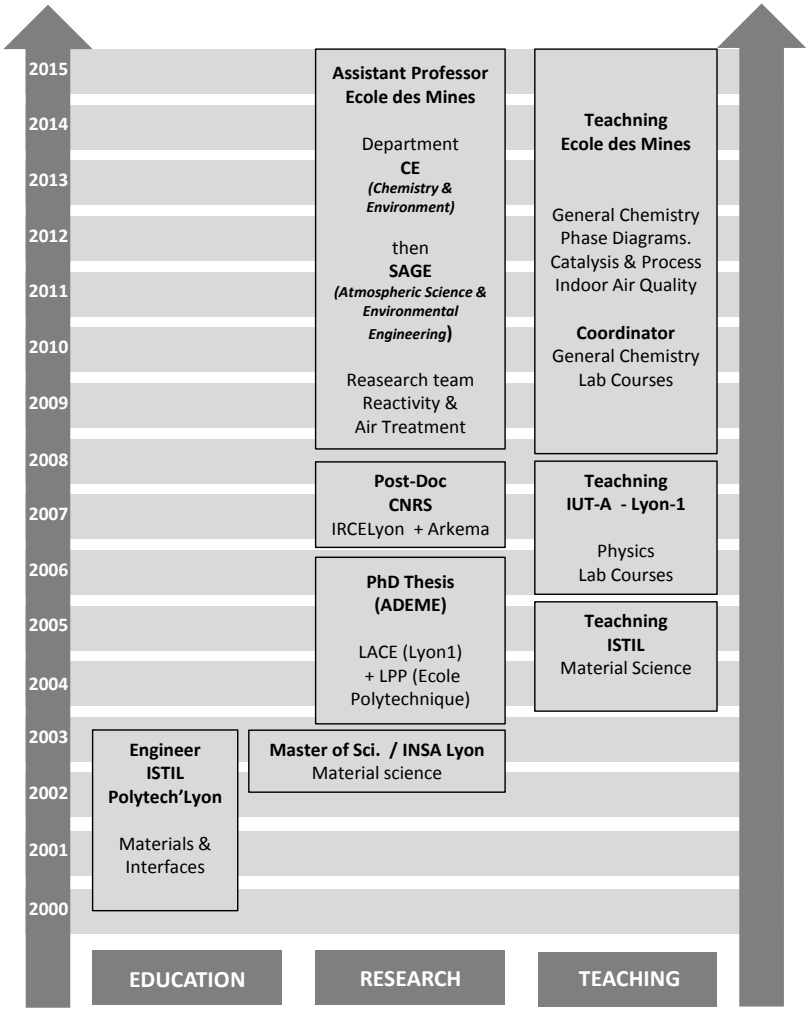

Figure 1 - Schematic of academic formation and career.

2003: research Internship

My research activities started in february 2003 as I joined the research group of Dr. G. Panczer and Prof. B. Champagnon in LPCML (*Laboratoire de Physico-Chimie des Matériaux Luminescents*, Lyon-1) and Dr. Jollivet (*Laboratoire du Comportement à Long Terme*, CEA-Marcoule). During this six-month internship I studied the long term behavior of glasses used for nuclear waste confinement using laser induced fluorescence (LIF) spectroscopy.

The use of Eu(III) as luminescent structural probe enabled the evaluation of the structural modifications induced on glasses by environmental lixiviation processes. More especially, the impact of lixiviation has been assessed on structural sites occupied by lanthanides. Results obtained during this internship directly led to the publication of a paper in *Journal of Non-crystalline Solids*.

This first experience of collaborative research made me more familiar with the academic world and confirmed my solid interest for research. Subsequently, I applied to a PhD related to physics, chemistry and environmental issues proposed in LACE (*Laboratoire d'Application de la Chimie à l'Environnement, Université Lyon-1*) and LPTP (*Laboratoire de Physique et Technologie des Plasmas, Ecole Polytechnique*). I have been recruited by Dr. Chantal Guillard (LACE), Dr. Antoine Rousseau (LPTP) and Anne Paillier (ADEME). This PhD was coordinated and financially supported by ADEME (*Agence de l'Envrionnement et de la Maîtrise de l'Energie*) in collaboration with two private companies, CIAT and Ahlstrom.

2003 to 2006: PhD Thesis

Context and objectives /

Research activities in the domain of air treatment are highly active since the mid-seventies. Two aspects were generally targeted: (i) limitation of pollutant emissions and (ii) abatement of VOCs. Regarding VOCs abatement, two different approaches are concomitantly developed: (i) trapping of VOCs and (ii) VOC oxidation.

Non-thermal plasmas (NTP) and photo catalysis are classified among the advanced oxidation processes. At the end of the nineties, the combination of non-thermal plasma with catalysis was successfully explored; consequently, the combination of non-thermal plasma with photocatalysis has been considered as a promising continuity.

The main objectives of this PhD were: (i) to understand the interaction between NTP and TiO_2 used as a photocatalyst, (ii) to describe oxidation reactions and processes occurring throughout the coupling of NTP with TiO_2 for VOC oxidation, (iii) determining the process parameters of interest for future industrial developments.

Achievements /

In agreement with ADEME and industrial partners, acetylene was used as a model VOC. The oxidation reaction of acetylene was investigated under each oxidation process and their coupling. Dedicated reactors were specially designed to address both fundamental and process issues. They were combined with appropriate analytical tools, mainly gas chromatography.

In a first step, acetylene oxidation mechanism was studied under photocatalytic treatment. The complete mineralization of the primary pollutant as well as oxidation pathway was evidenced. In a second step, the performances of NTP treatment were assessed, evidencing the fast kinetic of NTP compared to photocatalysis. Finally, acetylene removal was studied under combined treatments to explore their synergetic effect. The characterization of reaction intermediates and side-products enabled the determination of reaction pathways. The durability of TiO_2 under NTP exposure was addressed, and the role of adsorption in the coupling process pointed out.

This work contributed (i) to a step-forward in the understanding of plasma-material coupling and (ii) to the development of new indoor air treatment techniques. This PhD has been valorized by 7 papers published in international peer-reviewed journals.

2006 to 2008: Post-doc

Context and objectives /

Scientific skills developed during my PhD oriented my research activities toward deeper investigation of the potentialities of non-thermal plasma chemistry and more especially non-thermal plasma assisted chemical syntheses. *Arkema* company, in collaboration with CNRS, supported financially my 18 months post-doc at IRCELyon. This post-doc was coordinated by the '*pôle de compétitivité*' *Axelera*.

This post-doc aimed at investigating the potentialities of plasma to activate reactants and to orientate their recombination toward molecules with (i) higher added value, and (ii) at lower energy cost. H_2O_2 was the product of interest to be synthetized. NH_3 synthesis was investigated as well.

Achievements /

My post-doc was a strong and successful insight in the domain of chemical synthesis by plasma, combining non-thermal plasma, material science and analytical chemistry.

This study demonstrated the relevant use of non-thermal plasma to activate, safely and efficiently, O_2 and H_2 mixtures in order to synthetize H_2O_2. Moreover, it has been evidenced that the reaction yield of the process was considerably increased in the presence of TiO_2 material inserted inside the discharge zone. Heterogeneous processes induced by the presence of TiO_2 enabled the condensation of H_2O_2 and its stabilization via complexation reactions.

Developments related to this process have been valorized through one patent and one paper.

since 2008: Assistant Professor at Ecole des Mines

Research activities /

My main assignment as I was recruited in 2008 at Ecole des Mines in the D^{pt} SAGE was to creat and develop a new research axis dealing with air treatment processes applied to indoor air quality improvement. This activity had to be sited at the crossroad of fundamental research and applied industrial problematic, meaning in close collaboration with both academic and industrial partners.

The D^{pt} SAGE is an academic reference laboratory in analytical chemistry regarding gas phase analyses at ppb and event ppt levels. In that context I brought my expertise in the domain of (i) adsorption, (ii) photocatalysis, and (iii) non-thermal plasmas, and combined my proficiency with the solid analytical background of the lab.

Along the last 7 years, I created and developed the air treatment laboratory in the D^{pt} SAGE. This activity led so far to 6 academic and industrial research projects and 15 published papers. Meanwhile, 4 PhD have been defended and 2 are under preparation.

The central objective of my research activities at Ecole des Mines along the last seven years was to understand physical and chemical processes involved in the heterogeneous oxidation of volatile organic compounds (VOC). From a disciplinary point of view, my research activities rely on adsorption, non-thermal plasma and photocatalysis. From a technical point a view, significant developments have been performed regarding analytical chemistry and methods to address the fundamental and applied problematic of indoor air treatment.

Teaching activities /

Once I arrived at Ecole des Mines I have been involved in teaching activities from basic courses, in the first year, to more specialized lectures, in the second (*Mineure*, *Majeure*) and third years (*Option*, *Master Spécialisé*). The main lectures I give are: Phase Diagrams (2nd-year students), Catalysis (2nd-year students), and Indoor air Quality (3rd-year students).

Moreover, since 2011 I am coordinator of Chemistry Lab Courses proposed to 1st year students. This 64 hr experimental course requires both technical and staff management skills in order to ensure (i) operational equipment and (ii) optimal supervision of the students. From 8 to 10 Assistant Professors, Post-docs or PhD students contribute yearly to the supervision of 60 to 70 students.

In the context of the Chemistry Lab course I initiated and coordinated an educational project selected and financially supported by *Unisciel* in 2012.

In parallel each year I am involved in juries and supervisions of student projects; especially Research Projects proposed to 2nd-year students.

A-3 RESEARCH PROJECTS

Since my post-doc, I have coordinated and contributed to the development and proposal of various academic and industrial research projects at national and international scales. Six of them have been selected by evaluation committees; their respective contexts and objectives are summarized from Table 1 to Table 6. The technical and scientific content of the designated projects is detailed throughout the presentation of my research activities (Part-B to E). All these projects contributed (i) to the equipment of air treatment laboratory at D^{pt} SAGE and (ii) to the recruitment of PhD students and post-docs. The conception, structure and coordination of these projects are time-consuming, but unavoidable parts of my research activities.

Table 1 - Summary of PHOTOCOV project	**PHOTOCOV** **Photocatalytic oxidation of indoor air VOCs at ppb levels**				
Framework	Carnot MINES		*Duration:*	2008 - 2011	
Contributors	D^{pt} SAGE, Ecole des Mines, Douai			Coordinator	
Summary	The objective of the PHOTOCOV project is to identify and quantify secondary organic products formed during the photocatalytic oxidation of VOCs at typical indoor air ppb levels. This project aims at investigating for the first time (i) the kinetic of photocatalytic reactions at ppb levels and (ii) the carbon mass balance of such reactions at ppb levels.				
Budget	*Total cost:* 65 k€		*Grant:* 65 k€	*Grant for D^{pt} SAGE*	65 k€

Table 2 - Summary of RAMPE project	**RAMPE** **Regeneration of adsorbents under plasma exposure**				
Framework	ANR (French national research agency)		*Duration:*	2009 - 2012	
Contributors	Laboratoire de Physique des Plasmas, Ecole Polytechnique D^{pt} SAGE, Ecole des Mines, Douai IRCELyon, Université Lyon-1			Coordinator Partner Partner	
Summary	The objective of the RAMPE project is to assess the potentialities on non-thermal plasma surface discharges to achieve oxidative regeneration of VOC saturated sorbent surfaces. First, the adsorption of model VOCs has been characterized on selected sorbents; second two different approaches have been investigated: *in-situ* and *post-situ* plasma regenerations. The contribution of D^{pt} SAGE is focused on the *in-situ* regeneration of saturated sorbents and more precisely the investigation of (ii) environmental performances, (iii) sorbent ageing phenomena.				
Budget	*Total cost:* 860 k€		*Grant:* 430 k€	*Grant for D^{pt} SAGE*	100 k€

Table 3 - Summary of PHOTOCAIR project	**PHOTOCAIR** **Photocatalytic indoor air treatment**				
Framework	Carnot MINES		*Duration:*	2013 - 2015	
Contributors	D^{pt} SAGE, Ecole des Mines, Douai D^{pt} DSEE, Ecole des Mines, Nantes D^{pt} PRESIC, Ecole des Mines, Saint Etienne			Coordinator Partner Partner	
Summary	The objective of the PHOTOCAIR project is to assess, optimize and control the performances of a looped photocatalytic air treatment device under typical indoor air conditions. The contribution of the D^{pt} SAGE consists in (i) developing and validating sensor arrays for process control and optimization, and (ii) evaluating the long term performances of photocatalytic systems in the presence of indoor air typical co-pollutants.				
Budget	*Total cost:* 440 k€		*Grant:* 230 k€	*Grant for D^{pt} SAGE*	65 k€

Table 4 - Summary of PAni-TiO_2 project	**PAni-TiO_2** **New composite materials for air treatment systems**				
Framework	OSEO		*Duration:*	2009 - 2011	
Contributor	D^{pt} SAGE, Ecole des Mines, Douai			Coordinator	
Summary	The objective of the PAni-TiO_2 project is to develop and characterize innovative organic-inorganic composite materials for air treatment systems. The purpose of the materials combining photocatalytic TiO_2 with conducting polymer is to obtain a photocatalytically enhanced composite.				
Budget	*Total cost:* 100 k€		*Grant:* 50 k€	*Grant for D^{pt} SAGE*	50 k€

Table 5 - Summary of ETAPE project	**ETAPE** **Evaluation of performances and innocuity of photocatalytic air treatment devices close to real indoor air conditions**		
Framework	ADEME (CORTEA)	*Duration:*	2013 - 2016
Contributors	D^{pt} SAGE, Ecole des Mines, Douai D^{pt} DSEE, Ecole des Mines, Nantes		Coordinator Partner
Summary	The objective of the ETAPE project is to assess the performances and the innocuity of commercially available photocatalytic air treatment units. The originality of the project consists in the conception of innovative experimental setups able to reproduce typical indoor air conditions. Two complementary aspects are addressed: (i) the environmental assessment of performances and innocuity, (ii) the investigation of the process engineering to understand performances and limitations. The contribution of D^{pt} SAGE is related to the development of a large volume 40 m^3 experimental chamber to perform tests under validated and controlled typical indoor air conditions. This work will lead to significant recommendations and evolution of standards related to photocatalytic air treatment systems.		
Budget	*Total cost:* 510 k€	*Grant:* 220 k€	*Grant for D^{pt} SAGE* 110 k€

Table 6 - Summary of PSyCO project	**PSyCO** **Evaluation of the efficiency and sustainability of "air cleaning walls" under typical indoor air conditions**		
Framework	Carnot MINES	*Duration:*	2015-2016
Contributor	D^{pt} SAGE, Ecole des Mines, Douai		Coordinator
Summary	The objective of the PSyCO project is to evaluate the impact of commercially available "air cleaning walls" on indoor air quality. Experiments are carried out in the large volume experimental room developed at D^{pt} SAGE. Typical indoor air pollution is generated in the chamber in order to assess the long term air cleaning performances of the selected materials under different environmental conditions. As a result, this project will be useful to amend standards related to "air cleaning wall" widely available on the market.		
Budget	*Total cost:* 75 k€	*Grant:* 75 k€	*Grant for D^{pt} SAGE* 75 k€

A-4 RESEARCH EVALUATION ACTIVITIES

Throughout my research activities, from 2005 to 2015, I have been asked to contribute to research evaluation as (i) paper referee for international peer-reviewed journals, (ii) PhD thesis jury member, (iii) research project evaluator at national level, and (iv) conference scientific committee member. I am member of the international organizing committee of **SPASEC-20** (*Semi-conductor Photocatalysis and Solar Energy Conversion*) as well as **AOT-21** (*Advanced Oxidation Technologies for treatment of water, air and soil*) held in 2015 in San Diego, and **DUST-2016** (2nd International Conference on Atmospheric Dusts) held in June 2016 in Taranto. Moreover, I contribute to the national organizing committee of **SPEA-9** (*9th European Meeting on Solar Chemistry and Photocatalysis: Environmental Applications*).

Research evaluation activities related to PhD evaluation and paper reviewing are summarized in Table 7 and Table 8. Up to now, I have been involved into 6 PhD juries, among them, 4 as PhD supervisor (Olivier Debono, Loganathan Sivachandiran, Frédéric Batault and Christelle Barakat). Regarding paper reviewing processes, I generally receive 2 requests to review per month and accept or decline according to the scope of the submitted paper. Concerning research project evaluation, I am mainly involved in the ANR (French National Research Agency) reviewing process.

Table 7 - List of evaluated PhD as jury member.

Oxydation photocatalytique de composés organiques volatils et suivi de leurs intermédiaires réactionnels : étude en réacteurs statique et dynamique à des concentrations typiques de l'air intérieur (Supervisor) **Université de Nantes**	*Olivier Debono*
Regeneration of inorganic sorbents: investigation of adsorbed VOC oxidation using non-thermal plasma surface discharge. (Supervisor) **Ecole Polytechnique**	*Loganathan Sivachandiran*
Characterization and defluoridatio studies of active carbons derived from bio-materials of « typha angustata », « lagenaria siceraria » and, « acacia farnesiana » plants as adsorbents. (Internat[al]. Referee) **Andhra Loyola University, India**	*Yeleswarapu-Hanumantha Rao*
Synthèse et caractérisation d'oxydes mixtes de bismuth pour la photocatalyse dans le visible. (Jury member) **Collège de France**	*Marie-Anne Lavergne*
Influence de l'adsorption et des paramètres opératoires sur le traitement photocatalytique de composés organiques volatils en mélange dans les conditions de l'air intérieur. (Supervisor) **Université Lille-1**	*Frédéric Batault*
VOC abatement by plasma-catalyst coupling : from fundamentals to process engineering. (Supervisor) **Ecole Polytechnique**	*Christelle Barakat*

Table 8 - List of reviewed international peer reviewed journals and their corresponding impact factors.

Applied Catalysis B : Environmental	6.03
Chemical Engineering Journal	4.06
Journal of Environmental Management	3.19
Journal of Hazardous Materials	4.68
Journal of Physics D : Applied Physics	2.52
Plasma Chemistry Plasma Processing	1.60

A-5 ACADEMIC AND INDUSTRIAL PARTNERSHIPS

As exposed in the description of the research projects I contributed, my research activities are in collaboration with academic research laboratories with complementary skills, as well as industrial partners. Table 9 gives an overview of the industrial collaboration initiated since 2008 at Ecole des Mines de Douai on the air treatment research activity. Besides, Table 10 indicates my academic collaborations at national and international levels.

In November 2013, I obtained a one-month grant from Ecole des Mines to welcome Prof. Challapalli Subrahmanyam from *Hyderabad Indian Institute of Technology* (IIT) in D[pt] SAGE as invited Professor. This exchange was an opportunity to submit in 2012 an international collaborative research project to ANR international call for proposal.

Table 9 - List of industrial collaborations

➲ Delta Neu, Recherche et Développement, Armentières **(France)**	*Vivien Tricot* *Christophe Benjamin*
➲ PSA Peugeot-Citroën **(France)**	*Guillaume Meunier*
➲ Al-Ko Therm **(Germany)**	*Carsten Stuck*
➲ Lieherr-Aerospace **(France)**	*Lamia Dreibine*

Table 10 - List of academic collaborations

➲ Laboratoire de Physique des plasmas, UMR 7648 CNRS Ecole Polytechnique **(France)**	*Antoine Rousseau* *Olivier Guaitella*
➲ IRCELyon, UMR 5256 CNRS Université Lyon-1 **(France)**	*Daniel Bianchi* *Chantal Guillard*
➲ Department of Chemistry, Indian Institute of Technology, Hyderabad **(India)**	*Challappali Subrahmanyam*
➲ Laboratoire de Chimie de la Matière Condensée de Paris, UMR 7574 CNRS Université Pierre et Marie Curie / Collège de France **(France)**	*Sophie Cassaignon*
➲ D^{pt} Systèmes Energétiques et Environnement, GEPEA UMR 6144 CNRS Ecole des Mines / Université de Nantes **(France)**	*Laurence Le Coq* *Valérie Héquet*
➲ D^{pt} Procédés et Réactivité des systèmes solide-gaz instrumentation et capteur Centre SPIN, Ecole des Mines Saint-Etienne **(France)**	*Christophe Pijolat,* *Jean-Paul Viricelle*
➲ School of Engineering and Built Environment, Glasgow Caledonian University **(United Kingdom)**	*Natalia Chubar*

A-6 SUPERVISIONS IN THE CONTEXT OF RESEARCH ACTIVITIES

In the context of my research activities I had the opportunity to welcome, supervise and collaborate with 5 master students, 5 PhD students and 6 post-docs. Table 11 gives an overview of my supervision activities. In the column entitled "*context*" the first indication refers to the institution where the student or post-doc is affiliated from an administrative point of view; the second indication, between brackets, indicates the origin of the financial support. In the column entitled "Involv^{t}", the percentage indicated between brackets depicts my involvement rate in the supervision of the corresponding student.

Among the 5 master students I supervised, 4 of them followed a PhD thesis, one of them, Frédéric Batault, under my guidance.

Among the 5 PhD students I supervised, Prof. Nadine Locoge from D^{pt} SAGE was the director of Olivier Debono and Frédéric Batault. Both of them were also directed by Laurence Le Coq from Ecole des Mines de Nantes since they were financially supported by both laboratories. Dr. Antoine Rousseau from LPP Ecole Polytechnique was the director of Sivachandiran Loganathan as well as Christelle Barakat. From an organizational point of view, the PhD of Sivachandiran Loganathan as well as Christelle Barakat contributed to the ANR Rampe project. Sivachandiran Loganathan was mainly based in Ecole des Mines de Douai and Christelle Barakat was mainly based in LPP Ecole Polytechnique. Currently, Nadine Locoge is PhD director of Pamela Harb. This PhD thesis contributes to the ADEME Cortéa ETAPE project; subsequently Pamela Harb is also supervised by Laurence Galsomies from ADEME.

Among the 6 post-doc I supervised from 2009 to 2015, 4 of them were funded by research projects and 2 of them were financially supported by Ecole des Mines. I have shared the supervision of post-docs with different colleagues, depending on the topic of their research activities, Nadine Locoge (air treatment), Nathalie Redon (composite material characterization) and Veronique Riffault (mineral dusts in the atmosphere).

Table 11 - List of Master students, PhD students and Post-docs supervised from 2005 to August 2015.

Year(s)	Duration	Name	Context	Topic	Involvé[t]
Master of Science - Research Internship					
2008	6 months	**Julien COUBLE**	Université Lyon-1 (Univ Lyon-1)	Synthèse du peroxyde d'hydrogène par décharge à barrière diélectrique.	80 %
2011	6 months	**Sébastien CLAISSE**	UVHC (Ecole des Mines)	Elaboration de nano-composites hybrides pour application environnementales.	50 %
2011	6 months	**Frédéric BATAULT**	Université Lyon-1 (Ecole des Mines)	Etude de l'oxydation photocatalytique du trichloréthylène à l'échelle de la ppb.	80 %
2013	6 months	**Habib OURRAD**	Université Lyon-1 (Ecole des Mines)	Etude de l'oxydation photocatalytique du limonène à l'échelle de la ppb : étude des sous-produits gazeux et particulaires.	80 %
2014	6 months	**Benjamin TENEUL**	Chimie Lille (Ecole des Mines)	Mise en place et instrumentation d'une pièce expérimentale de grand volume.	100 %
PhD Thesis					
2008 - 2011	3 years	**Olivier DEBONO**	Université Nantes (Ecole des Mines)	Oxydation photocatalytique de composés organiques volatils et suivi de leurs intermédiaires réactionnels : étude en réacteurs statique et dynamique à des concentrations typiques de l'air intérieur. **[1]**	50 %
2010 - 2013	3 years	**Loganathan SIVACHANDIRAN**	Ecole Polytechnique (ANR)	Regeneration of inorganic sorbents: investigation of adsorbed VOC oxidation using non-thermal plasma surface discharge. **[2]**	80 %
2011 - 2014	3 years	**Frédéric BATAULT**	Université Lille-1 (Ecole des Mines)	Influence de l'adsorption et des paramètres opératoires sur le traitement photocatalytique de composés organiques volatils en mélange dans les conditions de l'air intérieur. **[3]**	50 %
2012 - 2015	3 years	**Christelle BARAKAT**	Ecole Polytechnique (CIFRE)	VOC abatement by plasma-catalyst coupling: from fundamentals to process engineering. **[4]**	25 %
2015 - 2018	3 years (work in progess)	**Pamela HARB**	Université Lille-1 (ADEME)	Etude des performances et de l'innocuité de systèmes de traitement photocatalytiques commerciaux dans une pièce expérimentale reproduisant les conditions de l'air intérieur. **[5]**	80 %
Post-docs					
2009	1 year	**Chandrasekaran SARAVANAN**	Ecole des Mines (Ecole des Mines)	Syntheses and characterizations of PAni / TiO_2 composite for photocatalytic applications.	50 %
2010	9 months	**Paul GRAVEJAT**	Armines (ANR)	Adsorption de l'isopropanol sur TiO_2 et régénération sous exposition plasma.	100 %
2013	9 months	**Louis OLIVIER**	Armines (Carnot Mines)	Etude de l'adsorption de NO_2 et de l'acétaldéhyde sur TiO_2.	80 %
2014	9 months	**Loganathan SIVACHANDIRAN**	Armines (ADEME)	Développement, équipement et validation d'une pièce expérimentale de grand volume pour l'étude de la qualité de l'air intérieur.	80 %
2015	9 months	**Olivier DEBONO**	Armines (Contrat indus.)	Etude des performances d'un système de traitement photocatalytique industriel : hauts débits / hautes concentrations.	100 %
2015 - 2016	1.5 years	**Manolis ROMANIAS**	Armines (Armines)	Evaluation of sorption properties and reactivity of mineral dusts regarding atmospheric VOCs.	80 %

A-7 PUBLICATIONS, COMMUNICATIONS & REPORTS

After a first publication in 2005, based on my research internship, I valorized my research activities through peer-reviewed publications all along PhD, post-doc and Assistant Professor with an average publication rate of 2.5 papers per year. Papers have been submitted to peer-reviewed journals in the fields of catalysis, non-thermal plasma and process engineering, leading to 22 publications. 18 publications out of the 22 papers have been published after my PhD defense. The list of the journals and the corresponding impact factors are reported in Table 12. The number of papers published in each listed journal is indicated in the last column. In August 2015, my total impact factor is 92.3 and my h-index is 12.

Table 12 - List of the Journals and corresponding impact factors.

Journal	Impact factor	Number of papers
Applied Catalysis B: Environmental	6.01	7
Chemical Engineering Journal	4.32	6
Journal of Physics D: Applied Physics	2.72	2
Plasma Chemistry and Plasma Processing	1.60	2
Applied Physics Letters	3.52	1
Journal of Physical Chemistry C	4.84	1
Catalysis Today	3.31	1
Journal of Photochemistry and Photobiology A	2.29	1
Journal of Non-Crystalline Solids	1.72	1
Total impact factor :	**92.3**	**22 papers**
h-index :	**12**	

In order to give a general overview of my publication activity, the number of published papers in peer-reviewed journals has been reported as a function of years between 2005 and 2015 in Figure 2. Similarly, the distribution of oral communication from 2005 to 2015 has been reported in Figure 3. Years characterized by low publication and communication rates respectively correspond to (i) the launch of my research activity at Ecole des Mines and (ii) a higher number of submitted research projects. The detailed list of published peer-reviewed papers from 2005 to May 2015 is reported in Table 13.

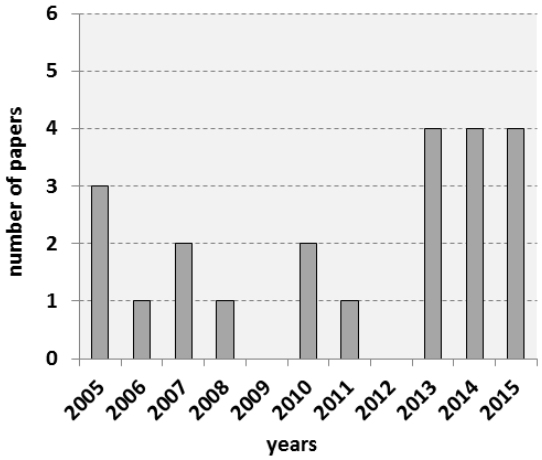

Figure 2 - Distribution of published peer-reviewed papers per year from 2005 to 2015

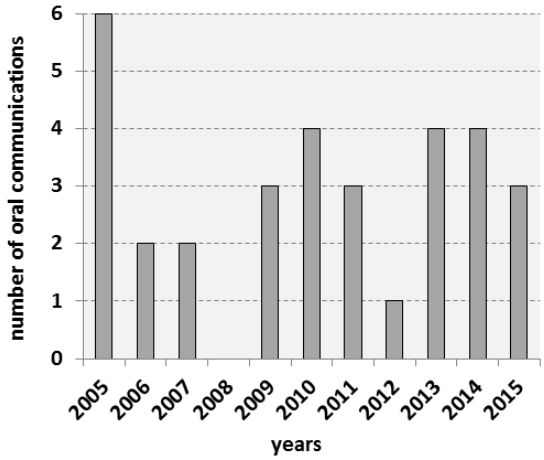

Figure 3 - Distribution of oral communications in national and international conferences per year from 2005 to 2015

Poster communications in national and international conference are not listed and detailed in the present document in order not to make it too long. Nevertheless, I contributed to 35 poster communications in national and international conferences from 2004 to 2015.

Table 13 - List of published papers (August 2015)

1- Determination of the environment of lanthanide ions in a simplified non-active nuclear glass and its weathering gel products – Europium as a structural luminescent probe.
F. Thevenet, G. Panczer, P. Jollivet, B. Champagnon
Journal of Non-Crystalline Solids, 351 (2005) 673 **[6]**

2- Photocatalytic degradation of acetylene over various titanium dioxide based photocatalysts
F. Thevenet, O. Guaïtella, J.-M. Herrmann, A. Rousseau, C. Guillard,
Applied Catalysis B: Environmental 61 (2005) 62 **[7]**

3- Photocatalyst activation in pulsed low pressure discharge
A. Rousseau, O. Guaitella, L. Gatilova, F. Thevenet, C. Guillard, J. Roepcke, G. Stancu,
Applied Physics Letters 87, 221501 (2005) **[8]**

4- Dynamics of the plasma current amplitude in a barrier discharge : influence of TiO_2 as a photocatalytic material
O. Guaitella, F. Thevenet, C. Guillard, A. Rousseau,
Journal of Physics D: Applied Physics 39 (2006) 2964 **[9]**

5- Oxidation of acetylene by photocatalytic process coupled with dielectric barrier discharge
F. Thevenet, O. Guaitella, E. Puzenat, A. Rousseau, C. Guillard,
Catalysis Today 122 (2007) 186 **[10]**

6- C_2H_2 oxidation by plasma / TiO_2 combination : influence of the porosity, and photocatalytic mechanisms under plasma exposure
O. Guaitella, F. Thevenet, E. Puzenat, C. Guillard, A. Rousseau
Applied Catalysis B: Environmental 80 (2007) 296 **[11]**

7- Influence of water vapour on plasma / photocatalytic oxidation efficiency of acetylene
F. Thevenet, O. Guaitella, E. Puzenat, C. Guillard, A. Rousseau
Applied Catalysis B: Environmental 84 (2008) 813 **[12]**

8- OH Radicals and H_2O_2 Molecules in the Gas Phase near to TiO_2 Surfaces
J. Thiebaud, F. Thevenet, C. Fittschen
Journal of Physical Chemistry C, 114 (2010) 3082 **[13]**

9- Synthesis of hydrogen peroxide using dielectric barrier discharge associated with fibrous materials
F. Thevenet, J. Couble, M. Brandhorst, J. L. Dubois, E. Puzenat, C. Guillard, D. Bianchi
Plasma Chemistry Plasma Processing 30 (2010) 489 **[14]**

10- Toluene photocatalytic oxidation at ppbv levels: kinetic investigation and carbon balance determination
O. Debono, F. Thevenet, P. Gravejat, V. Hequet, C. Raillard, L. Lecoq, N. Locoge
Applied Catalysis B: Environmental 106 (2011) 600 **[15]**

11- Isopropanol saturated TiO_2 surface regeneration by non-thermal plasma: Influence of air relative humidity
L. Sivachandiran, F. Thevenet, P. Gravejat, A. Rousseau
Chemical Engineering Journal, 214 (2013) 17 **[16]**

12- Gas phase photocatalytic oxidation of decane at ppb levels: removal kinetics, reaction intermediates and carbon mass balance
O. Debono, F. Thevenet, P. Gravejat, V. Hequet, C. Raillard, L. Le Coq, N. Locoge
Journal of Photochemistry and Photobiology A Chemistry 258 (2013) 17 **[17]**

13- Investigation of NO and NO_2 Adsorption Mechanisms on TiO_2 at Room Temperature
L. Sivachandiran, F. Thevenet, P. Gravejat, A. Rousseau
Applied Catalysis B: Environmental 142 (2013) 196 **[18]**

14- Non-Thermal Plasma Assisted Regeneration Of Acetone Adsorbed TiO_2 Surface.
L.Sivachandiran, F. Thevenet, A. Rousseau
Plasma Chemistry and Plasma Processing 33 (2013) 855 **[19]**

15- Acetylene photocatalytic oxidation using continuous flow reactor: gas phase and adsorbed phase investigation, assessment of the photocatalyst deactivation.
F. Thevenet, A. Rousseau, C. Guillard
Chemical Engineering Journal 244 (2014) 50-58 **[20]**

16- Regeneration of isopropanol saturated Mn_xO_y surface : comparison of thermal, ozonolysis and non-thermal plasma treatment.
L. Sivachandiran, F. Thevenet, A. Rousseau
Chemical Engineering Journal 246 (2014) 184-195 **[21]**

17- Oxidation of isopropanol and acetone adsorbed on TiO_2 under plasma generated ozone flow : gas phase and adsorbed species monitoring.
C. Barakat, O. Guaitella, F. Thevenet, A. Rousseau
Applied Catalysis B: Environmental 147 (2014) 302-313 **[22]**

18- Plasma Catalyst coupling for VOC removal and indoor air treatment: a review
F. Thevenet, L. Sivachandiran, O. Guaitella, C. Barakat, A. Rousseau
Journal of Physics D Applied Physics 47 (2014) 224011 **[23]**

19- Acetaldehyde and acetic acid adsorption under dry and humid conditions
F. Batault, F. Thevenet, V. Hequet, C. Raillard, L. Le Coq, N. Locoge
Chemical Engineering Journal, 264 (2015) 197-210 **[24]**

20- Limonene photocatalytic oxidation at ppb levels: assessment of gas phase reaction intermediates and secondary organic aerosols heterogeneous formation.
H. Ourrad, F. Thevenet, V. Gaudion, V. Riffault
Applied Catalysis B: Environmental 168-169 (2015) 183-194 **[25]**

21- Isopropanol removal using Mn_xO_y packed bed non-thermal plasma reactor: comparison between continous treatment and sequential sorption/regeneration.
L. Sivachandiran, F. Thevenet, A. Rousseau
Chemical Engineering Journal 270 (2015) 327-335 **[26]**

22- Acetaldehyde adsorption on TiO_2: influence of NO_2 preliminary adsorption.
F. Thevenet, L. Olivier, F. Batault, L. Sivachandiran, N. Locoge
Chemical Engineering Journal 264 (2015) 197-210 **[27]**

I have given 3 invited lectures in international conferences; corresponding references are reported in Table 14.

Table 14 - List of invited lectures.

1- Regeneration of Inorganic Sorbent Surface: Investigation of adsorbed VOC Oxidation using Surface Discharge
F. Thevenet
International Conference on Plasma Processing of Organic Materials and Polymers (PPOMP 2011), Kottayam, Kerala, India, November 25-27th 2011

2- Plasma-catalysis for VOC oxidation : comparison between continuous and sequential processes
F. Thevenet, L. Sivachandiran, A. Rousseau
AOTs-21 (Adavanced Oxidation Technologies), San Diego, USA, November 16-19th 2015

3- Photocatalytic oxidation of limonene in indoor air : gas phase, adsorbed phase and particulate matter investigation
F. Thevenet, H. Ourrad, V. Riffault
SPASEC-21 (Semi-Conductor Photocatalysis & Solar Energy Conversion), San Diego, USA, November 16-19th 2015

Moreover, 28 oral communications have been given in national and international conferences based on my research activities. The corresponding list is reported in Table 15 my name is underlined as I was the speaker.

Table 15 - List of oral communications given in national and international conferences (August 2015)

1- VOC removal by plasma-photocatalyst combination : comparison between a low and an atmospheric pressure discharge
A. Rousseau, O. Guaitella, L. Gatilova, F. Thevenet, C. Guillard, M. Hannemann, J. Roepcke
57th GEC (Gaseous Electronic Conference) Shannon - Ireland, September 2004

2- Combination of Photocatalysis and Non-Thermal Plasma for VOC Treatment
C. Guillard, F. Thevenet, O. Guaitella, A Rousseau
8th International Conference on Solar Energy and Applied Photochemistry, Louxor - Egypt, February 20-25th 2005

3- Plasma-photocatalyst synergy in a pulsed low pressure discharge
O. Guaitella, L. Gatilova, G. Stancu, J. Roepcke, F. Thevenet, C. Guillard, A. Rousseau
15ème CIP – Colloque International des Plasmas, Autrans - France, 5-9 Juin 2005

4- Dynamic of interaction between a pulsed plasma reactor and a porous semi-conductor surface
O. Guaitella, G Stancu, J. Roepcke, F. Thevenet, C. Guillard, A. Rousseau
XXVIIth ICPIG, Eindhoven - Pays Bas, july 18-22nd 2005

5- Photocatalytic removal of VOCs by powder and supported titania photocatalysts
F. Thevenet, E. Puzenat, O. Guaitella, A Rousseau, J.M. Herrmann, C. Guillard
7th European Congress of Catalysis (EUROPACAT VII), Sofia - Bulgarie, 27 Aout - September 1st 2005

6- Dégradation de l'acétylène par photocatalyse : approche cinétique et modélisation
F. Thevenet, E. Puzenat, O. Guaitella, A. Rousseau, C. Guillard
8ème JFJPC (Journées Francophones des Jeunes Physico-Chimistes), Marly-le-Roy - France, 28-30 Septembre 2005

7- Combination of atmospheric pressure dielectric barrier discharge and photocatalysis for C_2H_2 oxidation
F. Thevenet, O. Guaitella, C. Guillard, A. Rousseau
58th GEC (Gaseous Electronic Conference), San Jose - Californie - USA, October 2005

8- Mechanisms of the synergy of DBD with TiO_2 for C_2H_2 removal
O. Guaitella, F. Thevenet, C. Guillard, A. Rousseau
ESCAMPIG 18, LECCE, Italy, july 11-16th 2006

9- Plasma-photocatalysis combination for air pollutant removal: identification of the synergy mechanisms
O. Guaitella, F. Thevenet, C. Guillard, J. Roepcke, and A. Rousseau
59th GEC, Columbus, Ohio, USA October 10-13th 2006

10- Understanding of the plasma/photocatalyst synergy for VOC abatement
O. Guaitella, F. Thevenet, C. Guillard, A. Rousseau
ISPC, Kyoto - Japon, august 26-31st 2007

11- Reactional pathway of acetylene removal by non-thermal plasma and/or photocatalysis process
F. Thevenet, O. Guaïtella, F. Dappozze, E. Puzenat, A. Rousseau, C. Guillard
13th International Conference on Advanced Oxidation Technology for Treatment of Water, Air and Soil, Niagara Falls - USA September 24-27th 2007

12- Kinetic investigations of by-products formed during photocatalysis oxidation of toluene at indoor air levels
O. Debono, F. Thevenet, V. Hequet, C. Raillard, L. Lecoq, N. locoge
Healthy building 2009, Syracuse (USA), 15-19th September 2009

13- Kinetic investigations and reaction intermediates during photocatalytic oxidation of toluene at indoor air levels (ppb)
O. Debono, F. Thevenet, V. Hequet, C. Raillard, L. Lecoq, N. locoge
European Symposium on Photocatalysis, Bordeaux - France, 21-22nd September 2009

14- Dielectric and photoconductivity behaviour of Polyaniline- TiO_2 nanocomposites
C. Saravanan, N. Redon, F. Thevenet, J.L. Wojkiewicz
13th International IUPAC conference on polymers and organic chemistry, Montréal (Canada), 4-9th July, 2009

15- Photocatalytic oxidation of indoor VOCs at ppb levels : kinetics of by-products formation
O. Debono, F. Thevenet, V. Hequet, C. Raillard, L. Lecoq, N. locoge
239th ACS Meeting, San Francisco, March 21–25th 2010

16- Photocatalytic oxidation of VOCs in indoor air (ppb levels) : kinetic and by-product investigation, influence of VOC mixture
O. Debono, F. Thevenet, V. Hequet, C. Raillard, L. Lecoq, N. locoge
TiO_2 Photocatalysis: Fundamentals and Application (TiO2-15), San Diego, USA, November 15-18th , 2010

17- Regeneration of isopropanol saturated TiO_2 coatings using surface dielectric barrier discharges
P. Gravejat, F. Thevenet, O. Guaitella, A Rousseau
Advanced Oxidation Techologies for Treatment of water, air and soil (AOTs-16), San Diego, USA, November 15-18th , 2010

18- Non-thermal plasma synthesis of H_2O_2 : investigation of DBD and surface-DBD performance
F. Thevenet, J. Couble, M. Brandhorst, J.L. Dubois, D. Bianchi
Gaseous Electronic Conference (GEC), Paris, France, october 4-8th 2010

19- Intermediates Formation during Toluene Photocatalytic Oxidation at ppb Levels : Comparison between Batch and Dynamic Experiments
O. Debono, F. Thevenet, V. Hequet, C. Raillard, L. Lecoq, N. locoge
TiO_2-16th, San Diego, California, November 7-10th , 2011

20- Non thermal plasma surface discharge assisted regeneration of CO and CO_2 adsorbed TiO_2 : effect of humudity
L. Sivachandiran, F. Thevenet, P. Gravejat, A. Rousseau
18th International Colloquium on Plasma Processes (CIP 2011), Nantes, July 4-8th, 2011

21- Plasma regeneration of IPA saturated TiO_2 surface : influence of air relative humidity
L. Sivachandiran, F. Thevenet, P. Gravejat, A. Rousseau
IPS-2012 : 5th international workshop on plasma spectroscopy, Giens, France, may 13-16th 2012

22- Non-Thermal Plasma Driven Regeneration of IPA Saturated MnO_2 Surface
L. Sivachandiran, F. Thevenet, P. Gravejat, A. Rousseau
21st International Symposium of Plasma Chemistry (ISPC-21), Cairns, Australie, august 4-9th 2013

23- Non thermal plasma surface discharge assisted regeneration of CO and CO_2 adsorbed TiO_2 : effect of Humidity
L. Sivachandiran, F. Thevenet, P. Gravejat, A. Rousseau
Congrès International des Plasma (CIP), Paris, France, septembre 9-13th 2013

24- TiO_2 photocatalytic oxidation of indoor VOCs at ppb levels in a multi-pass dynamic reactor : influence of the mixture of VOCs on reaction intermediates concentrations
O. Debono, V. Hequet, C. Raillard, F. Thevenet, L. Le Coq, N. Locoge
245th ACS National Meeting, New Orleans, LA, USA, April 7-11th 2013

25- Ageing of TiO_2 Surface: Quantitative Assessment of NO and NO_2 Adsorption Mechanisms
L. Sivachandiran, F. Thevenet, A. Rousseau
Journées Européennes de Photocatalyse JEP-2013, Portoroz, Slovenia, September 25-27th 2013

25- Optimization of Photocatalytic Media Geometry for the Improvement of Indoor Air PCO Treatment
L*. Olivier, F. Batault, O. Debono, A. Subrenat, V. Hequet, C. Raillard, F. Thevenet, L. Le Coq, N. Locoge*
SPEA-8 : 8th european meeting on solar chemistry and photocatalysis, Thessaloniki, Greece, June 25-28th 2014

26- Regeneration of IPA saturated MnxOy surface : comparaison of thermal, ozonolysis, and non-thermal plasma treatment
L. Sivachandiran, F. Thevenet, A. Rousseau International Symposium on Non-Thermal/Thermal Plasma Pollution Control Technology and Sustainable Energy (ISNTP-9) Dalian, China, June 16-20th , 2014

27- Sorption properties and photocatalytic reactivity of standard and natural dusts with VOC
H. Ourrad, F. Thevenet, V. Riffault
International Conference on Atmospheric Dust 2014, Castellaneta-Marina, Italy, June 1-6th 2014

28- Limonene photocatalytic oxidation at ppb levels: characterization of gas phase and particulate phase side products
H. Ourrad, F. Thevenet, V. Gaudion, V. Riffault
XXXIVème édition du Colloque Annuel du Groupe Français de Cinétique et Photochimie (XXXIV - GFCP), Villeurbanne, 23-24 juin 2014

International patents based on my research activities are listed in Table 16

Table 16 - List of international patents (August 2015)

Combined treatment of gaseous effluents by cold plasma and photocatalysis / Traitement de l'air par couplage plasma / photocatalyseur supporté
International patent : WO 2007/051912 **[28]**

Method for producing hydrogen peroxide / Procédé de fabrication du peroxyde d'hydrogène
International patent : WO 2010/049634 A1 **[29]**

Finally, I authored 8 scientific reports as listed in Table 17.

Table 17 - List of scientific reports.

1- Master of Science – Final Report (July 2003)
Détermination de l'environnement des lanthanides et des actinides dans le verre de confinement SON68 et ses gels d'altération – Etude par sonde structural luminescente.
written under the supervision of Gérard Panczer

2- PhD Thesis Manuscript (Septembre 2006)
Elimination et mécanismes de degradation de l'acétylène par couplage plasma-froid photocatalyse
under the supervision of A. Rousseau & C. Guillard **[30]**

3- Post-doc – final report (March 2008)
Rapport final du projet Axelera plasma/H_2O_2
under the supervision of Daniel Bianchi

4- Study report (April 2011)
Evaluation de l'activation de photocatalyseurs à travers des vitrages automobiles.

5- PHOTOCOV project - final report (Sept. 2011)
Etude des composés organiques volatils formés au cours du traitement photocatalytique de l'air intérieur.

6- PAni/TiO_2 project – final report (Sept 2011)
Nouveau composites organiques-inorganiques pour systèmes de traitement d'air

7- RAMPE project – final report (November 2012)
Regeneration of inorganic sorbents under plasma exposure.

8- ETAPE project – 1st year report (July 2014)
Rapport intermédiaire du projet ETAPE « Evaluation des performances et de l'innocuité des systèmes de traitement d'air par photocatalyse ».

9- PhotoCair project – final report (July 2015)
Rapport final du projet PhotoCair « Traitement Photocatalytique de l'air intérieur »

A-8 SYMPOSIUM ORGANIZATION

In partnership with Didier Salmon from *Interscience*, a Belgian analytical instrument supplier, my colleague Nadine Locoge and I organized in D^{pt} SAGE at Ecole des Mines a one-day symposium dedicated to "**Recent advances in gas phase analyses"** on May 13th 2014. This symposium was dedicated to researchers and industrials interested in gas phase analyses for environmental and process engineering applications.

The symposium has been divided into three complementary sessions: (i) analyses of gases at ppb levels by micro-GC; (ii) analyses of concentrated gases; (iii) spectrometric methods for gas phase analysis. Nine speakers were invited from France, Belgium, Luxemburg and the Netherlands. They were requested to organize their 30-minute talks into two parts: (i) presentation of the analytical technique, method or development; (ii) illustration of the achievement through operational applications. Discussions, interactions and feedbacks were promoted all along the symposium between the speakers and the audience by the different chairmen. More than 50 participants, from academic as well as industry, have been welcomed for the first edition.

A-9 TEACHING ACTIVITIES

This section summarizes my contributions to teaching in the different Universities, Institutions and Schools from my PhD to my current position at Ecole des Mines (Table 18). Teaching activities are classified according to (i) their nature, (ii) the institution and (iii) the level of students. Please note that the level of students is indicated according to the French LMD classification (Licence-Master-Doctorat). The status of Assistant Professor or even full Professor at Ecole des Mines do not compel to any minimum level of teaching per year. As a consequence, the involvement in the teaching activities at Ecole des Mines is principally based on one's motivation. In the column entitles "*Remark*" indications are given when I have created and initiated myself the corresponding courses.

Table 18 - Synthesis of teaching activities from 2005 to 2015

	hr/year	Level	Institution	Topic	Remark
Lectures					
2005-2006	4 hr	Master 2	Université P & M Curie	Photocatalysis and plasma-catalysis coupling for environmental applications.	New lecture
Since 2010	12 hr	Master 2	Ecole des Mines	Indoor Air Quality : indoor air monitoring, current regulations and treatments.	New lecture
Since 2009	10 hr	Master 1	Ecole des Mines	Catalysis and industrial catalytic processes.	New lecture
Since 2010	26 hr	Master 1	Ecole des Mines	Phase Diagrams: applications to material science.	Renewed
Tutorial Classes					
2004-2005	24 hr	Master 1	Polytech'Lyon	Material Science: from structure to mechnanical properties.	New class
Laboratory Courses					
2005-2008	40 hr	Licence 2	Univ. Lyon-1	Physics laboratory courses.	ø
2008-2010	24 hr	Licence 3	Ecole des Mines	Physics laboratory courses.	ø
Since 2008	64 hr	Licence 3	Ecole des Mines	Chemistry laboratory courses.	50% renewed in 2011

Beside classical pedagogical activities, teacher at Ecole des Mines are highly encouraged to contribute to the supervision of student projects. Indeed, the project-based learning is highly promoted in the pedagogical strategy of Ecole des Mines. Subsequently, each year, students have to contribute or lead different types of projects. In that context I have supervised the following student projects.

Bibliographical projects / Till 2010 groups of two 1st-year students were in charge of a bibliographic study proposed by teachers from at Ecole des Mines. They had to find, summarize and discuss any relevant document related to the topic they had selected. The project led to (i) the writing of a bibliographic report where the formal structure was specifically evaluated, and (ii) an oral defense to present the documented topic. I supervised in 2009 and 2010 two bibliographical projects: (i) *Principle and application of photocatalytic concretes* and (ii) *Environmental impact of Le Havre harbor*.

Open project / During the 1st year (Licence 3), groups from 5 to 8 students have 80 hr to work on a technical or scientific problem proposed by teachers from Ecole des Mines, associations or industrial partners. This project is generally interdisciplinary and involves students from various options. The main objective is to stimulate their creativity and ability to collaborate. I supervised in 2009 an open project named "Anim&co". This project aimed at developing a game for ten year old children in order to make them aware of modern pollution issues. In a first step, students have completely developed the game and its rules, and then they have proposed this game to three "*CM2*" classes from Douai, in cooperation with teachers.

Research projects (PDR) / Since 2009, students in the 2nd year (Master 1) have 80 hr to discover some aspects of research activities at Ecole des Mines related to their future options. Groups of 2 students have to make first a short bibliographical report on the scientific topic they have selected. Then, they propose to the supervising teacher a strategy to answer the problematic they have to face. Students perform the experiments they have planned and then, present obtained results and conclusions during a one-day symposium to their colleagues and teachers. The list of the 11 research projects I have proposed and supervised is reported in Table 19.

Table 19 - List of supervised student research projects (PDR) and years.

Analyses of VOCs in an industrial working place	2010
Photocatalytic degradation of methylene blue: solar vs. artificial light	
Photocatalytic activity assessment of new PAni/TiO_2 composite materials	
Degradation of methylene blue by photocatalysis and Fenton reaction	2011
Degradation of methylene blue by Fenton reaction: influence of concentration	2012
Scaling of laboratory reactor dedicated to dye adsorption on activated carbon	
Degradation of methylene blue by Fenton reaction: influence of temperature	2013
Synthesis and coating of CeO_2 on Pyrex glass	
Determination of the specific area of fly ash from biomass burning	2014
Determination of a protocol to assess atmospheric particle oxidizing potential	
May analytical chemistry address problems related to bad breath ?	2015

A-10 SPECIFIC PEDAGOGICAL INPUT

In the context of Chemistry lab courses, my colleague Véronique Riffault and I submitted, to *Unisciel* a pedagogical innovative project entitled *VideoChem*. *Unisciel* is a GIS (Scientific Interest Group), and one of the 7 French UNT (Digital Thematic University). Digital Thematic Universities have been created with the support of the Technology branch at the Ministry of National Education, Higher Education and Research, and aim at gathering institutions working on similar topics in order to share and diffuse open educational resources based on common frameworks. *Unisciel* is hosted by Lille-1 University. The project has been submitted to the open call for proposal proposed by *Unisciel*.

The VideoChem project aimed at: (i) making the preparation of lab courses easier and more efficient for students, and (ii) giving to the students more autonomy and self-confidence irrespectively of their background in chemistry. Considering the huge growth of digital and video in the modern world, especially for young people, it was quite obvious that the new pedagogical tool we wanted to develop had to be (i) available on-line, (ii) at any time, (iii) short and (iv) striking. Thus, videos appeared as the most interesting media, even if it was a whole challenge for us. Veronique Riffault, Paul Gravejat and I wrote the scenario. Shots, video cuts and video editing have been efficiently performed by Stéphane Giszczewski from Ecole des Mines. The VideoChem

project is summarized in Table 20. Created video are available on the Ecole des Mines education digital platform named “Campus” and on-line through Canal-U (https://www.canal-u.tv/).

Table 20 - Summary of VideoChem project	**VideoChem**		
Framework	Unisciel	*Duration:*	2012 - 2013
Contributor	D^{pt} SAGE, Ecole des Mines, Douai		Coordinator
Summary	The main difficulty encountered by Chemistry lab courses supervisors was related to the heterogeneity of students. Indeed, students attending the Chemistry lab courses originate from different preparatory classes with various majors (Mathematic, Physics, Chemistry,…). Moreover, some of them were used to experimental courses, whereas others only had theoretical teachings. The objective of the VideoChem project was to propose videos to students to help them preparing lab courses. These short videos (2-3 min) aim at (i) introducing a protocol, (ii) detailing an instruments or (iii) showing the appropriate experimental procedure. Students are free to use or not these 11 videos available on the Ecole des Mines digital teaching platform *Campus*. Videos can be watched on-line either before lab courses for preparation, or during the class on available computers. The use of these videos (i) allows the students a more efficient preparation of lab courses, (ii) improves their autonomy and self-confidence and (iii) reduces the risk of accident, wound and damage due to inappropriate handling of instruments and chemicals.		
Budget	*Total cost:* 16 k€	*Grant:* 10 k€	*Grant for D^{pt} SAGE* 10 k€

A-11 ADMINISTRATIVE AND INSTITUTIONAL INVOLVMENTS

From 2006 to 2008, as post-doc, I was an elected member of the laboratory council of IRCELyon, representative of students and non-permanent researchers. From 4 to 6 half-day meetings were planned per year. The laboratory council discusses, proposes and votes the research and teaching strategy of the laboratory. This first experience made me more familiar with the management of a large scale public research laboratory.

Since January 2011, I am an elected member of the laboratory council of D^{pt} SAGE at Ecole des Mines, representative of Assistant Professors. The smaller size of SAGE compared to IRCELyon only requires 2 meetings per year and facilitates a less formal and more responsive management.

Since 2012, I supervise the activity planning of Vincent Gaudion, technician in my group. It mainly consists in weekly meetings and discussions to organize the schedule of Vincent based on missions, and in yearly individual interview in the presence of Nadine Locoge. I am his referee as regards of days-off and working hours.

Part B - INDOOR AIR AND AIR TREATMENT

*Adapted from **ADEME** publication AGIR! (2015)*

This section proposes a general overview of the main context of my research activities along the last seven years. Indoor air is a specific atmosphere which went through to significant changes during the last thirty years. Part-B is not an exhaustive review of indoor air problematic but aims at giving the main issues and the recent developments regarding indoor air treatment technologies.

B-1 INDOOR AIR QUALITY: CURRENT CONTEXT AND MODERN ISSUES

Introduction / Air pollution is a major problem that has been recognized hundred years ago along with the increase of population density and activities. In France, even if a royal decree, published in 1663, requested the drifting of grey waters at the outbound of Paris city to avoid unpleasant odors [31], the individual right to a healthy air was only recognized in the French legislation in 1996 [32]. Similarly, in an effort to reduce air pollution, in 1272 king Edward Ist of England threatened Londoners with harsh penalties if they did not stop burning coal in their houses. However, regular warnings along the following centuries did not prevent the Great London Smoke in the winter 1952 leading to more than 4000 deaths in the span of one week.

Air pollutants / More recently, the evolutions of modern lifestyles in developed countries led to the massive development of automobile, industry and synthetic materials, in parallel with a considerable increase of the time spent indoor (ca. 80%) emphasizing people's exposure to air pollutants. A summary of the main primary pollutants monitored in air related to their sources and potential health effects is reported in Table 21.

Pollutant	Natural Sources	Anthropogenic Sources	Human Health Effects
Carbon monoxide (CO)	Volcanic eruptions, forest fires, photochemical reactions in the troposphere	Motor vehicle exhaust, electrical generating facilities, and other incomplete combustion processes.	Blocks the ability of hemoglobin to transport oxygen to the cells of the body. At moderate concentrations, angina, impaired vision, and reduced brain function may likely result.
Nitrogen oxides (NOx)	Lightning storms and biological decay processes.	Primarily from fossil fuel combustion in electrical utilities, high-temperature operations, and operation of motor vehicle exhaust.	Eye, skin, and respiratory tract irritation. Pulmonary edema, bronchitis, bronchiolitis, and emphysema in moderate to high levels.
Sulfur oxides (SOx)	Biological decay processes, volcanic eruptions.	Burning of fuel (e.g. coal and oil) containing sulfur and during metal smelting and other industrial processes.	Respiratory illness, alterations in the lungs' defenses, and aggravation of existing heart or lung disease in susceptible populations.
Particulate matter (PM)	Pollen, bacterial, and fungal spores, dust, soot ash.	Electricity generation, industrial processes, fossil fuel combustion, waste disposal.	Decreased lung function, irritation of the airways, aggregated asthma, and heart problems. Small particles with less than 10 µm in diameter lead to the greatest risk.
Volatile organic compounds (VOCs)	Trees and other plants emit hydrocarbons (terpenes).	Solvent use, vehicular exhaust, industrial processes.	Eye, nose, and throat irritation, headaches, loss of coordination damage to liver, kidney, and central nervous system. Some are suspected or known to cause cancer in humans.

Table 21 - Primary air pollutants: sources and potential health effects.

Health and societal issue / The Indoor Air Quality (IAQ) became an important issue since the term "Sick Building Syndrome" (SBS) was first coined by the World Health Organization (WHO) in 1986 [33]. Generally, SBS is a situation in which occupants of a building experience acute health effects that seem to be linked to time spent in a building, but no specific illness or cause can be identified. Further, SBS complaints are generally associated with headache, eye, nose, or throat irritation, dry cough, dizziness, difficulty in concentrating, fatigue and odor sensitivity. Most of the complainants report relief soon after leaving the building. Hence, attention has been paid to monitor the indoor pollutants and to improve the air quality. As a consequence of SBS, several organizations such as the WHO, the United States Environmental Protection Agency (US-EPA), and the French (OQAI), have established a list of priority indoor air pollutants [34][35][36][37] based on the ubiquity, the concentrations and toxic effects of the involved substances. The degradation of indoor air quality has been well evidenced by the French (OQAI) [38] which mainly relates indoor air quality degradation to the massive presence of VOCs (Volatile Organic Compounds).

In spite of the health issue, studies on indoor air pollutants and sanitary impacts were initiated in the 80s. WHO evaluates the number of deaths due to air pollutants to 7 million people [39]. Among them, 4 million could be attributed to poor indoor air quality. As a health issue, indoor air pollution became a major concern [40][41][42]. Thus, indoor air quality was taken as a criterion of the HQE process (*Haute Qualité Environnementale*) [43] and became one of the key point of the 2nd-PNSE (*Plan national Santé Environnement*) [44]. Recently, the French Ministry of Environment conducted a study to evaluate the cost of air pollution weighing on the French medical system [45]. In France, air pollution induces 1.8 billion € expenses per year.

VOCs & indoor air / One of the first detailed review of VOC concentrations in indoor air of different kinds of buildings (houses, offices, schools, hospitals, established, new,…) was conducted in 1994 by Brown et al [46]. They gathered information from 50 worldwide studies and evaluated concentrations obtained from the published literature. They pointed out two main characteristics of VOCs in indoor air:

The mean concentration of individual VOCs in established buildings is generally below 50 µg/m^3, with most below 5 µg/m^3, while TVOC concentrations are much higher (e.g. 1000 µg/m^3 in dwellings), reflecting the large number of compounds present.	VOC concentrations in new buildings are much greater than those in established buildings, often by an order of magnitude or more, and appear to arise from construction materials and building contents, the VOC emission characteristics of which can be measured for source control.

Since then, numerous studies were conducted in different countries to address the specificities of VOCs in indoor air with more accuracy, in Germany (Hippelein [47],Schleibinger at al [48]), in France (Mosqueron et al [49][50]), in Finland (Edwards et al [51]), in Japan (Chikara et al [52]), in China (Liu et al [53]) and the USA (Hodgson et al [54], US-EPA [55]).

Sources / A large part of indoor air pollution by VOCs originates from sources located inside the building [56]. Outdoor air entering the building is another source of indoor air VOCs [57] especially in urban zones. Kostiainen identified more than 200 VOCs along a field campaign measurement in 26 houses and related the level of indoor VOCs with SBS occurrence [58]; this thorough monitoring of indoor air illustrates the diversity of VOCs. They are (i) emitted from the materials around us (household and consumer products, furnishing and building materials, office equipment, air fresheners, paints, paint strippers, household solvents, etc.), (ii) generated by our own activities (cooking, cleaning, tobacco smoking, etc.), (iii) infiltrated from outdoor air (traffic, biogenic and industrial emissions, etc), (iv) produced by microorganisms found in indoor environments (molds, bacteria) or (v) even produced through homogeneous or heterogeneous indoor air reactions.

Determinants / VOCs are ubiquitous in indoor environments but their concentrations depend on: (i) the total space volume, (ii) the pollutant sinks and sources, (iii) the air exchange rate with outdoor, (iv) the outdoor VOC concentrations [59], the presence of indoor or outdoor oxidants and the subsequent potential reactions. As a result, concentrations of individual VOCs are highly variable. Hence, publications frequently report the levels of Total Volatile Organic Compounds (TVOCs) rather than individual values [60]. Total indoor air VOCs concentrations hardly exceed 200 ppb in most of the dwellings. This value sounds low, however, depending on the nature (i.e. toxicity) of the VOCs it has to be decreased to diminish and people's exposure.

Diversity / A first and widespread approach consists in classifying the various monitored VOCs in indoor air according to their chemical families. VOCs belong to different chemical families: aromatic hydrocarbons, alkenes, alcohols, aliphatic hydrocarbons, aldehydes, ketones, esters, glycols, glycolethers, halocarbons, cycloalkanes and terpenes. Since the mid-1980s, when the German UBA (*Umwelt Bundesamt*) carried out first systematic indoor measurements, toluene and volatile halocarbons significantly decreased. However, the latter study conducted by the German Association of Ecological Research Institutes (AGÖF) shows that other substances are now found at higher concentrations than in the past. This trend is observed for aliphatic hydrocarbons with longer carbon chains which have, to a large extent, substituted other more volatile and toxic solvents [61]. Neilson et al [62] proposed in 2002 an overview of the relation between, sources and natures of the VOCs (Table 22).

The large-scale measurement campaign performed from 2003 to 2005 in France on 567 residences is highly informative about VOC diversity. This campaign evidenced that carbonyl compounds are characterized by the highest occurrences and the highest concentrations [38]. Indeed, formaldehyde, acetaldehyde and hexanal were monitored in 100% of the investigated dwellings.

Guidelines and regulations for indoor air / In France, OQAI initiated the classification of the main monitored pollutants in indoor air. This classification is based on the toxicity and the occurrence of the substances, leading to the creation of five priority groups. In 2002 a list of 70 classified pollutants was proposed. This list was completed in 2005 and 2010 with the introduction of other substances from specific places such as schools and

offices. In 2010, 1026 substances were listed and 359 were classified. Pollutants from the most priority group are: formaldehyde, benzene, acetaldehyde, dichlorvos, PM10 and radon; as a result, VOCs are particularly watched. At European scale, a similar classification has been initiated through the INDEX project. Based on the OQAI classification, the ANSES (*Agence National de Sécurité Sanitaire*) was in charge of the determination of the exposure threshold for the classified substances with the highest priority which led to the definition of guidelines reported in Table 23.

Outdoor sources	Traffic, industry	aliphatic and aromatic hydrocarbons; aldehydes; ketones; esters
Building material	Insulation, paint, plywood, adhesives	aliphatic and aromatic hydrocarbons; alcohols; ketones; esters
Furnishing material	Furniture, floor/wall coverings	aliphatic and aromatic hydrocarbons; alcohols; halocarbons; aldehydes; ketones; ethers; esters
Garage and combustion appliances	Vehicle emission, tobacco smoking, candles	aliphatic and aromatic hydrocarbons; aldehydes, amines
Equipment	Laser printers, photocopiers, computers, other office equipment	aromatic hydrocarbons; aldehydes; ketones; esters
Indoor activities	Cooking, tobacco smoking, use of water and solvents	amines; aliphatic and aromatic hydrocarbons; aldehydes; halocarbons

Table 22 – Source of emissions of indoor VOCs and corresponding chemical families.

Substance	Guidelines
formaldehyde	- short term Guideline: 50 µg.m^{-3} (40 ppb) 2h exposure - long term Guideline: 10 µg.m^{-3} (10 ppb) pour une exposition supérieure à un an
carbon monoxide	short term Guideline: - 10 mg.m^{-3} (9 ppm) 8 h exposure - 30 mg.m^{-3} (26 ppm) 1 h exposure - 60 mg.m^{-3} (51 ppm) 30 min exposure - 100 mg.m^{-3} (86 ppm) 15 min exposure
benzene	- short term Guideline : 30 µg.m^{-3} (9 ppb) 14 days exposure - medium Guideline : 20 µg.m^{-3} (6 ppb) from 2 weeks to one year exposure - long term Guideline: * 10 µg.m^{-3} (3 ppb) more than one year exposure * 0,2 µg.m^{-3} (60 ppt) whole life exposure
naphtalene	- long term Guideline: 10 µg.m^{-3} (2 ppb) more than one year exposure
trichlorethylene	- medium Guideline: 800 µg.m^{-3} (147 ppb) from 2 weeks to one year exposure - long term Guideline: 2 µg.m^{-3} (0,4 ppb) whole life exposure
tetrachloroethylene	- short term Guideline: 1380 µg.m^{-3} (200 ppb) from 1 to 14 days exposure - long term Guideline: 250 µg.m^{-3} (36 ppb) more than one year exposure

Table 23 - Exposure guidelines in indoor air proposed for high priority substances.

Germany promoted the concept of '*Better Indoor Air Quality*' since 1992; the Federal Government aimed at making a nation-wide uniform evaluation of indoor air through the definition of guideline values for indoor air pollutants. As a result, a set of guideline values was proposed for the following substances: toluene (1996), styrene (1998), dichloromethane (1997), pentachlorophenol (1997), carbon monoxide (1997) and nitrogen dioxide (1998) [63]. In the following, based on the various governmental initiatives, the WHO selected guidelines for indoor air quality regarding 9 pollutants in 2010: benzene, carbon monoxide, formaldehyde, naphthalene, nitrogen dioxide, polycyclic aromatic hydrocarbons, radon, trichloroethylene and tetrachloroethylene [64]. Indoor air quality guidelines are not legally binding and do not solve the sources of VOCs, nevertheless, they define and propose a reference framework for protecting the population from health effects related to air pollution exposure by inhalation. Guidelines contribute to the development of

recommendations and regulations that will ultimately reduce air pollution to a level compliant with public health.

International collaborations, such as French CSTB (*Centre Scientifique et Technique du Bâtiment*) and British BRE (Building Research Establishment) partnership through the Sustainable Building Alliance (SB Alliance), strengthened the development of guidelines and standard analytical procedures for indoor air quality evaluation in buildings. This approach led to significant advances, with the internationalization of the French national label "*NF Bâtiments Tertiaires – Démarche HQE®*" [65] as a legal certification for new buildings.

Regarding gas phase monitoring, regulations are gradually implemented. In France, decree n° 2011-1728 of December 2nd 2011 and decree n° 2012-14 of January 5th 2012, respectively aim at regulating indoor air quality in French public places dedicated to children (schools, kindergartens, day-care). These laws aim at making compulsory the monitoring of air quality in designated public places however, requirements are gradually planned from 2015 to 2023; they are not effective yet and may be postponed according to political decisions.

Regarding VOC emitted by commercial products, studies conducted in the last two decades have led to recent regulations to limit the emissions. For instance, in France and Germany, *ecolabels* and rating and classification systems such as *EMICODE*, *M1*, *Blue Angel* or *Indoor Air Comfort* are already applied and have impacted the marketplace, leading to the development of low-emission products.

In France, the law resulting from the *Grenelle-2* session requires the labelling of the emission class of any commercialized building material. The purpose of this requirement is twofold: (i) to favor the industrial development of low emission products, (ii) to favor the selection of low emission products by consumers. Commercialized materials since January 1st 2012 have to be labelled according to the « *arrêté du 19 avril 2011 relatif à l'étiquetage des produits de construction, de revêtement de mur et de sol, et des peintures et vernis* » [66]. This text defines a 10 VOC list; the emission class of a material (from A+ to C, Figure 4) is determined from the exposure concentration calculated from the emission rate of the 10 selected VOCs. The label refers to the lowest grade calculated among the 10 VOCs.

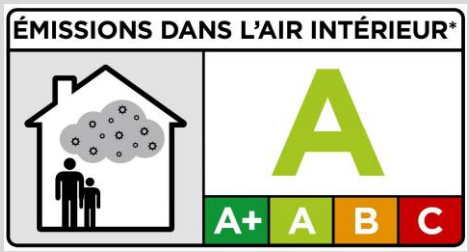

Figure 4 – Example of label related to material emission class according to French decree [66]

Energy, buildings & indoor air quality / Based on the *Grenelle de l'Environnement*, a general program was initiated in France; regarding buildings, it aims at reducing energy consumption by 38 % in existing buildings and at promoting innovative and smart solutions in the conception of new buildings. This program is directly subsequent to the French regulation on building thermal insulation, known as *RT-2012* [67][68]. These texts focus on three main actions: (i) building energetic efficiency, (ii) building energy consumption, and (iii) comfort in non-air-conditioned buildings. Since the very first French regulation on building thermal insulation in 1974 [69], the energy consumption of new buildings was divided by 2, thus evidencing the effectiveness of such regulations. The *Grenelle* law aims at dividing the current consumption by 3 in order to be lower than 50 $kWh_{ep}/(m^2.an)$, in accordance with the "low energy demand building" label. Similarly, other labels such as HPE (*Haute Performance Energétique*) or BBC (*Bâtiment Basse Consommation*) have been defined in order to be used as guidelines in the conception or upgrading of buildings. By 2020, requirements to satisfy these labels will be strengthened.

Two main watchwords are underlying the building energy regulations so far: (i) insulation and (ii) air tightness. As a result, considerable efforts are achieved to develop insulating solutions and decrease the natural and direct mechanical extraction of air from the building. The *RT-2012* typically recommends air renewal rates ca. 15 $m^3\ pers^{-1}\ h^{-1}$. However, during the last two years various organisms involved in indoor air quality monitoring such as ICEB (*Institut pour la Conception Ecoresponsable du Bâti*) [70][71] pointed out some mismatches between the recommendation of *RT-2012* and the expectation of OQAI as regards of indoor air quality. As a result, either air renewal rate expectations have to be increased, or indoor air has to be treated and recycled.

Current issues in indoor air quality / The situation of indoor air quality is presently the meeting point of two main contradictions:

(i) the impact of indoor air pollution on health is evidenced, nevertheless the legal monitoring of indoor air pollutants is not effective or highly limited and not uniform from one country to another,

(ii) indoor air quality is considerably degraded by inner sources of pollutants, however modern buildings are more and more insulated thus improving the pollutant confinement effect.

These aspects reveal the urgent situation regarding indoor air quality. Research could bring significant steps forward concerning both aspects.

Regarding indoor air quality monitoring and the assessment of people's exposure, the development of more responsive, easy to handle and low cost techniques, such as electronic sensor arrays, may make more operational the legal monitoring of indoor air pollutants. Besides, built surfaces in indoor environment do not only act as sources or sinks of pollutants, they may be considered as reactive platform and be involved in the conversion of pollutants. The deeper investigation of homogeneous and heterogeneous reactivity of indoor air pollutants could improve the understanding of indoor air pollutant fates and the development of more effective indoor air models. This approach may result in a more accurate forecast of indoor air toxicity or innocuity. These research axes are currently investigated by different laboratories through research projects [72].

Regarding the antagonist demand between energetic confinement and indoor air renewal to allow the extraction of pollutants, two trends have to be promoted: (i) the decrease of inner pollutant sources, (ii) the treatment and recycling of indoor air. As aforementioned, actions in the field of low emission materials are already effective and the conception of energetically efficient buildings with the lowest emission levels is more and more widespread and promoted in France thanks to the labelling regulation. However, this approach may not be sufficient and air treatment systems are more and more frequently implemented indoor to reduce the level of air pollutants. In the following section an overview of the existing air treatment techniques is presented to define the current issues in that domain.

Irrespectively of the approach ("monitoring and modeling" or "source reduction and treatment"), there is a need for experimental data determination in controlled environment. The development of both research axes requires significant experimental development regarding real scale experimental chambers, technically compliant with indoor air issues. This aspect is developed as short and mid-term perspective of my research activities in Part F.

Non-conventional indoor air issues / The challenge of indoor air quality commonly refers to health and comfort issues experienced by people in traditional or classical building or dwellings. However, the same problematic can be pointed out in many other places such as cars, trains, aircraft cabins, underground stations, etc… All these spaces have to face the same challenge related to inner sources of pollutants, air renewal, pollutant reactive conversion, air treatment to diminish people's exposure.

Few of these places have already been investigated in terms of pollutant diversity and sources. M. Verriele et al [73] proposed an original and accurate inventory of VOCs and odors in the interior of a motor vehicle. Compared to classical building indoor air, non-conventional indoor air places have to face specific problematic, for instance, (i) the massive presence of highly emitting synthetic material combined with potentially high temperatures in car vehicles, (ii) the high people density in aircraft cabins associated with the close vicinity of reactor engines. These fields of indoor air quality will have to be investigated as well in the coming years.

B-2 AIR TREATMENT TECHNOLOGIES

In the very specific context of indoor air, the main technological concern is to remove diluted, but diverse pollutants, typically at ppb levels, at a low energy cost. This context immediately excludes any technology based on the heating of indoor air effluent like in conventional thermal catalysis or saturated sorbents regeneration, for energy consumption reasons. Nowadays the most wide spread market technologies are based on adsorption or photocatalysis [74]. However, this section aims at giving a short overview of the existing air treatment technologies and at highlighting their relevance or not as regards of indoor air treatment.

Trapping methods / These methods merely rely on the transfer of the pollutants from one phase to another, solid or liquid. They do not induce any conversion of the trapped pollutants.

Condensation is based on the equilibrium between the liquid and vapor phase of an air-pollutant mixture; the vapor pressure of a solvent at equilibrium decreases as the temperature decreases. When the partial vapor pressure becomes greater than the vapor pressure, condensation takes place. Given the exothermic nature of this process, the system requires important cooling systems and is only economically applicable for very high pollutant concentrations [75], which is very far from any indoor air consideration [76].

Absorption consists in transferring the pollutants from the gas phase to a liquid phase. The latter can either consist of water or can be a reactive medium such as an acidic, basic or oxidative solution. This process is principally implemented for odor treatment downstream industrial processes and is very seldom used for VOCs [75][77].

Adsorption consists in transferring the pollutants from the gas phase onto a solid surface by passing the air flow into a packed bed reactor (PBR). The packing material is usually a porous substrate such as activated carbon or zeolites. Once the surface is saturated, the material is either replaced or regenerated. The latter usually consists in desorbing the pollutants using a heat transfer fluid or by direct heating of the material, after which the pollutant is sometimes collected, generally evolved or rarely destroyed. This method is mainly energetically efficient; it can also be used as a post treatment technique [78]. However, the main drawback of this method is the frequent maintenance due to the change of packed bed. Moreover, for economic reasons, filters or sorbent are often stored or incinerated, which is far from any sustainable development consideration. Nevertheless, adsorption is compliant with indoor air specificity.

Destructive methods / The objective of these methods is to degrade pollutants. Some of them may be characterized by VOC oxidation advancements leading to CO_2 and H_2O formation. They can be divided into three categories of treatment: biological treatment, thermal oxidation treatment and non-thermal oxidation treatment.

Biological treatment systems rely on the activity, development and metabolism of microorganisms to degrade contaminants from polluted air streams. It is widely used for odor treatment. In the case of VOC treatment, biofilters are used. The gas to be treated flows through a bio-chemical fixed bed reactor. More specifically, biofilms are formed on the surface by microorganisms and react with pollutants upon adsorption. Frequently used biofilter media are compost, peat, root wood, wood chips and their combinations [79]. This process requires humidity regulation between 40 and 60 % as well as a low pressure drop. Given the slow kinetics of biological processes, residence times are usually high (20 seconds to 2 minutes) and the flow rates typically ranges from 100 to 500 m^3/h, making the dimensions of the reactor usually important for industrial applications as regards of the air flow requirements [80]. Traditionally, biofilters were used to treat off-gases from sewage treatment plants, composting facilities and rendering plants, which mainly contain biological intermediate degradation products [79]. In recent years, further applications have been opened to this technology including food and tobacco producing and processing industries. As well as the treatment of waste gases containing industrial solvents and other volatile organic compounds.

In spite of the previously mentioned limitations which make this method poorly suitable to VOC abatement in the context of indoor air treatment, current projects are under development to adapt biological treatment to indoor. Such an approach raises the question of bio-aerosol release in treated air.

Non-catalytic thermal oxidation treatment relies on the gas heating at elevated temperatures, usually above 800°C, with a pollutant residence times ranging from 0.2 to 2 seconds. In the case of VOC treatment, CO_2 and water are ideally targeted. This method is poorly adapted to compounds containing heteroatoms such as sulfur, nitrogen or halogens (Cl, I, Br, F) as they respectively thermally decompose into SO_2, NOx or halogenated compounds such as Cl_2 or HCl. All these side products are subject to strict regulations [78] and require subsequent post-treatment. Furthermore, a minimum concentration of $1g/m^3$ or 1000 ppmv is generally required for the system to work in an auto-thermal regime [81]. The very dilute VOC concentration in indoor air renders this approach very costly and poorly environmentally friendly as most of the energy would be used to useless heating of air.

Catalytic thermal oxidation treatment operates in the presence of a catalyst to lower the activation energy of VOC oxidation and therefore to lower typical operating temperature (200-500°C), resulting in a considerably reduced energy demand [81]. However, the costs for the catalyst itself have to be taken into account. Drawbacks of thermal gas treatment, catalytic or not, for indoor VOC abatement, remain the high operating costs due to the low concentration of pollutants and the formation of secondary emissions like nitrous and sulfur oxides.

Non-thermal oxidation treatments, occasionally known as “cold” oxidation techniques, have gained a lot of attention for the treatment of VOCs in the past recent years for low energy demand reasons.

Photolysis consists in subjecting a gas or liquid to intense UV radiation to directly dissociate compounds absorbing UV wavelength. The extent of reaction is highly dependent on the type and concentration of (i) the organic pollutant, (ii) the radiation wavelength, and (iii) in the case of continuous processes, on the presence of additional oxidants such as O_3, H_2O_2 and HO°. This method is well adapted to water and wastewater treatment. However, in the case of gas treatment, high performance UV sources have to be used to obtain significant efficiencies making this method very costly and not well adapted to gas phase VOC abatement [81]. Main drawbacks of photolysis are (i) the general incomplete mineralization and the production of harmful intermediates [82], and (ii) the limited number of VOC sensitive to photolysis.

Photocatalysis operates in the presence of a catalytic materials activated by UV light. Irradiation of the photocatalyst with UV generates free radicals (through electron-hole pairs) able to undergo secondary reactions to oxidize pollutants adsorbed onto the photocatalyst [83]. This method is increasingly popular and suitable for a broad range of inorganic and organic pollutants. In the literature, the investigation of photocatalytic oxidation of VOCs for air treatment purposes is huge. However, the question of secondary pollutant generation is more and more raised and several studies have clearly evidenced that VOC photocatalytic oxidation may lead to secondary emission of oxygenated side-products and especially formaldehyde [15][17]. In front of the booming development of photocatalytic air treatment units on the market, regulations have been defined and are still under improvement in France; they stress specific expectation regarding formaldehyde release on autonomous systems [84][85], or integrated to air treatment units [86]. The proposed standards aim at framing this crucial drawback and regulate the market of photocatalytic devices. These standards are discussed in the following.

Non-thermal plasma (NTP) consists in generating activated molecules by applying an electrical discharge to a gas, most frequently air [87]. The applied electrical energy is used to produce and accelerate electrons which in turn generate highly reactive species [88].The most significant advantage of non-thermal plasma generated in ambient air is the production of highly reactive oxidizing radicals such as O° and HO°, and also O_3. Such species are produced at room temperature and at a low energy cost compared to any other method. These species later react with hazardous compounds to form non-hazardous or less hazardous substances [89]. The main advantage of this method is the low energetic cost compared to previously mentioned techniques, photocatalysis and photolysis. However, this method is seldom used yet as a self-consisting technology because of constraints such as (i) poor VOC mineralization, (ii) by-product formation like CO or (iii) generation of ozone [90].

A more effective use of NTP emerged along the last twenty years, through its combination with heterogeneous catalysts, so-called *plasma-assisted catalysis*. Indeed, from the 90s to 2000, air treatment techniques have mainly been individually investigated and developed. Adsorption, non-thermal plasma and photocatalysis were separately studied by distinct research teams. In the early 2000s, individual processes have been coupled. Synergetic effects between non-thermal plasma and materials have been rapidly evidenced;, thus research efforts have been focused on the understanding of the physics and chemistry involved in the coupling processes.

Plasma assisted catalysis consists in first approach in coupling non-thermal plasma with a catalytic material to overcome some of the main problems encountered with NTP alone and to diminish energetic consumption of thermal catalysis. Firstly, the material with sorption properties acts as a pre-concentrator regarding the gas phase species, thus increasing the interaction probability between the active species generated by the plasma and the pollutant. Positive effect on pollutant removal is generally attributed to the increase of pollutant residence time inside the discharge zone. Rapidly, the nature of the catalyst has been shown as key parameter to improve the selectivity of the process by (i) favoring CO_2 formation [91][92], (ii) minimizing by-product formation [91][93] and (iii) dissociating ozone at the reactor output [94][95][96]. Further, depending on the position of the catalyst with respect to the discharge, an increase in reactive species production can be achieved due to the formation of active species in the pore volume [97][98]. Due to these effects, coupling NTP to catalyst greatly improves energy efficiencies of VOC conversion [99][100][101][102] making this approach highly appealing for air treatment.

Wrap up /

Among the various air treatment technologies available, few of them are actually and effectively compliant with indoor air characteristics at reasonable cost and low environmental impact; namely adsorption, photocatalysis and non-thermal plasma. They all show advantages and drawbacks which means that the choice of an air treatment technique has to be adapted to the environment and the pollution to be treated. Side-product formation is recurrently designated as the dark side of destructive methods and this aspect tends to be overcome by coupling different methods to achieve better mineralization rates as well as conversion rates. Plasma-material coupling and more precisely plasma-catalyst coupling has already been investigated, and evidenced good performances. Before 2010, the understanding of plasma-catalyst coupling was merely empirical and systematic studies led to the selection of some interesting catalysts to be associated to plasma.

Heterogeneous systems / As further discussed in Part-D, the key point of plasma-catalyst coupling relies in the introduction of sorption phenomena in the discharge zone; sorption singularities may concern pollutants as well as oxidizing species. Indeed, the presence of a material, solely sorbent or even catalytic, inside the discharge zone, introduces a heterogeneous contribution in the homogeneous plasma system. More generally, the three air treatment techniques compliant with indoor air share the common characteristic of being heterogeneous processes. This aspect has to be investigated deeper, from a fundamental point of view as well as from a process point of view, in order to understand, optimize and efficiently couple adsorption, photocatalysis and plasma-material. This conclusion underlies my experimental development and my research activities presented in the following.

Since adsorption is the meeting point of all these three air treatment techniques, it is introduced and described in Part-C in order to structure the main fundamental and experimental outlines of my research activities. Then, obtained results related to plasma based heterogeneous oxidation of VOCs are detailed in Part-D. Then, achievements in the domain of photocatalysis for indoor air treatment are reported in Part-E.

Part C - ADSORPTION: FUNDAMENTALS & EXPERIMENTAL DEVELOPMENTS

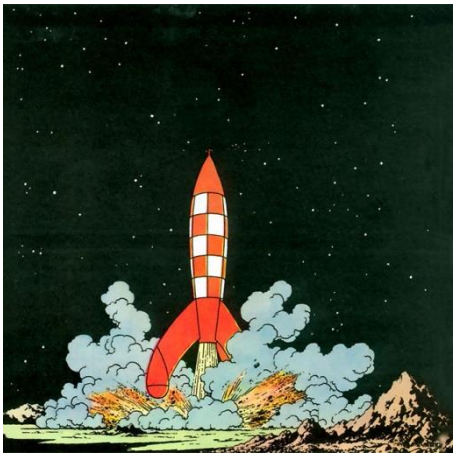

The purpose of this section is to propose a formal overview of the main fundamentals on adsorption. It aims at being introductive and general, as would be a lecture on that topic; however it is regularly illustrated with mentions to the distinctive behavior of TiO_2 regarding VOCs since it is one of the system of interest for most of this manuscript.

This theoretical section aims at drawing the main outlines of the fundamentals which governed the experimental development I achieved in order to address my different research axes : in Part-D (plasma-material) and Part-E (photocatalysis). Interestingly such heterogeneous experimental developments are non-conventionally transposed to natural dust sorption properties assessment as further exposed in Part-F.

C-1 INTRODUCTION TO ADSORPTION

The experimental investigations of adsorption mainly originate from two distinct research fields: surface science and catalysis. The experimental protocols and the objectives may considerably differ between these two domains. Studies related to surface science are generally focused on adsorption modes such as the various interaction of a VOC onto TiO_2 surface, irrespectively of its potential use as (photo)catalyst, and generally remain qualitative. Experiments are frequently carried out under high vacuum and consider well defined crystallographic orientations of the investigated solid surface [103]. In the perspective of air treatment heterogeneous process investigations, such experimental protocols seem to be disconnected from typical atmospheric conditions, i.e. atmospheric pressure, ambient temperature and in the presence of moisture.

In the domain of catalysis and photocatalysis, a significant part of the reported studies are dedicated to the investigation of liquid or gaseous species on TiO_2 surface. Some results are obtained in the complete absence of catalyst activation, subsequently without any catalytic reactivity. On the contrary, some others are extracted from the analysis of the catalytic reaction kinetic. However, these studies consider adsorption phenomena as one step of the global catalytic process and poorly quantitatively address the various adsorption modes and their respective evolutions throughout the catalytic process [104]. However, it is important to address these aspects of the heterogeneous reaction to determine whether reactants compete or not on the catalytic surface. Moreover, it has shown that the catalytic reaction can only be modeled considering different adsorption modes for the reactants [105]. The most widespread model used to describe adsorption phenomena is Langmuir model.

C-2 LANGMUIR MODEL

The Langmuir model proposes a description of the interaction between gas phase molecules with solid surface [106]. It relies on 4 main restrictive hypotheses which may, to some extent, induce a gap between the proposed model and the reality of adsorption:

Adsorption occurs on a single type of site.

Adsorption energy does not depend on the amount of adsorbed molecule.

Adsorption is a physical or chemical interaction without any modification of the molecule.

Adsorption occurs through a single layer of molecules on the surface.

The model proposed by Langmuir is based on kinetic considerations. Indeed, adsorption equilibrium corresponds to the situation when adsorption rate is equivalent to desorption rate. The adsorption rate is related to collision number of the gaseous molecules on the solid surface, subsequently, it is proportional to partial pressure. The proportion factor k_A ($mol.s^{-1}.Pa^{-1}$) comprises the collision effectiveness between gas phase molecules and the solid surface. Since adsorption only occurs on the non-covered fraction of the surface, adsorption rate is proportional to the unoccupied fraction of the surface. In order to define and represent this fraction, the coverage rate θ is defined as the fraction of the surface covered by adsorbed molecules. The unoccupied fraction is $(1 - \theta)$. The adsorption rate can be described as a function of the partial pressure P (Pa) as reported in Equation 1.

$$r_{ads} = k_A . P(1 - \vartheta) \qquad \textbf{Equation 1}$$

Desorption rate is related to thermal agitation of the interacting molecules. Thus, it is proportional to the adsorbed amount. This amount can be expressed by the coverage of the surface θ. In that case, the proportional coefficient is k_D ($mol.s^{-1}$), and the desorption rate can be expressed as reported in Equation 2.

$$r_{des} = k_D . \vartheta \qquad \textbf{Equation 2}$$

The global adsorption rate is defined as the difference between r_{ads} et r_{des}. The kinetic equation of adsorption can be rewritten converting the partial pressure into the gas concentration C (ppm) and the surface coverage into adsorbed quantity q (mol). The adsorbed amount can be normalized by the quantity of sorbent (g) and/or the specific surface of the sorbent ($m^2.g^{-1}$). As a result, q is respectively expressed in mol g^{-1} and mol m^{-2}, and Equation 3 is obtained. Kinetic adsorption constants k_A' (ppm^{-1} s^{-1}) and k_D' (s^{-1}) are the correspondingly

modified k_A and k_D. The constant q_m (mol) is introduced and represent the maximum adsorbed amount at highest coverage (θ = 1).

$$\frac{dq}{dt} = k'_A.C(q_m - q) - k'_D.q \qquad \textbf{Equation 3}$$

When the adsorption equilibrium is reached, the adsorbed amount does not vary since adsorption and desorption rates are equal. Thus, the adsorbed amount can be expressed as a function of the concentration of gas phase species. The obtained equation is reported in Equation 4.

$$q = q_m \frac{K.C}{1 + K.C} \qquad \textbf{Equation 4}$$

The mentioned constant *K* (ppm^{-1}) is the so-called "*adsorption constant*" of the considered gas onto the considered solid; it is expressed as the reverse of the concentration unit. This constant depicts the affinity between the molecule and the surface. It can be related to the enthalpy of the adsorption-desorption process *ΔH* ($kJ.mol^{-1}$) and to the temperature *T* (K) as reported in Equation 5.

$$K = K'.e^{\frac{-\Delta H}{R.T}} \qquad \textbf{Equation 5}$$

The pre-exponential factor *K'* is dependent on the temperature as well. This dependence is depicted by Equation 6 and coms from statistic physics as described by Chafik et al [107]. In Equation 6, *h* is the Plancke constant, *m* (kg) the mass of the molecule and k_B ($J.K^{-1}$) the Boltzmann constant. Based on the international system, *K'* is expressed in Pa^{-1}.

$$K' = h^3(2\pi.m)^{\frac{-3}{2}}(k_B.T)^{\frac{-5}{2}} \qquad \textbf{Equation 6}$$

The maximum adsorbed amount q_m is the asymptotic quantity proposed by this model at high concentrations. It is related (i) to the density of adsorption sites of the considered surface for the considered molecule and to the surface covered by a single molecule [108].

In the case of the existence of several adsorption site for the same molecule on a given surface, adsorbed amounts on each type of site can be described by Equation 4 with different values for q_m et *K*. Then, the total adsorbed amount is expressed by Equation 7.

$$q = \sum_i q_{mi} \frac{K_i.C}{1 + K_i.C} \qquad \textbf{Equation 7}$$

In order to match with reality and integrate phenomena which were not initially comprised by the basic form of the Langmuir model, this model has been modified, especially the variation of *ΔH*, which is frequently considered since such phenomenon is regularly observed.

In the continuity of the adsorption of a molecule onto a solid surface, the surface could be abruptly exposed to pure non-sorptive carrier gas, thus dropping the gas phase molecule concentration of the investigated gas to zero. In that case, it is experimentally observed that a fraction of the adsorbed molecules desorbs; this amount of desorbed molecules is called "reversibly adsorbed fraction". The amount that remains adsorbed on the surface is called "irreversibly adsorbed fraction". This behavior is not described by the model proposed by Langmuir, it correspond to a non-equilibrium desorption [109].

C-3 COMPETITIVE ADSORPTION

As emphasized in part-B, the reality of indoor air consist in a inconstant multi-pollutant and multi-VOC mixture, subsequently, all these gas phase species may interact with solid surface used in air treatment process. This aspect may be integrated as a Langmuir model evolution. The case of different gas phase pollutant interaction with the same kind of adsorption site leads to competitive adsorption. The subsequent determination of the

non-occupied fraction of the solid shall take into account the site occupation by any VOC interacting with the considered type of site. Thus, Equation 4 is modified as reported in Equation 8 which describes the adsorbed quantity of one gas phase species among others interacting with the solid as a function of the adsorption constants and concentration of other gaseous species. Equation 8 evidences the fact that, under competitive adsorption, each VOC is adsorbed in a lower amount than in the case of its single adsorption.

$$q = q_m \frac{K.C}{1 + \sum_i K_i.C_i}$$ **Equation 8**

The main limitation of the Langmuir model relies in the hypothesis of mono-layer adsorption, which considerably bounds its application to low concentrations and coverages. In order to overcome this drawback, other models can be employed such as BET model.

C-4 MODEL OF BRUNAUER-EMMETT-TELLER (BET)

The model proposed by Brunauer, Emmett and Teller [110] is an extension of the Langmuir model. In the BET model, authors have considered that molecules may not only directly interact with the uncovered solid surface, but also with preliminary adsorbed molecules. As a result, the surface may be simultaneously partly uncovered and partly covered by various layers of molecules. The adsorption of molecules on uncovered solid surface as well as preliminary covered areas can individually be described by the Langmuir model. Based on these considerations, the variation of the adsorbed molecule quantity with their gas phase pressure is reported in Equation 9. In that Equation, q_m corresponds to the amount of molecule required to reach a mono-layer coverage on the solid surface and c_{BET} is a constant of the model which relates the affinity of molecule for uncovered surface compared to covered surface.

$$q = q_m \frac{c_{BET} \frac{P}{P_{sat}}}{\left(1 - \frac{P}{P_{sat}}\right)\left(1 + \frac{P}{P_{sat}}(c_{BET} - 1)\right)}$$ **Equation 9**

C-5 INFLUENCE OF HUMIDITY

Another key parameter regarding the heterogeneous behavior of gas phase molecules on solid surface is relative humidity. Indeed, even if water vapor is rarely considered as a major pollutant in indoor air, excluding exceptionally high levels of moisture; it is massively present in the gas phase and may compete with other species when interacting with a solid surface. Typical indoor levels of relative humidity range from 40 to 70%, corresponding to concentrations ranging from 10 000 to 30 000 ppm for usual indoor temperatures. Compared with typical indoor air levels for VOCs around 100 ppb, the impact of moisture on VOC heterogeneous interaction is far from being negligible. Apart from theoretical considerations on adsorption processes, any experimental study dedicated to indoor air treatment has to take into account the influence of relative humidity on the process performances.

There are different ways of considering the impact of water vapor on pollutant adsorption on solid surface. In a first approach, the variation of the pollutant adsorption enthalpy ΔH with relative humidity can be explored [111]. However, water molecules can simply be considered as another gas phase molecule interaction with the solid surface, competing with gas phase pollutants. In the context of Langmuir model, Equation 8 can be used to model the influence of water vapor. Then, it can be rewritten as reported in Equation 10. In that Equation, K (ppm^{-1}) and K_W (ppm^{-1} ou $\%_{RH}^{-1}$) respectively correspond to adsorption constants of typical pollutant and water, and C (ppm) and C_W (ppm ou $\%_{RH}$) respectively correspond to pollutant and water gas phase concentrations. This approach is widely used to model the influence of water vapor on VOC adsorption onto sorbents.

$$q = q_m \frac{K.C}{1 + K.C + K_W.C_W}$$ **Equation 10**

Equation 10 can be rewritten as a pseudo Langmuir equation as in Equation 11; then, K_H et q_{mH} are the corresponding pseudo parameters.

$$q = q_{mH} \frac{K_H . C}{1 + K_H . C}$$ **Equation 11**

Calculations evidence that q_{mH} is equivalent to q_m, meaning that competition with water poorly affects the total adsorbed amount of pollutant, however, values obtained for K_H, as obtained from Equation 12 are lowered by the presence of moisture. These theoretical tendencies have to be confronted to experimental results.

$$K_H = \frac{K}{1 + K_W . C_W}$$ **Equation 12**

The impact of moisture does not only affect adsorption competition. Indeed, the presence of moisture levels typical of indoor air may considerable influence the chemical surface state of the solid. These aspects have been addressed in details by Henderson [112]. In the case of metal oxides which are widely used solid for heterogeneous oxidation processes, in the absence of moisture, the solid surface is weakly hydroxylated. When exposed to typical indoor air levels of moisture, the hydroxylation rate of the surface is considerably increased because of frequently observed water dissociative adsorption. This phenomenon is well reported on TiO_2 [113]; regarding that metal oxide, a complete surface hydroxylation is reported for RH values higher than 30% at ambient temperature. Noticeably, the presence of such species on the surface may significantly affect the sorption properties of gas phase molecules [108].

C-6 EXPERIMENTAL PROTOCOLE FOR HETEROGENEOUS PHENOMENA INVESTIGATION

Introduction / Various experimental protocols can be used to address adsorption. Most of these methods only exploit data obtained under adsorption equilibrium since adsorption kinetic may be influenced by several physical phenomena, such as diffusion or local temperature fluctuations, which poorly affect the equilibrium state. This section aims at presenting experimental approach developed throughout my research activities to explore adsorption phenomena involved in photocatalysis and non-thermal plasma regeneration of sorbents along my research activities. Subsequently it mainly refers to the investigation of the "VOC - metal oxide" systems; however, analogous procedures have been applied to investigate NOx, O_3, CO and CO_2 interactions with solid surfaces.

Main experimental achievements have been developed in the context of the PhD theses of Loganathan Sivachandiran [2] and Frédéric Batault [3], they are gathered and summarized in the following.

Equilibrium partitioning in closed system / This basic experimental method, known as EPICS [111], consists in introducing VOC vapors in a tightly closed vessel containing the investigated solid used as sorbent [114]. The purpose of this setup is to determine the amount of VOC adsorbed per gram of sorbent q_e (mol.g^{-1}) for various VOC concentrations in the gas phase C_e (ppm) using a mass balance. The adsorbed amount n_e (mol) is the difference between the total amount of VOC adsorbed in the vessel and the remaining amount once adsorption equilibrium is reached. The initially introduced amount n_0 is known and depends on the VOC generation technique. This amount could be expressed as a concentration in the vessel prior to any adsorption; however, this concentration has a questionable meaning since adsorption simultaneously occurs with the VOC mixing in the vessel. The amount n_g is determined by gas phase analysis of the VOC concentration in the vessel atmosphere once equilibrium is reached: C_e. Considering the volume of the vessel, n_g is determined. The amount of VOC adsorbed per mass unit or per specific surface unit of the sorbent sample can be obtained. The introduction of various initial concentrations makes possible the determination of (C_e, q_e) couples leading to the adsorption isotherm of the corresponding VOC on the sorbent. Moreover, the static mode used for this method questions the problematic of diffusion inside the material. This experimentally simple method can be advantageously complemented by the dynamic breakthrough method.

Breakthrough method and breakthrough curve / The breakthrough method is an experimental technique that enables the quantitative investigation of adsorbed species at equilibrium for a given concentration. It consists in exposing the investigated material used as a sorbent to a defined concentration step of VOC and to follow the evolution of the VOC concentration at the breakthrough reactor outlet. A permanent equilibrium is achieved in the breakthrough reactor along the experiment. Initially, the desorption rate is low since low

amounts of VOCs are adsorbed (Equation 2). Meanwhile, the adsorption rate is high since the surface offers numerous unoccupied adsorption sites (Equation 1). The VOC feeding rate at the reactor outlet has generally to be lower than the global adsorption rate. In that case, all introduced molecules are adsorbed and the VOC outlet concentration is null. Along the adsorption process, the VOC adsorbed amount increases which induces a gradual decrease of the adsorption rate and a gradual increase of the desorption rate. The global adsorption rate tends to decrease. When adsorption and desorption rates are equal, the adsorption equilibrium is reached and the global adsorption rate is null. Then, the VOC concentration at the reactor outlet is equal to the inlet concentration.

If the progression of the flow through the reactor did not induce any distortion of the concentration front, the global adsorption rate could be determined at any time through a mass balance calculation. However, the reactor and the sorbent necessarily induce delay and distortion of the concentration front between the inlet and the outlet of the reactor. This temporal contribution is known as the reactor "mixing curve". The temporal profile of the VOC at the reactor outlet results in the convolution of the reactor mixing curve with the ideal VOC breakthrough curve. The determination of the reactor mixing curve is an advance experimental requirement to any breakthrough curve interpretation. Integrating the delay between the reactor mixing curve and the breakthrough curves enables the quantitative determination of the total adsorbed amount.

Ambient temperature desorption / This experimental step consists in flushing the breakthrough reactor, once the breakthrough is achieved, i.e. the equilibrium is reached, with pure non-sorptive carrier gas. Under these conditions a definite fraction of the formerly adsorbed species may desorb; it is released at the reactor downstream and induces a transient concentration burst at the reactor downstream. This phenomenon leads to a delay in the concentration profile decay. Similarly to breakthrough curve interpretation, the integration of the delay between the monitored temporal profile of VOCs along flushing and the reactor flushing mixing curve enables the quantitative determination of the reversibly adsorbed amount. The difference between the calculated totally adsorbed and reversibly adsorbed amounts leads to the quantitative determination of the irreversibly adsorbed amount remaining on the sorbent surface.

Adsorption isotherms / The plotting of reversibly or irreversibly adsorbed amounts as a function of the inlet gas phase species concentration for a given temperature is the adsorption isotherm. These curves are required to calculate parameters used in the Langmuir model. One of the interests of the breakthrough method compared to EPICS is the quantitative distinction between reversible and irreversible fractions and the determination of their respective adsorption isotherms. This approach is highly informative regarding the global interaction of the gas phase species with the solid surface. The determination of Langmuir model parameter is achieved through experimental data fitting.

Langmuir parameter determination / First, adsorption isotherm fitting can be achieved by considering the linear relationship between the reverse of gas phase concentration and the reverse of adsorbed amount.

$$\frac{1}{q} = \frac{1}{q_m} + \frac{1}{q_m . K}\frac{1}{C}$$ **Equation 13**

A linear regression based on experimental data gives a numerical determination of parameters with their uncertainties. However, linear fitting data treatment emphasizes the weight of data at the lowest concentrations and weakens high concentration points. In the case of highly dispersed data the fitting quality is rapidly lowered as exposed on Figure 5. In order to improve the fitting quality and the subsequent accuracy of q_m (µmol.m^{-2}) and K (ppm^{-1}), a new data processing has been proposed by F. Batault [3] in his PhD thesis It aims at minimizing least-squares on direct experimental data and not their reverse values. It has been named "*direct fitting*" method. The improvement provided by this approach is illustrated on Figure 5.

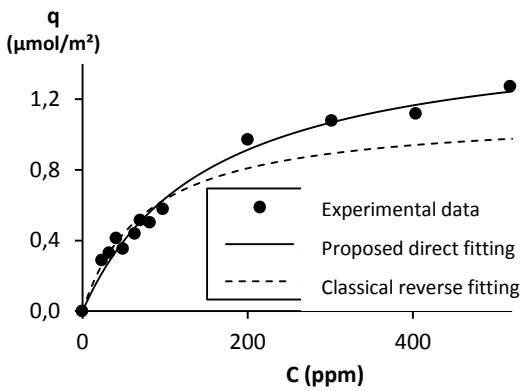

Figure 5 – Comparison of reverse fitting and direct fitting for Langmuir parameter determination from adsorption isotherm.

Temperature programmed desorption (TPD) / This step of the protocol consists in heating the sorbent-sorbate system in order to induce desorption of formerly adsorbed species. It is classically adapted from Redhead [115]. The heating ramp is adapted and regulated in order to distinguish the different desorbed species along the temperature increase. This step is performed after ambient temperature in order to avoid the massive desorption of weakly bonded species which may shade desorption of irreversible adsorbed modes. The carrier gas flowing across the reactor drifts the desorbed species which are monitored at the reactor outlet. Temperature of the inner part of the reactor is recorded to correlate desorbed species with temperature. This step is typically performed under nitrogen in order to minimize oxidation of sorbates on the solid surface prior to desorption. However, in the case of metal oxide, thermal activation of the solid may lead to oxidation reaction induced by lattice oxygen atoms even under inert gas.

Qualitative interpretation of TPDs / First, TPDs are qualitatively interpreted. The number of desorption peaks and their position is highly informative regarding the diversity of adsorption modes comprised into the irreversibly adsorbed fraction. In the case of reactive adsorption and/or reactive desorption the released species along the TPD differ from the inlet compound. These results, combined with literature data address the nature of the adsorption modes.

Quantitative interpretation of TPDs / Second, TPDs can be quantitatively interpreted to calculate adsorption enthalpies corresponding to the identified adsorption modes, as well as the variation of enthalpies with surface coverage. To that end, the temporal evolution of the quantity adsorbed along the TPD is determined through mass balance calculation: q_{calc}. This calculation considers that desorption remains close to equilibrium all along the temperature increase. This assumption has been evaluated in the PhD thesis of Frédéric Batault [3] using the criteria proposed by Kanervo et al. [116]. It has been used to attest the validity of the adsorption experimental setups developed and used. It has been shown that the desorption temporal profile obtained by TPD is effective for adsorption-desorption equilibrium enthalpy determination ΔH (kJ.mol^{-1}). Authors propose to determine the simulated adsorbed quantity which corresponds, in the case of two desorption peaks A and B, to the sum of the adsorbed quantities at equilibrium and the non-desorbed amount as peaks are processed (Equation 14).

$$\mathrm{q_{sim}} = \mathrm{q_{mA}}\frac{\mathrm{K_A.C}}{1+\mathrm{K_A.C}} + \mathrm{q_{mB}}\frac{\mathrm{K_B.C}}{1+\mathrm{K_B.C}} + \mathrm{q_{restant}} \qquad \textbf{Equation 14}$$

The gas phase concentration, C (ppm) is the downstream monitored concentration. The adsorbed amounts q_{mA}, q_{mB} and $q_{restant}$ (µmol.m^{-2}) are parameters. K_A et K_B (ppm^{-1}) are determined from measured temperature T enthalpies of each mode (Equation 15). To characterize a possible dependence of ΔH with surface coverage, enthalpies are calculated as linear functions of the coverage θ. The surface coverage is determined from adsorbed amount q_{calc} obtained from TPD. The respective amounts of peaks A and B are calculated as reported in Equation 17 and Equation 18. The simulated amount depends on concentration, measured temperature as well as q_{calc}. Parameters are q_{mA}, q_{mB}, $q_{restant}$, $\Delta H_{A,\theta=0}$, $\Delta H_{A,\theta=1}$, $\Delta H_{B,\theta=0}$, $\Delta H_{B,\theta=1}$. They are tuned to overlay $q_{sim}(t)$ and $q_{calc}(t)$.

$$K_i = K'.e^{\frac{-\Delta H_i}{RT}} \quad i = A,B \qquad \textbf{Equation 15}$$

$$\Delta H_i = \Delta H_{i,\vartheta=0} + \vartheta_i.(\Delta H_{i,\vartheta=1} - \Delta H_{i,\vartheta=0}) \qquad \textbf{Equation 16}$$

$$\vartheta_A = \frac{q_{calc} - q_{mB} - q_{restant}}{q_{mA}} \qquad \textbf{Equation 17}$$

$$\vartheta_B = \frac{q_{calc} - q_{restant}}{q_{mB}} \qquad \textbf{Equation 18}$$

Multiple breakthrough procedure / For experimental effectiveness purposes, the "*multiple breakthrough*" has been implemented to our adsorption experimental procedure; it has efficiently been developed and validated in the PhD thesis of Frédéric Batault [3]. In order to obtain several "adsorbed quantity" vs. "concentration" data couples within only a single experiment, "*multiple breakthrough*" curves have been carried out. To

perform a multiple breakthrough, the inlet flow VOC concentration describes several increasing steps. The time between each concentration increment is kept long enough to reach the equilibrium. The equilibrium is known to be reached when the outlet concentration remains constant and corresponds to the input concentration. Multiple breakthroughs have been performed with various first step concentrations to make sure that the data obtained from a first step and from the other steps are comparable. This approach makes possible a complete adsorption isotherm determination within a single breakthrough experiment; it has been efficiently employed and published by my research group in the following papers: Batault et al [24], Thevenet et al [27].

Graphical summary of sorption experiments / An overview of a complete adsorption experimental sequence is reported on Figure 6, it the experimental illustration of the abovementioned theoretical steps.

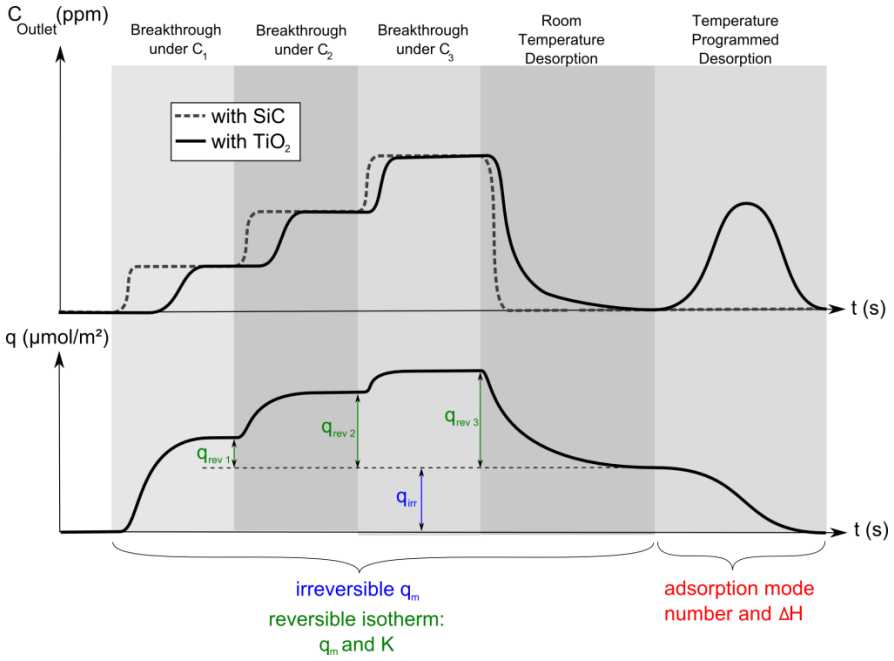

Figure 6 - Theoretical plots of (i) Breakthrough curve, (ii) Room Temperature Desorption (RTD) and (iii) Temperature Programmed Desorption (TPD), showing the reactor outlet VOC concentration, the calculated adsorbed quantity and the obtained quantitative and qualitative data along the different experimental steps, adapted from [3] and [24].

C-7 DEVELOPED EXPERIMENTAL SETUPS FOR ADSORPTION INVESTIGATION

Introduction / Two main setups have been developed along my research activities at Ecole des Mines to address adsorption and more generally heterogeneous phenomena from an experimental point of view. The first setup is dedicated to the complete determination of gas phase species sorption parameters onto a defined solid surface; it allows the complete experimental sequence exposed in Figure 6. It has been dedicated to the determination of VOC sorption parameters on TiO_2 surface for photocatalytic indoor air treatment (Part D), and to the investigation of TiO_2 surface ageing in the presence of NO_2 and the corresponding impact on VOC adsorption (Part E). The second experimental setup is dedicated to adsorption characterization along with the investigation of the plasma-sorbent regeneration process. Subsequently, the process setup consists in a dual sorption and non-thermal plasma reactor.

A third experimental setup related to adsorption is currently under development and validation. It will be dedicated to the investigation of mineral dusts sorption properties. Briefly, it consists in the coupling of DRIFTS cell, for *in-situ* monitoring of the mineral dust surface coverage and sorption modes by VOCs, with SIFT mass spectrometer for simultaneous quantitative sorption parameter determination.

Fundamental experimental setup / Fundamental experiments on adsorption are carried out in a fix-bed flow reactor. This quartz-made reactor includes a bulb and U-shaped tubing. The tubing inner and outer diameters are respectively 4 and 6 mm. The bulb inner diameter is 15 mm and its length is 30 mm. The sorbent bed is placed in the bulb bottom. The typical sorbent mass used for experiments ranges from 20 to 120 mg, depending on the sorption abilities of the sorbents and sorbates. A quartz wool plug is used to maintain the sorbent bed in the reactor. The reactor and the sorbent bed are depicted in Figure 7.

The reactor can be by-passed using two three-way valves. During thermal pretreatment and thermal desorptions, the reactor is heated with a tubular furnace with a heating rate of 10 to 40 K/min, up to 673K. The sorbent temperature is continuously monitored using a K-type thermocouple located inside the reactor. Its tip is located in the center of the sorbent bed. The gas stream relative humidity is monitored with a *Testo* probe (± 1 % accuracy), to make sure the sorbent is subjected to the targeted relative humidity condition.

SIFT mass spectrometry / In order to address the fast temporal dynamics of gas phase species concentrations at the reactor outlet, Selected Ion Flow-Tube (SIFT) mass spectrometry (*Syft* Voice 200) is used. SIFT mass spectrometry is based on analytes chemical ionization. This technology generates three precursor ions: H_3O^+, NO^+ and O_2^+. Precursor ions are sequentially selected by a first quadrupole. Then, they react with analytes in a flow tube to produce ionized molecules, which are separated by a second quadrupole and counted. This device enables the calculation of analyte theoretical concentrations using: the kinetic of ionization reactions in the flow tube, the ionized molecule and remaining precursor quantities, and the residence time inside the flow tube. This calculation is based on theoretical data, and can be affected by the operating conditions. For more reliable concentration measurements, this mass spectrometer is regularly experimentally calibrated, using dilution bench and VOC certified cylinders. Typical detection limits of VOCs with SIFT-MS range from 10 to 50 ppb.

FTIR spectroscopy / The detection and quantification of the species of interest can be completed by Fourier Transform Infrared (FTIR) spectrometer *Antaris IGS*, especially in the case of NOx and COx which are not monitored by SIFT-MS. A heated 10 m optical-path cell coupled with a liquid nitrogen cooled MCT (Mercury Cadmium Telluride) detector is used. FTIR spectra are collected using Result-3 software with a spectral resolution of 0.5 cm^{-1}. Detection limits are determined as three times the signal-to-noise ratio in the spectral regions of interest. Typical detection limits for CO and CO_2 with FTIR are lower than 100 pbb, in the case of VOCs they range from 100 ppb to 1000 ppb.

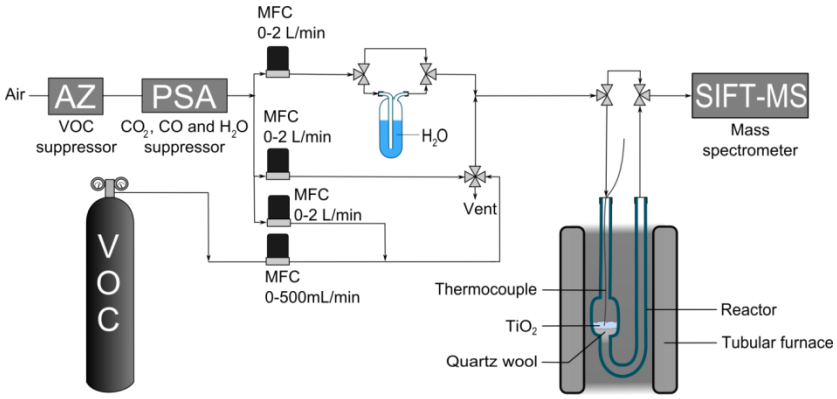

Figure 7 - General scheme of the fundamental experimental setup dedicated to adsorption, adapted from [3] and [24].

MFC : Mass Flow Controllers.
AZ : Zero Air generator.
PSA : Pressure Swing Adsorption air purifier.
VOC : Volatile Organic Compound.
SIFT-MS : Selected Ion Flow Tube Mass Sectrometer.

Process experimental setup / Experiments dedicated to process purposes, especially in the case of plasma-sorbent coupling have been achieved using the setup depicted on Figure 8. This setup enables the investigation of breakthrough curves and the quantitative determination of reversibly and irreversibly adsorbed fractions. However, the size and the structure of the sorbent bed does not match with the expectations proposed by Kanervo et al [116], thus temperature programmed desorption are not as reliable as they would be using the fundamental setup. Nevertheless, the process setup is highly already informative and is closer from process operational considerations.

The process experimental setup for adsorption is used as a continuous flow reactor. A Pyrex glass tube characterized by 17 mm of outer diameter, 14.6 mm of inner diameter and 1.2 mm of wall thickness was used as a reactor. Considering that in the context of the investigated process the reactor has to be compliant with in situ non-thermal plasma regeneration, it is been designed as a plasma reactor too. Copper wires are inserted in a capillary glass tube having wall thickness of 2 mm. It is used as main electrode and fixed in the middle of the larger Pyrex tube which leads to a 5.3 mm discharge gap. Thus, the obtained configuration is a double dielectric barrier discharge. The process experimental setup for adsorption is a classical packed bed reactor. The discharge gap is filled in with glass beads; the diameter of the beads is 2 mm. VOC, NOx or COx diluted in air or

nitrogen are sent through the packed bed with tuneable concentrations from 100 ppb to 1000 ppm. Similarly, the nature of the sorbent deposited on packed bed glass beads can be varied. Typically, TiO_2, MnO_2 [16][18][19][21], Al_2O_3 and activated carbon sorption properties have been investigated using this process experimental setup.

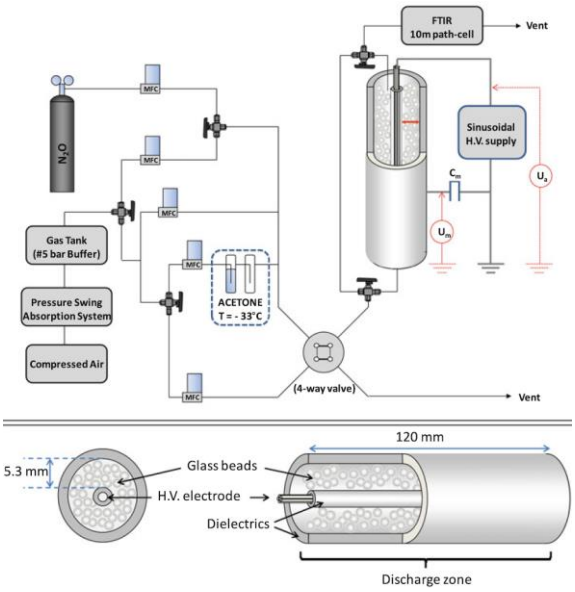

Figure 8 - General scheme of the process experimental setup dedicated to adsorption characterization and subsequent plasma regeneration of the sorbent. The present scheme, adapted from Sivachandiran et al [19], is devoted to acetone adsorption on TiO_2 and plasma regeneration. The nature of the adsorbed species can be varied, and the sorbent coated on glass beads as well.

The quantification of gas phase species is performed downstream the reactor generally by Fourier Transform Infrared Spectroscopy (FTIR, Thermo Scientific). The spectrometer is equipped with a liquid nitrogen cooled MCT (mercury cadmium telluride) detector and a 10 m length optical path cell. A resolution of 0.5 cm^{-1} is been used and 16 scans are selected as constant spectrum acquisition parameters for all experiments. Background spectra are taken under pure air at 0.5 cm^{-1} resolution with 500 scan.

Conclusion /

The role of heterogeneous phenomena and more especially the question of adsorption and its characterization have been highlighted during the PhD of Olivier Debono [1] dedicated to photocatalytic reaction investigation at ppb levels (Part-E). Experimental developments have subsequently been carried out in order to address these sorption phenomena in the context of plasma-material and photocatalysis investigations.

Corresponding experimental developments have been validated and used throughout (i) the PhD thesis of Frédéric Batault [3] regarding the fundamental experimental setup (Figure 7) and (ii) the PhD thesis of Sivachandiran Loganathan [2] regarding the process experimental setup (Figure 8). Developed experimental setups have been highly informative as regards of their respective PhD objectives in the domain of plasma-material interaction as well as photocatalysis for indoor air treatment. Developed protocols have been also used during the PhD of Christelle Barakat [4].

Distinctive performances of the developed setups and diagnostics are: (i) their ability to be operated with various pollutants from VOCs to COx and NOx and even in the presence of multi-pollutant atmosphere, (ii) the low detection limits of SIFT-MS and FTIR which can be efficiently completed by GC and HPLC measurements as presented further, (iii) the compliance of these experimental setup with various relative humidity levels in order to be as close as possible to effective environmental conditions.

Main results obtained from the process experimental setup related to the plasma-sorbent research axis are principally reported in Part-E. Main results obtained using the fundamental experimental setup related to the investigation of VOC sorption parameters on TiO_2 surface are presented and exploited in Part-F.

Part D - PLASMA BASED HETEROGENEOUS OXIDATION OF VOCs

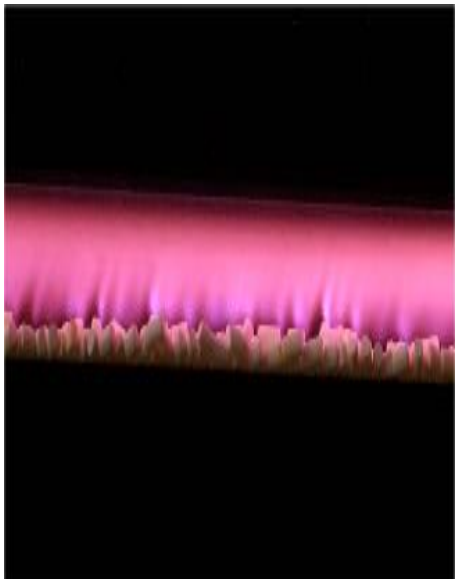

This section aims at giving an overview of my research activities in the domain of plasma-material coupling for VOC oxidation.

In a first part, I depict the scientific context of non-thermal plasma coupling with materials as I initiated that research activity at Ecole des Mines.

Then, I raise the different research axes I developed along the last 7 years: (i), comparison of continuous direct plasma treatment of VOCs with sequential plasma regeneration of VOC saturated sorbents, (ii) investigation of *in-situ* plasma regeneration of sorbent as regards of their interests and limitations and (iii) ageing of materials coupled to non-thermal plasma in order to give more insights on the process sustainability. Most of the results presented and discussed in this section have been obtained in the context of ANR RAMPE project and industrial collaboration relying on two PhD theses: Sivachandiran Loganathan and Christelle Barakat [2][4].

D-1 FROM NON-THERMAL PLASMA to PLASMA-MATERIAL and PLASMA-SORBENT COUPLING

Did you say plasma ? / In physics and chemistry, plasma is a state of matter similar to gas in which certain portions of the species are ionized. It is a combination of charged particles, positive ions and negative electrons. The term plasma was first introduced by Langmuir in 1928 because the multi-component and ionized gas he observed reminded him of blood plasma. Langmuir wrote: "*Except near the electrodes, where there are sheaths containing very few electrons, the ionized gas contains ions and electrons in about equal numbers so that the resultant space charge is very small. We shall use the name plasma to describe this region containing balanced charges of ions and electrons*" [117]. Plasmas naturally occur but can also be effectively man-made in laboratory and industry, which provides opportunities for numerous applications, including thermonuclear applications, electronics, lasers, fluorescent lamps, ozone production and many others.

Depending on the relative temperature of the species, we can distinguish three main types of plasmas: high temperature plasmas, thermal plasmas and non-thermal plasmas. The critical parameter between these different types of plasmas is electron, ion and gas characteristic temperatures, summarized in Table 24.

Table 24 - Classification of plasmas and related physical characteristics adapted from [118].

Plasma type	Temperatures	Example
High temperature plasma (equilibrium plasma)	$T_e \approx T_i \approx T_g = \ 10^6 - 10^8 K$	Laser fusion plasma
Thermal plasma (quasi-equilibrium plasma)	$T_e \approx T_i \approx T_g \leq 2 \times 10^4 K$	Arc plasma, plasma torches RF inductively coupled discharges
Non thermal plasma (non-equilibrium plasma)	$T_e \gg T_i \approx T_g = 300 \ldots \ 10^3 K$	Glow, corona, dielectric barrier discharges, plasma needle, etc

The different types of plasmas are also distinguished by the ratio of density of charged species to that of neutral gas, corresponding to plasma ionization degree. As ionization degree is close to 1, it is referred to completely ionized plasma, a typical property of high temperature or thermal plasmas. As ionization degree is low, the so called weakly ionized plasma allows the gas to remain at, or close to, room temperature and atmospheric pressure, making non-thermal plasmas more compliant with industrial constraints. The main advantage of non-thermal plasmas is their high chemical efficiency. As little or no heat is produced, nearly all input energy is converted to energetic electrons [119].

Non-thermal Plasmas / In electric discharges, energy from the electric field is first accumulated by the electrons. Due to their small mass, electrons are selectively accelerated under the influence of the electric field. Upon collisions with the neutral gas, they transfer a small portion of their energy to heavier particles. For this reason, the electron temperature in plasma is initially higher than that of heavy particles. Examples of low pressure and non-thermal plasmas are glow discharges, inductively (ICP) and capacitively (CCP) coupled plasmas, radiofrequency (RF) discharges, widely used in modern electronics. However, at atmospheric pressure, it is necessary to limit the ionization degree to maintain non-equilibrium conditions by imposing : (i) low discharge current, (ii) short discharge pulses, (iii) micro-discharges or (iv) dielectric barrier discharge.

Dielectric barrier discharges / Among these different technologies, DBDs gained a lot of attention because of their relative experimental simplicity. The flexibility of their geometrical configurations along with their operating medium and parameters makes easier the up scaling from laboratory to industry [120]. Dielectric barrier discharges were first introduced by Werner von Siemens in 1857 in a published paper on electrostatic induction [121]. He described a silent discharge apparatus dedicated to ozone synthesis from air or oxygen. Till 1930s the DBD, or silent discharge, was exclusively used for ozone production.

Dielectric barrier discharges are characterized by the presence of one or more insulating material, namely the dielectric barrier, in between the electrodes, separated by a gap of a few millimeters. If the gap between the two electrodes is packed with a material, it is referred to as a packed bed reactor, leading to surface discharges. The dielectric barrier most frequently consists in glass, quartz, ceramics, or polymers [122].The presence of the dielectric barrier avoids spark formation, its presence also impedes direct current transfer. The discharge is generated using an alternative current voltage. The applied electric field has to be high enough to cause breakdown in the considered gas volume. DBDs usually occur in a number of individual small ionized channels,

known as micro-discharges and observed as thin bright filaments. The micro-discharge physics is based on the initial avalanche-to-streamer transition leading to streamer formation.

NB: Considering that dielectric barrier discharges have been selected as non-thermal plasma technology for air treatment applications presented and discussed in this manuscript, it is generally referred to as "plasma", "non-thermal plasma" or "discharge".

Non-thermal plasma induced chemistry in air / The electric energy applied to the DBD is initially transferred to electrons in the form of kinetic energy (1-20 eV). Upon inelastic collisions with the bulk gas molecules, electrons transfer a portion of their energy in the form of chemical and physical processes leading to: (i) excited gas molecules losing their energy through photons emission or collisions, (ii) neutral species ionization of and subsequent formation of positively charged species, and (iii) molecule dissociations into neutral species or negative ions upon electron attachment or dissociative ionization reactions, as summarized on Figure 9.

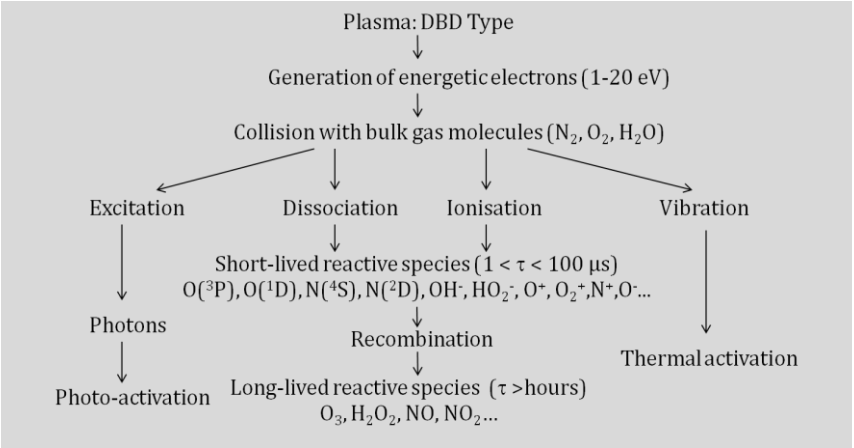

Figure 9 - Physical and chemical processes taking place upon non-thermal plasma generation on humid air, adapted from [123] and [4].

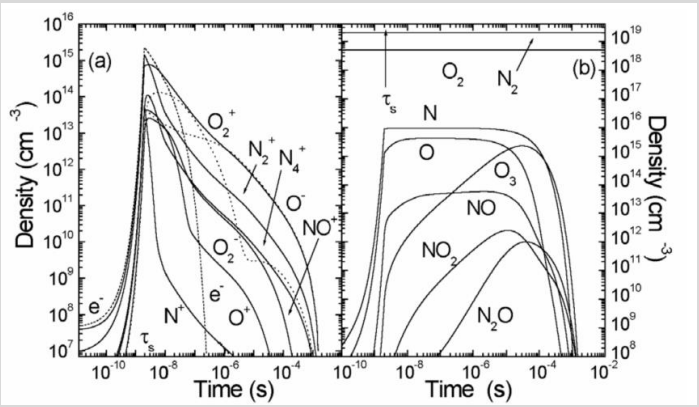

Figure 10 - Temporal evolution of the densities of charged and neutral species in streamer propagating in air, adapted from [124].

Remarkably, Barni et al. [124] depicted the temporal evolution of charged and neutral species in a streamer. After the brief phase of streamer formation, showing a roughly exponential growth of charged particles, electrons are quickly removed and a molecular ion plasma is left over, slowly fading due to recombination and diffusion within few microseconds. Neutral gas-phase evolves at a slower pace and ozone becomes dominant just before the streamer channel starts being dissipated by diffusion within a few milliseconds. Figure 10 emphasizes the distinction between short life time species, namely oxygen and nitrogen based ions, as regards to long life time species such as ozone. Interestingly, non-thermal plasmas ignited in air are powerful sources of oxidizing species.

Environmental applications / Non-thermal plasma environmental applications started at the beginning of the XXth century with the use of plasma generated ozone for water depollution. Later on, this type of treatment process is still successfully developed [125] for pesticides and antibiotics degradation. Regarding air treatment, research activities really started in the 1970s. The individual action of non-thermal plasma ignited in air is

mainly related to gas phase activation. A gas phase plasma discharge changes the chemistry of the bulk gas in several ways. As a consequence non-thermal plasma induces homogeneous reactions. Particularly, when ignited in air, it may degrade the contaminants into partially oxidized hydrocarbons, and convert NO to NO_2. Regarding NOx, some preliminary studies have been achieved in 1927 [126], but main results and applications were gained in the early 2000s [127][128][129]. Besides NOx, non-thermal plasmas were more and more applied to volatile organic (VOC) compound removal and oxidation along the last 20 years as further discussed.

Early works in the field of plasma-material coupling / From a chronological point of view, the coupling of non-thermal plasmas with catalytic materials results from more general studies dealing with the coupling of non-thermal plasma with various solids. Basically, physicists were interested in introducing solids characterized by high relative permittivity, like $BaTiO_3$, inside non-thermal plasma discharge zones, in order to improve the discharge characteristics. In that framework, Ogata et al [130] coupled non-thermal plasmas with $BaTiO_3$, $BaTiO_3/Al_2O_3$, and metal loaded Al_2O_3. These authors clearly evidenced that the chemical composition of the material not only improves the discharge electrical characteristics but also promotes the degradation of VOCs sent in the air stream compared to simple discharges. They evidenced that improvements regarding VOCs oxidation, especially mineralization, are not correlated to the modification of the discharge electrical parameters by the coupling material, but directly instigated by the surface reactivity of the inserted solid. In parallel, Oda et al [131] suggested that some catalytic surfaces like TiO_2/V_2O_5 may be activated by the discharge itself. After 2000, the synergetic effect between non-thermal plasma and catalytic surface was clearly evidenced and reported. As a result, research activities have been oriented toward the understanding of the physics and chemistry involved in the plasma-catalyst interaction.

Toward plasma-material coupling and understanding / Numerous papers have been published from 1998 to 2004 on plasma-catalyst coupling. They all pointed out the synergetic effects and tried to raise and validate various hypotheses to explain this positive interaction. Thus, first review articles on this topic were published beyond 2004 [132][133]. More recently two reviews on plasma-material coupling were published in 2014 in *Journal of Physics D: Applied Physics*: (i) Neyts and Bogaerts [134] aim at giving a comprehensive overview of plasma-catalyst coupling and emphasizes the positive contribution of modelling and simulation to the understanding of such a process; (ii) Thevenet et al [23] highlight the positive contribution of *in situ* adsorbed phase diagnostics to elucidate reaction pathways and the subsequent plasma-material interactions.

In the early 2000s, four main axes related to material characteristics were pointed out as potential explanations to the observed positive interaction between non-thermal plasma and materials for VOC abatement :

Catalytic activity ***Porosity*** ***Geometry*** ***Sorption properties***

Catalytic activity / Various catalysts have been coupled to NTP discharges e.g., Al_2O_3, γ-Al_2O_3, TiO_2 [135], MnO_2 [136], ZrO_2 and combination of metal oxides [137]. The activation of various catalytic surfaces, mainly metal loaded catalysts, have been confirmed by Hammer et al [138], Kirkpatrick et al [139] and Ayrault et al [140]. For instance, Ayraut et al. [140] have shown that platinum metallic particles have a room temperature catalytic activity under DBD exposure for 2-heptanone conversion by comparing the same support (honeycomb monolith) with and without metallic particles. This last paper perfectly illustrates the catalyst activation by plasma for 2-heptanone removal. The conversion of 2-heptanone is reported as function of reactor temperature for three different types of treatment. In the case of thermal catalytic treatment, no conversion is noticed below 200°C. However, the conversion gradually, and typically, increases till 80% at 450°C. Plasma treatment performed alone at room temperature leads to of conversion of around 45% of inlet VOC. Finally, the introduction of the same thermal catalyst in the plasma operated at room temperature enables a conversion of 70% with a very low energetic consumption. Interestingly the material may also change the chemistry of bulk gas. For instance, some catalysts such as MnO_2, can decompose plasma generated ozone to form oxygen and oxygen radicals [141]. These radicals can further react with adsorbed compounds in the vicinity of the reaction site responsible for the ozone decomposition.

Porosity / In 2002, Holzer et al [97] as well as Song et al [98] evidenced the positive effect of a porous material inserted in a discharge. Because of the diffusion of the species inside the porous structure of alumina and silica, authors pointed out the positive influence of porous materials on (i) active species lifetime increase and (ii) VOC residence time increase. As evidence by Roland et al [142], the porosity of the material can be used as a reactive platform to create new reactive species. Indeed, Authors evidenced the presence of long lifetime

surface bounded oxygen on Al_2O_3 in the form of either Al-O° or Al-O-O° by using Electron Paramagnetic Resonance (EPR) technique. Technically, the EPR technique revealed a change in the magnetic properties within the pores of the alumina after NTP treatment, and the presence of Al-O° or Al-O-O° was confirmed by a technique called electron spin echo envelope modulation (ESEEM). Furthermore, surprisingly, this Al-O° or Al-O-O° groups persists even if Al_2O_3 is exposed to a reducing gas like Ar, N_2 and He. Authors have evidenced that Al-O° or Al-O-O° must be formed by rearrangement of surface bound oxygen atoms in Al_2O_3 during IPC treatment.

Geometry / Various geometries of plasma-catalytic reactors have been tested [143][144][145][146][147]. The catalyst positioning in plasma-catalytic systems shows a significant influence on VOC removal. Two main configurations shall be distinguished: (i) if the catalyst is right inside the plasma discharge the configuration if typically called ***In*-Plasma Catalysis** (IPC), (ii) if the catalyst is placed downstream the plasma discharge it corresponds to the so-called ***Post*-Plasma Catalysis** (PPC). In the case of IPC, if materials are introduced into a non-thermal plasma reactor as pellets and completely fill the discharge gap, it would form the so-called and widespread packed-bed reactor (PBR) which is characterized by numerous contact points in between pellets and electrodes. From a physics point of view, the average electric field in a PBR will be enhanced compared to the empty reactor because of the short distance and the adjacency of contact points. When ignited in air, a higher electric field is expected to favor oxygen dissociation processes and formation of oxidative radicals, less energy being lost in nitrogen vibrational excitation. The presence of high permittivity pellets like TiO_2, $BaTiO_3$ or zeolites increases the local electric field and reduces the gas breakdown voltage [148][149][150].

Apart from the fact that IPC and PPC represent two different approaches in air treatment processes [151] their comparison is highly informative as regards of plasma-material coupling from a fundamental point of view. In order to discriminate surface reactions from gas phase reactions, Roland et al [152] have used a non-volatile organic compounds coated on various catalysts. They have evidenced the interaction of plasma discharge on catalyst surface by using two various experimental setups and different catalysts. In the first set of experiment, eicosane ($C_{20}H_{42}$) is adsorbed on catalysts such as γ-alumina, α-alumina, silica gel, and quartz. When eicosane coated catalyst is placed downstream to the plasma (PPC), it has been evidenced that there is no removal and/or conversion of eicosane on α-alumina, silica gel or quartz, whereas about 50% of the adsorbed eicosane is removed from γ-alumina. In the second set of experiment, eicosane adsorbed catalyst is placed inside the NTP discharge region (IPC), and a significant removal is observed for all cases including quartz. Furthermore, they have reported that, during PPC, in the cases of α-alumina, silica gel, and quartz, ozone is not able to oxidize the adsorbed hydrocarbon. The most energetic species, such as oxygen atom, are able to oxidize the eicosane as long as they have time to reach the surface of the catalyst. On the other hand, γ-alumina has shown a significant oxidation of eicosane during PPC, presumably owing to γ-alumina ability to decompose ozone and produce highly active oxygen atoms on the surface. These experiments evidence the role of short and long lifetime species produced by NTP. In the case of IPC all the species generated by the plasma may interact with the surface and the adsorbed compounds; this may lead to an enhancement of the oxidative processes, but may also lead to the storage of undesired poisoning species on the surface. During IPC, VOC can be activated and oxidized by the reactive species as well as by direct electronic impact. In the case of PPC, only long life time species reach the surface of the material; as a consequence the reactivity is related to the kinetic constant of the long life time species with the VOCs to be treated.

Sorption properties / Adsorption and desorption of pollutants from the material surface are key parameters in coupling. Indeed, the adsorption of VOCs on catalyst surface would change its retention time and even its concentration in the discharge zone. In addition, desorption of obtained products makes possible the renewal of pollutants on the surface. In order to take part from (i) high specific surface and (ii) potential surface reactivity, authors suggested favoring photocatalytic materials inside discharges, namely SnO, ZnO and TiO_2. In 2003, Ogata et al [153] confirmed the positive impact of high specific surface materials. Apart from pollutant adsorption and desorption, material sorption and stabilization properties can be used regarding oxidizing species. Indeed, O atoms adsorption on a catalytic surface under plasma exposure was assessed using isotopic exchange by Kim at al [154]. The surface of various catalysts was pretreated under a mixture of He and $^{18}O_2$. Then, benzene oxidation was monitored using mass spectrometry in the presence of $^{16}O_2$ in the gas phase. The presence of CO and CO_2 containing ^{18}O atoms was evidenced after 30 minutes of plasma treatment. These measurements show that under plasma exposure, reactive O-containing groups are produced onto the surface and stabilized on long time scales. These groups are adsorbed on surfaces and are available for further reactions.

Material modifications under plasma exposure / As evidenced using Raman spectroscopy and X-ray diffraction during my PhD [30], even under energetic non-thermal plasma operated during several days, the insertion of the material inside the discharge gap does not lead to any structural modification of TiO_2 bulk structure. Indeed, energetic species delivered by the discharge are from far insufficient to damage or modify the material bulk lattice. However, the surface chemistry and surface morphology of the coupling material can be considerably modified. Under NTP treatment, materials might be affected in two different ways:

❶ **The oxidation state** of metal oxides can be influenced when exposed to plasma discharge. This was evidenced by observing Mn_3O_4 after exposing Mn_2O_3 catalyst to NTP treatment [155]. This low-valent (Mn_3O_4) is known to have a large oxidation capability. Similarly, Wallis et al [156] reported that due to plasma-catalyst interactions, less Ti-O bonds are found on TiO_2 surfaces.

❷ **The morphology** of the material surface can be changed. It is widely reported that in NTP catalyst hybrid configurations new types of active sites with unusual but valuable catalytic properties may be formed [157]. Moreover, the formations of ultrafine particles with higher specific surface and less-perfect crystal lattice having a large number of vacancies have also been noticed. On the contrary, Wallis et al. [156] noticed that BET surface area can be reduced after plasma exposure. For instance, in the case of HZSM-5 zeolite catalyst a reduction of the surface area of 45% was measured while this was only about 6% for TiO_2 catalysts. Moreover, especially in the case of metal loaded catalysts, the discharge may enhance the dispersion of active catalytic components. It has been shown that NTP influences the stability and catalytic activity of the exposed catalyst materials [155].

Special insight into plasma-photocatalyst coupling / Among the catalysts used in DBD, photocatalysts have a very particular chemical activity. Photocatalysts are semi-conductors activated by photons which create electron-hole pairs, inducing oxidation or reduction reactions at the surface of the material with adsorbed molecules. TiO_2 is one of the most efficient photocatalysts for VOC treatment. The plasma-TiO_2 combination has been studied since 1999 and its benefit was initially shown on toluene [158][159], benzene [160-164] and a few other molecules [165-167]. It was reported that NTP coupled with TiO_2 photocatalytic reactor shows comparatively better conversion on acetylene decomposition and Guaitella et al [11] as well as Chung-Liang et al [168] found that TiO_2 packed bed reactor shows around 40% better reactivity than simple NTP reactors.

Role of UV / As reported in my PhD [30], the role of the UV that may be emitted by the plasma itself on the activation of TiO_2 has been studied. However, in typical experimental setups, UV and energetic particles produced by the plasma were not sufficient to activate TiO_2 nano-particles. Nevertheless, it can be pointed out that, with external UV lamps, a synergetic activation of the photocatalyst is possible. Indeed, photocatalytic reactions occur under plasma exposure and are more efficient in the plasma phase than in neutral gas phase. This effect was attributed to the positive interaction of plasma generated radicals and ozone on UV activated TiO_2 surface.

Role of O_3 / The use of ozone in photocatalytic process was described by Ohtani et al [169]. They have shown that photocatalysis aided by ozone is more efficient because O_3 can be decomposed on activated TiO_2. However, Guaitella et al [11] did not observe any improvement of 1000 ppm C_2H_2 destruction when the catalyst was located downstream the discharge and exposed to long life time reactive species such as ozone. Only a small increase of CO_2 production was measured when external UV lamps was switched on showing that O_3 was involved in photocatalytic oxidation of C_2H_2. It was concluded that short life time species from the plasma are then involved in C_2H_2 oxidation by photocatalytic processes.

My research Issues in plasma-material coupling /

The introduction of a material inside the discharge gap basically implements heterogeneous reactivity into the system. The presence of the material: (i) shortens the discharge gap, (ii) modifies the plasma characteristics and the discharge behavior. More especially, the material changes the VOCs decomposition mechanisms owing the VOC adsorption onto the material surface. Reactive species such as oxygen radicals and ozone, produced by plasma, can be transported to the material surface as well. These species may alter and/or take part to the chemical environment of the

material surface. Then, they may adsorb and/or react with the adsorbed molecules. As a consequence, coupling a material with a NTP will have mainly two effects: first, it modifies the energy transferred to the gas (lower breakdown voltage, change of the electron energy…); second, it promotes gas-surface transfers of plasma produced reactive species and pollutants. As I started my research activity in the domain of plasma-material coupling at Ecole des Mines, three main questions were raised:

➲ What is the impact of plasma on the material adsorbed phase chemistry ?
➲ What is the impact of material on plasma gas phase chemistry ?
➲ What is the effective role of the material ? Is it solely used as a sorbent, or as a catalyst ?

Beside catalytic properties of the coupling materials, the meeting point of the abovementioned questions are the sorption phenomena of pollutants and oxidizing species onto the coupling material. Classically, as I started my research activities on plasma-material coupling this process was inferred as a continuous process, meaning that the plasma was continuously ignited directly on the coupling material (IPC) on at the coupling material upstream (PPC).

I proposed to orientate research efforts on an innovative sequential coupling consisting in two distinctive and consecutive steps: first pollutants are adsorbed on the material used as a sorbent; second, plasma discharge is ignited on the saturated material. Two motivations underlined this concept: (i) the sequential approach makes possible the qualitative and quantitative investigation of the dynamic sorption and plasma oxidation phenomena which may give significant new fundamental insights in plasma-material coupling, (ii) the sequential approach represents an innovative air treatment process which may lead to energy savings and more optimized use of material sorption and catalytic properties. In the following of Part-D obtained results in that research axis are structured according to the following three main points.

❶ Continuous vs. sequential couplings / Most of published results in the domain of plasma-material describe continuous operating conditions; it means that: (i) a constant amount of pollutants flows through the plasma-/catalyst reactor and (ii) the non-thermal plasma discharge is permanently ignited. The main drawback of such process is that the plasma has to be continuously switched on, creating constant energy demand.

The alternative approach I proposed is (i) to adsorb pollutants, then (ii) to regenerate the saturated sorbent using NTP. This approach means that the discharge is sequentially ignited; indeed the ignition of the plasma would be related to the coverage of the material surface by pollutants since it is used as a sorbent. Besides eventual technological advantages, the sequential process makes the evaluation of the process performances more straightforward:

- the absolute quantity of adsorbed pollutant can be precisely known,
- mainly surface reactions have to be considered,
- carbon balance is accessible and can be completed by consecutive thermal desorption,
- *in-situ* surface analyses may be performed.

❷ Sorbents as relevant coupling materials / The sequential coupling requires high sorption properties of the coupling material to remove the targeted pollutants. Sorbents such as activated carbon (AC) are frequently used to adsorb gaseous VOCs. But they do not efficiently adsorb the lightest pollutants, i.e. characterized by the lowest molecular weights, such as formaldehyde [170][171]. Therefore, alternative sorbents such as alumina (Al_2O_3) [172], and synthetic zeolite [173] in granular form are also used. All of these materials are characterized by high specific surface. Regarding non-thermal plasma characteristics and considering former presented studies on plasma-catalyst interaction, the most relevant sorbents to be coupled to plasma should be able to effectively benefit from plasma generated oxidizing species. It is necessary to characterize sorption properties on the coupling material regarding VOCs and simultaneously to evaluate the ability of the coupling materials to benefit from plasma generated oxidizing species. To that end, we focused on metal oxides.

❸ **Metal oxides as coupling materials /** Metal oxides appear as the best candidates since they combine (i) good adsorption properties for VOCs, (ii) tuneable surface reactivity compliant with oxidation reactions and hydrophilicity, and (iii) resistance to long-term plasma exposure. Compared to zeolites they can be coated on structured substrates; compared to activated carbon they promote chemisorption of VOCs rather than physisorption and make possible the characterization of the process carbon mass balance. For these reasons, TiO_2, MnO_2, CeO_2 and their mixtures have to be considered. The chemisorption of carbonyls and carboxylic acid on TiO_2 as detailed by Batault et al [24] with acetaldehyde and acetic acid perfectly exemplify the sorptive and reactive properties of such metal oxide regarding VOCs from indoor air. Moreover, as shown by Barakat et al this material is able to benefit from short life-time as well as long life-time oxidizing species, thus inducing oxidation processes on its surface [22]. The positive interaction between plasma generated species and such p-type and n-type semi-conductors is highlighted by Oyama et al [174] through ozone heterogeneous reactivity on metal oxides. However, it is necessary to evaluate the sustainability of metal oxides when exposed to pollutants and plasma generated species. Poisoning phenomena have to be addressed in order to identify and overcome potential limitations of the process related to surface deactivation.

In the following of Part-D, different aspects of the plasma-sorbent coupling are addressed in order to highlight the current understanding, the performances, and the limitations of such an air treatment process. Presented results have mainly been obtained throughout the PhD theses of Loganathan Sivachandiran [2], Christelle Barakat [4] and Frédéric Batault [3] in the context of ANR Rampe project, Institut-Carnot PhotoCair project, as well as Al-Ko Therm collaboration. First, the interest of sequential plasma sorbent coupling from an energetic point of view is discussed. Second, the physical and chemical issues as well as process performances regarding model VOC treatment are presented. Third, ageing aspect of materials used as sorbent and coupled to plasma are assessed to evaluate the long term performances of the process. As above mentioned, metal oxides are the most compliant materials, MnO_2 (or more generally MnxOy) and TiO_2 have been selected as sorbents of interest for plasma coupling.

D-2 COMPARISON BETWEEN CONTINUOUS and SEQUENTIAL PROCESSES for INDOOR AIR TREATMENT

Introduction / The objective of section D-2 is to compare the performances of a continuous NTP treatment. It has been assessed using Mn_XO_Y packed bed reactor, with a sequential adsorption/non-thermal plasma regeneration process. Owing to the redox properties of MnO_2, it has been widely used as a catalyst in industrial processes. The multiple oxidation states of Mn atoms in a single mineral facilitate catalyzing oxidative processes [175]. It is also well known that, at room temperature, MnO_2 shows high ozone decomposition efficiency [176][177][178][179]. MnO_2 is widely used as a thermal catalyst, however, in the PhD theses of Loganathan Sivachandiran [2] and Christelle Barakat [4], it is used as a sorbent and catalytic surface inserted in the discharge zone of a DBD reactor. Regarding both approaches (continuous and sequential), the same (i) reactor, (ii) packing material (Mn_XO_Y) and (iii) model VOC have been used, but operated according to the two distinct configurations. The experimental setup used in this section refers to Figure 8. The efficiency of both processes has been evaluated in terms of (i) energy efficiency, (ii) primary VOC removal, (iii) side-product formation and (iv) mineralization aspects.

Analytical devices for ppb level measurements / Two analytical devices have been employed in this study. Considerable efforts have been made on the analytical technique reworking to characterize the species of interest at ppb level in order to be relevant with indoor problematic. As a result, both analytical instruments are able to quantify efficiently the species of interest at ppb levels.

FTIR spectroscopy / The Fourier transform infrared (FTIR) spectrometer used for these studies in presented in section C-7 p43. In order to illustrate our analytical achievements with this instrument, the detection limits of the species of interest are reported in Table 25.

SIFT mass spectrometry / The Selected Ion Flow Tube Mass Spectrometer used for these studies is presented in presented in section C-7 p43. In order to illustrate our analytical achievements with this instrument, the detection limits of the species of interest are reported in Table 25.

Table 25 - Detection limit of FTIR and SIFT-MS for species of interest in section D-2.

FTIR		SIFT - MS		
species	detection limit (ppb)	species	ion source	detection limit (ppb)
CO	76	formaldehyde	H_3O^+	25
CO_2	20	acetaldehyde	H_3O^+	20
IPA	1 400	IPA	NO^+	20
acetone	80	acetone	NO^+	25
N_2O	50			

Abatement of IPA by continuous process / In order to characterize the removal of IPA using continuous treatment close to indoor air concentration, 320 ± 20 ppb of IPA diluted in dry air are continuously sent through non-thermal plasma (NTP) discharge at 296 K. The obtained temporal profile of IPA concentration at the reactor downstream is reported in Figure 11. The discharge is ignited at t = 0 with a constant input power of 0.82 ± 0.02 W. Before t = 0, the 320 ppb IPA diluted in air are already sent into the reactor in order to reach the adsorption equilibrium in the system prior to any treatment. Indeed, if 320 ppb IPA were sent in the packed bed reactor simultaneously with the discharge ignition, IPA abatement monitored at the reactor downstream would not only be due to the plasma treatment, but also to the adsorption of IPA on Mn_xO_y. In that case, the intrinsic abatement performances of NTP would not be correctly evaluated. Thus, the discharge is ignited once IPA concentration at the reactor outlet has reached the input concentration. Thus, as can be seen on Figure 2, prior to t = 0, IPA concentration at the reactor outlet is 320 ± 20 ppb.

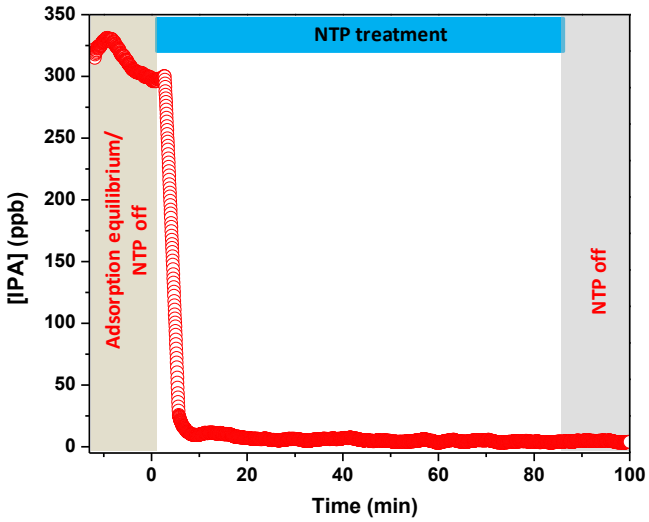

Figure 11 - Temporal profiles of IPA monitored at the reactor downstream using SIFT-MS. The continuous NTP treatment is performed from t = 0 to t = 85 minutes under dry condition with 0.82 W input power.

At t = 0, the NTP discharge is ignited for 85 minutes. In the following, we will distinguish two different phases of the plasma ON time: (i) the first one is the transient phase during which monitored gas phase species are not all stabilized yet, this transient phase lasts less than 30 min; (ii) the second phase is the steady state treatment (t > 30 min), all species concentrations are constant, which makes possible the evaluation of the pollutant conversion by the process operated in continuous mode.

As soon as NTP discharge is ignited, IPA concentration at the reactor downstream falls down. Beyond 15 minutes, the concentration of IPA tends to stabilize to a concentration lower than 10 ppb. Regarding IPA conversion by continuous NTP discharge, a span of 15 min, typically from 40 to 55 min, is considered to calculate IPA conversion and subsequent total carbon mass balance. IPA conversion is calculated on that time span using Equation 1, where, $[IPA]_{in,}$ and $[IPA]_{out}$ respectively represent the IPA inlet and outlet concentrations. 98% of IPA conversion is achieved as calculated on the defined steady state range. Beyond 15 minutes, IPA conversion is constant as long as the discharge is operated. Longer treatments, from 3 to 4 hours, have been performed leading to the same observations. From an IPA conversion point of view, continuous NTP Mn_xO_y packed bed treatment offers excellent performances.

$$\text{IPA conversion (\%)} = \left[\frac{[IPA]_{in} - [IPA]_{out}}{[IPA]_{in}} \right] X\ 100 \qquad \textbf{Equation 19}$$

Interestingly, beyond 85 minutes of treatment the discharge is switched off, however, in spite of the constant 320± 20 ppb IPA input, its concentration at the reactor downstream remains lower than 10 ppb. IPA is not converted by NTP anymore, but this behavior suggests that IPA adsorbs on the packed bed material. This hypothesis has been confirmed by complementary experiments showing that IPA concentration slowly increases along 12 hours, corresponding to a progressive breakthrough of the VOC on Mn_XO_Y once the discharge is turned off. This phenomenon indicates that adsorption sites are available on Mn_XO_Y, meaning that NTP prevents any deactivation of the coupling material during VOC treatment.

Gas phase reaction intermediates produced during IPA continuous treatment / During the continuous treatment of IPA, only three gas phase reaction intermediates have been identified and quantified: acetone, acetaldehyde and formaldehyde. Their behaviors are contrasted. Acetone is produced only at the beginning of the plasma treatment, whereas acetaldehyde and formaldehyde are monitored as long as the discharge is on.

As can be seen on Figure 12, during the first 10 minutes of non-thermal plasma treatment, a burst of acetone is noticed at the reactor downstream. Acetone maximum concentration reaches 2650 ppb. However, beyond 10 minutes of treatment, concentration remains lower than the SIFT-MS detection limits during the whole process (<25 ppb). Two hypotheses could explain the acetone massive transient production: (i) NTP ignition may lead to desorption of acetone produced during the equilibrium step; (ii) non-thermal plasma may shift the adsorption equilibrium of IPA on Mn_XO_Y surface toward desorption and convert desorbed IPA into acetone. Considering that the heat of adsorption of acetone is expected to be lower than the one of IPA [26], only traces of acetone could be present on the surface prior to t = 0, which means that the first hypothesis is not valid. As a consequence, it can be suggested that acetone transient production is related to a fast oxidation of adsorbed IPA to reach a new equilibrium state compliant with the plasma exposure of Mn_xO_y surface.

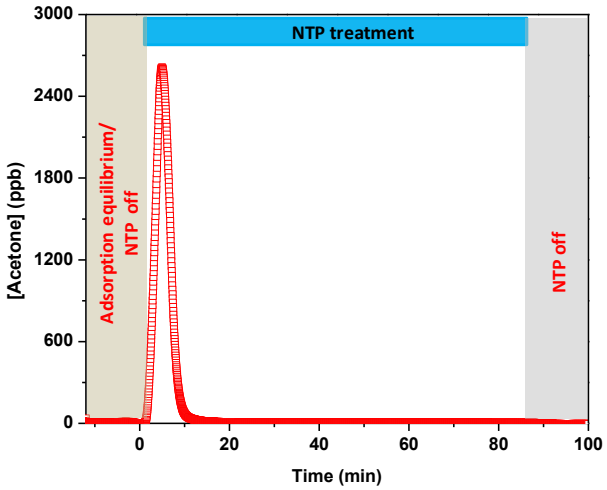

Figure 12 - Temporal profile of acetone monitored at the reactor downstream using SIFT-MS. The continuous NTP treatment is performed from t = 0 to t = 85 minutes under dry condition with 0.82 W input power.

Before NTP ignition, neither acetaldehyde nor formaldehyde is identified in the air stream. When the discharge is on, these species are produced after few minutes (Figure 13). Their concentrations increase and tend to stabilize between 30 and 45 ppb for acetaldehyde, and between 125 and 175 ppb for formaldehyde. As soon as NTP discharge is turned off, both species concentrations return to zero in a time span compliant with the reactor purging. The steady state production of acetaldehyde and formaldehyde is nevertheless characterized by significant fluctuations which could be correlated to the fluctuation (i) in the IPA inlet concentration and (ii) in the NTP input power. The temporal profiles of these two species reported in Figure 13 suggest that they mainly originate from the continuous conversion of IPA by the discharge in the packed bed reactor. As a consequence, similarly to IPA steady state conversion, steady state amounts of produced acetaldehyde and formaldehyde have been determined by averaging their respective concentrations on a 15 minutes time span from 40 to 55 min. Obtained values are integrated to the process carbon mass balance and discussed further. Compared to acetone, these two oxidation intermediates are characterized by low concentrations, but are produced all along the process.

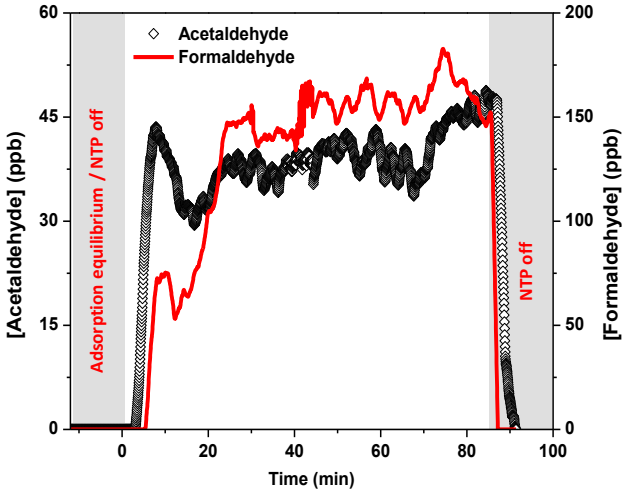

Figure 13 - Temporal profiles of acetaldehyde and formaldehyde monitored at the reactor downstream using SIFT-MS. The continuous NTP treatment is performed from t = 0 to t = 85 minutes under dry condition with 0.82 W input power.

Quantification of CO and CO_2 produced during IPA continuous treatment / Mineralization induced by oxidative processes is a key parameter which is poorly assessed in the domain of indoor air treatment since it requires very low detection limits regarding CO_2 and CO quantifications. This point has been addressed here. CO_2 and CO are both produced during the 320 ± 20 ppb IPA continuous NTP treatment. The temporal profiles of CO_2 and CO determined by FTIR are reported in Figure 14.

As NTP discharge is ignited, CO and CO_2 are produced. During the first 30 minutes of treatment, both concentration profiles are characterized by intense production peaks (Figure 14). The outlet concentrations of CO and CO_2 respectively reach 1.8 and 18.0 ppm. When the discharge is ignited, IPA adsorption equilibrium on Mn_xO_y may change. As discussed earlier, a fraction of desorbed IPA is converted into acetone and transiently released at the reactor downstream; another fraction is mineralized into CO and CO_2.

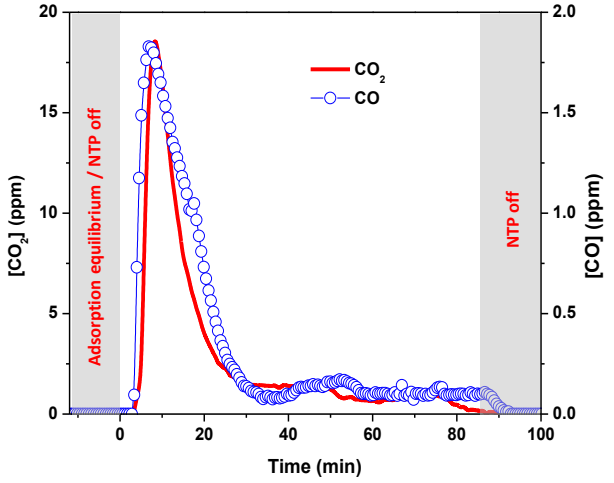

Figure 14 - Temporal profiles of CO and CO_2 monitored at the reactor downstream using FTIR. The continuous NTP treatment is performed from t = 0 to t = 85 minutes under dry condition with 0.82 W input power.

Beyond 30 minutes of continuous treatment, CO and CO_2 productions are almost constant as long as the discharge is operated. Therefore, it can be assumed that, after 40 min of NTP discharge, only IPA is converted into acetaldehyde, formaldehyde and mineralized into CO_2 and CO. Averaged concentrations of CO and CO_2 between 40 and 55 minutes are respectively 0.12 ppm and 1.0 ppm. These steady state values, corresponding to a continuous treatment regime, have been used to assess the process carbon mass balance.

Carbon mass balance of IPA continuous treatment / To account the process efficiency, the carbon mass balance recovered during the continuous NTP treatment of IPA has been determined. In order to evaluate the process performances in a steady state regime, only IPA conversion and CO, CO_2, acetaldehyde and formaldehyde steady state productions have been considered. Thus, quantitative data used for carbon mass balance calculation have been determined beyond 40 minutes of treatment. Results are reported on Figure 15.

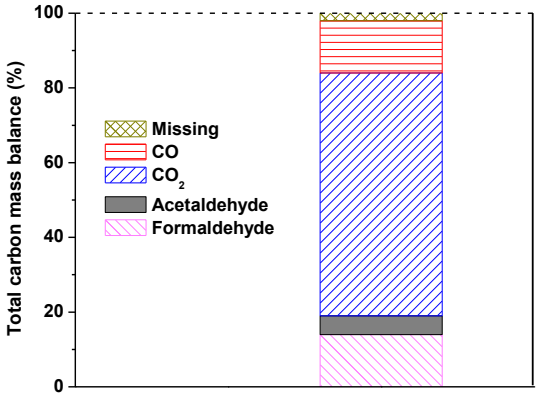

Figure 15 - Carbon mass balance recovered by continuous NTP treatment during the process steady state regime with a constant 0.82 W input power. At the reactor inlet, 320 ± 20 ppb of IPA, diluted in air, are continuously sent.

IPA treatment by sequential adsorption on Mn_XO_Y and NTP regeneration / After evaluating the performances of the *continuous process*, we are now considering the performances of the *sequential process*. Firstly, IPA is removed from the contaminated air by adsorbing on Mn_XO_Y surface till the breakthrough of IPA at the packed bed reactor outlet. Then, IPA reversibly adsorbed fraction is flushed under zero air. Secondly, *in-Situ* NTP treatment is applied to oxidize the irreversibly adsorbed IPA from Mn_XO_Y surface. NTP treatment is performed for 30 min under pure dry air and at 296 K. Finally, temperature programmed desorption (TPD) is carried out on NTP treated Mn_XO_Y surface to complete the total carbon mass balance and to evaluate the efficiency of *in-Situ* NTP treatment.

Adsorption of IPA on Mn_XO_Y surface / IPA adsorption on Mn_XO_Y is achieved by sending 165 ppm of IPA at the reactor inlet concurrently with N_2O which does not adsorb on Mn_XO_Y and can subsequently be used as a breakthrough tracer. The complete adsorption and ambient flushing sequence is presented on Figure 16. The delay between IPA breakthrough curve and N_2O mixing curve makes possible the quantification of the total amount of IPA adsorbed on the Mn_XO_Y packed bed. Under our experimental conditions 4.3 ± 0.05 µmol m^{-2} of IPA are adsorbed on Mn_XO_Y surface. As shown in Figure 16 concurrently with IPA breakthrough, acetone is monitored at the reactor outlet. The production of acetone is transient and clearly related to IPA adsorption. Acetone is not produced anymore once IPA breakthrough is over. The total amount of acetone released in the gas phase is 0.34 ± 0.05 µmol m^{-2}, corresponding to less than 8% of consumed IPA. Acetone originates from the conversion of a fraction of the total consumed IPA, which attests of minor reactive adsorption of IPA on Mn_XO_Y.

The delay between IPA flushing curve and the corresponding N_2O profile can be integrated to determine the reversibly adsorbed fraction of IPA, which corresponds to weakly adsorbed IPA molecules. Under our experimental conditions 1.0 ± 0.05 µmol m^{-2} of IPA are reversibly adsorbed on Mn_XO_Y surface. Considering the IPA reversibly adsorbed fraction and the acetone produced, the irreversibly adsorbed fraction of IPA is determined as 3.0 ± 0.05 µmol m^{-2}. This fraction corresponds to strongly bonded IPA molecules on Mn_XO_Y surface. The fact that the flushing step is operated under pure zero air shifts the adsorption equilibrium toward a surface state corresponding to a saturation obtained with very low IPA concentrations in the gas phase. Subsequently, the obtained Mn_xO_y surface covered by irreversibly adsorbed IPA is exposed to non-thermal plasma *in-situ* regeneration.

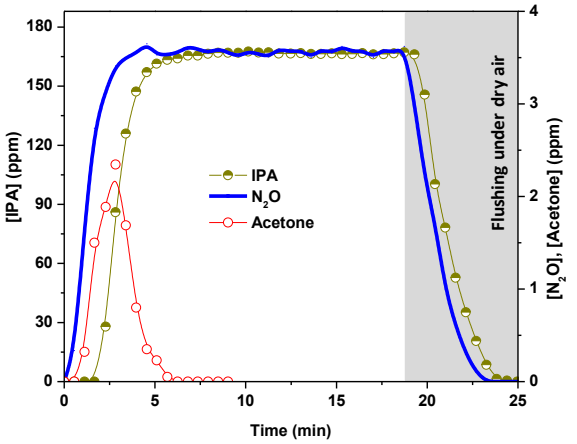

Figure 16 - Breakthrough and flushing temporal profiles of 165 ppm IPA and 3.7 ppm N_2O, used as a tracer, on Mn_xO_y coated reactor at 296 K. During adsorption, IPA and N_2O are diluted in dry air, flushing is achieved under pure dry air.

Non-thermal plasma regeneration of IPA adsorbed Mn_XO_Y surface / The non-thermal plasma regeneration of irreversibly adsorbed IPA on Mn_XO_Y surface is performed under dry air during 30 minutes. This NTP treatment time span has been defined according to the species temporal profile presented and discussed further. The organic reaction intermediates have been identified at the reactor downstream by SIFT-MS, simultaneously with CO and CO_2 by FTIR.

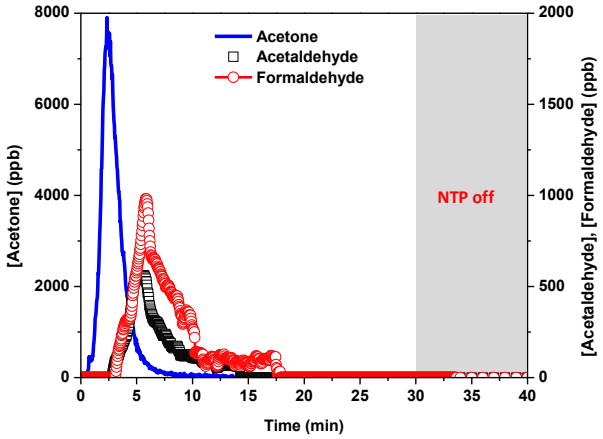

Figure 17 - Organic gas phase species monitored at the reactor downstream using SIFT-MS during the 30 minutes NTP regeneration performed on IPA saturated MnXOY surface. NTP discharge is carried out under dry air with 0.82 W input power.

As shown on Figure 17, acetone, acetaldehyde and formaldehyde are the only three organic intermediate species monitored at the reactor downstream. IPA has not been detected, indicating that very low amounts of IPA desorb from Mn_XO_Y surface. The nature of the organic species is the same than for continuous treatment of gas phase IPA, suggesting similar oxidation pathways. Acetone is produced as soon as the discharge is ignited on saturated Mn_XO_Y surface. The transient production of acetone is short in time and intense; acetone maximum concentration is reached within 2.5 minutes but returns to zero after 8 minutes of NTP treatment. Unlikely, formaldehyde and acetaldehyde are monitored at the reactor downstream beyond 3 minutes of treatment, once the largest fraction of acetone has been released. Their transient productions reach maximum values between 6 and 7 minutes and return to zero beyond 15 minutes of treatment.

Acetone is the first reaction intermediate produced during IPA decomposition either by thermal or catalytic methods [21]. During the first three minutes of treatment, Mn_XO_Y surface coverage by IPA is close to 1. Assuming that the heat of adsorption of acetone on Mn_XO_Y is lower than the one of IPA, similarly to TiO_2 [180] and as proposed by Sivachandiran et al [21], most of acetone produced in the first minutes of NTP is released in the gas phase and IPA oxidation advancement does not go further than acetone. However, after few minutes of treatment, the surface coverage becomes lower than 1, which makes some adsorption sites available. As a consequence, a fraction of produced acetone molecules may remain in the adsorbed phase and get further oxidized under NTP action. This could explain the delayed formation of acetaldehyde and formaldehyde after 3 minutes of treatment. Beyond 7 minutes of treatment, the surface coverage is low enough to make possible the adsorption of all acetone molecules produced which can be converted into further oxidized products.

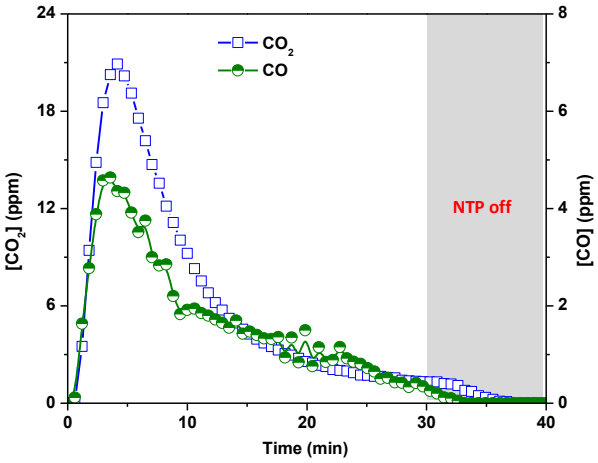

Figure 18 - CO and CO_2 monitored at the reactor downstream using FTIR during the 30 minutes NTP regeneration performed on IPA saturated Mn_xO_y surface. NTP discharge is carried out under dry air with 0.82 W input power.

CO and CO_2 are produced as soon as the discharge is ignited; their respective temporal profiles are reported on Figure 18. This behavior suggests that either adsorbed IPA and acetone or released in the gas phase can be

directly mineralized. They are homothetic, but the level of CO_2 exceeds by a factor 5 to 6 the level of CO all along the 30 minutes regeneration step. CO and CO_2 are still monitored after 17 minutes of treatment, i.e. on a time span without any organic intermediate production in the gas phase. This means that organic reaction intermediates from the adsorbed phase are oxidized under the NTP action and released in the gas phase once mineralized. This mechanism is all the more plausible that it occurs after 18 minutes of treatment, i.e. once Mn_XO_Y surface coverage has been considerably decreased. Once CO and CO_2 concentrations at the reactor downstream become respectively lower than 0.5 and 1 ppm, the discharge is switched off. Within 2.5 and 5 minutes, the concentrations of CO and CO_2 return to 0, showing that they directly originate from NTP oxidation.

Carbon mass balance of adsorbed IPA plasma regeneration / The total carbon mass balance recovered by *In-Situ* NTP treatment has been determined by considering the irreversibly adsorbed IPA 3.0 ± 0.05 µmol/m² (which corresponds to 6.4 ± 0.05 µmol) as 100%. All reported species quantified at the reactor downstream have been taken into account. Their temporal profiles have been integrated and their relative contributions in the carbon balance of the NTP regeneration have been calculated. Within 30 min of NTP treatment, 69% of total carbon mass balance has been recovered with 47% of CO_2 and 9% of CO contributions. Similarly, 13% is contributed by organic intermediate species quantified using SIFT-MS (11% acetone, 1% acetaldehyde and 1% formaldehyde) (Figure 19).

The missing fraction of the carbon mass balance (31%) could be attributed to adsorbed species remaining on the packed bed material after the *in-Situ* NTP treatment. In order to assess the nature and the amount of the remaining adsorbed species, a temperature programmed desorption (TPD) is performed under 1 L/min dry N_2 on the packed bed reactor. The reactor temperature is linearly increased from 296 to 673K, with the heating rate of 0.4 K/s. During the TPD, organic species have been monitored by SIFT-MS and CO and CO_2 have been monitored using FTIR. Interestingly, no organic intermediate species have been monitored by SIFT-MS during TPD. Beside, 1.8 ± 0.05 µmol CO_2 and 0.1 ± 0.05 µmol CO have been quantified by FTIR at the reactor outlet. These values respectively correspond to 28 and 2% of the carbon mass balance. Including these species, the carbon balance is completed up to 99%. The direct production of CO_2 from adsorbed reaction intermediate during thermal treatment of metal oxide surface has been reported by Sivachandiran et al [19]. Based on that work, it is possible to suggest that the missing carbon balance mainly consisted in adsorbed carboxylic acids, especially formic acid, desorbing as CO_2 under heating.

A key point to assess the performance of any air treatment technique is the amount of energy spent (i) to decompose the VOC, and (ii) to produce CO_2. Therefore, based on the experiments carried out, IPA removal efficiencies of both approaches are compared and reported in the following section.

Comparison of continuous vs. sequential treatment / Considering Figure 15 and Figure 19, the determination of the respective carbon mass balances makes possible to compare both processes in terms of VOC abatement and mineralization. From that point of view, the continuous treatment appears to be superior since (i) 98% of IPA is converted and (ii) the mineralization rate reaches 78%, which is 1.4 times higher than sequential treatment. However, regarding indoor air quality, a third criterion must be taken into account: the amount of organic side-products. In the domain of indoor air treatment technologies, this aspect dealing with secondary pollutants was rarely considered in spite of the fact that organic side-products themselves may decrease indoor air quality. For instance, in the domain of photocatalytic indoor air treatment considerable efforts have been achieved to assess this aspect during the last five years [15][17]. In the case of NTP continuous treatment, 20% of the treated IPA is converted into organic side products, namely acetaldehyde (6%) and formaldehyde (14%), whereas only 13% of the treated IPA is converted into secondary organic gaseous species during sequential treatment. From that point of view, the sequential treatment appears to be more efficient.

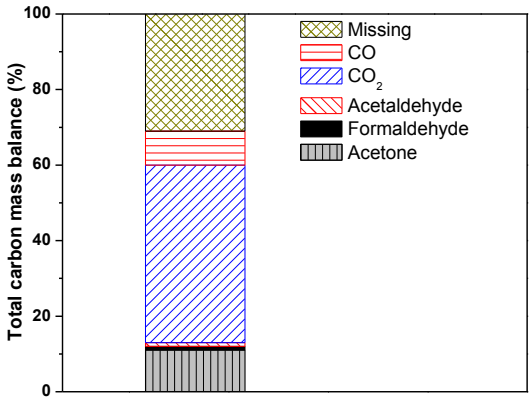

Figure 19 - Carbon mass balance recovered after 30 min of NTP treatment on IPA adsorbed Mn_XO_Y surface under dry air. NTP is ignited with a constant 0.82 W input power.

Apart from the nature and the relative abundances of the species treated and produced, energetic performances of both processes have to be assessed and compared. Performances of the continuous treatment have been determined on a steady state regime. Considering IPA inlet concentration, 0.22 µmol of IPA have been treated on that time range. Meanwhile, the constant 0.82 W input power, corresponds to 740 J deposited in the packed bed reactor. Dividing the energy consumed by the amount of treated IPA, it is possible to define the IPA removal efficiency (η_{IPA}) expressed in J μmol^{-1} as detailed in Equation 20. As reported in Table 26, the removal of one µmol of IPA using the continuous treatment requires the consumption of 3350 J. Similar calculations have been made for the sequential treatment. Performances of the sequential treatment have been evaluated on a 30 minutes time span because transient phenomena induced by NTP are completed within that time range. The IPA removal efficiency has been calculated as 230 J μmol^{-1} for the sequential treatment. As a result, the removal of one µmol of IPA requires 14.5 times less energy with the sequential treatment compared to the continuous treatment.

η_{IPA} *(J/µmol)* = **deposited energy** *(J)* / **amount of removed IPA** *(µmol)* **Equation 20**

η_{CO2} *(J/µmol)* = **deposited energy** *(J)* / **amount of produced CO_2** *(µmol)* **Equation 21**

In order to assess CO_2 production energetic cost, equivalent calculations can be made to determine the CO_2 production efficiency by dividing the energy consumed by the amount of CO_2 produced as defined in Equation 21. Interestingly, CO_2 production efficiency is 1725 J/µmol in the case of the continuous treatment, and 163 J/µmol in the case of sequential treatment (Table 26). The energetic cost to produce one µmol of CO_2 is almost 11 times lower in the case of sequential treatment. These findings highlight the advantage of sequential adsorption/NTP-regeneration over continuous NTP treatment. Therefore, sequential adsorption/NTP regeneration process is much more energetically efficient to remove and mineralize VOCs in indoor compared to continuous NTP treatment.

treatment mode	NTP investigated time span	Injected power	amount of IPA removed	IPA removal efficiency η_{IPA}	CO_2 production efficiency : ηCO_2	mineralization rate	total carbon balance recovered
continuous	900 s	0.82 W	0.22 µmol	3 350 J/µmol	1 750 J/µmol	**78%** CO_2 : 65 % CO 13%	98%
sequential	1 800 s	0.82 W	6.40 µmol	230 J/µmol	163 J/µmol	**56%** CO_2 : 47 % CO 9%	69%

Table 26 - Comparison of continuous and sequential adsorption - NTP-regeneration processes.

Wrap up & conclusion on *continuous* and *sequential* processes comparison /

The treatment of IPA under typical indoor air conditions has been achieved (i) with direct and continuous non-thermal plasma and (ii) with sequential adsorption on Mn_XO_Y and non-thermal plasma regeneration. It is possible to find experimental conditions enabling the proper comparison of both processes using the same packed bed reactor. From an IPA abatement point of view, both processes lead to satisfying performances: IPA conversion by continuous plasma reaches 98% and adsorption efficiently traps IPA. From a reaction intermediate release point of view, which is a key point regarding indoor air treatment systems and quality, the continuous process is characterized by a higher amount. Indeed, 20% of the continuous process carbon mass balance is accounted by organic intermediates, whereas only 13% is reached by sequential process. More precisely, the contribution of formaldehyde, which is a regulated compound in indoor air, is far higher with continuous process (13%) compared to sequential process (1%). From a mineralization point of view, the performance of the continuous process is significantly higher since 78% of the carbon mass balance is accounted by CO_2, whereas it only reaches 56% for the sequential process.

Finally, the most striking difference between both processes is the energy demand. Indeed, the energy consumed to convert and/or mineralize the same amount of IPA is 14.5 times lower using sequential process compared to continuous process. Similarly the energy demand to produce the same amount of CO_2 is 10 times lower using the sequential process. Based on these results, sequential processes combining adsorption with non-thermal plasma regeneration should be privileged for energetic and air quality reasons. However, efforts should be made to improve their mineralization ability and to improve the carbon mass balance completion through the investigation of other kinds of sorbents.

Corresponding results have been obtained by L. Sivachandiran in the first year of his PhD [2], and valorized through a publication in Chemical Engineering Journal in 2015 [26].

D-3 NTP REGENERATION OF IPA SATURATED Mn_xO_y SURFACE COMPARED TO OTHER TECHNIQUES

In order to investigate the performances of non-thermal plasma regeneration of VOC saturated metal oxides, this approach has been compared to two other classical techniques: direct thermal regeneration and ozonolysis. A detailed description of this study based on IPA saturated MnxOy packed bed reactor regeneration by *in-situ* non-thermal plasma has been published by Sivachandiran et al [21] in 2014 in Chemical Engineering Journal. Main results are summarized below.

Mn_XO_Y coated glass beads packed-bed reactor (Figure 8) has been used for isopropanol (IPA) storage under gas-flowing condition at 296 K. Atmospheric pressure gas phase Fourier Transform Infrared Spectroscopy (FTIR) and online Thermal Desorption coupled with Gas Phase Chromatography and Mass Spectrometry (TD-GC-MS) have been respectively used to quantify and to identify the gas phase species produced during the regeneration processes. This study mainly aims at comparing three different techniques to regenerate the IPA saturated Mn_XO_Y surface, namely (i) Direct Thermal Treatment (DTT), (ii) Ozonolysis and (iii) *In-Situ* Non Thermal Plasma Treatment (NTP).

First, it was demonstrated that Mn_XO_Y can be used as an efficient sorbent material for IPA removal. Among the investigated methods, the dry air thermal treatment (DTT) has shown 94% of surface regeneration efficiency. However, 35% of total carbon mass balance is contributed by desorbed IPA and 22% is contributed by acetone. Compared to DTT process, the dry air ozonolysis has shown lower surface regeneration efficiency of 41%, with 23% of CO_X and 12% of acetone contributions. Regarding the IPA desorption and acetone formation, DTT and dry air ozonolysis methods are disfavored. In the case of *In-Situ* NTP treatment it was noticed that, all adsorbed IPA have been converted into other oxidized species. However, only a maximum of 66% of irreversibly adsorbed IPA have been removed from the Mn_XO_Y surface. Thus, it was evidenced that, even after 30 min of NTP treatment, thermal treatment is necessary to complete the total carbon mass balance. From a process point of view, and considering high mineralization and low VOCs desorption as the main criteria, among the studied methods, the *In-Situ* NTP treatment has shown better regeneration efficiency, and twice more CO_2

selectivity. Notably, dry air *In-Situ* NTP treatment prior to thermal treatment has significantly improved the mineralization. The order of mineralization efficiency and/or COx selectivity can be written as follows: *In-Situ* NTP > dry air ozonolysis > dry air DTT.

D-4 INVESTIGATION OF *in-situ* NON-THERMAL PLASMA REGENERATION: ROLE OF RELATIVE HUMIDITY (RH)

Introduction / In this section, the NTP regeneration of IPA saturated TiO_2 surface is investigated to clarify the environmental performances of such a process. IPA was adsorbed up to the breakthrough on a TiO_2 coated packed bed reactor (Figure 8). Reversibly and irreversibly adsorbed IPA fractions on TiO_2 were quantified. The influence of air relative humidity was especially investigated since moisture is always present in treated effluents and H_2O may considerably impact both adsorption and oxidation processes. After the adsorption step, IPA saturated TiO_2 was submitted to *in-situ* NTP. The plasma injected power was determined as a function of air relative humidity. Influence of humidity on IPA total oxidation, total carbon balance and TiO_2 surface regeneration are investigated and discussed.

Experimental procedure / Figure 20 represents the schematic of IPA adsorption and regeneration cyclic procedure using the adsorption / non-thermal plasma reactor (Figure 8).

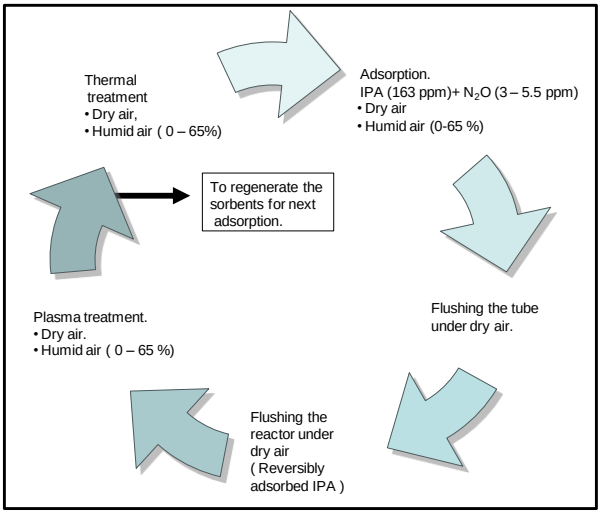

Figure 20 - Schematic of the VOC adsorption and *in-situ* non-thermal plasma and thermal regeneration experimental cyclic procedure.

Influence of air RH on non-thermal plasma injected power / Figure 21 represents the evolution of plasma injected power as a function of air RH%. The injected power was measured for 10 different air RH, from 0%, to 65%, at constant applied voltage of 10 kV and 1000 Hz frequency. It can be mentioned that the injected power globally increases with humidity at constant applied voltage. Injected power varies from 0.35 W under dry air to 1.83 W for 65% RH. The sigmoid profile of injected power as a function of air RH may be attributed to the evolution of TiO_2 surface coverage by H_2O molecules. The increase of H_2O surface coverage onto TiO_2 may lead to (i) a decrease in the coating dielectric constants [181] and (ii) an increase in the surface conductivity. As reported by Kai-Uwe and Eisenreich, TiO_2 surface is covered by a complete water monolayer above 30% RH in air [182]. The inflexion point noticeable at 30-35% RH on Figure 21 could be correlated to the water monolayer formation onto the sorbent surface.

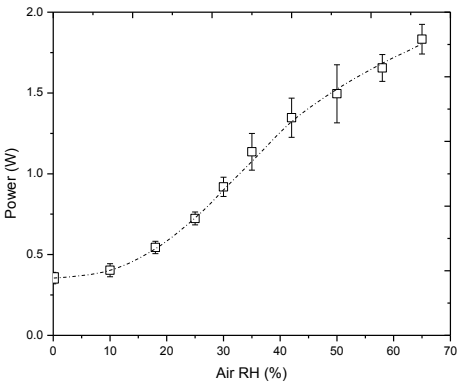

Figure 21 - Evolution of the plasma injected power as a function of air relative humidity (RH). The applied voltage and frequency are fixed as 10 kV and 1000 Hz. The injected power was measured by (q–V) Lissajous Method.

Influence of air RH on IPA adsorption on TiO_2 / Under real operating conditions of VOC adsorption and regeneration on TiO2, humidity is permanently present in the air and may considerably impact adsorption mechanisms and further oxidation processes. Thus, the influence of air RH on amount of IPA adsorbed over TiO2 surface at ≈ 295 K was studied; the reversibly and irreversibly adsorbed IPA quantities were determined and reported on Figure 22 for each investigated RH. The amount of irreversibly as well as reversibly adsorbed IPA decreases continuously with increasing relative humidity. As soon as introducing the humidity, IPA adsorption decreases steeply from, 275 µmol g-1 to 175 µmol g-1 at 10% RH, this 1.6 times decrease in IPA adsorption can be attributed to the competitive adsorption between IPA and water molecules. The amount of H2O represented by a 10% RH in air at 295 K is 2600 ppm. Compared to the 163 ppm of IPA in the inlet gas stream during the adsorption phase, the partial pressure ratios between IPA and H2O clearly favors H2O adsorption in the competitive process even with the lowest air RH.

From 0 to 35% RH, even if the co-adsorption of water clearly hinders IPA adsorption, the partition between reversibly and irreversibly adsorbed IPA is not modified. As reported on insert of Figure 22, the percentage of irreversibly adsorbed IPA is almost constant to 82 ± 2%, air RH varying from 0 to 35%. The adsorption process is globally hindered by the presence of water, but the reversible and irreversible adsorption modes are still allowed. On this RH range, as reported by Kai-Uwe and Eisenreich [182], IPA adsorption sites on TiO_2 surface are decreased by the presence of H_2O molecules but still accessible since the complete surface coverage by water is not achieved. On the contrary, over 35% RH, a water monolayer is expected to be formed. The percentage represented by irreversibly adsorbed IPA increases to 94% under 65% RH. On high RH range (>35%), IPA adsorption globally decreases as RH increases, more especially, the weakly hydrogen-bonded adsorption mode appears to be clearly disfavored. In parallel, it can be suggested that a third strong adsorption mode may appear for the highest RH. Indeed, considering (i) the formation of water multilayer on TiO_2 surface, and (ii) the high solubility of IPA into water; part of irreversibly adsorbed IPA may be also solvated in water multilayer, rather than directly interacting with TiO_2 surface for the highest RH.

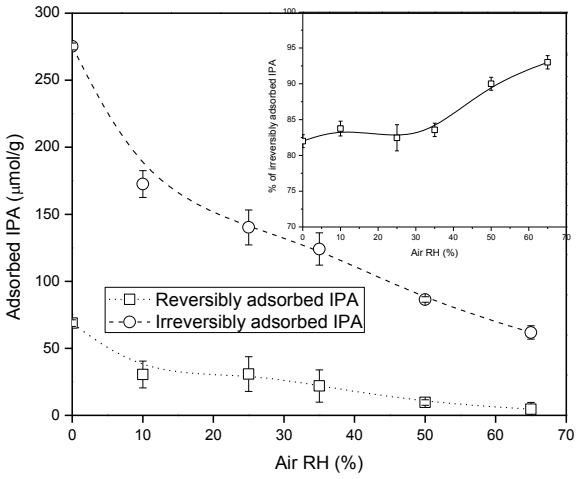

Figure 22 - Influence of air relative humidity (RH) on IPA reversible and irreversible adsorbed fractions on TiO_2 at ambient condition.

Plasma assisted regeneration of TiO_2 saturated surface under 35% RH / To investigate the influence of NTP surface discharge on VOC saturated surface regeneration close to indoor air condition, adsorptions of IPA on TiO_2 under various RH were performed. Plasma treatment was done with corresponding adsorption air RH Temporal profiles of species monitored along the plasma treatment under 35% RH are on Figure 23.

As shown on Figure 23, during the first seconds of discharge ignition (t<100 s), a significant amount of IPA desorbs along with the formation of CO and CO_2. At this stage, the plasma treatment of adsorbed IPA shows two simultaneous effects: (i) desorption of the initial VOC; (ii) mineralization of the VOC. In the presence of 35% RH, IPA desorption under plasma treatment occurs from 0 to 230 s. The amount of IPA desorbed by the plasma treatment under 35% RH is 67 µmol g^{-1} corresponding to 54% of the irreversibly adsorbed IPA. It can be suggested that the ignition of the surface discharge modifies the competitive adsorption equilibrium between IPA and water toward IPA desorption. In order to highlight the influence of air RH on IPA plasma induced desorption, the fraction of IPA desorbed during the plasma treatment (i.e.: desorbed IPA (µmol g^{-1}), divided by irreversibly adsorbed IPA (µmol g^{-1})) was normalized by the plasma deposited energy during the desorption process (J^{-1}). Obtained data are reported on Figure 24 as a function of air RH.

The effect of plasma induced desorption is inferior to 1.10^{-4} J^{-1} under dry air. From 10 to 65% RH, the fraction of plasma desorbed IPA per Joule ranges from 1.35 to 1.65 10^{-3} J^{-1}. For the same deposited energy, the presence of moisture in the adsorption and treatment gas stream multiplies by a factor 15 the IPA desorption. Thus, it is the combined effect of plasma ignition and H_2O molecules which cause IPA desorption. Therefore, we suggest that HO° radicals, produced by dissociative electron collision with H_2O, got chemisorbed on TiO_2, leading to a re-hydroxylation of the pre-treated TiO_2 surface. Subsequently, adsorbed IPA would be replaced by hydroxyl groups and desorbed. Since the molar fraction of H_2O is already superior to IPA concentration at 10% RH by one order of magnitude, the phenomenon is poorly influenced by the RH and occurs since the lowest RH.

Figure 23 - Gas phase products monitored in the reactor downstream as a function of time. t=0 corresponds to plasma ignition. IPA adsorption and plasma treatment were both done under 35% RH.

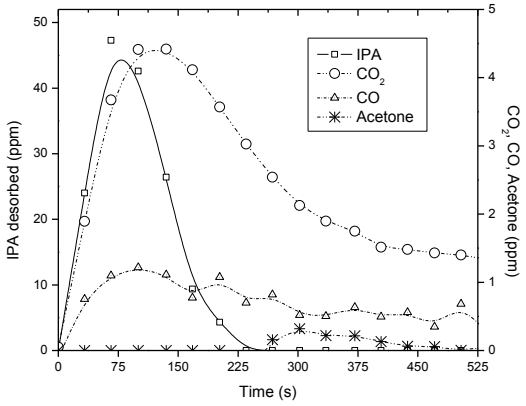

Figure 24 - Fraction of IPA desorbed per Joule during plasma treatment as a function of air relative humidity (RH). IPA adsorption and plasma treatment were done under corresponding air RH.

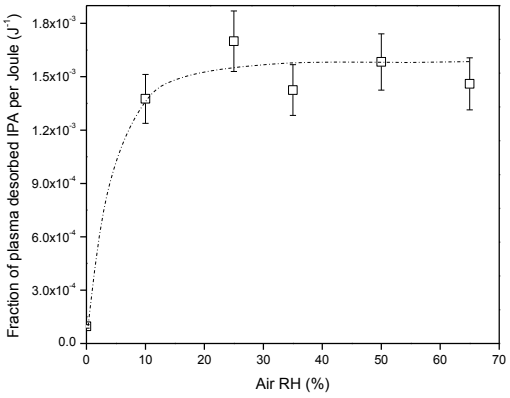

Carbon balance under 35% RH / In spite of a significant plasma-H_2O induced IPA desorption, the simultaneous production of CO and CO_2 attests of the reactivity induced by the plasma since the very beginning of the treatment. Moreover, after 230 s of treatment, CO, CO_2 and acetone are monitored downstream the reactor corresponding to the oxidation of the remaining adsorbed fraction of IPA. Figure 25 gives an overview of IPA saturated TiO_2 plasma treatment, in the presence of 35% RH. This figure reports the various percentages represented by plasma desorbed IPA, CO, CO_2 and acetone after 60 minutes of plasma treatment, i.e. once signals are returned to zero. Percentages are calculated from the contribution of each species into the carbon mass balance based on irreversibly adsorbed IPA. Figure 10 underlines the fact that within 60 minutes of treatment, 82% of the initially adsorbed carbon has been removed from the surface. We suggest that the 18% missing carbon balance are present on TiO_2 surface as adsorbed species; they consist either in polymerized organic species which are not sensitive to the plasma oxidation, or in adsorbed CO_2, produced by plasma treatment, since TiO_2 is able to adsorb significant amounts of carbon dioxide and carbonates.

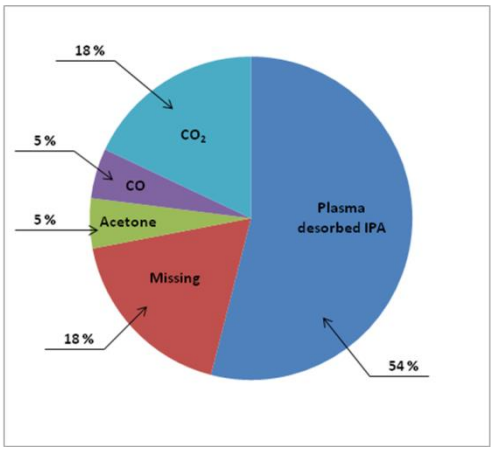

Figure 25 - Overview of IPA saturated TiO_2 plasma treatment carbon balance under 35% air RH.

Influence of air RH on plasma assisted mineralization / Irrespectively of the air relative humidity, plasma treatment was done up to CO and CO_2 signals return to zero at the reactor outlet. As discussed in prior section, the aim of this study is to investigate the influence of air relative humidity on the regeneration process, independently of injected power variations. Subsequently, the fraction of CO, or CO_2, produced (i.e.: amount of CO, or CO_2, produced (µmol g^{-1}), divided by irreversibly adsorbed IPA (µmol g^{-1})) was normalized by the plasma deposited energy during CO, or CO_2, formation process. The fraction of CO and CO_2 produced per Joule is reported as a function of air relative humidity on Figure 26 . CO_2 produced per Joule of injected energy is almost constant up to 35% RH. Furthermore, it is multiplied by 2 from 50 to 65 % RH. The fraction of CO produced per Joule follows the same trend; it increases slowly but continuously up to 35%. Similarly to CO_2 a steep increase in CO production per Joule is noticed over 35% RH.

Below 35% RH, TiO_2 surface is not completely covered by adsorbed water molecules, meaning that the adsorption of IPA can directly take place on TiO_2 surface. Water molecules surrounding adsorbed IPA, either in the gas phase or in the adsorbed phase, do not seem to play any significant role into IPA mineralization mechanism at low RH since CO and CO_2 productions are not considerably modified. On the contrary, as RH exceeds 35%, the fraction of CO and CO_2 produced per Joule is highly increased. As earlier discussed, under highly humid conditions (RH > 35%), strong adsorption modes of IPA are favored. Whatever the strong adsorption mode (non-dissociated, dissociated or dissolved into H_2O multilayer), IPA is stabilized on the sorbent and solvated by H_2O molecules. We suggest that this configuration is the most suitable for IPA oxidation into CO and CO_2, improving simultaneously the amount of HO° produced by the discharge and their contact with the VOCs to be oxidized.

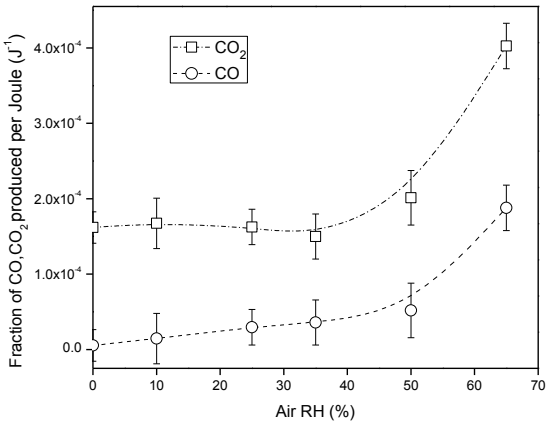

Figure 26 - Fraction of CO and CO_2 produced per joule during plasma treatment. IPA adsorption and plasma treatment were done under corresponding air RH.

Influence of air RH on carbon mass balances / The total carbon balance was determined considering irreversibly adsorbed IPA as 100%. As reported on Figure 27 the missing carbon balance after plasma treatment varied between 64% (dry air) to 9% (50% RH). It clearly appears that moisture promotes the plasma surface regeneration. In order to complete 100% carbon balance and to evaluate the remaining adsorbed species after plasma treatment, the reactor was heated up to 703 K under dry air with a flow rate of 1000 mL min^{-1}. This step is called thermal treatment. It is always performed after the plasma treatment. Carbone balances can be

calculated for the plasma treatment alone, and for the thermal treatment alone. The sums of those two carbon balances correspond to the total carbon balance of the process. Figure 27 represents the carbon balances calculated after (i) plasma treatment, (ii) thermal treatment, (iii) plasma + thermal treatment, as a function of air relative humidity.

The carbon balance achieved by plasma treatment takes into account IPA, CO, CO_2 and acetone. It increases from 36 to ca. 90% with increasing the air RH from 0 to 65%, showing the positive influence of moisture on plasma regeneration efficiency. Indeed, the introduction of moisture simultaneously improves IPA mineralization and decreases acetone formation.

No IPA was monitored at the reactor outlet during thermal treatment. CO_2, CO, and acetone were the only detected species. The contributions of CO_2 and CO respectively range from 4 to 8.2% and from 1 to 4%. Fluctuations do not appear to be correlated to the air relative humidity. CO_2 and CO may originate either (i) from plasma preliminarily oxidized species which get converted into CO_2 and CO in the presence of air at 700 K; or (ii) from CO_2 and CO, formerly produced by the discharge, which remained adsorbed onto TiO_2. In the case of CO_2, the second hypothesis is supported by the work of Luo and Ollis [183] who report the capacity of TiO_2 surface to adsorb CO_2 and carbonates. Nevertheless, they do not report any quantitative measurements which would have been compared with the amount of CO_2 we desorbed from our sorbent. In the case of CO, both hypotheses can be considered.

Except in the case of dry air treatments where the total carbon balance is limited to 54%, from 10 to 65% RH the total carbon balances are all higher than 92% and even reach 97% in the presence of 50% RH. Successive IPA adsorptions and treatments made under dry air lead to reproducible adsorbed amounts of IPA and equivalent results during regeneration. This indicates that, in spite of a low total carbon balance under dry air, adsorption properties of TiO_2 surface are not altered by poisoning polymerized species. The regeneration processes appear to be efficient, but we suggest that organic species like formaldehyde or acetic and formic acids may be produced and released. These species are characterized by low extinction coefficients, leading to high detection limit with direct FTIR monitoring even with long-path cell devices. In the presence of moisture, the diversity of products is limited since 96% of the carbon balance can be recovered only taking into account IPA, CO_2, CO and acetone.

Figure 27 - Influence of air RH on carbon balance calculated after (i) plasma treatment; (ii) thermal treatment performed after plasma treatment. The IPA adsorption, plasma and thermal treatment were done under corresponding air RH varied between 0 to 65%.

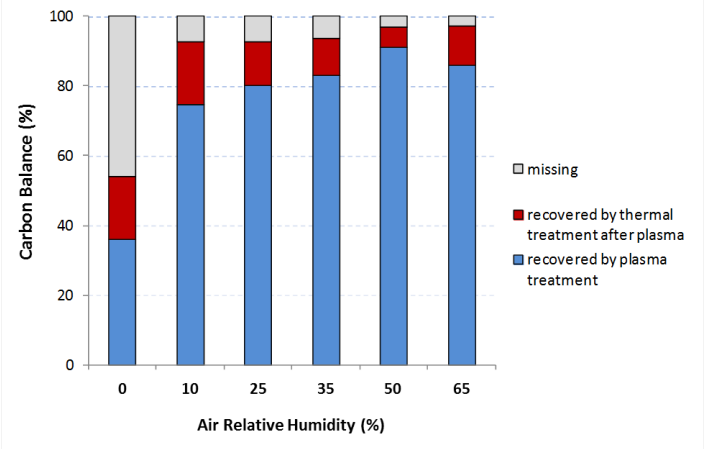

Conclusion /

In this section, the regeneration of IPA saturated TiO_2 surface has been investigated. The sequential approach in plasma-material combination, consisting first in using the material as a sorbent, and second in exposing the saturated surface to a discharge, appears as a very promising technique. The role of air RH has been investigated through each step of the process. Even if moisture considerably hinders the adsorption of IPA on TiO_2, it promotes the mineralization of the model molecule and diminishes acetone formation which is the main side product.

TiO_2 surface coverage by water molecule considerably impacts:

(i) plasma injected power;

(ii) IPA adsorption modes;
(iii) IPA reactivity under plasma exposure.
These three points have been quantitatively assessed.

Taking into account moisture on a large RH range enables to predict the process behavior when operated close to real indoor air conditions. TiO_2 surface reactivity plays a key role in the adsorption step as well as during the plasma regeneration step. Carbon balances based on gaseous species monitored during 1h plasma treatments evidenced that packed bed reactor configuration is appropriate for TiO_2 surface regeneration. Based on these encouraging results, this approach could be extended to multi-VOC atmosphere.

Corresponding results have been obtained by L. Sivachandiran during his PhD [2] in the context of ANR RAMPE project, they have been valorized through a publication in Chemical Engineering Journal in 2013 [16] and a second in Plasma Chemistry & Plasma Processing in 2013 [19].

D-5 *post-situ* NON-THERMAL PLASMA REGENERATION: DUAL GAS PHASE & SURFACE MONITORING

Introduction / The regeneration of IPA saturated TiO_2 surface using post-plasma reactor has been especially investigated through the PhD Thesis of Christelle Barakat et al. [4], in order to understand the individual role of long lifetime oxidative species, namely O_3, on adsorbed VOCs. The direct interaction of ozone with the metal oxide surface was first evaluated, then, the impact of O_3 on adsorbed IPA was assessed. The gas phase as well as the adsorbed phase was monitored.

Experimental procedure / The experimental procedure consists of five steps, it involves either an experimental setup corresponding to the one depicted in Figure 7 in the gas phase approach experiments or a DRIFTS cell setup in the case of adsorbed phase approach. In both setups, the sorbent bed is placed at the discharge downstream to be exposed only to the long life-time plasma generated specie, i.e. O_3.

❶ *Pretreatment* of the TiO_2 sample at 300°C to remove water and other adsorbed hydrocarbon species to guarantee surface repeatability.
❷ *Adsorption* of the pollutant on TiO_2 surface: the gas flow containing the pollutant passes through the sorbent bed and is gradually concentrated on the surface until saturation of the sorption sites.
❸ *Flushing with synthetic dry air flow* to remove reversibly adsorbed species. Flushing the adsorbent bed with pure air desorbs the molecules with the weakest heats of adsorption, i.e. physisorbed species, leaving only the irreversibly adsorbed molecules on the catalyst surface.
❹ *Surface exposure to ozone* by switching on the non-thermal plasma. Ozone generated by the plasma oxidizes the adsorbed molecules. The plasma is turned off after 70 minutes and the system is purged under dry synthetic air flow for a few minutes.
❺ *Temperature programmed oxidation* under air flow at 300°C is performed in order to oxidize the remaining adsorbed species and to regenerate the surface and complete the carbon balance.

Interaction of ozone with the sorbent surface / The sorbent surface is exposed to 20 ppm of O_3 generated by the plasma stage during 70 minutes. Figure 28 shows the temporal evolution of O_3 at the sorbent reactor outlet under three different conditions: (i) without TiO_2 in the reactor, (ii) with 200 mg of clean TiO_2 in the reactor, (iii) with 200 mg of IPA saturated TiO_2 in the reactor.

As long as the sorbent reactor remains empty, ozone produced by the upstream plasma reaches the FTIR cell within a few minutes. When TiO_2 is introduced in the sorbent reactor, a significant difference is noticed on O_3 breakthrough curves; even after 70 min plasma, O_3 outlet concentration does not reach the input value. This behavior indicates that O_3 is consumed on TiO_2 surface. The presence of TiO_2 in the sorbent reactor induces the decomposition of a fraction of O_3. The continuous increase of O_3 concentration at the outlet of the sorbent reactor indicates that the decomposition efficiency of O_3 on clean TiO_2 decreases with time. This behavior is consistent with an increasing coverage of strong Lewis acid sites, making them less and less available for further ozone adsorption.

Figure 28 - Temporal evolution of O_3 at the sorbent reactor outlet under three different conditions for the sorbent reactor: empty reactor, reactor with TiO_2, reactor with TiO_2 adsorbed with IPA. Ozone is produced by the upstream discharge (50Hz, 10kV, 68.2mW, 5.5J/L), adapted from [4].

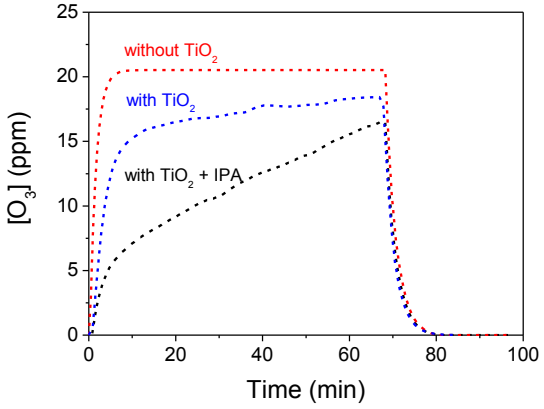

When TiO_2 surface has been formerly saturated by irreversibly adsorbed IPA, the consumption of ozone is enhanced. This suggests that ozone is simultaneously consumed by TiO_2 Lewis acid sites and by adsorbed IPA. Thus IPA is expected to produce oxidized by-products when exposed to ozone. The difference between ozone consumption on clean TiO_2 and ozone consumption on IPA saturated TiO_2 corresponds to a quantity of ozone of 1.3 µmol/m^2. The temporal evolution of O_3 consumption during the plasma ON phase can be estimated from the difference between the curves with TiO_2 and with TiO_2 and IPA. This temporal evolution is compared with the IPA oxidation products: acetone, CO and CO_2, presented in Figure 29.

Figure 29 - Temporal evolution of O_3 at the sorbent reactor outlet under three different conditions for the sorbent reactor. Ozone is produced by the upstream discharge (50Hz, 10kV, 68.2mW, 5.5J/L), retrieved from [4].

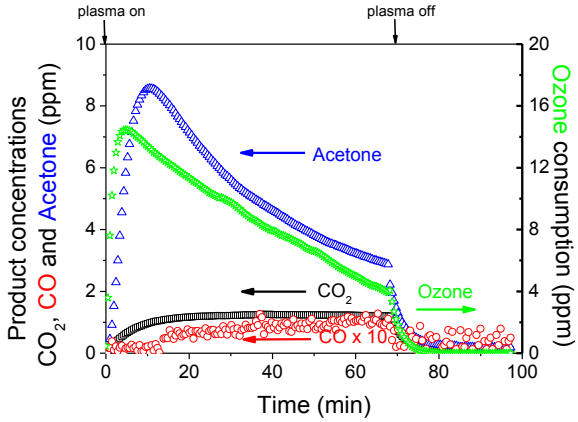

Adsorbed IPA oxidation by O_3 : gas phase approach / Figure 29 displays the evolution of the gas phase species detected during the exposition of IPA saturated TiO_2 surface to the 20 ppm ozone flow. IPA oxidation product concentrations are reported on the left axis. Ozone consumed as a consequence of the IPA adsorbed on the TiO_2 surface is reported on the right axis. The complete oxidation into CO and CO_2 remains relatively weak and a strong desorption of intermediate byproducts is observed with the acetone desorption. The mineralization of IPA into CO and CO_2 is first discussed.

Organic intermediates: As soon as the discharge is turned on, a transient production of acetone with a maximum at 10 minutes is observed. The total amount of gas phase acetone produced within 70 minutes is 1.2 µmol m^{-2}. Acetone is known to be an intermediate in IPA oxidation into CO_2 and CO. The amount of acetone detected in the gas phase is high since it corresponds to more than 22% of the irreversibly adsorbed IPA. It is worth noting that ozone consumption also exhibit a maximum and then follows the same characteristic decay time as acetone. Thus, O_3 consumption seems to be related to acetone production. Maximum O_3 consumption occurs around 5 minutes, significantly before the maximum of acetone in the gas phase. This means that a first step involving O_3 must occur before acetone desorption. We can make the hypotheses that O_3 is first responsible for acetone production on the surface and desorption of acetone is triggered by another mechanism.

Mineralization: As the plasma is turned on, CO_2 production is directly noticed and O_3 starts to be consumed. CO_2 concentration reaches a plateau (ca. 1.2 ppm) within 20 minutes. Then, its production remains constant until the plasma is switched off. Around 12 minutes after plasma ignition, CO is latently observed with a concentration that slowly increases with time until plasma is turned off. We can consider that CO is produced since the beginning of the plasma ignition, but the concentrations evolved remains below the FTIR detection limits during the first 12 minutes. CO is produced as long as O_3 is sent on IPA covered TiO_2; nevertheless the level of CO hardly exceeds 80 ppb, which is 15 times lower than CO_2. The production of CO_2 and CO, along with the immediate O_3 consumption of adsorbed IPA confirms that O_3 is able to oxidize, as well as mineralize, TiO_2 adsorbed IPA. Subsequently, IPA oxidation can be first evaluated through the mineralization of the adsorbed organic matter into CO_2 and CO (Equation 22).

$$Mineralization\ (\%) = \frac{Q_{CO_2} + Q_{CO}}{3 \times Q_{IPA_{irr.}}} \times 100 \qquad \textbf{Equation 22}$$

This mineralization rate, expressed in %, is calculated as the ratio of the total amount of carbon, Q_{CO2} and Q_{CO}, resulting from the oxidation of IPA into CO_2 and CO, respectively, over the carbon quantity of the pollutant initially adsorbed on the surface Q_{IPAirr}. The amounts of CO and CO_2 produced are obtained from the integration of their temporal profiles. They can be expressed as a function of TiO_2 specific surface area. During the exposition of IPA saturated TiO_2 surface to plasma generated O_3, the amount of CO_2 produced is 0.27 µmol m^{-2} and the amount of CO produced is 0.016 µmol m^{-2}. These values could also be expressed per Joule of injected power leading to 8.5 nmol J^{-1} and 0.5 nmol J^{-1} for CO_2 and CO, respectively. Substituting the produced quantities of CO_2 and CO in µmol m^{-2} into equation 1 gives a mineralization rate of only 2%.

Adsorbed IPA oxidation by O_3 : adsorbed phase approach / After the adsorption-flushing step discussed in the previous section, the discharge is turned on in order to generate O_3 upstream the sorbent reactor; ozone inlet concentration is 23 ppm. The evolution of the adsorbed species monitored by DRIFTS during the ozonation of the surface is shown in Figure 30, IPA adsorption step was previously monitored using the same technique.

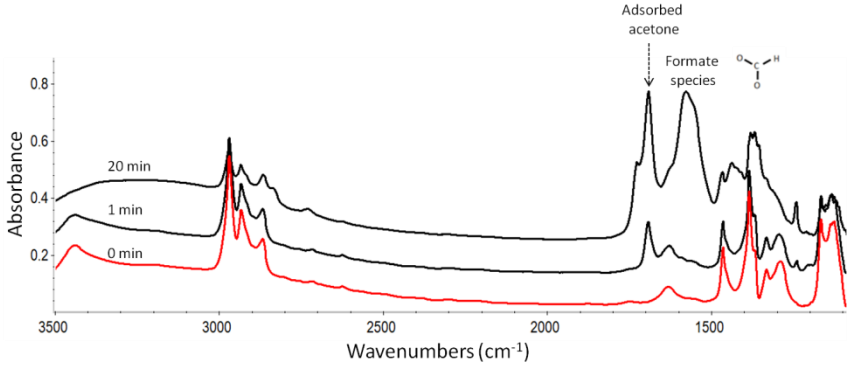

Figure 30 - Evolution of surface species adsorbed on TiO_2 during ozone generation under 200 ml/min of 20%O_2/Ar (200Hz, 2kV, 11.7mW, 4.7J/L).

On the spectrum corresponding to t = 0, the IPA peak at 2973 cm^{-1} attributed to IPA is at its highest and no carbonyl vibration ($\nu_{C=O}$) is detected. This indicates that no acetone can be detected as long as the plasma is turned off. Once the plasma is turned on, all the bands corresponding to IPA adsorption modes decrease and new bands appear at 1696 cm^{-1} and 1553 cm^{-1}. The band at 1696 cm^{-1} is characteristic of the ($\nu_{C=O}$) vibration mode of the carbonyl group in acetone and the band at 1553 cm^{-1} is characteristic of the ($\delta_{as\ COO}$) vibration mode of formate species. After 20 minutes of plasma, a band at 1701 cm^{-1} appears on the IR spectrum. This band is ascribed to ($\nu_{C=O}$) of an aldehyde species (acetaldehyde or formaldehyde) [184]. The temporal evolution of the peaks characteristic of both adsorption modes of IPA can be followed by plotting the TiO_2 surface coverage of dissociated IPA ($\delta_{O\text{-}H}$ = 1252 cm^{-1}) and non-dissociated IPA ($\delta_{C\text{-}O}$ = 1131 cm^{-1}) as a function of time. Obtained data are plotted on Figure 31.

It clearly appears on Figure 31 that the temporal decays of both IPA adsorption modes during ozonation are the same. This means that, independently of the adsorption mode, dissociated and non-dissociated IPA on TiO_2 show the same reactivity with ozone or its oxidative decomposition products. Simple models described in the literature suggest that O_3 decomposes on TiO_2 surface, leading to O_2 in the gas phase and an adsorbed O atom. This species is considered as the main oxidizing species and a Langmuir-Hinshelwood kinetic model could be proposed to describe the reaction between the adsorbed VOC and the adsorbed O atoms.

Figure 31 - Evolution of dissociated and non-dissociated IPA surface coverages on TiO_2 during the ozonation phase under 200 mL/min of 20% O_2/Ar and 23 ppm of O_3 (DRIFTS measurements).

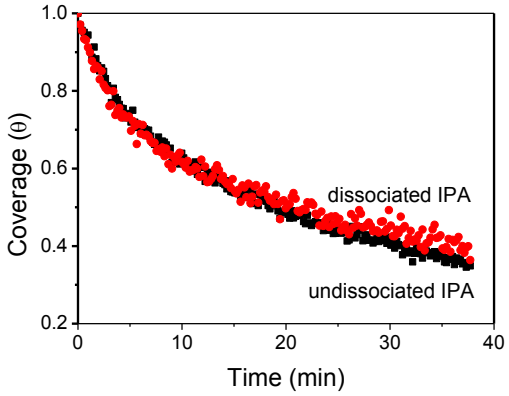

Conclusion /

In this section, potentialities of *post-situ* plasma regeneration, i.e. O_3 exposure regeneration were assessed. The simultaneous analysis of gas phase and adsorbed species by FTIR and DRIFTS measurements are informative to understand the mechanisms of IPA and acetone oxidation on TiO_2 exposed to plasma generated O_3 flow. Currently, *in-situ* characterization is only achieved in the case of post-plasma treatment since only reactant gases have to be sent to the surface; experimental developments are in progress in order to perform such *in situ* characterizations in the *in-situ* coupling. First developments have been performed in collaboration with IRCELyon designing transmission FTIR cell to investigate material surface in the same reactor than plasma discharge.

Regarding *post-situ* plasma treatment of saturated TiO_2, CO_2, CO and a transient acetone production are observed in the gas phase during surface ozonation. Similarly to photocatalysis, acetone seems to be the main intermediate in IPA oxidation into CO_2 and H_2O; however, mineralization remains low compared to *in-situ* plasma regeneration. This work mainly emphasizes the fact that *in-situ* configuration is more effective than *post-situ* for VOC oxidation and sorbent regeneration, and that *in-situ* monitoring developments are required. Further challenge is the development of *in-situ* characterization techniques applied to *in-situ* plasma treatment.

Presented results originate from the PhD thesis of Christelle Barakat [4] and have been valorized so far through two publications, one in Applied Catalysis B: Environmental [22] in 2014 another in a review article in Journal of Physics D: Applied Physics [23] in 2015.

D-6 AGEING OF MATERIALS COUPLED TO PLASMA

Introduction / Along the investigation of plasma-sorbent coupling, attention has been paid to the sustainability of the investigated process. Beside the oxidation of VOCs trapped on the sorbent surface, it is required to avoid any rapid ageing of the sorbent, i.e. poisoning of the surface through sorption and/or reactive site hindering. Concerning both main investigated metal oxides (TiO_2 and MnxOy) two kinds of species have been pointed out for their potential poisoning effect: carboxylic acids and NO_2.

Regarding carboxylic acids, first results have been obtained through the investigation of acetone adsorption on TiO_2 and subsequent regeneration by *in-situ* plasma exposure. Results are detailed in the article published by our research group in 2013 in Plasma Chemistry and Plasma Processing [19]. The typical interaction of carboxylic acids onto TiO_2 surface will not be exposed in this section since it is addressed in Part-E. The question of surface ageing will only be illustrated here through NOx impact on TiO_2 surface. Results presented here have been published in two papers: a first one dealing with NO_2 reactive sorption mechanisms on TiO_2 in *Applied Catalysis B: Environmental* in 2013 [18] and a second one dealing with the impact of NO_2 preliminary adsorption on VOC subsequent adsorption published in 2015 in *Chemical Engineering Journal* [27].

NOx (NO and NO_2) are mainly formed when nitrogen from air combine with oxygen at high temperatures for instance in thermal power plants, welding, and combustion engines. Besides, it is well reported that, when NTP is ignited in air (mixture of N_2/O_2) it produces higher oxides of Nitrogen compounds such as NO, N_2O, NO_2 and HNO_3 in concentration of few hundreds of ppb to some ppm depending on deposited energy [185][186]. Furthermore in NTP process under air, the major part of NOx is contributed by NO_2 due to the rapid oxidation of NO with highly active ozone produced by NTP [187].

The level of NO and NO_2 in indoor air are respectively in the range of several hundred ppb and less than a hundred ppb [188]. National Institute for Occupational Safety and Health (NIOSH) suggested that the Immediately Dangerous to Life and Health (IDLH) concentration of NO_2 is 20 ppm. Studies focused on risk assessment have shown that high outdoor NO_2 concentration observed in residential areas contributes to increased respiratory and cardiovascular diseases and mortality [189].

Therefore, in the case of air treatment systems based on plasma-material coupling, VOCs are generally the targeted compounds, but the metal oxide surface is exposed to the wide diversity of species present in the air stream or generated by the system itself. Among them, NOx may dramatically influence VOC adsorption processes and decomposition mechanisms [190][191], which may also impact the system efficiency and ageing.

NO_2 is a radical molecule, with a high electron affinity [192] (2.3 eV). Therefore, on TiO_2 surface, it can react to the metal center namely Ti^{4+} sites through O, N, or a combination of both. Dalton et al [193] have reported that, TiO_2 effectively converts NO_2 to harmless nitrates species under UV radiation in continuous flow reactor. On the other hand, Sorescu et al [194] have found that, NO weakly adsorbs on TiO_2 and desorbs around 127 K. However, metal oxides are used in NO_X storage technologies, where the release of NO_X at higher temperatures is a key issue [195]. Interestingly, there was not enough study on NO_2 storage and quantification on TiO_2 with flowing condition, and under typical ambient indoor air conditions.

Experimental procedure / The experimental setup used in this section corresponds to the one described on Figure 8. Before NO_2 adsorption, the TiO_2 coated packed-bed reactor was pre-treated under dry air at 703 K for 1 h (1 L min^{-1}) to remove the chemically adsorbed water molecules, VOCs and possible traces of adsorbed species (carbonates, nitrates...). NO_2 adsorption was performed at room temperature (296 K) along with tracer N_2O (3 - 5.5 ppm) diluted in dry air. Once NO_2 breakthrough is reached, lines were flushed with pure air by by-passing the reactor. Then, the reactor was flushed under dry air in order to quantify the reversibly adsorbed fraction of NO_2. Thereafter, Temperature Programmed Desorption (TPD) was performed under Nitrogen, from 296 K to 703 K with a ramp of 1.1 K s^{-1}. Species in the reactor downstream were continuously monitored by FTIR spectroscopy from the beginning of NO_2 adsorption to the end of thermal regeneration.

NO_2 adsorption and quantification on TiO_2 / Prior to NO_2 adsorption studies, NO adsorption has been addressed. We evidenced that NO does not adsorb on TiO_2 under ambient conditions [18]. To investigate the NO_2 adsorption mechanisms on TiO_2 under ambient condition, 23 ppm of NO_2 were sent in the feed gas concurrently with tracer N_2O (4.5 ppm). Breakthrough curves are reported in Figure 32.

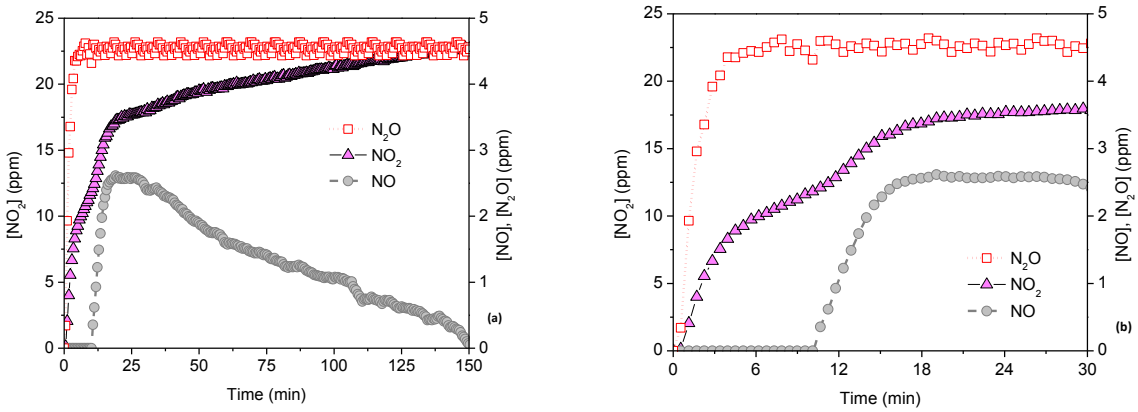

Figure 32 - Temporal profiles of NO_2 breakthrough curve on TiO_2, overlaid with N_2O tracer breakthrough curve: a) Full adsorption sequence, b) Focus on first 30 min.

Main observations from Figure 32 are:
❶ There is a significant delay between system mixing curve and NO_2 breakthrough curve; it evidences that NO_2 shows a quantifiable adsorption on TiO_2 under ambient condition.
❷ NO is produced; it evidences that NO_2 reactively adsorbs on TiO_2 and produces gas phase NO.
❸ Delayed evolution of NO leads to the hypothesis that the NO production probably depends on the amount of NO_2 adsorbed on TiO_2.
❹ The tracer N_2O concentration remains constant and corresponds to input concentration, indicating that N_2O is not produced during full sequence of NO_2 adsorption.

The interaction of NO_2 on TiO_2 surface has been intensively studied by authors for various experimental conditions like, (i) different NO_2 partial pressures, (ii) various temperatures ranging from 323 to 573 K [191][196]. Remarkably all authors have reported the production of NO in the gas phase, and formation of nitrates on TiO_2 surface.

As shown in Figure 32, NO_2 breakthrough concentration increases rapidly, followed by a slower increase with evolving NO in the gas phase. For the whole adsorption process, approximately 150 minutes are required to reach NO_2 steady state at the reactor downstream. The total amount of adsorbed NO_2 has been calculated by integrating the area between tracer N_2O and NO_2 breakthrough curve. Under our experimental conditions 8.3 ± 0.3 µmol m^{-2} of NO_2 are adsorbed on TiO_2 after breakthrough. The uncertainty in amount of NO_2 adsorbed, and NO produced have been calculated by repeating the experiment four times under the same experimental conditions. Furthermore, the monitoring of NO during NO_2 adsorption at room temperature evidences that, without any illumination of the photocatalyst, reactive adsorption occurs. The total amount of NO produced during this whole course of adsorption is quantified as 2.7 ± 0.3 µmol m^{-2}. Hence, the amount of NO_2 adsorbed could be more precisely denoted as NO_2 consumed in the following sections.

In order to get a better understanding on NO evolution profile, the first 30 minutes of NO_2 breakthrough curve is focused and presented in Figure 32-b. During the first 10 minutes of NO_2 adsorption, approximately 50% of feed gas NO_2 has been consumed on TiO_2. However, during this period of time NO is not noticed in the gas phase downstream the reactor. In particular, NO is produced after 10 minutes and reaches the maximum (2.7 ppm) within 6 minutes (approximately after the 16^{th} minutes of the adsorption process). Moreover, NO formation is a transient process, after 30 minutes, NO production drops back to zero. Therefore, the absence of NO during first 10 minutes of NO_2 adsorption suggests that, NO_2 coverage on TiO_2 has to reach a threshold to initiate the NO production. As abovementioned, no significant amount of NO adsorbs on TiO_2 surface under our experimental conditions, thus, it can be assumed that all NO produced during adsorption has been monitored in the gas phase. The total amount of NO produced represents 33% of total consumed NO_2 along the complete adsorption sequence. Therefore, the ratio between $NO_{2(consumed)}$ and $NO_{(produced)}$ is 3:1. Similar findings were reported by Despres et al [197] and Haubrich et al [196]. Despres et al [197] have investigated the NO_2 storage capacity on TiO_2 at 473 K, for 500 ppm of NO_2 inlet concentration, and reported a slightly lower NO_2 storage capacity of 2.2 µmol/m^2 on TiO_2. This lower adsorption phenomenon can be attributed to the adsorption performed at higher temperature, nevertheless, the authors also reported the ratio of 3:1 between $NO_{2(consumed)}$ and $NO_{(produced)}$ which is in good agreement with our findings.

Haubrich et al [196] investigated NO_2 adsorption steps on TiO_2 (110) under Ultra High Vacuum (UHV) conditions, by using photoemission and XANES experiments as well as theoretical density functional (DFT) calculations. They have reported that NO_2 adsorbs on TiO_2, and produce one NO in the gas phase through disproportionation reaction between two adsorbed NO_2 molecules by leaving one NO_3 on TiO_2 surface. Furthermore, Rodriguez et al [198] reported the fact that the adsorbed NO_3 is formed by disproportionation reaction and not by direct reactive adsorption of NO_2 on O-vacancy sites on TiO_2 surface, and the remaining adsorbed NO_3 is electro neutral in nature. Besides, they also reported the migration of O vacancies from subsurface to the surface during NO_2 adsorption. In addition, authors suggested the same mechanism for other metal oxides like CeO_2, CuO, ZnO, Cr_2O_3 and Fe_2O_3. In brief, a NO_2 adsorption mechanism on TiO_2 surface at room temperature is generally reported as the disproportionation of two NO_2 into one NO_3 and one NO, without any precise species quantification support. Thus the expected ratio between $NO_{2(consumed)}$ and $NO_{(produced)}$ would be 2:1, which is clearly not in accordance with our experimental quantitative measurements (3:1) and other authors [197]. Therefore, the general mechanism suggested for NO_2 adsorption on TiO_2 at room temperature should be deeply reconsidered.

On the other hand Apostolescu et al [199] investigated NO_2 adsorption mechanisms on Al_2O_3 at 323 K using Diffuse Reflectance Infrared Fourier Transformation spectroscopy (DRIFTS). On Al_2O_3 surface, NO_2 adsorbs in a reactive way and produces NO_3 in adsorbed phase and NO in the gas phase. In particular, they have reported the ratio of about 3:2:1 between $NO_{2(consumed)}$, $NO_{2(desorbed)}$ by TPD performed after NO_2 adsorption and $NO_{(produced)}$ in the gas phase during NO_2 adsorption, respectively. Furthermore, the authors have confirmed the fact that, the NO formation proceeds through three successive reactions as follows:

1. Two adsorbed NO_2 undergo disproportionation reaction and produce NO_3^- and NO^+ on Al_2O_3,
2. NO^+ is highly reactive; hence it reacts with Al_2O_3 lattice O^{2-} and produce NO_2^-,
3. NO_2^- further reacts with another adsorbed NO_2 and produces adsorbed NO_3^- and gas phase NO.

Therefore, we propose a similar mechanism for NO_2 adsorption on TiO_2 at room temperature and under dry air flowing condition as follows (Equation 23 to Equation 27):

$$2\,NO_{2\,(gas)} \leftrightarrows 2\,NO_{2\,(ads)} \quad \textbf{Equation 23}$$

$$2\,NO_{2\,(ads)} \rightarrow NO_3^-{}_{(ads)} + NO^+{}_{(ads)} \quad \textbf{Equation 24}$$

$$NO^+{}_{(ads)} + O^{2-}{}_{(TiO2\ S.L.)} \rightarrow NO_2^-{}_{(ads)} \quad \textbf{Equation 25}$$

As TiO_2 surface coverage "θ" by $NO_2^-{}_{(ads)}$ and $NO_3^-{}_{(ads)}$ exceeds 0.2, then the Equation 26 occurs:

$$NO_2^-{}_{(ads)} + NO_{2\,(ads)} \rightarrow NO_3^-{}_{(ads)} + NO_{(gas)} \quad \textbf{Equation 26}$$

The global mechanism can be summarized as follows (Equation 27):

$$3\,NO_{2\,(ads)} + O^{2-}{}_{(TiO2\ S.L.)} \leftrightarrows 2\,NO_3^-{}_{(ads)} + NO_{(gas)} \quad \textbf{Equation 27}$$

As reported in Equation 27 three NO_2 molecules are involved in two consecutive disproportionation reactions to produce one NO in the gas phase. Thus, the theoretical ratio is 3:1 between $NO_{2(consumed)}$ and $NO_{(produced)}$, which is in agreement with our quantitative measurements performed downstream the adsorption reactor. Moreover, as shown in Equation 27 two NO_3^- species have been stored on TiO_2 to produced one NO in the gas phase. Therefore, this proposed mechanism could be quantitatively assessed by determining the total amount of NO_3^- stored on TiO_2 surface.

Hence, the NO_2 saturated TiO_2 has been subjected to Temperature Programmed Desorption (TPD); results are discussed in the following section.

Temperature programmed desorption of NO_2 saturated TiO_2 surface / To assess the proposed NO_2 adsorption mechanisms on TiO_2 at room temperature, TPD have been performed on NO_2 saturated TiO_2 under N_2 flow. Prior to TPD, the reactor was thoroughly flushed under N_2 at 296 K. It was found that neither NO nor NO_2 have been detected in the reactor downstream, indicating that all consumed NO_2 has been strongly adsorbed on TiO_2 at room temperature. During TPD, the total N_2 flow has been kept constant at 1 L min^{-1}. The NO_2 saturated TiO_2 reactor was heated up to 703 K, with a heating rate of 1.1 K s^{-1}. The obtained temporal profile of monitored species is reported on Figure 33. The most important observation is that only NO_2 has been monitored during the course of thermal desorption. In addition, TPD has been performed until NO_2 concentration reaches zero in the reactor downstream, making possible the complete quantification of NO_2 desorbed.

Figure 33 - Temporal profile of NO_2 desorbed during temperature programmed desorption (TPD) of NO_2 (23 ppm) saturated TiO_2 surface. Thermal treatment was performed under Nitrogen (1 $L.min^{-1}$) with a temperature ramp of 1.1 $K.s^{-1}$. Temperature ramp is displayed in the insert which is a focus on the first 15 minutes of TPD.

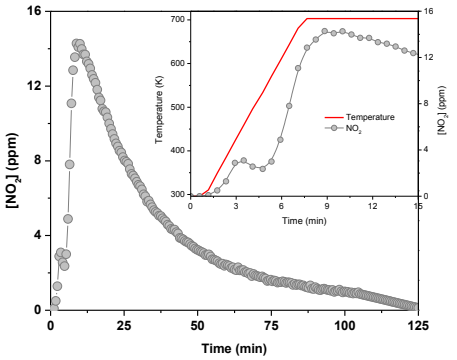

As shown in Figure 33, NO_2 desorbs in two distinct peaks (inserted figure with temperature profile). First, very narrow peaks centered approximately at 3 minutes, and second a broad peak at 9 minutes. These two peaks have been quantified separately and discussed. The first peak at 3 minutes can be attributed to desorption of weakly adsorbed NO_2^-, or NO_3^- from TiO_2 surface; the corresponding desorption temperature is low : 450 K. The broad peak, at 9 minutes, corresponds to the strongly adsorbed species, desorbing at higher temperature, more than 580 K. Haubrich et al [196] evidenced the decomposition of NO_3^- over 520 K by *in-situ* FTIR spectroscopy. Furthermore, according to our proposed mechanisms, the strongly adsorbed NO_3^- species are produced by consuming the surface lattice O^{2-}. Therefore, during thermal treatment it is likely to produce NO_2 by leaving O^- to TiO_2 surface lattice. By considering our proposed mechanisms, the broad second peak can be attributed to the decomposition of chemisorbed NO_3^- into NO_2 in the gas phase as mentioned in Equation 28.

$$NO_{3\,(ads)}^{-} \xrightarrow{\triangle Q} O_{(ads)} + NO_{2\,(g)} \qquad \textbf{Equation 28}$$

Approximately 0.2 ± 0.1 µmol m^{-2} of NO_2 have been quantified by integrating the first peak desorbed at 450 K. In addition, 5.4 ± 0.1 µmol m^{-2} of NO_2 have been quantified from the second peak integration. Therefore, approximately 5.6 ± 0.1 µmol m^{-2} of NO_2 have been removed from TiO_2 surface along the TPD, corresponding to 67% of the total consumed NO_2. Thus, for 23 ppm of inlet concentration, the ratio between consumed NO_2 and thermally desorbed NO_2 can be written as 3:2. Furthermore, assuming the distinction between both peaks, the TPD profile shows that, 97% of thermally desorbed species are represented by the second peak. This shows that 97% of consumed NO_2 have been stored as strongly adsorbed NO_3^- on TiO_2 surface. **As a conclusion, from a qualitative and a quantitative point of view, NO_2 reactive adsorption on TiO_2 surface could be described by the proposed mechanism.**

Control of TiO_2 surface coverage by NO_2 / Figure 34 shows the temporal profiles of NO_2 and N_2O breakthrough curves and NO transient formation curve on fresh TiO_2 surface. NO_2 adsorption on TiO_2 is performed under dark condition and in dry air with a constant flow rate of 600 mL min^{-1}. At the reactor inlet, 30 ppm of NO_2 and 5 ppm of tracer N_2O are concurrently introduced. During adsorption, NO_2 concentration at the reactor downstream increases until the surface is saturated. As above described, NO is evolved in the gas phase after 6 minutes of adsorption. And the NO concentration reaches the maximum value between 15 and 20 minutes of adsorption. When the surface tends to reach saturation, NO concentration gradually decreases. In particular, it reaches zero when the surface is completely saturated. Both NO_2 and NO temporal profiles are overlaid with the system mixing curve obtained from the temporal profile of N_2O. Five different adsorption experiment sets have been carried out, they differ by their adsorption times ranging from 150 s to 5000 s. Each set of experiment has been repeated four times in order to assess the reproducibility.

Figure 34 - Temporal profiles of NO_2 and NO monitored at the reactor downstream under dark conditions and at 296 K. For adsorption, 30 ppm of NO_2 and 5 ppm of N_2O balanced with zero air are concurrently sent at the reactor inlet with a total flow rate of 600 mL min^{-1}.

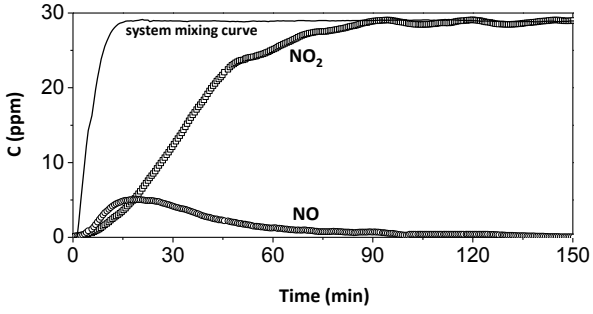

Considering the mechanism depicted from Equation 23 to Equation 27, the stable ad-species present on saturated surface are : (i) irreversibly adsorbed $NO_{2\,(ads)}^-$ and (ii) $NO_{3\,(ads)}^-$ species. Regarding $NO_{3\,(ads)}^-$ species, Hadjiivanov et al [200] reported that NO_2 adsorption on TiO_2 surface leads to the formation of monodentate as well as bidentate $NO_{3\,(ads)}^-$ species on Ti^{4+} sites. Although $NO_{2\,(ads)}^-$ is a reaction intermediate, it coexists with $NO_{3\,(ads)}^-$ on partially covered surface. Therefore, in the following discussion the notation " $NO_{x\,(ads)}^-$ " is used to represent the adsorbed $NO_{2\,(ads)}^-$ and $NO_{3\,(ads)}^-$ species. Subsequently, the coverage rate θ is used to characterize the surface coverage due to NO_2 adsorption. The parameter θ is defined as the ratio between $NO_{x\,(ads)}^-$ adsorbed amount along partial adsorption and the total amount of $NO_{x\,(ads)}^-$ adsorbed on saturated TiO_2 surface.

As reported in Figure 34, from NO_2 adsorption breakthrough curve, it is possible to determine the total amount of NO_2 consumed on TiO_2 surface and the total amount of evolved NO for various adsorption times. The total amount of NO_2 consumed is obtained by integrating the area between the NO_2 breakthrough curve and the N_2O system mixing curve and the total amount is expressed in µmol m^{-2}. Similarly, the amount of NO produced is directly quantified from NO concentration temporal profile. Consumed NO_2 values are reported in Table 27. In the following, $q(NO_{x\,(ads)}^-)$ represents the sum of $NO_{2\,(ads)}^-$ and $NO_{3\,(ads)}^-$ adsorbed amounts per surface unit. The proposed mechanism contains the following points:

1. There is a θ threshold regarding the production of NO in the gas phase.
2. Below this θ threshold, the stoechiometric ratio between consumed NO_2 and $NO_{x\,(ads)}^-$ is 2:2
3. Beyond the θ threshold, the stoechiometric ratio is 3:2

Thus, $q(NO_{x\,(ads)}^-)$ is quantified by multiplying the consumed NO_2 amount by 1 or 2/3, depending on the adsorption process advancement. The values related to saturated surface are considered as references to calculate θ when $\theta < 1$. The uncertainty values are determined from the dispersion of the measurements obtained during the repeated experiments. Table 27 reports the amounts of NO_2 consumed per surface unit for the different adsorption times and the corresponding $q(NO_{x\,(ads)}^-)$ amounts and θ values.

Based on Table 27, four different surface coverages (0.05, 0.1, 0.55 and 0.92) can be considered to evaluate the impact of NO_2 on acetaldehyde adsorption. The first two are lower than NO formation threshold and the last two are above NO formation threshold. Acetaldehyde adsorption parameters, i.e. irreversibly adsorbed fraction (q_{irr}), reversibly adsorbed fraction (q_{rev}) and adsorption constant (K) have been determined for each selected values of θ.

Table 27 - Amounts of NO_2 consumed per surface unit for various adsorption times. Total $q(NO_{x\,(ads)}^-)$ is calculated as the total amount of $NO_{2\,(ads)}^-$ and $NO_{3\,(ads)}^-$ per surface unit. Covering of TiO_2 surface by NO_2 is represented by the θ parameter varying from 0 to 1.

Adsorption time (s)	Total consumed NO_2 (µmol m^{-2})	Total $q(NO_{x\,(ads)}^-)$ (µmol m^{-2})	θ
150	0.19 ± 0.1	0.19 ± 0.05	0.05 ± 0.02
300	0.38 ± 0.05	0.38 ± 0.05	0.10 ± 0.02
1450	3.03 ± 0.3	2.02 ± 0.15	0.55 ± 0.05
2400	5.01 ± 0.4	3.34 ± 0.27	0.92 ± 0.05
5000	5.47 ± 0.4	3.65 ± 0.27	1

Acetaldehyde adsorption on clean TiO_2 surface / Figure 35 shows acetaldehyde breakthrough curve overlaid with the N_2O system mixing curve during breakthrough and flushing steps on clean TiO_2 surface. During adsorption, 20 ppm of acetaldehyde balanced with dry air is sent to the reactor inlet. The acetaldehyde concentration at the reactor outlet increases till the adsorption equilibrium is reached. Then the reactor is flushed under dry air. During flushing, the reversibly adsorbed acetaldehyde fraction desorbs. Flushing is stopped as the acetaldehyde concentration returns to zero.

Adsorbed acetaldehyde amounts on fresh TiO_2 surface are 8.61 µmol m^{-2} ± 10% for the irreversibly adsorbed fraction and 0.42 µmol m^{-2} ± 10% for the reversibly adsorbed fraction, corresponding to a total adsorbed amount of 9.03 µmol m^{-2} ± 15%. These experimental data are coherent with those obtained with 20 ppm inlet concentration of acetaldehyde as obtained Frédéric Batault during his PhD thesis [3] with fundamental setup.

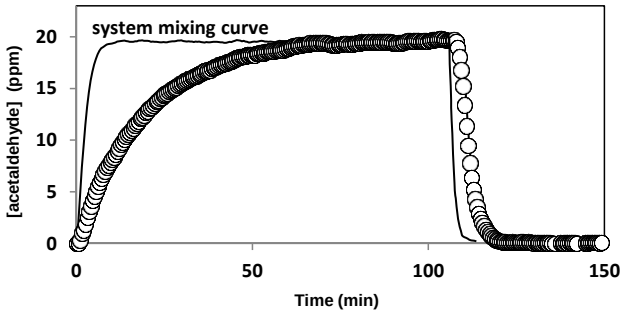

Figure 35 - Acetaldehyde breakthrough and flushing curves overlaid with N_2O system mixing curves on clean TiO_2 surface. During adsorption, 20 ppm of acetaldehyde and 5 ppm of N_2O are concurrently sent to the reactor inlet. Adsorption is performed under dry air with 600 mL min^{-1} total flow rate, at 296 K and under dark conditions.

Adsorption of acetaldehyde on clean TiO_2 surface has been investigated with acetaldehyde inlet concentrations ranging from 5 to 300 ppm. For each inlet concentration, reversible and irreversible fractions have been quantified, they exhibit contrasted behaviours. Indeed, the irreversibly adsorbed fractions is poorly influenced by acetaldehyde inlet concentration, which suggests that even with 5 ppm inlet concentration, all irreversible adsorption sites can be covered. In contrast, the reversibly adsorbed fraction of acetaldehyde shows a typical Langmuir isotherm behaviour with respect to acetaldehyde inlet concentration. This isotherm, determined on clean TiO_2 surface, is reported on Figure 37. It enabled the calculation of the maximum reversibly adsorbed amount on clean TiO_2 surface as : q_{revm} = 1.6 ± 0.2 µmol m^{-2} and the adsorption constant of reversibly adsorbed acetaldehyde on clean TiO_2 surface as 0.010 ± 0.002 ppm^{-1}.

Acetaldehyde adsorption on preliminary NO_2 exposed TiO_2 surface / Acetaldehyde adsorption and desorption have been performed for the various selected values of θ, i.e. various surface coverages by $NO_x^-{}_{(ads)}$ species. Acetaldehyde, NO, NO_2 and N_2O concentrations are monitored at the reactor downstream. For each θ values, acetaldehyde adsorption has been repeated three times. It has to be noted that neither NO nor NO_2 have been monitored at the reactor outlet during acetaldehyde adsorption on $NO_x^-{}_{(ads)}$ covered TiO_2 surface. This finding emphasizes the fact that acetaldehyde adsorption does not affect the chemisorbed NO_2^- and/or NO_3^- species on TiO_2 surface under our experimental conditions. For each experiment both irreversibly and reversibly adsorbed fractions of acetaldehyde have been quantified and correlated to θ values.

Impact of NO_2 preliminary adsorption on acetaldehyde irreversibly adsorbed fraction / Figure 36 shows the amount of irreversibly adsorbed acetaldehyde per surface unit as a function of θ, i.e. $NO_x^-{}_{(ads)}$ surface coverage. The vertical error bars are determined by the minimum and maximum q_{irr} values quantified from the repeated experiments. The horizontal error bars correspond to the uncertainty related to θ as reported in Table 2. It can be noticed in Figure 36 that the irreversibly adsorbed fraction decreases with the increase of TiO_2 surface coverage by $NO_x^-{}_{(ads)}$ species. At high surface coverage, irreversibly adsorbed acetaldehyde (q_{irr}) reaches a minimum value of 1.3 ± 0.5 µmol m^{-2}, which corresponds only to 12% of the irreversibly adsorbed amount on fresh TiO_2 surface. This result emphasizes the negative impact of NO_2 preliminary adsorption on acetaldehyde irreversible adsorption.

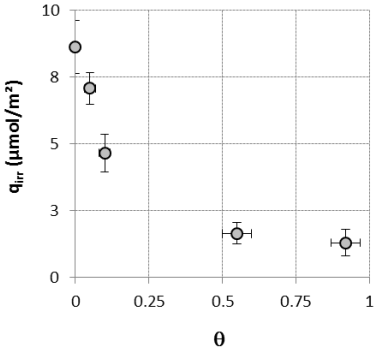

Figure 36 - Irreversibly adsorbed acetaldehyde fractions on TiO_2 as a function of θ, i.e. $NO_x^-{}_{(ads)}$ surface coverage. Acetaldehyde adsorption on fresh and aged TiO_2 is performed under dry air and at 296 K.

The first hypothesis that can be proposed to explain this significant impact is the competitive adsorption between one $NO_2^-{}_{(ads)}$ and/or $NO_3^-{}_{(ads)}$ ad-species and one acetaldehyde molecule to access Ti^{4+} sites. If this hypothesis were valid, it would mean that the adsorption of one $NO_x^-{}_{(ads)}$ species would prevent the adsorption of one acetaldehyde molecule. However, a significant discrepancy can be pointed out regarding the corresponding ratio. Indeed, Table 28 reports the quantified amounts per surface unit of irreversibly adsorbed acetaldehyde for the various θ values. From these values $-\Delta q_{irr}$ has been calculated. It represents the absolute value of the difference between irreversibly adsorbed acetaldehyde (q_{irr}) on fresh TiO_2 surface and irreversibly

adsorbed acetaldehyde (q_{irr}) on corresponding NO_2 exposed TiO_2 surface (θ). In addition to that, the $-\Delta q_{irr}$ / $q(NO_x^-{}_{(ads)})$ ratio is also calculated for each θ value. It represents the average number of acetaldehyde molecule prevented from adsorbing per one $NO_x^-{}_{(ads)}$ species present on TiO_2 surface. Remarkably, at low θ, this ratio reaches values as high as 8 to 10, meaning that the presence of one $NO_x^-{}_{(ads)}$ species on the surface prevents the adsorption of 8 to 10 acetaldehyde molecules. Subsequently, a simple competitive adsorption is not satisfactory to explain the negative impact of NO_2 ageing on acetaldehyde adsorption. Remarkably, the $-\Delta q_{irr}$ / $q(NO_x^-{}_{(ads)})$ ratio is not constant with the different investigated θ values. Indeed, it drops down to 2.2 for θ = 0.92 which is the lowest values.

The impact of $NO_x^-{}_{(ads)}$ on acetaldehyde irreversible adsorption is remarkable; the observed phenomena may result from the combination of two main effects related to the pre-adsorption of $NO_x^-{}_{(ads)}$ species:

❶ According to the literature [201][202], acetaldehyde adsorption scarcely leads to the adsorption of single acetaldehyde molecules on TiO_2 surface, but mostly produces 2-butenal through β-aldolization and dehydration reactions. Such reactive adsorption indirectly promotes acetaldehyde adsorption on TiO_2 surface by consuming adsorbed acetaldehyde. 2-butenal, as well as acetaldehyde, adsorbs on Ti^{4+} sites through carbonyl function groups. Thus, it can be suggested that the competitive adsorption of $NO_x^-{}_{(ads)}$ on Ti^{4+} sites may also impact 2-butenal adsorption. Therefore, it can be suggested that the covering of one Ti^{4+} site by a $NO_2^-{}_{(ads)}$ or $NO_3^-{}_{(ads)}$ species may prevent the irreversible adsorption of two acetaldehyde molecules. Even if this consideration could not be sufficient to explain the massive negative impact of $NO_x^-{}_{(ads)}$ pre-adsorption on acetaldehyde adsorption, since it would decrease the $-\Delta q_{irr}$ / $q(NO_x^-{}_{(ads)})$ ratios only by a factor 2, it has to be considered as one of the possible impacts of pre-adsorbed $NO_x^-{}_{(ads)}$ species.

Table 28 - Acetaldehyde adsorbed amounts on fresh and NO_2 exposed TiO_2 surface. Decreases in adsorbed acetaldehyde amounts $-\Delta q_{irr}$ and $-\Delta q_{irr}$ / $q(NO_x^-{}_{(ads)})$ are determined from fresh and NO_2 exposed acetaldehyde adsorption data.

ϑ	Acetaldehyde q_{irr}	$-\Delta q_{irr}$	$-\Delta q_{irr}$ / $q(NO_x^-{}_{(ads)})$
	µmol m^{-2}	µmol m^{-2}	
0.00	8.61 ± 0.28	0	Ø
0.05	7.07 ± 0.34	1.52	8.0
0.10	4.66 ± 0.68	3.93	10.3
0.55	1.65 ± 0.09	6.94	3.4
0.92	1.29 ± 0.41	7.3	2.2

❷ $NO_x^-{}_{(ads)}$ species may not only impact 2-butenal adsorption but also 2-butenal formation. As reported by Raskó and Kiss [201] 2-butenal is produced through aldol reaction by consuming one lattice oxygen $O^{2-}{}_{(lattice)}$ from TiO_2 surface. Furthermore, as reported in Equation 25, on TiO_2 surface, the intermediate species NO^+ necessarily consumes lattice oxygen $O^{2-}{}_{(lattice)}$ to produce NO_3^-. Therefore, it can be proposed that the pre-adsorption of NO_2 on TiO_2 surface could significantly decrease the amount of available $O^{2-}{}_{(lattice)}$ required for 2-butenal formation. As a consequence, 2-butenal formation could be hindered, which would considerably decrease irreversibly adsorbed acetaldehyde fraction.

Impact of NO_2 preliminary adsorption on acetaldehyde reversibly adsorbed fraction / Figure 37 reports the adsorption isotherms of the reversibly adsorbed acetaldehyde fractions for different TiO_2 surface ageing by NO_2 at 296 K. Isotherms are obtained from acetaldehyde adsorption and flushing experiments. For each θ value, experiments have been performed for different acetaldehyde inlet concentrations ranging from 5 to 300 ppm. It can be assumed in Figure 37 that, irrespectively of the surface ageing θ, the reversibly adsorbed fraction (q_{rev}) depends on the gas phase acetaldehyde concentration accordingly to Langmuir model [106], as described in Equation 29.

In Equation 29, q_{rev} (µmol m^{-2}) represents the amount of acetaldehyde adsorbed on TiO_2 surface at equilibrium, q_{revm} (µmol m^{-2}) is the maximum adsorbed amount corresponding to surface saturation, K represents the adsorption constant, and C is acetaldehyde gas-phase concentration at equilibrium. The fitting curves reported on Figure 37 were obtained from regression using Langmuir model on experimental data. Regressions are used to determine the values of K and q_{revm}. Figure 38 reports the evolution of q_{revm} and K as a function of θ, from fresh (θ = 0) to aged (θ = 0.92) TiO_2 surface by NO_2.

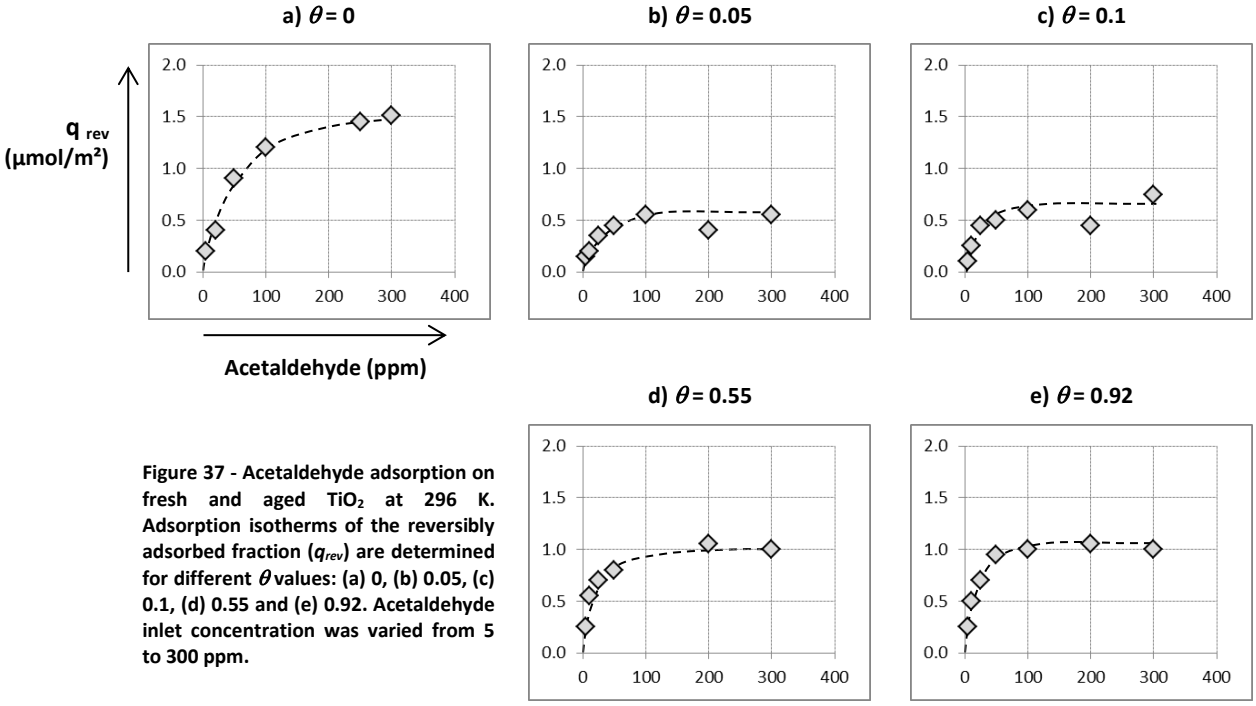

Figure 37 - Acetaldehyde adsorption on fresh and aged TiO_2 at 296 K. Adsorption isotherms of the reversibly adsorbed fraction (q_{rev}) are determined for different θ values: (a) 0, (b) 0.05, (c) 0.1, (d) 0.55 and (e) 0.92. Acetaldehyde inlet concentration was varied from 5 to 300 ppm.

$$q_{rev} = q_{revm} \times \frac{K.C}{1 + K.C}$$ **Equation 29**

It can be noticed on Figure 38 (a) and (b) that, compared to clean TiO_2 surface, the various surface ageing strongly impact q_{revm} as well as *K*. Indeed, the presence of $NO_{x\ (ads)}^-$ on the surface decreases the amount of reversibly adsorbed acetaldehyde even for the lowest values of θ. For instance, as soon as θ reaches 0.05, q_{revm} is decreased by 65%. Interestingly, q_{revm} slightly varies with increasing θ, but uncertainties on q_{revm} do not make possible the determination of any clear tendency. Considering that the reversibly adsorbed fraction of acetaldehyde mainly occurs on OH surface group, the first hypotheses to explain this behaviour would be the decrease of OH surface groups by $NO_{x\ (ads)}^-$ species. Indeed, Hadjiivanov et al [200] demonstrated that, on TiO_2 surface, the adsorbed NO_2 and/or NO_X^- species increase the surface acidity by consuming, the basic surface OH groups. Therefore, it can be proposed that the lowering of surface OH group density due to NO_X^- species may decrease the fraction of reversibly adsorbed acetaldehyde.

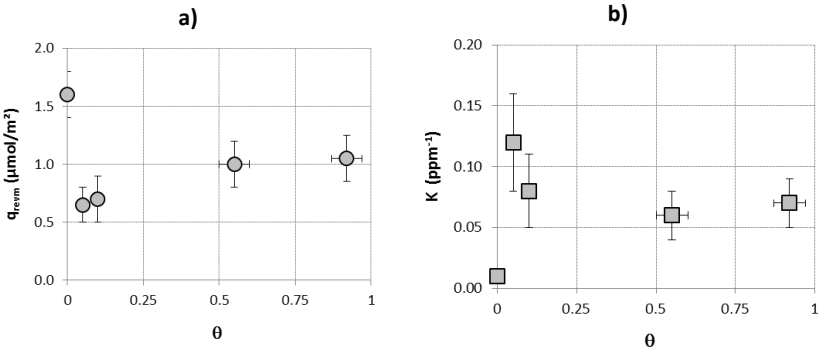

Figure 38 - Evolution of a) maximum reversibly adsorbed amounts of acetaldehyde (q_{revm}), and b) reversibly adsorbed acetaldehyde adsorption constant (*K*), reported as a function of NO_2 ageing on TiO_2 surface, i.e. θ. These data are determined from Langmuir model regression using experimental isotherms.

Beside, a second hypothesis could be raised; indeed, the presence of $NO_{x\ (ads)}^-$ species may considerably change the adsorption mode of reversibly adsorbed acetaldehyde. This hypothesis is supported by the observtion of *K* variations with θ. Surprisingly, the adsorption constant of acetaldehyde is multiplied by a factor ranging from 7 to 11 as soon as $NO_{x\ (ads)}^-$ species are present on TiO_2 surface. This phenomenon suggests that the interaction between acetaldehyde and aged TiO_2 surface is probably changed in nature, compared to clean TiO_2 surface. The ionic structure of TiO_2 adsorbed $NO_{x\ (ads)}^-$ species may induce stronger electrostatic interactions between acetaldehyde and the aged photocatalyst surface. This hypothesis is supported by the work of Rodriguez et al.

[XXX] who reported that adsorbed NO_X^- species modify the thermochemical stability of O vacancies on TiO_2 surface and facilitates their migration from bulk to the surface which could provide new adsorption sites. The investigation of TiO_2 surface ageing and subsequent acetaldehyde adsorption using diffuse reflectance infrared spectroscopy could help identifying the nature of reversible adsorption sites.

Conclusion /

Beside adsorption and subsequent oxidation of VOCs, the presence of NO_2 in the plasma-sorbent treated effluent may considerably impact the surface chemistry of metal oxide based sorbents.

First, this study evidenced that, depending on TiO_2 surface coverage by NO_2, at room temperature, NO_2 adsorbs in a reactive way by evolving NO in the gas phase and leading to two chemisorbed nitrates. A new NO_2 adsorption mechanism on TiO_2 at room temperature has been proposed and evidenced by quantitative measurements performed downstream a breakthrough reactor. Interestingly, based on the proposed mechanism, it has been evidenced that it is possible to control the coverage rate of TiO_2 surface by $NO_{x\,(ads)}^-$ species, namely $NO_{2\,(ads)}^-$ or $NO_{3\,(ads)}^-$.

Second, the adsorption of acetaldehyde on TiO_2 has been qualified and quantified on fresh and NO_2 aged TiO_2 surface. The quantities of irreversibly and reversibly adsorbed fractions, as well as the adsorption constant *K*, are impacted by the preliminary adsorption of NO_2. NO_2 preliminary adsorption tends to decrease the amount of irreversibly adsorbed acetaldehyde. This effect is characterized by the $-\Delta q_{irr} / q(NO_{x\,(ads)}^-)$ parameter and varies with $NO_{x\,(ads)}^-$ species. The effect of direct competitive adsorption combined with the hindering of acetaldehyde condensation on the surface are proposed to explain the observed phenomenon. Similarly, the reversibly adsorbed fraction of acetaldehyde is negatively impacted by NO_2 preliminary adsorption. The first hypothesis proposed to explain this behaviour if the consumption of OH groups by $NO_{x\,(ads)}^-$ species. However, considering the sudden variation of the adsorption constant *K* for the lowest surface coverages by $NO_{x\,(ads)}^-$ species, it is suggested that a new adsorption mode of acetaldehyde is induced by the presence of $NO_{x\,(ads)}^-$ species on TiO_2 surface, this could be confirmed using *in-situ* spectroscopy of adsorbed species such as DRIFTS (Diffuse Reflectance Infrared Fourier Transform Spectometry).

This study quantitatively evidences for the first time the remarkable impact of NO_2 preliminary adsorption on the consecutive adsorption of a VOC on TiO_2. It is clearly shown that the presence of $NO_{x\,(ads)}^-$ species on TiO_2 surface modifies the surface chemistry and the subsequent VOC sorption properties of TiO_2. Thus, this result questions the long term behaviour of TiO_2 when used as a coupling material in-side or downstream a plasma discharge. Considering that, in the case of plasma-material coupling, the role of TiO_2 is highly related to its sorption properties, long term performances of such processes should be addressed. Similarly, in catalytic or photocatalytic processes, the decrease of VOC adsorption on TiO_2 may considerably hinder the global conversion rate of VOCs. These aspects should be investigated in order to give new insights on the long term performances of heterogeneous oxidation processes under real operating conditions.

These results have been obtained through the ¨PhD Theses of Loganathan Sivachandiran and Frédéric Batault in the context of ANR RAMPE project and Institut Carnot PhotoCair project. They have been valorised by a first publication in *Applied Catalysis B: Environmental* [18] in 2013 and a second in *Chemical Engineering Journal* [27] in 2015.

D-7 MAIN OUTCOMES OF THE RESEARCH AXIS

The investigated approach in plasma-material coupling consists in adsorbing the pollutant on a porous adsorbent which is sequentially regenerated by plasma; the proposed approach offers interesting possibility from fundamental understanding to applied processing : (i) from a fundamental point of view, this approach makes possible the distinction between volume and surface phenomena, (ii) the accurate characterization of VOC adsorption onto the coupling material and reaction combining in-situ adsorbed phase and gas phase monitoring techniques enables complete characterization of the process carbon mass balances, (ii) from an applied point of view, it has been evidenced that in the case of IPA treatment using MnO_2 as coupling material, the sequential regeneration of saturated sorbents by plasma consumes 14 times less energy and non-thermal plasma regeneration offers higher mineralization than direct thermal treatment, and better sorbent regeneration compared to *post-situ* (ozonolysis) process.

Through the PhD theses of Loganathan Sivachandiran [2] and Christelle Barakat [4], both fundamentals and applied aspects of the sorbent coupling have been investigated. Interestingly, obtained results were used by AL-KO engineers to design AL-KO PURE. This system is devoted to the treatment of indoor airstreams containing ppb levels of VOCs. AL-KO PURE will be on the market in the course of the year 2015. A first version was installed in the LPP lab to perform a set of performance tests to evaluate the abatement of several selected VOCs.

The key point of such process is the pre-concentration step of the targeted pollutants on a sorbent:

➲ oxidative species are directly generated in the sorbent surface vicinity to optimize reactions,
➲ surface chemistry of the sorbent can be used to enhance oxidation as synergetic effect,
➲ emission of side-products is prevented not to generate secondary contaminants,
➲ residence time of pollutants is high and mineralization (conversion into CO_2) is enhanced.
➲ the discharge is sequentially ignited leading to significant energy savings,
➲ the process is operative for any concentration range, even indoor ppb levels, since the pre-concentration step buffers pollutant concentration fluctuations.

So far, only the feasibility of sequential adsorption/non thermal plasma regeneration process was evidenced, even if the crucial role of water vapour has been thoroughly addresses, model VOCs have been used (isopropanol, acetone) far from typical indoor air conditions. Nevertheless, these preliminary investigations emphasized the crucial role of:

- **sorbent surface chemistry (ozone decomposition, redox properties),**
- **sorbent morphology (porosity, specific surface),**
- **pollutant adsorption parameters on the sorbent (adsorption constant, maximum adsorbed amount)**
- **water interaction with the considered sorbent and the targeted pollutants,**
- **sorbent physical impact on plasma deposited energy.**

Based on the results obtained throughout this research axis, future development are oriented toward the development of tailored material to be coupled with plasma. The use of commercially available materials was a first step, but it does not provide a sufficient and reliable range of (i) specific surfaces, (ii) morphology, (iii) porosity and (iv) crystalline phases. Therefore, the synthesis of the targeted materials with required characteristics is targeted. Metal oxides characterized by labile oxygen atoms could be especially selected and investigation should be focused on CeO_2. Meanwhile, experimental developments have to be carried on to be able to monitor the material surface even under non-thermal plasma exposure. The synthesis of materials optimized for plasma coupling may also lead to the development of specific treatment, such as the individual abatement of formaldehyde.

These aspects are detailed in Part-F as research perspectives.

Part-E PHOTOCATALYTIC OXIDATION OF VOCs UNDER TYPICAL INDOOR AIR CONDITIONS

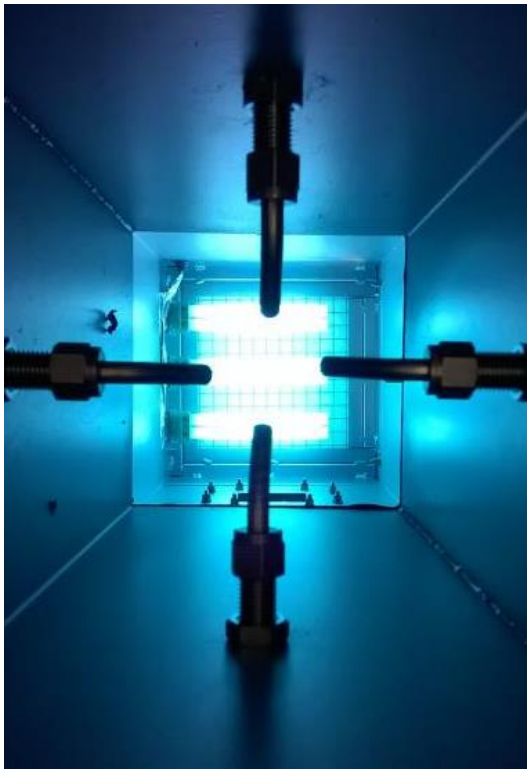

This section aims at giving an overview of the main results I obtained in the framework of indoor air VOC photocatalytic oxidation. This research axis represents a significant step forward in the domain of photocatalysis applied to indoor air treatment. It has been achieved in a context where photocatalysis was greatly questioned regarding its performances and, above all, its effective innocuity for indoor air. Our approach did not consist in unreasonably promoting photocatalysis, but in giving facts and results to assess its applicability to tangible indoor air problematic.

First, some basics are recalled about photocatalysis and its application to indoor air problematic. Then, experimental developments achieved to address this question are presented. Obtained results are comprehensively reported in two steps: (i) complete investigation of the ppb level reaction (kinetic of primary pollutant removal, reaction intermediates, mineralization, carbon mass balances), (ii) understanding multiple VOC photocatalytic treatment through sorption parameter determination.

Reported results have been obtained throughout the PhD theses of Olivier Debono [1], and Frédéric Batault [3] in the context of PhotoCOV and PhotoCair research projects

E-1 PHOTOCATALYSIS versus INDOOR AIR

About basics of photocatalysis / Photocatalysis is an advanced oxidation technology based on the activation of a semi-conducting material using a proper radiation. For efficiency, operation and cost reasons the most widespread photocatalyst is TiO_2. This material can be activated by incident wavelengths lower than 390 nm, leading to the creation of photo-induced electron-hole (e^-/h^+) pairs in the material lattice. These pairs mainly recombine in the material; however, some of them can reach the semi-conductor surface and get involved into oxidation and reduction reactions with the various compounds adsorbed onto TiO_2.

As the photocatalyst is placed in ambient air, major species interacting on TiO_2 surface are H_2O and O_2. Considering the reaction with photo-generated holes, H_2O leads to the formation of adsorbed hydroxyl radicals (HO°); in parallel, reaction of oxygen with electrons leads to the formation of $O_2^{\circ-}$ radicals. Thus, as TiO_2 is irradiated and in contact with air the photocatalyst surface get covered by highly oxidizing radicals.

When VOCs or any other environmental pollutant access the photocatalyst surface they can undergo adsorption onto TiO_2 as well. Then, pollutants may react according to two main paths: (i) reaction with photo-generated electrons or holes, corresponding to the *direct reactivity*; (ii) reaction with oxidizing species present on the photocatalyst surface corresponding to *indirect reactivity*. In both cases, observed reactions lead to the oxidation of the pollutants. Such oxidation reactions may allow the complete mineralization of organic compounds to produce CO_2 and H_2O when the contact time with the photocatalyst is long enough. The whole range of organic compounds is sensitive to photocatalytic oxidation because of the presence of HO° et $O_2^{\circ-}$ radicals, characterized by high oxidizing potentials. Other typical inorganic pollutants of air such as NO, NO_2 and O_3 are also characterized by a strong reactivity onto TiO_2 [104].

Photocatalytic air treatment process / Along the last thirty years, photocatalysis was initially applied to water purification in the 80s and 90s [203][204], then by the end of the 90s air treatment has been targeted [205]. Regarding air treatment applications, two approaches are generally considered:

➲ ***In the passive mode***, the photocatalyst is placed in the volume to be treated and natural diffusion of the pollutants in air ensures the contact between pollutants and photocatalytic media as well as the diffusion of photocatalytic reaction products. This type of treatment generally relies on the development of photocatalytically active building furniture such as cements, walls, paintings or glasses.

➲ ***In the active mode***, the air to be treated is extracted and sent onto the photocatalytic media. In order not to be drifted by the treated air flow, the photocatalyst has to be deposited and anchored on a substrate compliant with air treatment processes. Various substrates have been investigated: fibers, foams, grids, honeycombs, etc… The treated air may flow along the photocatalytic media or even cross the substrate. Such configurations are typically inserted into air treatment units or found in autonomous air treatment devices.

Active photocatalytic air treatment / Since the 2000s, the most widespread photocatalytic air treatment devices are the active one. In spite of the intense research activities about new photocatalytically active materials, the number of published scientific papers and patents per year dealing with active mode treatment along the last ten years is around ten times higher than those dealing with the passive mode [206]. In order to regulate the development of this market in France, standard have been published [84][85]. So far, these texts only deal with autonomous air treatment devices. However, ongoing projects such as Epurateur3 aim at widening the available standards to photocatalytic systems integrated to air handling units [207].

From air treatment to INDOOR air treatment / Till the early 2000s, most of scientific studies dealing with VOC abatement using photocatalysis applied to indoor air purification were achieved under experimental conditions non-compliant with the reality of indoor air in terms of VOC concentration, VOC diversity and humidity. Typically inlet concentrations in the investigated photocatalytic systems were ca. tens, hundreds or thousands of ppm. Authors considered that observed performances on the ppm range would be easily extrapolated to few ppbs. This point was extremely questionable considering the three orders of magnitude between tests and reality which may considerable impact (i) adsorption processes and (ii) reaction kinetic. In 2003, the photocatalytic oxidation of VOCs was interestingly investigated by Ao et al [208][209] with sub-ppm concentrations. Remarkably, authors investigated the photocatalytic oxidation of benzene, toluene, ethyl-

benzene and xylene with 200 ppb inlet concentration and in the presence of NO in order to take into account the cocktail effect of indoor air pollutants. In 2008, the wide diversity of VOCs in indoor air has been first addressed by Hodgson et al [210]. Authors considered two mixtures of typical indoor air VOCs, one with 10 VOCs representative of household cleaning products, another containing 27 VOCs characterized by high occurrence in indoor air. Finally, through the development of efficient analytical devices and compliant reactors, Sleiman et al [211] and more especially Olivier Debono, during is PhD at Ecole des Mines [1] and through his published papers [15][17], investigated (i) the reaction pathways and kinetics of VOC photocatalytic oxidation at typical ppb levels, (ii) the nature of the reaction intermediates produced along the photocatalytic reaction, and (iii) the impact of relative humidity on the reaction to mimic realistic conditions.

In the context od my research activities, advances in the domain of photocatalytic air treatment at ppb level have been determined by the development of appropriate analytical devices in order to enable first the assessment of (i) primary pollutant abatement and (ii) side-product formation. One of the most problematic challenges of photocatalytic reaction characterization at ppb level was to quantify CO and CO_2 produced by the photocatalytic oxidation of few tens of ppb of VOCs. This challenge was successfully tackled by Olivier Debono during his PhD Thesis [1][15][17].

Structure of Part-E / First, the investigation of VOC photocatalytic oxidation is reported at ppb level. Kinetic is characterized and a special attention is paid to side product formation and mineralization. Carbon balances established in the ppb range are proposed to characterize the photocatalytic reaction on that typical indoor air concentration range. Then, the determination of VOC sorption parameter on TiO_2 is presented. Obtained data are discussed and used to interpret the simultaneous photocatalytic oxidation of 5 VOCs in a final section. Results presented and discussed in Part-E originate from the PhD Theses of Olivier Debono [1] and Frédéric Batault [3]. Most of the reported results have been published [15][17][25][24], some are currently under valorization.

E-2 EXPERIMENTAL DEVELOPMENTS FOR ppb RANGE INVESTIGATION OF PHOTOCATALYTIC REACTIONS

Model VOCs / Studies on the ppb range investigation of photocatalytic reactions have been performed using model VOCs. First, during the PhD of Olivier Debono [1], the individual behaviors of **toluene**, **decane**, **limonene** and **trichloroethylene** have been investigated on the ppb range. The first three VOCs have been selected (i) because of their high occurrence in indoor air, (ii) because of their different sources in indoor air and (iii) because of their contrasted chemical structure. Trichloroethylene is not a typical indoor air VOC but its behavior is highly questioned in the context of dry cleaning activities where photocatalytic treatment units have been employed to treat chlorinated VOCs. Moreover, it considerably differs from other VOCs regarding chemical and physical properties. In a second step, the individual behaviors of **formaldehyde**, **acetaldehyde** and **acetic acid** have been investigated during the PhD of Frédéric Batault [3]. These VOCs were selected in order to address (i) the behavior of the major carbonyl VOCs found in indoor air and (ii) the behavior of a typical carboxylic acid since this chemical family is regularly point out as poisoning or deactivating VOCs on TiO_2. The sorption parameters on TiO_2 of selected VOCs have been quantitatively determined. The obtained set of results has been used to interpret the mixing effect of multiple VOC photocatalytic degradation.

VOC generation system / A VOC generation system was developed in order to produce a controlled air flow containing from one to five VOCs at tunable ppb level. “Zero-air” is generated by a purification system combining zero air generators and pressure swing adsorption (PSA) devices, which remove VOCs, CO_2 and moisture from ambient air leading to residual amounts of VOCs and CO_2 respectively lower than 10 ppt and 10 ppb.

Calibrated gas cylinder of VOCs balanced in nitrogen or liquid VOCs placed in a pressurized stainless steel tank are used as concentrated VOC sources. Zero-air and gaseous VOC flows are regulated and diluted with appropriate ratios using mass flow controllers (MFC). For all experiments, the concentration of VOCs can be tuned from 50 to 900 ± 20 ppb. Before each experiment, the gas mixture is directly sent to the appropriate analytical system, by by-passing the batch reactor, in order to check the VOC input concentrations.

Relative humidity regulation system / Downstream the VOC generator the gas stream contains 10 ppm of H_2O corresponding to a relative humidity lower than 0.01%. Humidity measurements were performed by Fourier Transform Infrared Spectroscopy (FTIR) as described later. An additional gas line enabled the regulation of H_2O

concentration, i.e. relative humidity, at the outlet of the VOC generator to 15 500 ppm; corresponding to a relative humidity of 50% at 25°C. In order to investigate the influence of water vapor, reactions were performed in the presence of (i) 10 ppm of water, so-called dry conditions, or (ii) 15 500 ppm of water, so-called wet conditions.

Reaction Chamber / Photocatalytic experiments were carried out in a 120 L Pyrex chamber developed and described by Olivier Debono during his PhD [1]. Briefly, this cylindrical reaction chamber is 935 mm high with an inner diameter of 470 mm. This large volume allows the sampling and analysis of the reaction chamber at each step of the reaction advancement. UV irradiation is obtained from nine *PL-L-40 Phillips* UV lamps emitting a broad band centered at 365 nm and without any emission below 350 nm. It was determined that the photon flux is homogeneous in the chamber with an average of 10 ± 1 mW cm^{-2} using a spectro-radiometer in 70 different spots of the reaction chamber. The temperature is regulated at 23 ± 1 °C using four fans located at the back of the UV insulating box. The photocatalyst powder (100 mg) is sieved on a Pyrex plate in order to ensure the dispersion of the material. The circular Pyrex support is positioned 5 cm above the bottom of the reactor. Before each experiment, the chamber is purged with 50% humid air, under UV irradiation, for 12 hours in order to clean the internal surface of the chamber and the photocatalyst as efficiently implemented by Debono et al [OD Toluene]. This procedure ensures the reproducibility of the experiments.

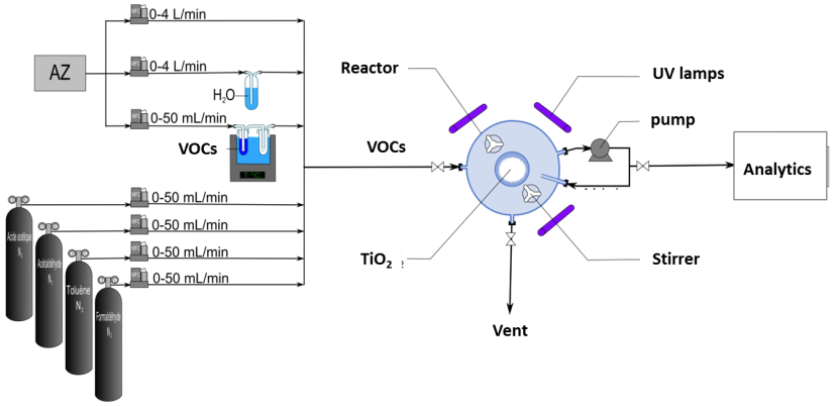

Figure 39 – Upper view of the experimental setup dedicated to photocatalytic investigation of VOC oxidation at ppb levels in the 120 L reaction chamber, retrieved from [3].

All the experiments were performed under static and dry air conditions. In order to reach the adsorption equilibrium, in dark conditions, the targeted concentrations of VOC at 500 mL min^{-1} total flow rate are sent into the chamber for 14 hours. Then, the reaction chamber is closed. The chamber sealing has been evaluated through VOC static decay along 24 hr and remains lower than 5% [1]. Before switching on the UV-irradiation, initial concentrations of VOC are measured twice. At t = 0 the UV-irradiation is started, then, the reaction chamber mixture is regularly monitored along the irradiation time in order to characterize the removal kinetics. Compared to dynamic flow reactors, the use of a batch reactor, or stirred tank reactor, to investigate VOC removal makes possible the characterization of the complete temporal decay, thus encompassing the various advancements of the oxidation reaction, and making accessible the reaction kinetic.

Gas phase analyses / Gas phase analyses are performed using mainly three different analytical devices: (i) Gas Chromatography (GC) coupled to MS and FID for VOC identification and quantification, (ii) derivatization and liquid Chromatography (HPLC) coupled to UV spectrometry for carbonyl VOC monitoring, (iii) Fourier Transform Infrared (FTIR) spectroscopy for CO and CO_2 measurements and (iv) SIFT mass spectrometry for VOCs.

Gas Chromatography For each VOC analysis by GC, 1 L of the gas mixture is sampled online (Gerstel Thermo-Desorption System, TDS) from the chamber and pre-concentrated on a multi-sorbent cartridge (Carbopack X; Carbopack B; Carbopack C) at a constant flow rate of 100 mL min^{-1}. A maximum of 10 L, i.e. less than 10% of the total chamber volume, is sampled in order not to significantly modify the reaction mixture inside the chamber during the photocatalytic treatment. Therefore, 10 analyses are allowed and performed during each experiment to determine the temporal profiles of VOCs and reaction intermediates by GC. After thermal desorption of the cartridge, compounds are conducted by He used as carrier gas toward a cryogenic trapping capillary tube (Cooled Injection System, CIS), filled with Carbopack B, in order to refocus the analytes at -100 °C. The gas chromatographic analysis is carried out by a 6890N/5975B type instrument from Agilent Technologies equipped with an Agilent DB-5MS

chromatographic column (60 m × 0.32 mm × 1 µm). Samples are eluted using a thermal ramp of 15 °C min^{-1} from 0 to 250 °C. This column is connected to two different detectors using a calibrated Y-shaped restriction. Therefore, analytes are concurrently transferred to (i) a Flame Ionization Detector (FID), dedicated to compound quantification, and to (ii) a Mass Spectrometer (MS) dedicated to compound identification. The parameters of the TD-GC analytical system are summarized in Table 29.

Table 29 - Thermo-desorption and gas chromatography parameters.

Thermodesorption system	Initial temperature	10	°C
	Temperature ramp	50	°C.min^{-1}
	Final temperature	250	°C
	Final time	10	min
	Flow rate	50	mL.min^{-1}
Refocusing on CIS and injection into GC	Initial temperature	-100	°C
	Temperature ramp	12	°C.s^{-1}
	Final temperature	250	°C
	Final time	10	min
Gas Chromatographic system	Initial temperature	0	°C
	Initial time	4	min
	Temperature ramp	15	°C.min^{-1}
	Final temperature	250	°C
	Flow rate	4	mL.min^{-1}

The FID calibrations of the different intermediate compounds identified using the mass spectrometer were performed in the ppb range. These substances were obtained from two different sources: (i) certified gas cylinders from Praxair, or (ii) vaporized liquid VOCs from Aldrich. The detection limit of each compound quantified in this study ranges from 5 to 50 ppt.

Derivatization and liquid chromatograpghy / Formaldehyde is usually reported as a major by-product during the photocatalytic oxidation of VOCs, however, the above-mentioned GC analytical method is unable to detect this carbonyl species. Therefore, gas samples were collected online on Waters Silica cartridges impregnated with 2,4-dinitrophenylhydrazine (DNPH). More generally, this analytical method enables the quantification of the lightest carbonyl compounds. Apart from formaldehyde, obtained results were crosschecked with GC quantification to ensure the metrological connection of the various analytical methods. The derivatization of carbonyls is achieved at a flow rate of 100 mL min^{-1} for a total volume of 1 L and leads to the formation of hydrazones which are eluted and analyzed by high performance liquid chromatography (Waters Alliance 2695) coupled with a UV detector (Waters 2487). The detection limit obtained for formaldehyde using this method is 5 ppb.

FTIR spectroscopy / Instrument specifications for CO and CO_2 analyses are detailed in section C-7 p43

SIFT mass spectrometry / Instrument specifications are detailed in section C-7 p43.

Photocatalyst adsorbed phase analyses by DRIFTS / In the case of limonene photocatalytic oxidation, the in-situ monitoring of the photocatalyst surface under UV irradiation has been performed directly in a DRIFT cell (Harrick, Praying Mantis) coupled with a FTIR spectrometer (Nicolet 6700).The inlet of the cell is connected to the VOC generation system. A 20 mg bed of TiO_2 particles is placed on the grid inside the DRIFT cell. This configuration allows a constant gas flow through the catalyst bed. Two ellipsoidal mirrors focus the infrared beam at the upper part of the catalyst bed and collect the scattered light to the MCT detector. UV irradiation of TiO_2 is performed from the outer part of the DRIFT cell. UV-LEDs are used to irradiate the photocatalyst surface with a photon flux of 2.5 mW cm^{-2}. The emission spectrum of the UV-LEDs is centered at 365 nm.

Prior to any photocatalytic experiments, the catalyst is thermally pretreated at 400°C for 1 hour under zero air flow (250 mL min^{-1}) in order to clean the surface and ensure reproducibility. After thermal pretreatment, a reference spectrum with 500 scans is recorded at room temperature. Then the cell is swept with 5 ppm of limonene diluted in air under a 250 mL min^{-1} air flow. Under these conditions, the adsorption equilibrium of limonene can be monitored by DRIFTS. The equilibrium is reached ca. within one hour of adsorption. Before UV irradiation, the cell is thoroughly flushed under zero air for about 2 hours in order to remove the reversibly

adsorbed fraction of limonene. Finally, UV irradiation is performed under zero air flow and the evolution of the adsorbed phase is followed by DRIFTS.

Particulate phase analyses / In the case of limonene photocatalytic oxidation, particle size data have been collected every four minutes over 44 channels in the range 5.5 to 350.4 nm using a Scanning Mobility Particle Sizer (SMPS) Grimm 5403. The SMPS consists of a Condensation Particle Counter (CPC) coupled with a Diffusion Mobility Analyzer (DMA). Aerosols are sampled at a flow rate of 300 mL min^{-1}, through a ¼" stainless steel tubing placed 10 cm above the photocatalyst bed. The residence time of the particles in the tube was estimated to be 1.6 s. In order to keep the overall reactor volume (hence the pressure) constant, experiments are performed in a dynamic state where zero air is added in the reactor to compensate for each sample taken. Dilution was taken into account as explained in the Results section.

E-3 KINETIC OF PHOTOCATALYTIC VOC OXIDATION AT ppb LEVELS

First approach with limonene / The decay profile corresponding to 750 ppb d-limonene photocatalytic degradation is plotted as a function of irradiation time and reported on Figure 40. In order to describe the evolution of the d-limonene degradation rate, Equation 30 is used. In Equation 30, *r* is the VOC removal rate as a function of reactant concentrations C_1 and C_2; *k* is the reaction rate constant, n_1 and n_2 are the partial reaction orders regarding each reactant. During the photocatalytic oxidation reaction, limonene reacts either with photo-generated holes or with hydroxyl and superoxide radicals formed on the surface of the photocatalyst. Considering a steady-state approximation for these reactants, which is all the more valid since limonene initial concentration is in the ppb range, Equation 30 can be simplified as reported in Equation 31. In Equation 31, *[lim]* represents the concentration of d-limonene, k_{app} is the pseudo reaction constant, *n* is the order of the reaction and *t* the irradiation time. Equation 32 results from the linearization of Equation 31.

$$r = k.C_1^{n_1}.C_2^{n_2} \qquad \textbf{Equation 30}$$

$$r = -\frac{d[lim]}{dt} = k_{app}.[lim]^n \qquad \textbf{Equation 31}$$

$$\ln\frac{-d[lim]}{dt} = n.\ln([lim]) + \ln(k_{app}) \qquad \textbf{Equation 32}$$

It is then possible to evaluate k_{app} and *n* from the linear regression of experimental data. Under our experimental conditions, a linear relationship is confirmed by plotting *ln (-d [lim] / dt)* as a function of *ln ([lim])* for three different experiments (Figure 40). It makes possible the evaluation of k_{app}, from the intercept at the origin, and *n*, from the slope of the linear regression fit. The value of *n* was found to be equal to 1.04 ± 0.06. Thus, the limonene photocatalytic removal can be described by a mono-exponential decay corresponding to a pseudo first-order kinetic. In addition, the average value of k_{app} was calculated as 0.23 ± 0.04 h^{-1}. The main results are: (i) photocatalytic reactions can be explored and described on the ppb range and (ii) the classically reported first order reaction observed on ppm range is still valid on the ppb range.

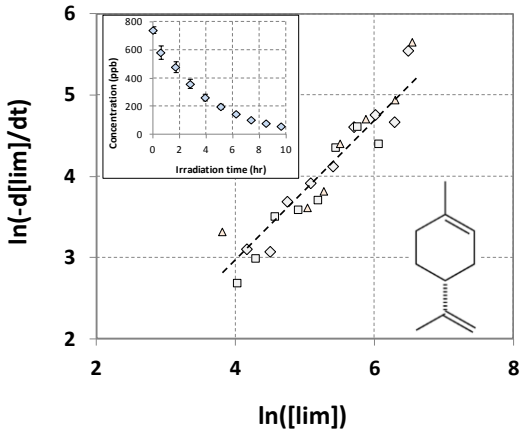

Figure 40 - Evolution of *ln(-d[lim]/dt)* as a function of *ln([lim])* obtained from three photocatalytic degradations of limonene on TiO_2 under dry air with 750 ppb initial concentration. Data are obtained from the temporal profiles of limonene photocatalytic oxidation reported in insert.

Impact of concentration and relative humidity on removal kinetic / The photocatalytic reaction kinetic has been investigated for other VOCs on the whole ppb range. The photocatalytic oxidations of toluene and decane were carried out for various initial concentrations ranging from 50 to 800 ppb under dry and wet conditions.

➲ ***Toluene /*** First, in order to investigate the experiment reproducibility, the photocatalytic removal of 800 ppb of toluene was successively investigated 5 times during 20 hours without any regeneration procedure between the degradations. Toluene, and more generally aromatic compounds are largely designated as poisoning or deactivating species in photocatalysis. The obtained removal profiles were characterized by a standard deviation lower than 10 ppb. The fact that toluene removal can be performed with such reproducibility indicates that no by-product compounds irreversibly poisoned the photocatalyst surface on short terms experiments. Nevertheless, the photocatalyst regeneration procedure has been performed between degradations to ensure long term experiment reproducibility. Decay profiles of toluene observed under dry air are reported in Figure 41 as a function of irradiation time.

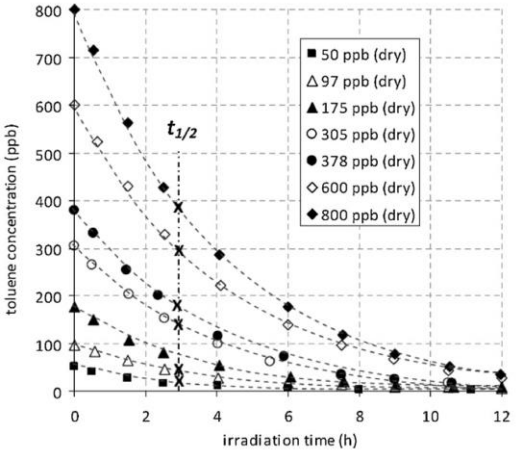

Figure 41 - Evolution of toluene concentration as a function of irradiation time during the photocatalytic oxidation of toluene under dry air.

The graphical determination of the half reaction time ($t_{1/2}$) under dry air for each reaction (Figure 41) indicates that this parameter does not depend on toluene initial concentration on the investigated concentration range. This point was noticed for both dry and wet series of experiments. Values of $t_{1/2}$ are 3.0 and 2.7 hr, respectively during dry and wet air toluene removal. The fact that $t_{1/2}$ does not depend on reactant initial concentrations suggests that toluene photocatalytic removal at ppb level is a pseudo-first-order reaction on the whole range.

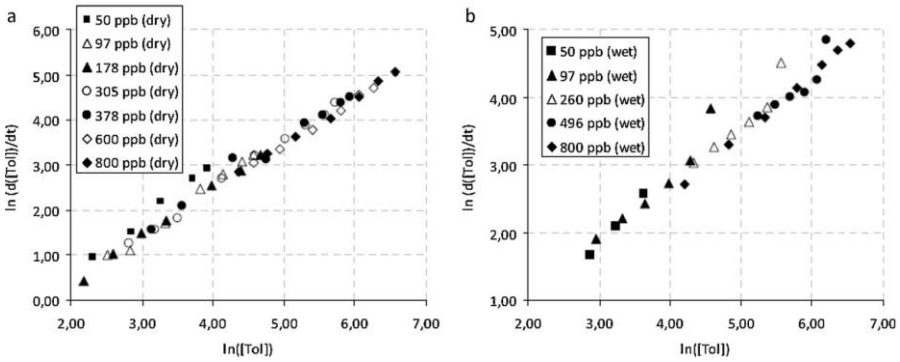

Figure 42 - Evolution of ln(d[Tol]/dt) as a function of ln[Tol.] : a) under dry air (10 ppm H_2O); b) under wet air (15 500 ppm H_2O).

Figure 42 reports the evolution of *ln(-d [Tol] / dt)* as a function of *ln([Tol.])* during photocatalytic reactions performed under dry (a) and wet (b) air for various toluene initial concentrations. Linear evolutions can be noticed under both conditions for each reaction. This linear behaviour enables the determination of the reaction order *n* and the reaction constant *k* for each photocatalytic reaction. Data obtained on same series of experiments (dry or wet) are characterized by a low dispersion. Therefore, average values were calculated for each condition. Average values of *n* are equivalent under dry and wet air, respectively 1.07 ± 0.06 and 1.03 ± 0.08, confirming for both series of experiments a pseudo-first-order reaction. On the contrary, reaction rate values appear to be slightly influenced by the presence of water vapour: 0.19 ± 0.03 h^{-1} and 0.22 ± 0.02 h^{-1} respectively under dry and wet air. In the presence of humidity, the minor increase of *k* is coherent with the

decrease of $t_{1/2}$, suggesting a slight enhancement of the photocatalytic reactivity due to the formation of HO° radicals. Nevertheless, the positive influence of water vapour on toluene disappearance is weak in comparison to the dispersion of the experimental data, it is not possible to evidence clearly any significant effect of H_2O.

➲ ***decane /*** Similar investigations performed with decane evidenced that (i) decane removal follows a pseudo-first order reaction kinetic on the ppb range as well and that (ii) *k* values tend to increase with the decrease of decane initial concentration, under both dry and wet air (Table 30). This trend is described by the Langmuir-Hinshelwood law that takes into account in the kinetic models several steps of the mechanism including the adsorption of the molecules onto the catalyst surface. The fact that the apparent kinetic constants depend on the initial concentrations also means that modeling each degradation rates by a first order reaction rate is also an approximation. In fact, the corresponding mechanisms are more complex.

Table 30 - Reaction constants of the photocatalytic oxidation of decane, C_0^{Dec} = 34 - 810 ppb; RH = 0 or 50 %.

Dry air		Wet air	
$[Dec]_0$ (ppb)	k (h^{-1})	$[Dec]_0$ (ppb)	k (h^{-1})
34	0.286 ± 0.003	53	0.440 ± 0.020
92	0.216 ± 0.001	94	0.340 ± 0.010
219	0.219 ± 0.002	283	0.202 ± 0.003
494	0.196 ± 0.003	500	0.175 ± 0.004
800	0.173 ± 0.001	810	0.132 ± 0.002
Average of coefficients ± standard deviation	**0.22 ± 0.04**	**Average of coefficients ± standard deviation**	**0.26 ± 0.13**

The influence of humidity on the degradation rate was studied for different alkanes in the past but any general trend cannot be extracted from those studies [212]. However, it seems that water vapour can have two contrary effects: (i) promotion of the degradation by the formation of hydroxyl radicals [213], (ii) for higher humidity, inhibition of the degradation by competition with VOCs for the adsorption on the active sites of TiO_2. When varying humidity, several studies showed that the two effects can be predominant, depending of the humidity; other studies reported that only one of these effects can be visible. For example, Twesme et al [214] reported that the degradation rates of several alkanes reach their maximum at a relative humidity of 40 % under 70° C. Below 40 %, promotion by hydroxyl radicals is predominant whereas, above 40 %, inhibition by a competition for adsorption become predominant. On the contrary, Shang et al [215] evidenced a continuous decrease of the degradation rate of heptane when the relative humidity is increased from 0 % to 60 %. This result was also obtained by Boulamanti and Philippopoulos [212] who reported a similar trend for several C_5-C_7 alkanes with water vapor concentrations ranging from 0 to 37 000 ppm. Those reported contradictory effects of humidity on alkane degradation rates may be attributed to the various experimental conditions used to operate degradation tests: concentration levels of alkanes, continuous or discontinuous VOCs supply to the reactor, temperature, investigated RH range. Looking at the obtained kinetic constants for decane on the ppb range, we can assume that water vapor, via hydroxyl radicals, has a very weak impact on photocatalytic oxidation kinetic under our experimental conditions.

Wrap up of toluene, decane and limonene photocatalytic removal at ppb level /

Likewise ppm range investigations, individual photocatalytic oxidations of toluene, decane and limonene are characterized by pseudo-first order kinetics. This behavior means that reaction rate is proportional to the respective VOC concentrations, this aspect is has definitely to be taken into account from a chemical engineering point of view in the designing of indoor air treatment devices.

As underlined by Lin et al [216], concentration changes in the lowest ranges induce remarkably high changes in the degradation rate compared to higher ranges of concentration. This behavior is related to the higher sensitivity of the adsorption step in the lowest concentration range. Regarding reaction constants usual behavior observed on the ppm range is a strong variability of reaction constants with VOC structures. This aspect is reported for instance by Raillard et al [217]. Such behavior is generally attributed to the chemical and physical properties of the VOCs which impacts the interaction between the VOC and the photocatalyst surface: VOC structure, VOC sorption parameters, solubility, Henry's constant, and reactivity toward HO° radicals. All these interactions typically result in highly contrasted behaviors between VOCs as illustrated by Alberici and Jardim [218] on the ppm range. As reported on Figure 43, first kinetic constants determined here on the ppb range for toluene, decane and limonene reveals very close values. Considering the

uncertainties associated to the determined values of *k*, and in spite of the contrasted structures of the VOCs, surprisingly no clear reactivity distinction can be made between the three VOCs, neither under dry air nor under wet air. Beyond the respective reactivity of the model VOCs under photocatalytic oxidation, another process may govern their removal kinetic: adsorption. Adsorption can be suggested as a significant influencing parameter in the ppb range photocatalytic oxidation of VOCs. Results reported on Figure 43 question the sorption behaviors of the three VOCs on the ppb range. This aspect is addressed in section E-8.

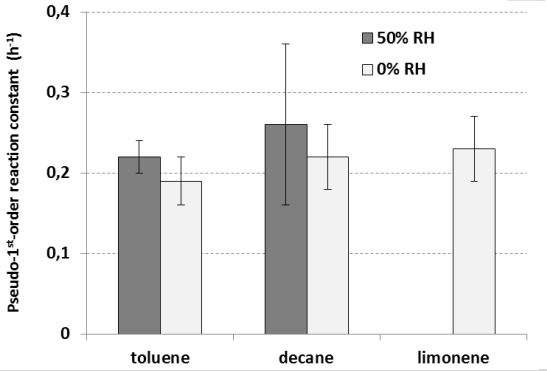

Figure 43 – Comparison of toluene decane and limonene pseudo-first order reaction rates determined on the ppb concentration range, under dry air (10 ppm H_2O, 0% RH) and wet air (15 500 ppm H_2O, 50% RH) for toluene and decane.

Distinctive behavior of trichloroethylene (TCE) / The removal kinetic of TCE has been investigated through three main degradation reactions with 100, 280 and 550 ppb initial concentrations both under dry (0% RH) and humid air (50% RH). The evolutions of TCE concentrations have been followed during a maximum of 6 hr. Temporal profiles of TCE are reported on Figure 44. Irrespectively of initial concentration and humidity, TCE removal profile unexpectedly exhibits a sigmoid shape: TCE degradation starts since the beginning of UV irradiation, but removal rate tend to increase. Within 4 hr, TCE is removed from the reaction chamber. Compared to toluene, decane and limonene, the increase in removal rate leads to shortened times for complete removal. Kim and Hong report TCE degradation rates 4 times higher than that of methanol and acetone and 20 times higher than that of toluene [219] on the ppm range. Our result qualitatively shows that with lower concentration by three orders of magnitude, the same phenomenon is still noticeable.

With a continuous feed of toluene and TCE, Young et al [220] observed that toluene conversion descreases beyond 24 hr treatments whereas TCE conversion keeps constant. They correlate these behaviors to the action of Cl° radicals produced by TCE photocatalytic oxidation and suggest that these radical may promote the photocatalytic reaction. This phenomenon could be valid even in the ppb range concentration.

Based on temporal profiles displayed on Figure 44, it can be calculated that TCE removal rate increases till an irradiation time ranging from 30 min to 1h30min depending on TCE initial concentration. Then it decreases till the end of the reaction and the reactant gradual exhaust. As noticed in the case of toluene, decane and limonene, a typical pseudo first order reaction is characterized by a continuous decline of the reaction rate along the whole reaction time span. Similarly to formerly studied VOCs, TCE is initially attacked by HO° radicals. Unlike toluene, decane and limonene, this attack leads to the formation of Cl° radicals which may react with TCE. According to NIST Kinetic Database, reaction constant between TCE and HO° radical is 20 times lower than the reaction constant between TCE and Cl° radicals [221]. Subsequently the increase of TCE reaction rate along the first hour of reaction can be related to the gradual production of Cl° radical.

Compared to dry air experiments, reaction rates calculated from wet air experiment are 1.5 times higher. Ou and Lo [222] as well as Li Puma [223] noticed such an inhibition effect of relative humidity from 10 to 90 % on TCE degradation rate with initial concentrations ranging from 1 to 80 ppm. Our results confirm the hindering effect of water vapor on ppb range reactions. Two hypotheses can be raised to explain the impact of RH:
❶ TCE adsorption capacity on TiO_2 is diminished in the presence of H_2O as suggested by Ou and Lo [222],
❷ Under humid air, the surface density of some species such as H_2O, $HO^{\bullet}$, H^+ or HO^- increase; they may react with Cl° radicals and subsequently diminish their available amount by scavenging effect.

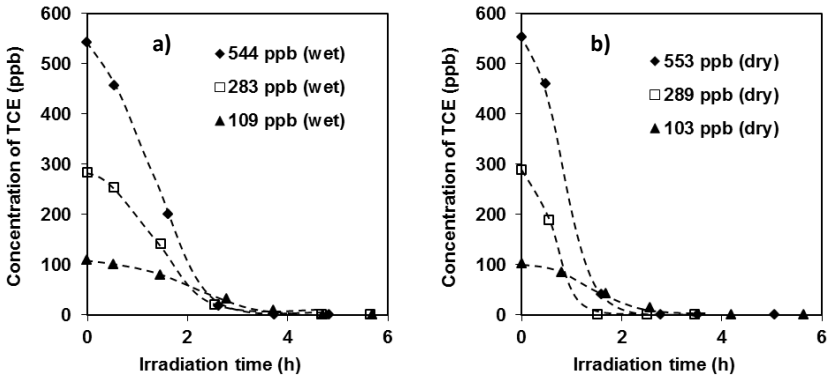

Figure 44 - Temporal evolutions of trichloroethylene concentration along its photocatalytic oxidation for various initial concentrations a) under dry air (10 ppm H_2O); b) under wet air (15 500 ppm H_2O).

Along the photocatalytic degradation of TCE, 5 reaction intermediates have been identifies and quantified: cloromethane, chloroethane, dichloromethane, trichloromethane and phosgene. The last three were already reported as reaction intermediates with ppm range initial concentrations of TCE [224][225]. Dichloroacetyle chloride is, with phosgene, the major reaction intermediates, but it has not been detected here.

Conclusion on TCE degradation at ppb level /

This study evidenced that the very specific kinetic behavior of TCE formerly evidenced on the ppm range is still valid on the ppb range. The production of Cl° radical is a key issue since it may not only impact the reaction kinetic but also it may induce cross-reactivity in the case of multi-VOC degradation. For instance, Cl° radicals generated by TCE degradation under typical indoor air conditions may react with aromatic rings if toluene is present in the treated air leading to chlorinated aromatic compounds as side-products.

The production of phosgene as reaction side-product is a key issue as well. Indeed, authors performing the ppm range photocatalytic degradation of TCE estimated that even if the formation of phosgene was observed, its production along ppb range treatment of TCE would be poorly probable. Based on our analytical development, we can assume that more than 150 ppb of phosgene are produced along the photocatalytic degradation of 550 ppb of TCE.
Considering that the irreversible toxicity threshold of phosgene for short term (1 hr) exposure is 500 ppb [226], the photocatalytic degradation of chlorinated compounds must be carefully addressed, even when applied to indoor air chlorinated VOC concentrations.

Multiple VOC removal kinetic / In order to get closer to typical indoor air conditions, the photocatalytic degradation of toluene, decane and TCE has been studied in the presence of 50% RH (15 500 ppm H_2O). Corresponding results are reported on Figure **45**.

Two distinct phases can be noticed. Prior to 18 hr of irradiation, the three model VOCs are characterized by a gradual concentration decrease. Toluene and decane are both impacted by the presence of other VOCs; their initial degradation rates calculated at t = 0 are respectively divided by a factor ca. 3 and ca. 2. The most impacted VOC is TCE. Indeed, the initial degradation rate of TCE is divided by a factor 40 and no more increase of the degradation rate can be noticed on the first hour of treatment. Interestingly, once toluene and decane conversion rate get higher than 80 %, i.e. after 20 hours of irradiation, a significant increase of the three degradation rates are noticed. Within one hour, toluene and decane are removed from the reaction chamber. The most striking effect is noticed on TCE temporal profile where the removal kinetic is radically changed.

Different axes have been investigated by Olivier Debono [1] to interpret these results evidencing a sequential treatment of the selected VOCS: (i) competition between the different VOCs to react with HO° radicals, (ii) competitive adsorption between the VOCs as regards of their potentially contrasted heats of adsorption on TiO_2, (iii) consumption of TCE generated Cl° radical by other VOCs than TCE. However, the lack of available data corresponding to the defined experimental conditions did not lead to any conclusive interpretation. Nevertheless, considering the temporal profiles the hypothesis of competitive adsorption was favored.

Subsequently, these results were the main motivation for deeper investigation of VOC adsorption on TiO_2 as reported in section E-8.

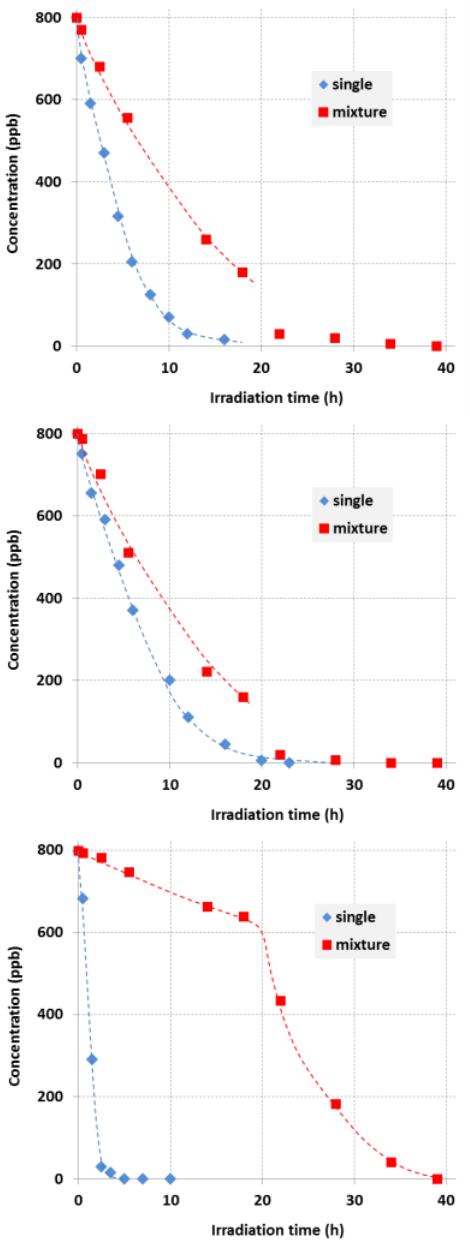

Figure 45 - Temporal evolutions of a) toluene, b) decane and c) TCE during their photocatalytic degradation in the presence of 50% RH, data obtained for single VOC degradation or mixture degradation are reported on the same graph.

Conclusion on primary VOC ppb level removal kinetics /

This first approach of VOC photocatalytic oxidation at ppb level confirmed that pseudo-first-order kinetics are applicable on ppb range to describe VOC degradation, except for the investigated chlorinated VOC. Reaction constants have been determined for individual VOC removal of toluene, decane and limonene. Interestingly, no significant effect of water vapor (0% vs. 50%) was evidenced for the considered VOCs. However, the impact of VOC mixture on the removal kinetic is considerable, even with only three VOCs in the ppb range. No reliable interpretation has been proposed at that time, but competitive adsorption is suggested as the governing phenomenon. Based on these results, this point has been specifically addressed further.

E-4 PHOTOCATALYTIC GAS PHASE REACTION INTERMEDIATES AT ppb LEVELS

Introduction / Thorough investigations of organic gas phase reaction intermediates and side-products have been performed for toluene, decane and limonene photocatalytic oxidation at ppb levels. The main objective of this study is to identify and quantify the widest diversity of reaction intermediates in order to assess the propensity of photocatalytic treatment to generate organic side products under indoor air conditions. First, lists of the identified and quantified reaction intermediates are given for each three model VOC. Then, a detailed discussion about limonene reaction intermediate study is proposed.

Toluene as primary pollutant / During toluene removal, reaction intermediates formation and removal were monitored with abovementioned analytical techniques. 15 VOC were evidenced in the reaction chamber gas phase. Compounds are listed in Table 31 and classified according to their chemical natures. The same reaction intermediate diversity was found for each reaction, irrespectively of toluene initial concentration (50-800 ppb). Among the identified reaction intermediates, 12 of them were quantified. Traces of benzene, phenol and propanal have been identified, but reliable quantifications have not been performed for these compounds because of the weakness of their signals. All VOC temporal profiles are characterized by (i) a formation period, (ii) a maximum concentration, (iii) a removal period. It is means that they do not accumulate in the chamber but could be removed with sufficient reaction advancement. The temporal position of the maximum is listed in Table 31 for each reaction intermediate.

Benzaldehyde, o-, m-, and p-cresols are characterized by the shortest maximum temporal positions, thus, they can be considered as toluene primary reaction intermediates in the gas phase. Indeed, Coronado and Soria [227] reported that toluene reaction onto TiO_2 leads to the formation of benzyl radical and subsequently, in the presence of O_2, to the formation of peroxybenzyl radicals. Then, benzaldehyde is formed and a HO° radical is released. Besides, cresols are produced by the direct attack of HO° radicals on the aromatic ring. Even if benzaldehyde appears as a key point into toluene photocatalytic oxidation pathway, the highest concentration of benzaldehyde in the gas phase does not exceed 3.5 ppb. Benzaldehyde is supposed to be rapidly oxidized into benzoic acid in the adsorbed phase by hydroxyl groups [228]. During the conducted experiments, no benzoic acid was detected in the gas phase. This compound, condensed at room temperature, accumulates on photocatalyst surface. Similarly, Marci et al [229] reported the presence of benzoic acid as reaction intermediate during toluene photocatalytic oxidation only in the adsorbed phase. However, this compound is sensitive to photocatalytic oxidation. For instance, benzene, identified as traces in the reaction chamber, may proceed from photo-Kolbe reaction on benzoic acid.

Aromatics	t_{MAX} (h)	D.L. (ppt)	***Ketones***	t_{MAX} (h)	D.L. (ppt)	***Aldehydes***	t_{MAX} (h)	D.L. (ppt)	***Others***	t_{MAX} (h)	D.L. (ppt)
Benzene	Ø	3	Acetone	>12	15	Formaldehyde	>14		2-methylfurane	1.5	5
Phenol	Ø	7	Butanone	8	12	Acetaldehyde	>14	43			
Benzaldehyde	1.5	5	M.V.K.	2.5	12	Acroleine	4	29			
o-cresol	1.5	5				Propanal	Ø	35			
m+p-cresol	1.5	6				Pentanal	2.5	9			
						Heptanal	2.5	7			

Table 31 - List of the reaction intermediates identified in the gas phase during toluene photocatalytic degradations. For each compound : "t_{MAX}" corresponds to the temporal position of the maximum concentration during the photocatalytic degradation of 800 ppbv of toluene; "D.L." indicates the detection limit of the compound using the GC analytical method.

Non-cyclic reaction intermediates originate from aromatic ring-opening reactions. Aldehydes are the major compounds in terms of diversity and concentration in the gas phase. Nevertheless, the presence of 2-methylfurane suggests recombination phenomena occurred in a minor way. Lightest reaction intermediates (acetone, acetaldehyde, formaldehyde) are characterized by the highest t_{MAX}. With 20 ppb maximum concentration, formaldehyde can be considered as the major gaseous reaction intermediate regarding concentration. This step of toluene photocatalytic oxidation pathway is rarely investigated in details by authors since it leads to the formation of numerous and various aliphatic compounds which are generally considered as sensitive to photocatalytic oxidation. Under our conditions, it appears that lighter compounds are not removed from the gas phase within 12 hour experiments. One hypothesis is that adsorbed reaction intermediates accumulated on the photocatalyst surface are slowly oxidized into acetone, acetaldehyde and formaldehyde several hours after toluene and gaseous reaction intermediates removal. This hypothesis could be confirmed

through the investigation of CO and CO_2 formation. The formation of CO and/or CO_2 after 14 hours of irradiation would be an evidence for adsorbed reaction intermediates photocatalytic oxidation.

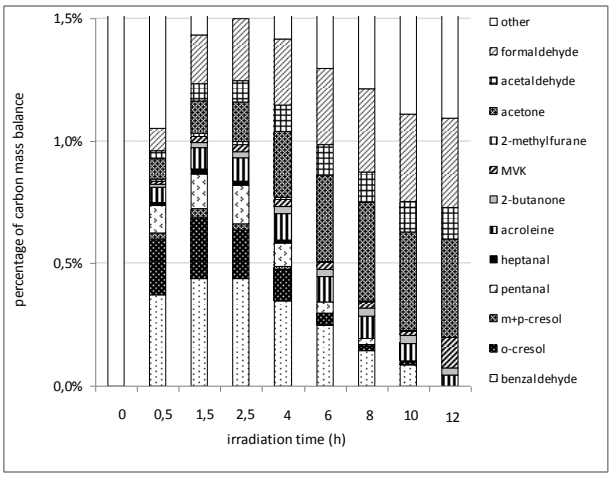

Figure 46 - Contribution of the identified gaseous organic reaction intermediates to the reaction carbon mass balance, during the photocatalytic degradation of 800 ppb of toluene in the presence of 15 500 ppm of H_2O for various irradiation times.

As reported on Figure 46, the contribution of the identified gaseous reaction intermediates into the reaction carbon balance only ranges from 1 to 1.5 % until 12 hours of irradiation. The fact that a low percentage of the carbon balance is released in the gas phase during the photocatalytic process is a positive point regarding air treatment in that emissions of reaction intermediates are limited as regards to initial concentration of pollutant. Figure 46 evidences the evolution of reaction intermediate diversity as a function of the oxidation reaction advancement. During the reaction first two hours, aromatic compounds represent from 60 to 75% of the gaseous reaction intermediate carbon mass balance. After 10 hours of reaction, more than 80% of the gaseous reaction intermediate carbon mass balance is made of aliphatic oxidized VOC containing less than 4 carbon atoms. The low concentration of reaction intermediates in the gas phase during the oxidation process can be balanced by the toxicity of the considered compounds. For instance, formaldehyde has to be carefully examined in the frame of air treatment devices qualification. After 12 hours of batch treatment, formaldehyde, acetone and acetaldehyde represent more than 80% of the gas phase reaction intermediate carbon mass balance.

Decane as primary pollutant / During the photocatalytic degradation of decane under wet air, 18 reaction intermediates were identified in the gas phase. The detected compounds are listed in Table 32 and classified according to their chemical natures. Three different decanones and three different decenes were identified. Nevertheless, as the position of the unsaturation within these compounds was not precisely determined, they are gathered under the names x-decenes and x-decanones in Table 32. The majority of the identified intermediates were carbonyl compounds and alcohols.

Table 32 - List of reaction intermediates identified in the gas phase during decane photocatalytic degradations. For each compound, "t_{MAX}" stands for to the temporal position of the maximum concentration during the photocatalytic degradation of 800 ppb of decane under 50% RH.

Aldehydes	t_{MAX} (h)	Ketones	t_{MAX} (h)	Alcohols	t_{MAX} (h)	Others	t_{MAX} (h)
Formaldehyde	13.7	Acetone	12	Ethanol	9.6	Methyl acetate	12
Acetaldehyde	9.6	2-butanone	9.6	1-propanol	Ø	x-decenes	2.3
Propanal	9.6	Methylvinylketone	6.1	Isopropanol	Ø		
Acroleine	9.6	x-decanones	4.3				
Butanal	6.1						
Pentanal	6.1						
Hexanal	6.1						
Heptanal	4.1						
Octanal	Ø						

Hexanal, octanal, 1-propanol and isopropanol have been detected but not quantified but of the analytical system detection limits. Similarly to toluene, the temporal profiles of decane intermediates consist in three phases: (i) intermediate formation, (ii) reaching of a maximum concentration (t_{MAX}), (iii) decrease of the intermediate concentration. The irradiation time (t_{MAX}) corresponding to the maximum concentration is reported in Table 32 for each intermediate. This time almost linearly increases as the number of carbons contained in the compound decreases. This is consistent with the advancement of the degradation reaction. In the case of intermediates with the highest number of carbon atoms, such as heptanal or x-decanones, the

maximum concentrations were reached before 5 h of irradiation. On the contrary, in the case of formaldehyde, the removal step begins only after 14 h of irradiation. Most of the quantified intermediates required more than 20 hours to be completely removed from the gas phase, whereas decane is completely removed from the gas phase at this irradiation time. Moreover, after 25 h of irradiation, some intermediates such as acetaldehyde or acetone are not completely removed yet. In order to explain the delay in the photocatalytic degradation of these light intermediates, the following hypothesis can be proposed: after the complete removal of decane and high molecular weight reaction intermediates from the gas phase, some strongly adsorbed reaction intermediates may remain on the surface of TiO_2 and would be slowly oxidized into lower molecular weight compounds such as formaldehyde or acetaldehyde. Based on the temporal profiles of the decane reaction intermediates and on literature, Debono et al proposed a detailed reaction pathway for decane photocatalytic oxidation at pbb level [17] based on six main reaction steps.

The influence of decane initial concentration on intermediate quantities was investigated on the ppb range. By increasing the decane initial concentration from 50 ppb to 800 ppb, three main observations can be reported:

❶ The same diversity of reaction intermediates is monitored in the gas phase, suggesting the reaction pathway is not modified while changing the initial concentration of pollutant on the ppb range.

❷ The ordering of intermediate temporal profiles was not sensibly modified. Only the duration of intermediates complete degradation was diminished by decreasing decane initial concentration from 800 to 50 ppb. Thus, the decane initial concentration only affects the irradiation time necessary to eliminate the reaction intermediates.

❸ Finally, the amounts of reaction intermediate in the gas phase increased along with decane initial concentration.

This last point is illustrated in Figure 47 with acetaldehyde: the maximum concentration of acetaldehyde measured in the gas phase is plotted versus decane initial concentration for dry and wet air conditions. Linear relations are obtained for acetaldehyde as an intermediate product of decane PCO with 80% and 94% of confidence for dry and wet air respectively. This linear trend is also observed for formaldehyde and propanal. These results confirm that the reaction pathway is not modified while changing the pollutant initial concentration at ppb level.

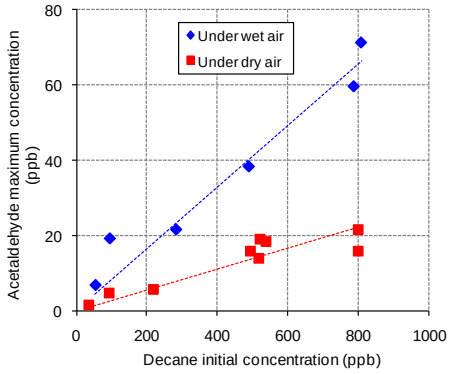

Figure 47 - Maximum acetaldehyde concentration as a function of initial decane concentration (squares: dry conditions; diamonds: wet condition (50% RH)).

Limonene as primary pollutant / During the limonene photocatalytic degradation on ppb range, a total of 20 VOCs have been identified and quantified in the gas phase. As reported in Table 33, the majority of the reaction intermediates are non-cyclic oxygenated VOCs. In contrast, the study of Poncet-Vincent [230] clearly highlighted the predominance of 8 different terpenoids among the reaction intermediates during the photocatalytic degradation of limonene, with an initial concentration exceeding 600 ppm. However, in this study, only 3 carvones are identified and quantified. This difference can be ascribed to the fact that, in the study of Poncet-Vincent [230], the reaction was performed at high concentrations, promoting a high surface coverage of the catalyst, which may favor the subsequent release of intermediates in the gas phase. In our study performed at ppb levels, we suggest that most of the heaviest and partially oxidized reaction intermediates, especially terpenoids, remain adsorbed on the photocatalyst surface, this point is addressed further through DRIFTS experiments.

The temporal profiles of the reaction intermediates are determined throughout the degradation of limonene. Two types of temporal profiles are observed in this study: (i) primary intermediates which are characterized by an initial formation rate different from zero at t=0, (ii) secondary intermediates which are characterized by an

initial formation rate equal to zero from t=0 up to a defined reaction time so called "delay time" and noted t_{delay} in Table 33. For each reaction intermediate, the time for which the maximum concentration was reached (t_{Cmax}) is listed in Table 33.

a)

Aldehydes	formula	t_{Cmax} (h)	Ketones	formula	t_{Cmax} (h)	Terpenoids	formula	t_{Cmax} (h)
Acetaldehyde	C_2H_4O	2.7	Acetone	C_3H_6O	1.6	d-Carvone	$C_{10}H_{14}O$	7.3
Heptanal	$C_7H_{14}O$	5	M.V.K.	C_4H_6O	5	l-Carvone	$C_{10}H_{14}O$	6.2
Methacrolein	C_4H_6O	5	2-Butanone	C_4H_8O	5	Carvomenthenal	$C_{10}H_{16}O$	2.7
2,3-dihydrofurane	C_4H6O	5						
Butanal	C_4H_8O	6.2						
Pentanal	$C_5H_{10}O$	7.3						
Formaldehyde	CH_2O	6.2						

b)

Carboxylic acids	formula	t_{delay} (h)	t_{Cmax} (h)	Alcohols	formula	t_{delay} (h)	t_{Cmax} (h)
Acetic acid	$C_2H_4O_2$	0.5	7.3	1-butanol	$C_4H_{10}O$	0.5	6.2
Pentanoic acid	$C_5H_{10}O_2$	1.6	7.3	Ethanol	C_2H_6O	1.6	5

Terpenoids	formula	t_{delay} (h)	t_{Cmax} (h)
T.M.P.	C_8H_{16}	0.5	6.2
Methyl acetate	C_3H_6O	0.5	7.3
2-pentanone	$C_5H_{10}O$	1.6	6.2

Table 33 - List of primary (a) and secondary (b) reaction intermediates identified and quantified in the gas phase during the photocatalytic oxidation of 750 ppb of limonene under dry air; "t_{Cmax}" indicates the maximum of the temporal profiles, and "t_{delay}" indicates the initial formation time of the secondary intermediates. (*M.V.K = Methyl Vinyl Ketone; T.M.P. = 2,4,4-trimethyl-1-pentene)*

Temporal evolutions of primary intermediates are reported in Figure 48. All terpenoids are characterized by the same initial formation rate on the first two hours of experiments. However, it can be noticed that their maximum concentrations are not reached at the same time in all three cases; they range between 3 and 6 hours of irradiation. These three reaction intermediates retain the terpenoid structure of d-limonene. In this study, the total amount of carvones quantified in the gas phase remains lower than 0.8 ppb and limited in time.

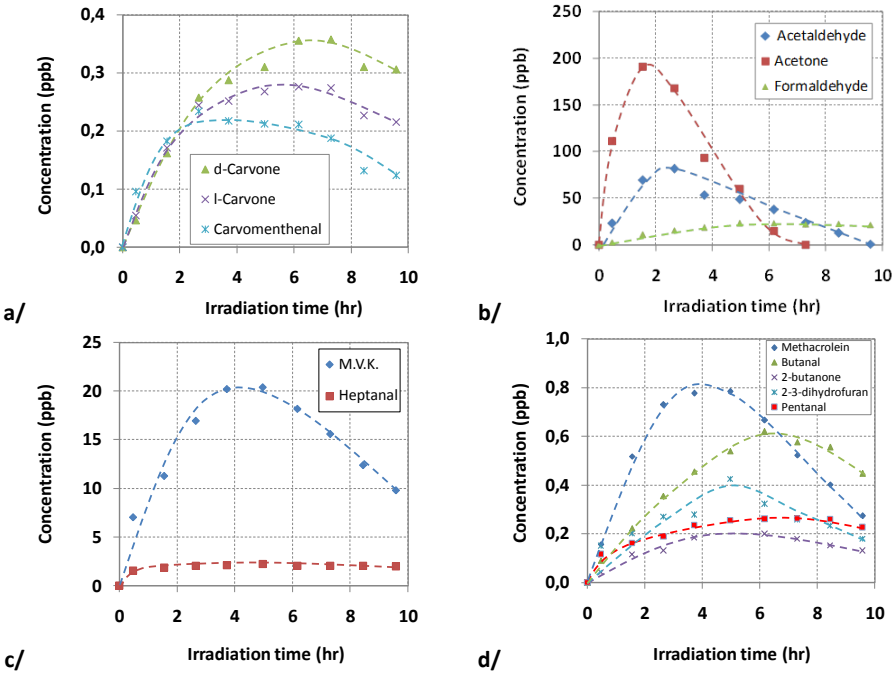

Figure 48 - Temporal profiles of the primary reaction intermediates during photocatalytic oxidation of 750 ppb of limonene on TiO_2 under dry conditions. (*M.V.K = Methyl Vinyl Ketone*).

Primary intermediates other than carvones do not contain any cyclic structure suggesting they originate from the ring-opening of limonene or terpenoid intermediates. As shown in Figure 48 b, c and d, carbonyls are the major gas phase reaction intermediates in terms of variety and concentration. Unexpectedly, formaldehyde is not quantified as the most abundant intermediate. Acetaldehyde and acetone can be considered as major gaseous intermediates regarding their concentrations, with respective maximum concentrations of 82 and 190 ppb, after only 3 hours of irradiation. Furthermore, they disappear from the gas phase simultaneously with the removal of limonene, whereas other carbonyl species, and especially formaldehyde, remain in the gas phase. This behavior suggests that acetaldehyde and acetone directly originate from the degradation of gas phase

limonene. The maximum concentrations of primary intermediates containing between 4 and 5 carbon atoms (methacrolein, butanal, 2-butanone, 2-3 dihydrofuran, pentanal) are reached after 4 hours of irradiation. They can be derived from the degradation of limonene or from the oxidation of intermediate compounds present in the adsorbed phase.

The temporal profiles reported in Figure 49 correspond to secondary reaction intermediates. These compounds are detected in the reaction chamber beyond 0.5 and 1.5 hour of irradiation. In previous articles from our group [15][17] dealing with the toluene and decane photocatalytic degradations at ppb levels and using the same reactor and analytical devices, no secondary intermediates were identified, all detected substances being formed since t = 0. The formation of secondary reaction intermediates requires the achievement of first reaction steps. Some of the secondary reaction intermediates, such as acetic acid, methyl acetate and ethanol, are characterized by low molecular weights and t_{Cmax} values from 5 to 7 hours. This suggests that they originate from the subsequent oxidation of gas phase primary intermediates. However, other secondary intermediates, such as trimethyl-1-pentene, pentanoic acid and 2-pentanone, contain between 5 and 8 carbon atoms. Their maximum concentrations are relatively high, from 5 to 50 ppb, and they are observed between 6 to 8 hours of irradiation. Such characteristics suggest that these species may mainly originate from the oxidation of heavy reaction intermediates adsorbed on the photocatalyst surface. This hypothesis is discussed while evaluating the photocatalytic reactivity of the adsorbed phase (section E-5).

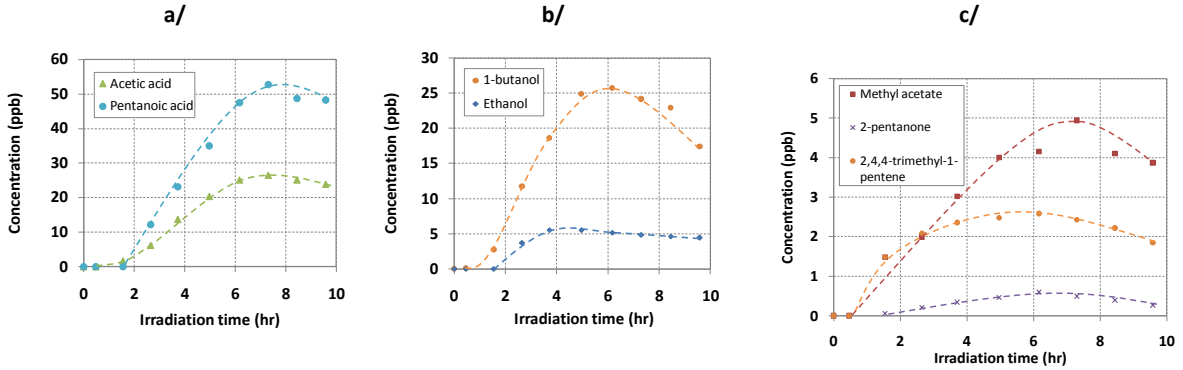

Figure 49 - Temporal profiles of the secondary reaction intermediates during the photocatalytic oxidation of 750 ppb of limonene on TiO_2 under dry conditions.

Conclusion on gas phase reaction intermediates at ppb level /

Obtained results on the characterization of gas phase reaction intermediates produced along toluene, decane and limonene photocatalytic oxidation at ppb level are the sole detailed investigation in the domain. The development of the well instrumented large volume batch reactor makes possible the investigation of the whole oxidation reaction advancement. As a result, reaction intermediates can be described in their diversity and related to the various reaction advancements. Precise quantifications made possible the innovative evaluation of gas phase reaction intermediates contribution in the reaction carbon mass balance. Interestingly, amounts of gas phase reaction intermediate depend on the nature of the oxidized VOC; however, they remain lower than 12% for limonene, 5% for decane and 1.5% for toluene.

Interestingly, these studies are highly informative as regards of photocatalysis innocuity for indoor air treatment. Gas phase reaction intermediates are generally pointed out as secondary sources of pollutants along photocatalytic treatment. Indeed, such species as released along the oxidation reaction, but their respective amounts remain limited compared to initial primary pollutant.

E-5 INSIGHT ON ADSORBED PHASE DURING LIMONENE PHOTOCATALYTIC OXIDATION

Introduction / This aspect has mainly be evaluated during the photocatalytic oxidation of limonene at ppb levels. Considering the low amount of terpenoid compounds monitored in the gas phase and the formation of secondary intermediates containing more than 5 carbon atoms beyond 6 hours of irradiation (Section E-4, limonene), complementary experiments were carried out to investigate the photocatalyst adsorbed phase. These experiments have been performed using a DRIFT cell in order to investigate: (i) the adsorption of limonene on TiO_2 and (ii) the fate of adsorbed species under UV irradiation. The adsorption of limonene on TiO_2

leads to the appearance of typical absorption bands at 2974, 2923 and 2875 cm^{-1} associated to the C-H stretch vibration of methyl groups. More precisely, the band at 2923 cm^{-1} has been used to follow limonene adsorption, desorption and conversion on TiO_2. The experiment was divided into three steps : (i) 5 ppm limonene diluted in air are sent into the DRIFTS cell on the surface of TiO_2, and limonene adsorption is monitored, (ii) the DRIFTS cell is flushed with zero air to remove the reversibly adsorbed limonene, (iii) the photocatalyst surface is illuminated with UV-LEDs.

***In-situ* monitoring of limonene photocatalytic oxidation /** Figure 50 reports the evolution of the band at 2923 cm^{-1}, corresponding to limonene, along the three experimental steps. During the adsorption step, the saturation of the band is observed within 1.1 hour, confirming the complete coverage of limonene adsorption sites on TiO_2 surface. Beyond 1.1 hour, the flushing step induces a steep decrease in the amount of adsorbed limonene corresponding to desorption of reversibly adsorbed, i.e. physisorbed, limonene from TiO_2 surface. Then, the band at 2923 cm^{-1} tends to stabilize, indicating that TiO_2 surface is mainly covered by irreversibly adsorbed limonene.

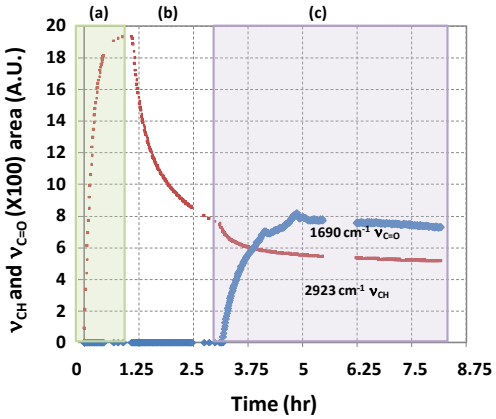

Figure 50 - DRIFTS temporal evolutions of the band at 2923 cm^{-1} corresponding to ν_{CH} from adsorbed limonene, and the band at 1690 cm^{-1} corresponding to $\nu_{C=O}$ from adsorbed carbonyl compounds, during (a) the adsorption of limonene, (b) the flushing under zero air and (c) the UV illumination on TiO_2 surface.

As soon as illumination starts, two main phenomena can be observed on Figure 50. First, the band at 2923 cm^{-1} corresponding to limonene ν_{CH} decreases, meanwhile, the band at 1690 cm^{-1} corresponding to $\nu_{C=O}$ for adsorbed carbonyl compounds increases. The apparition of the band at 1690 cm^{-1} simultaneously with UV illumination attests of the adsorbed phase oxidation of limonene. Moreover, UV irradiation also induced the apparition of absorption bands attributed to formates and alkenes, confirming the oxidative conversion of limonene. Formates and alkenes absorption bands are intense enough to be clearly identified, but remain too weak to accurately plot their temporal evolutions. The decrease in the ν_{CH} band at 2923 cm^{-1} indicates the consumption of adsorbed limonene molecules by photocatalytic processes. More precisely, the appearance of ν_{sCOO} and ν_{asCOO} corresponding to formate and $\nu_{C=O}$ corresponding to carbonyls confirms that adsorbed limonene molecules are oxidized. However, the relatively weak decrease in the ν_{CH} band at 2923 cm^{-1} (only 25% after 2 hours of irradiation) suggests that most of the reacted limonene remains in the adsorbed phase. As suggested in section E-4, the hypothesis of partially oxidized terpenoids accumulated on TiO_2 is strengthened. Thus, the adsorbed phase could be considered as a pool of terpenoid compounds which may (i) lead to the release of various reaction intermediates and (ii) be gradually mineralized along the photocatalytic reaction.

E-6 SECONDARY ORGANIC AEROSOLS (SOA) AS PHOTOCATALYTIC SIDE-PRODUCTS

Homogeneous reactions between limonene and oxidants such as ozone lead to the formation of both gaseous [231] and particulate products [232]. As reported in Section E-4, limonene photocatalytic oxidation produces a wide variety of gaseous intermediates during the first hours of treatment, among which many of them such as terpenoids and carboxylic acids have vapor pressures low enough to partition between the gas and particulate phases during the heterogeneous oxidation of limonene and thus to contribute to SOA formation. Indeed, we evidenced particle formation during the photocatalytic oxidation of 750 ppb limonene.

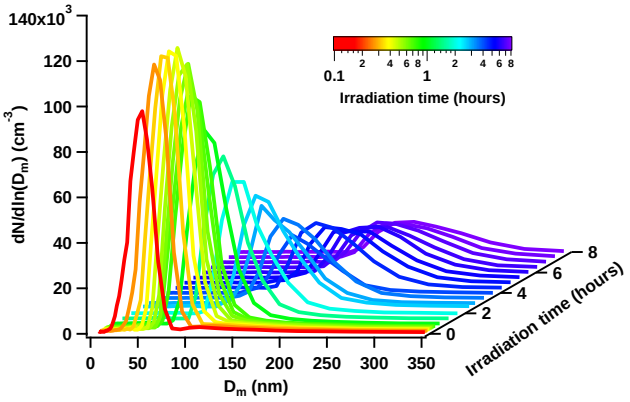

Figure 51 - Evolution of the SOA number size distribution during the photocatalytic oxidation of 750 ppb of limonene under dry conditions (t=0 corresponds to the beginning of UV irradiation).

Before switching on the UV lamps, no particles were monitored in the reaction chamber. In the CPC mode, SOA formation was detected after 6 min of irradiation, indicating that their production requires the presence of precursor compounds in the gas phase. Figure 51 presents the number size distribution obtained by connecting the DMA upstream the CPC and sampling the batch reactor mixture about every five minutes during the first 45 minutes after irradiation then every half hour up to 8 hours. The temporal profiles show a unimodal distribution whatever the time with a particle modal diameter shifting from 51.5 nm after 10 minutes to about 80 nm when the maximum number concentration is reached (i.e. at 24 minutes of irradiation) and further to 192 nm after 8 hours of irradiation. The number decrease and average size increase is expected, due to particle coagulation or condensation onto preexisting aerosols for ultrafine particles and semi-volatile vapors to form larger particles at higher irradiation times.

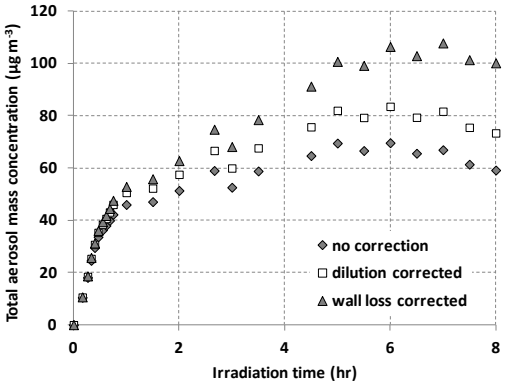

Figure 52 - Aerosol mass concentrations measured during the photocatalytic oxidation of 750ppb of limonene under dry conditions as a function of irradiation time, after taking into account dilution effects and wall losses in the reactor.

The SOA mass concentration could be calculated from SMPS size distributions assuming spherical particles with a density of 1.25 g cm^{-3} [233]. Due to the regular addition of known amounts of zero air (for a total of about 30 L) in order to keep the reactor at atmospheric pressure despite sampling, a dilution effect had to be taken into account. The dilution factor was calculated at each sampling point and ranged between 1 and 24% for 10 minutes and 8 hours of irradiation, respectively. Figure 52 shows the aerosol mass concentration before and after correction for the dilution effect. Aerosol wall losses in the reactor were estimated using a method previously developed and used in other studies [234], in which the loss rate is assumed to be first order and independent of the particle size. Only data points after the formation of new particles had stopped, i.e. after 5 hours of irradiation were taken into account. The rate constant, k_{loss}, could be derived from Equation 33 where M(t) is the aerosol mass concentration measured at time t and corrected for dilution, and C a constant.:

$$\ln M(t) = -k_{loss}.t + C \qquad \textbf{Equation 33}$$

The slope of the linear fit led to a value of k_{loss} = 0.046 hr^{-1}, similar to previously reported values [234]. Wall loss and dilution corrections were applied to the experimental data as illustrated in Figure 52. The overall corrections were less than 15% until 1 hour of irradiation but reached up to 70% for the last experimental point, mostly due to wall loss corrections. SOA formation is a complex process, involving the gas-particle conversion of oxidized VOCs. In order to better assess the chemical mechanisms during the partitioning of semi-volatile hydrocarbons between the gas and particle phases, the SOA time-dependent growth curve is modeled by

plotting the aerosol mass formed (ΔM) as a function of the amount of limonene reacted (Δ[Lim]) during the first 4 hours of irradiation of a specific experiment, during which the limonene concentration was determined with a high-time resolution by SIFT-MS measurements.

Figure 53 - Time-dependent growth curve of ultrafine particles detected during the photocatalytic oxidation of 750 ppb of limonene under dry conditions

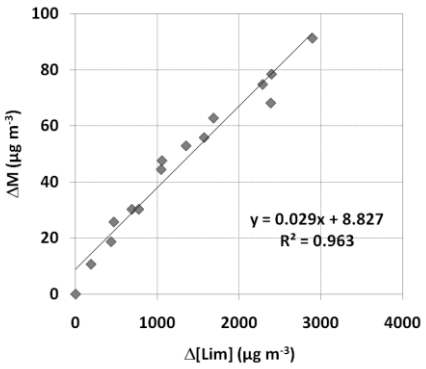

Figure 53 shows the SOA time-dependent growth data observed during limonene photocatalysis under dry conditions. The aerosol mass increases linearly till the consumption of ca. 70 % of limonene after 4 hours of irradiation. This was observed in many previous studies such as Coeur-Tourneur et al [235]. Due to the lack of limonene concentration values at longer reaction times and since it was not entirely consumed after 4 hours, we could not confirm previous findings from Ng et al [233] who observed that limonene growth curves (like other terpenoids with more than one double bond) showed a typical behavior when oxidized by OH or ozone, with aerosols still formed after the terpenes had been entirely consumed. They suggested that for this type of species, SOA formation is not only due to a rate-limiting step linked to the first-generation products, but that secondary products resulting from their further oxidation are rate-determining as well. In our case, the aerosol total mass concentration seems to stabilize in the reactor after 5 hours of irradiation once experimental data have been corrected for dilution and wall losses. This could suggest either an underestimation of the wall loss rate or a different oxidation mechanism in the case of adsorbed limonene. The first assumption has been tested by applying a wall loss rate of 0.2 hr^{-1}, i.e. a factor of 5 higher than what has been measured, without changing the observed trend for the total aerosol mass concentration. The reaction of OH with limonene has already been assumed to proceed mostly via the attack of the OH radical on the endo double bond rather than on the exo one [233] to explain the preferential formation of non-volatile products during the first reaction steps. Our results suggest that this phenomenon is even enhanced when limonene is adsorbed on TiO_2.

This study is the first to evidence the formation of organic particles during the photocatalytic degradation of VOCs. From an air treatment perspective, further experiments are required to characterize particle composition and therefore their potential impact on health. However, this study strongly questions the use of photocatalytic air treatment systems in the presence of household cleaning products or air fresheners.

E-7 PHOTOCATALYTIC MINERALIZATION OF VOCs AT ppb LEVELS

Introduction / Based on infrared spectroscopy analytical developments, CO and CO_2 productions have been monitored during the photocatalytic oxidation of toluene, decane and limonene. Since limonene has been described in details throughout sections E-4, E-5 and E-6, it illustrates the mineralization section as well. Similarly to toluene and decane, in spite of the fact that limonene is removed from the gas phase within approximately 12 hours, the formation of CO and CO_2 was monitored during 24 hours in order to investigate the mineralization process beyond VOC total removal. CO and CO_2 temporal profiles are reported in Figure 54.

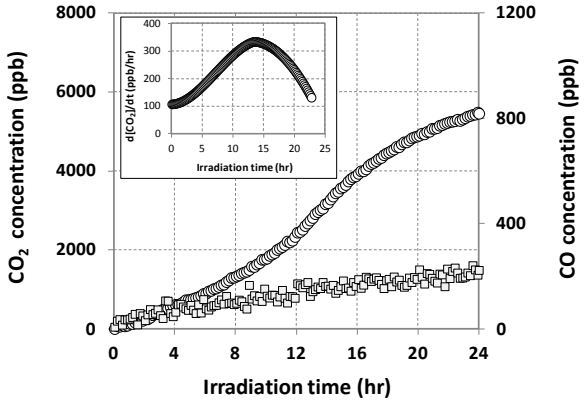

Figure 54 - Temporal evolutions of CO and CO_2 concentrations during the photocatalytic oxidation of 750 ppb of limonene under dry conditions. Open circles: CO_2; open squares: CO. The evolution of CO_2 formation rate (ppb h^{-1}) has been calculated from CO_2 temporal profile and reported in insert.

The concentrations of CO and CO_2 in the batch reactor continuously increased along the 24-hour experiment. CO and CO_2 are produced from the first oxidation steps since their initial formation rates at t=0 are respectively 30 and 110 ppb h^{-1}. It can be seen on Figure 54 that the formation of CO_2 is clearly favored compared to CO formation; after 24 hours, the concentration of CO_2 exceeds the concentration of CO by a factor of 24. The continuous increase of CO and CO_2 along the experiment evidences that organic matter is mineralized during the photocatalytic removal of limonene and far beyond.

CO_2 temporal profile is characterized by a sigmoid shape indicating that the CO_2 formation rate varies along the photocatalytic process. To assess this point, their evolution has been calculated as a function of irradiation time and reported on Figure 54, where their variation can be divided in two parts. First, a significant increase is noticed from 0 to 14 hours of illumination; on that time interval, the CO_2 formation rate reaches a maximum value of 340 ppb hr^{-1}. Second, a substantial decline of the CO_2 formation rates is observed beyond 14 hours. This behavior can be correlated to the evolution of organic species to be oxidized in the batch reactor. Indeed, CO_2 production is directly impacted by the structure and the oxidation state of the VOCs to be treated, i.e. the number of elementary steps to produce CO_2. From 0 to 14 hours, the increase in the CO_2 formation rate can be related to the advancement of the organic compound oxidation state with time. This point is supported by the nature and the temporal profiles of reaction intermediates in the gas and adsorbed phases. The opening of the terpenoid ring and the shortening of the carbon chain both promote mineralization rate.

Similar trends in CO_2 production rates were reported by Debono et al [15] during the investigation of toluene photocatalytic mineralization at ppb level in a batch reactor. However, the evolution of CO_2 formation rate is completely different in the case of decane photocatalytic oxidation which confirms the correlation between structure and mineralization kinetic [17]. Beyond 14 hours, the decline in the CO_2 formation rate can be correlated to the gradual depletion of organic reaction intermediates from both the gas and adsorbed phases. It is important to note that in spite of limonene removal from the reactor after 10 hours of treatment, the mineralization process still goes on; in particular, CO_2 concentration reaches 5,490 ppb after 24-hour illumination, corresponding to 74% of the reaction carbon mass balance. Conversion of the gas phase and also adsorbed phase reaction intermediate is a key step in the mineralization process.

Results obtained on toluene, decane and limonene mineralization are the first to quantitatively evidence the formation of CO and CO_2 on a ppb range photocatalytic reaction. This achievement makes possible the ppb range determination of photocatalytic reaction carbon mass balances.

E-8 CARBON MASS BALANCES OF PHOTOCATALYTIC REACTIONS AT ppb LEVELS

Introduction / The complete determination of the reaction carbon mass balances during the photocatalytic oxidation of VOCs at ppb level was an extremely challenging task that was first tackled by Olivier Debono during his PhD [1]. This experimental difficulty has been overcome through the analytical developments not only related to VOC monitoring but also through the very innovative CO and CO_2 quantification at ppb levels during the PhD theses of Olivier Debono [1] and Loganathan Sivachandiran [2]. This section is illustrated through the typical behavior of limonene.

The question of adsorbed VOC at t = 0 in the carbon mass balance / The preparation of the reaction chamber requires 14 hours in order to reach the adsorption equilibrium. This means that a steady state can be reached regarding the partition of VOCs in the gas phase and in the adsorbed phase. During the experiments, measurements of organic compounds are only performed in the gas phase, whereas a fraction of VOC molecules is present at the beginning of the reaction on the photocatalyst surface. Those adsorbed molecules are supposed to react rapidly at the beginning of UV illumination and will take part to the carbon balance of the photocatalytic reaction regarding organic intermediate and CO_2 formation. The question is to determine the portion of VOCs initially adsorbed on the photocatalyst in order to evaluate their potential contribution into the carbon balance.

Demeestere et al [111] have precisely investigated the equilibrium partitioning of various VOC on P25-Degussa TiO_2 surface, and determined for instance toluene adsorption constant as a function of temperature, concentration and relative humidity. At 298 K, in the presence of 400 ppb of toluene in our reaction chamber, corresponding to $1.8x10^{18}$ molecules in the gas phase, $3.2x10^{14}$ toluene molecules are adsorbed on the photocatalyst under dry conditions (10 ppmv H_2O) and $1.15x10^{14}$ toluene molecules are adsorbed under wet conditions (15 500 ppmv H_2O). Thus, the ratios between toluene amount in the gas phase and the adsorbed phase are around 3600 and 10 000 respectively under dry and wet conditions. Obee and Brown [236] suggest that toluene mainly adsorbs on TiO_2 surface hydroxyl groups. Thus, based on Mills and Le Hunte [237] considerations on TiO_2 active sites and adsorption sites it is possible to deduce the number of sites on the photocatalyst from: the OH surface density, the Brunauer-Emmet-Teller (BET) specific surface, and the mass of photocatalyst. In the presence of 100 mg of P25-Degussa TiO_2 we assume that the number of active/adsorption sites is superior to $5x10^{16}$. This implies that at t=0, less than 0.64 % and 0.23 % of TiO_2 sites are supposed to be occupied by toluene respectively in the dry and wet conditions. The ratios of toluene amounts between the gas and the adsorbed phase and TiO_2 surface coverage suggest that (i) the initial adsorbed toluene molecules are not significant in the photocatalytic reaction carbon balance; (ii) the absence of induction period at the beginning of the photocatalytic reactions which would be due to adsorbed toluene removal is coherent.

Carbon mass balance determination throughout limonene photocatalytic oxidation / Since the photocatalytic oxidation reaction are carried out in a batch reactor, their carbon mass balance of the reaction have been calculated based on the initial VOC concentration present in the 120 L chamber at t = 0, corresponding to 100% of the reactor carbon mass balance. Then, it is possible to determine the contribution of the various classes of compounds to the carbon mass balance: gas phase organic reaction intermediates, CO & CO_2, and SOA. Finally, a global overview of the carbon mass balance is proposed. This approach has been performed for toluene, decane and limonene for various reaction advancements, i.e. different reaction times. It is illustrated here with limonene.

Contribution of limonene gas phase organic reaction intermediates / The simultaneous quantification of limonene removal and reaction intermediates formation makes possible the calculation of their respective contributions into the reaction carbon mass balance as a function of oxidation process advancement in order to depict the partitioning of the various species. Assuming that the amount of carbon remains constant during the experiments performed in batch mode, the contribution of each gaseous compound to the carbon mass balance of the reaction has been calculated. The contributions of the VOCs belonging to the main classes (alcohol, terpenoid, ketone, etc.) are reported on Figure 55 for 0 to 9.6 hours of irradiation.

The contribution of organic compounds identified and quantified in the gas phase ranges from 5.8% to 12.5% of the reaction carbon mass balance. The maximum value of 12.5% is reached after only 2.7 hours of treatment. It corresponds to a massive release of aldehydes and ketones during the first steps of the oxidation process. This maximum value is higher than those obtained under similar conditions with toluene (1.5%) and decane (5%).

Thus, the structure of the VOC considerably influences the amounts of reaction intermediates released in the gas phase. Beyond 3.7 hours of treatment, the contribution of gas phase carboxylic acids and alcohols (secondary reaction intermediates) becomes predominant. The global contribution of gas phase reaction intermediates to the carbon mass balance tends to decrease mainly because of the carbonyl compound removal. After 9.6 hours of treatment, secondary reaction intermediates account for more than 75% of the total gaseous reaction intermediates. Despite their high number of carbon atoms, terpenoids monitored in the gas phase are characterized by a contribution which does not exceed 0.1% of the gaseous reaction intermediates on the whole investigated time range. This value confirms a massive adsorption of the terpenoid species all along the photocatalytic process.

Figure 55 - Contributions of the gaseous organic reaction intermediates to the carbon mass balance as a function of UV irradiation time, during the photocatalytic oxidation of 750 ppb of limonene in dry conditions

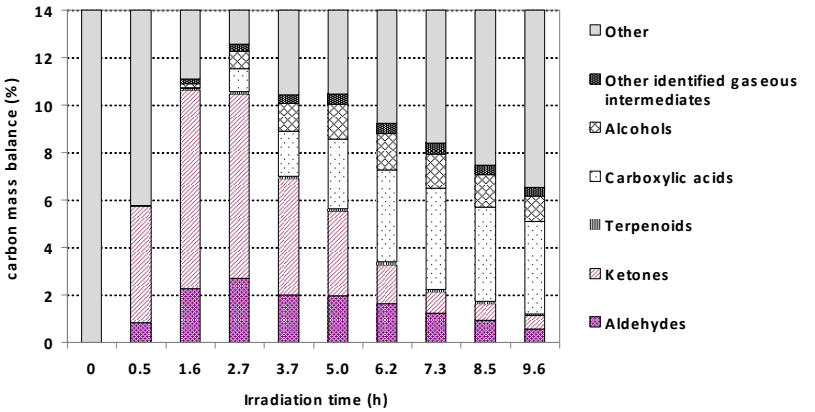

Contributions of CO and CO_2 to the carbon mass balance / The contributions of CO and CO_2 to the reaction carbon mass balance have been calculated for different irradiation times ranging from 0 to 24 hours of treatment and reported on Figure 56. Unsurprisingly, compared to CO_2, the contribution of CO in the carbon mass balance is minor; indeed, it remains lower than 3% whereas CO_2 accounts for 74% after 24 hours of reaction. The continuous increase of CO and CO_2 contributions in the carbon mass balance attests that no deactivation phenomenon of the photocatalyst occurs under our experimental conditions. As a result, the massive adsorption of limonene and terpenoid intermediates on the surface does not lead to an irreversible coverage of photocatalytic reactive sites. Compared to limonene removal which occurs within 10 hours, mineralization is significantly delayed and requires more than 24 hours. However, the fact that 77% of the carbon mass balance is represented by CO and CO_2 attests of the performances of the photocatalytic process to achieve complete oxidation of terpenoids.

Figure 56 - Contributions of CO and CO_2 to the carbon mass balance as a function of UV irradiation time, during the photocatalytic oxidation of 750 ppb of limonene in dry conditions.

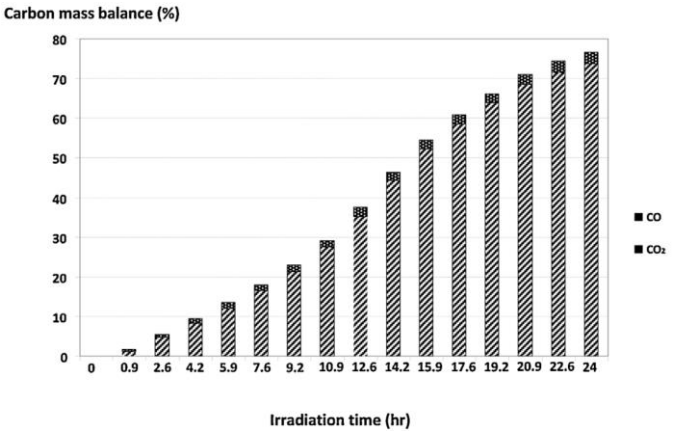

Contributions of SOA to the carbon mass balance / The contribution of SOA to the reaction carbon mass balance has been assessed. First, the volume of SOA formed per m^3 has been evaluated from particle counting data assuming that particles are spherical. Then, considering a density of 1.25 g cm^{-3} for SOA produced from limonene [233], the mass concentration of particle has been calculated. Finally, the number of carbon atoms involved in SOA per m^3 has been determined considering an average (organic matter/organic carbon) ratio of 1.6 [238]. These data have been used to evaluate the contribution of SOA to the carbon mass balance as a function of the photocatalytic reaction advancement from 0 to 8 hours. As reported on Figure 57, the

contribution of SOA in the carbon mass balance never exceeds 2%. In spite of the fact that the evaluation of SOA contribution relies on several hypotheses, it clearly appears that their contribution is one order of magnitude lower than organic gaseous intermediates. The contribution of SOA in the carbon mass balance continuously increases from 0 to 6 hours and then remains constant.

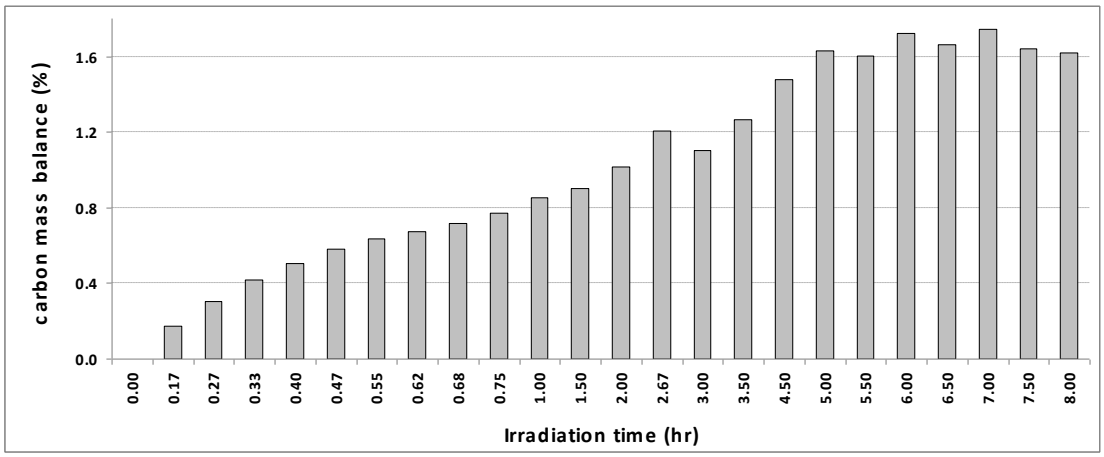

Figure 57 - Evaluation of the contribution of detected SOA to the carbon mass balance as a function of UV irradiation time, during the photocatalytic oxidation of 750 ppb of limonene in dry conditions.

Limonene photocatalytic oxidation carbon mass balance overview / Figure 58 gives an overview of the reaction carbon mass balance from 0 to 9.6 hours of treatment. The respective contributions of limonene, gaseous reaction intermediates, particulate matter, CO and CO_2 are plotted. The contribution of particulate matter in the carbon mass balance of a photocatalytic oxidation process is assessed for the first time. After 9.6 hours of batch treatment, more than 90% of limonene is removed from the gas phase. However, only 40 % of the carbon balance is characterized and 60% remains unidentified. Considering the diversity and the performances of the analytical techniques used in this study, we can assume that the unidentified fraction at 9.6 hr can mainly be attributed to species adsorbed on the photocatalyst. This hypothesis is based on (i) the DRIFTS experiments and (ii) the recovery of more than 77% of the carbon balance through CO and CO_2 after 24 hours of irradiation.

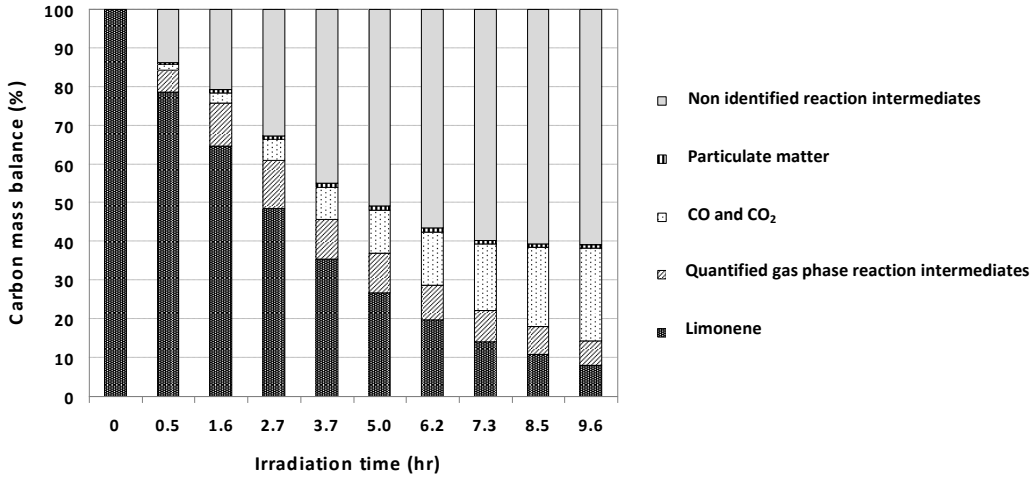

Figure 58 - Respective contributions of limonene, identified gaseous reaction intermediates, CO, CO_2, particulate matter and non identified reaction intermediates into the carbon mass balance of 750 ppb limonene photocatalytic oxidation in dry conditions.

Conclusion on carbon mass balance determination / The complete determination of reaction carbon mass balances during VOC photocatalytic oxidation of at ppb level was an analytical chemistry challenge. Main achievements have been obtained during the PhD of Olivier Debono. Obtained results enable a complete description of oxidation reaction and evidenced that photocatalytic removal of indoor air VOCs is achievable.

E-9 MAIN OUTCOMES of THE PHOTOCATALYTIC OXIDATION KINETIC STUDIES AT ppb LEVELS

The photocatalytic oxidations of toluene, decane, limonene and trichloroethylene at ppb levels have been investigated from complementary points of view. First, a complete characterization of the gas phase was performed by the monitoring of reaction intermediates, CO and CO_2 as a function of treatment time. Regarding limonene, the identification of adsorbed phase by-products has been successfully performed using an infrared in-situ monitoring of the photocatalyst surface. Finally, the formation of particulate by-products was evidenced for the first time.

The results showed that ppb level photocatalytic heterogeneous treatments follows a pseudo first order kinetic, except for TCE. From 15 to 20 VOCs have been identified and quantified in the gas phase as organic reaction intermediates, depending on the structure of the primary pollutant. Formaldehyde, acetone and acetaldehyde are the most abundant gaseous reaction intermediates; this point has to be noticed as regards of indoor air. Innovative analytical developments made possible the monitoring of CO and CO_2, which enabled the determination of carbon mass balances. Such an approach gives a comprehensive overview of the photocatalytic reaction advancement.

For limonene investigation, the implementation of DRIFT spectroscopy enabled to identify the increasing population of carbonyls, formates and alkenes as adsorbed species under UV irradiation. Although the DRIFT method used in this study did not allow quantifying the oxidized species, carbon mass balance calculations based on the quantified intermediates evidence that their abundance in the carbon balance is significant (more than 60%) after 10 hours of photocatalytic treatment.

Similarly to ozonolysis and photooxidation reactions, the photocatalytic oxidation of limonene leads to the fast, but not instantaneous, formation of secondary organic aerosol, confirming that they originate from the gas-particle conversion of reaction intermediates formed during the photocatalytic process. From an indoor air quality point of view, it is important to notice that it is the lowest contribution to the carbon mass balance among the quantified reaction intermediates. However, the photocatalytically produced particles are characterized by submicron diameters and high oxygen content. As a consequence they may deeply penetrate lungs and be easily metabolized. Further investigations with other biogenic hydrocarbons would be interesting in order to assess their behavior in real scale photocatalytic air treatment systems.

Regarding multiple VOC treatment, a sequential treatment VOCs has been evidenced. This phenomenon would be highly hindering in the case of real air treatment. The hypothesis of competitive adsorption is proposed to explain this phenomenon. However, experimental data related to VOC adsorption onto TiO_2 have to be determined before going further.

Results obtained in the framework of the PhD theses of Olivier Debono [1], Loganathan Sivachandiran [2] and Frédéric Batault [3] led to significant steps forward in the evaluation of the compliance of photocatalytic technology to indoor air problematic since they developed and validated experimental setups and analytical instruments to quantitatively address the photocatalytic reaction in the specific context of indoor air with three main performance criteria: (i) primary pollutant removal, (ii) gaseous and particulate side-product release, (iii) mineralization.

E-10 DETERMINATION of VOC ADSORPTION PARAMETERS ON TiO_2

Introduction / Adsorption plays a key role throughout the VOC photocatalytic oxidation process and kinetic behavior. As reported in section E-3, it may lead to VOC mixture sequential treatment or even photocatalyst deactivation. The aim of this work is to determine qualitative and quantitative data regarding VOC adsorption on TiO_2. This study has been performed with five different VOCs. Since the purpose of this study is to understand the role of adsorption as regard of photocatalytic reaction for indoor air treatment, these VOCs (i) are characterized by significant occurrences in indoor air, (ii) are representative of VOC diversity in indoor air, (iii) originate from various chemical families, (iv) contrasted in terms of molecular weights and functional groups. Selected VOCs are: formaldehyde, acetaldehyde, acetic acid, toluene and decane.

Adsorptions of the five VOCs onto TiO_2 have been studied under both dry and humid conditions. Dry and humid experiments provide complementary pieces of information to identify the adsorption modes, in accordance with literature. The Langmuir model parameters (adsorption constant (K), reversible and irreversible maximum adsorbed amounts ($q_{m\ rev}$ and $q_{m\ irr}$), and adsorption enthalpy ΔH) are determined for each VOC .Three experimental methods have been used: breakthrough curves, room temperature desorptions and temperature-programmed desorptions. Reactor used in this study is described in Figure 7 and experimental procedure is detailed in section C-6.

In this section, results obtained on acetaldehyde and acetic acid are detailed. Section E-10 is divided in four parts, first acetaldehyde and acetic acid individual studies are presented, then. Based on experimental results, a model for acetaldehyde and water co-adsorption is proposed, taking into account the specific interaction between acetaldehyde and water molecule. Regarding acetic acid, a reactive adsorption pathway is proposed. Finally obtained data are gathered and compared to classify the 5 investigated VOCs according to their typical behavior on TiO_2 surface.

Acetaldehyde adsorption on TiO_2 in dry condition / Multiple breakthrough curves and Room Temperature Desorptions (RTD) of acetaldehyde on TiO_2 have been performed in the 20-520 ppm concentration range. These experiments make possible the calculation of the adsorbed quantities under different concentrations and the remaining adsorbed quantity after zero air exposure. Figure 59 shows one of these experimental multiple breakthrough curves. TiO_2 has been successively submitted to 62 ppm, 82 ppm and 97 ppm acetaldehyde concentrations to reach the corresponding adsorption equilibriums. Then, it is submitted to a zero air flushing to desorb the reversibly adsorbed fraction corresponding to the third adsorption equilibrium. The total adsorbed quantity reaches 17.5 µmol m^{-2} during the first concentration step. During the following adsorption steps, it only increases by 0.08 and 0.06 µmol m^{-2}. During the RTD, the total adsorbed amount decreases by 0.68 µmol m^{-2} leading to a remaining adsorbed amount of 16.9 µmol m^{-2}. It can first be noticed that only a small part of the adsorbed acetaldehyde desorbs during the RTD. Most of acetaldehyde adsorption in dry condition is irreversible: the reversibly adsorbed fraction is only 4 % of the total adsorbed quantity at the third step. It can also be noticed that the quantity adsorbed during the first step is huge, relatively to the quantities adsorbed during the second and the third steps. Multiple breakthrough and RTD sequences have been performed 8 times with different step numbers and different first-step concentrations. Every time, the first step adsorbed quantity represents more than 97% of the last-step total adsorbed amount. It means that the irreversibly adsorbed fraction is mainly adsorbed during the first step of each experimental sequence. The irreversibly adsorbed amount calculated for the last step can thus be used to calculate the reversibly adsorbed quantity of every step for each experimental sequence.

Based on the 8 multiple breakthrough sequences, reversibly and irreversibly adsorbed quantities have been determined for various concentrations of acetaldehyde ranging from 20 to 520 ppm. The eight values of the irreversibly adsorbed fraction have been obtained and averaged. Standard deviation has been calculated to determine the uncertainty associated to the irreversibly adsorbed amount. The obtained value is 14.6 ± 4.8 µmol m^{-2}.

The reversibly adsorbed quantities increase with the VOC concentration. Then, they have been plotted as a function of acetaldehyde gas-phase concentration Figure 60. Each point is the average of three experimental values. This curve has been fitted with the Langmuir model in order to determine the adsorption parameters ($q_{m,rev}$ and K) of the reversibly adsorbed mode. Parameters obtained from this set of experiment are $q_{m,rev}$ = 1.61 ± 0.22 µmol m^{-2} and $K = 6.6.10^{-3} \pm 1.2.10^{-3}$ ppm^{-1}. The $q_{m,rev}$ value of the reversibly adsorbed

fraction is one order of magnitude lower than the irreversibly adsorbed fraction one. This difference will be discussed further with adsorption mode considerations.

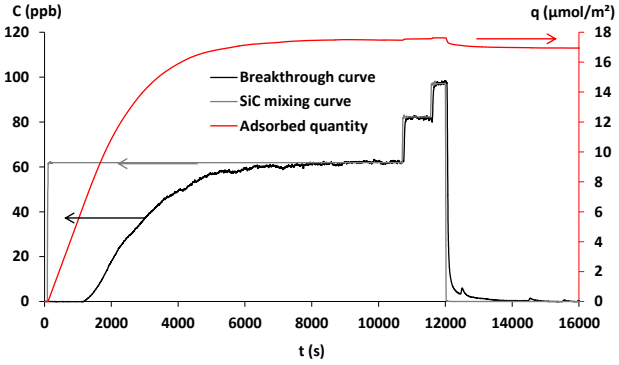

Figure 59 - Multiple breakthrough and Room Temperature Desorption (RTD) sequence typical curves for acetaldehyde experiments in dry air : Breakthrough curve on TiO_2 (black line) and SiC mixing curve (grey line) outlet concentrations and calculated adsorbed quantity (red line) versus time.

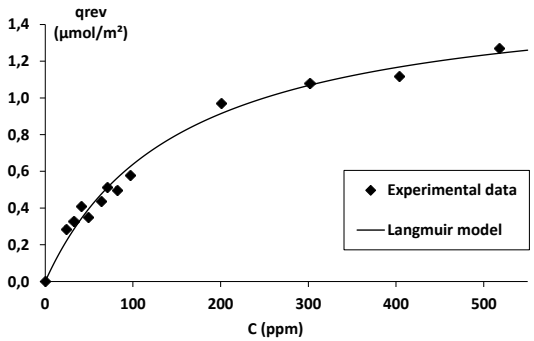

Figure 60 - Acetaldehyde reversibly adsorbed fraction isotherm on P25 TiO_2 under dry condition, at 23 ± 1 °C.

Acetaldehyde adsorption modes on TiO_2 in dry conditions / The adsorption modes corresponding to the observed reversible and irreversible fractions were investigated with the Temperature-Programmed Desorption (TPD) method, and compared with available literature data. Following the multiple breakthrough curve and RTD experimental sequences, TPDs have been conducted to characterize the adsorption modes from the irreversibly adsorbed part. Figure 61 shows the outlet concentration curve obtained during one of these TPD. TPD are performed under a 100 mL min^{-1} nitrogen flow, with a 15.6 K min^{-1} heating rate.

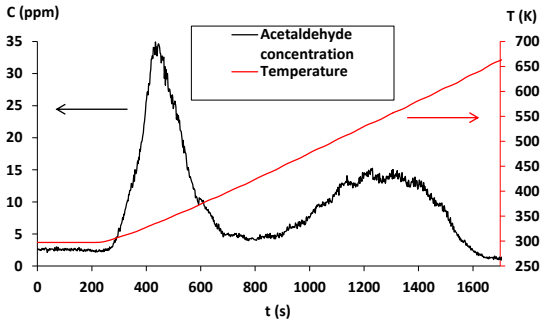

Figure 61 - Temporal profile of acetaldehyde desorbed along the Temperature-Programmed Desorption (TPD) on P25 TiO_2, under 100 mL/min dry N_2 flow and 16 K/min heating.

The TPD curve shows two distinct peaks, corresponding to two adsorption modes. Among the remaining adsorbed quantity after the RTD, only 2 % desorbed as acetaldehyde during the TPD. Most of the irreversibly adsorbed acetaldehyde molecules are not released as acetaldehyde during the TPD. Ethanol, acetic acid, 2-butenal (crotonaldehyde), benzene, carbon monoxide and carbon dioxide have been detected at the reactor outlet during the TPD. The difference between the irreversibly adsorbed quantity and the quantity desorbed as acetaldehyde during the TPD can be correlated to the adsorption modes of acetaldehyde on TiO_2. Acetaldehyde adsorption modes onto TiO_2 are described in literature. Acetaldehyde adsorbs first molecularly as a poorly stable mode by H-bond onto -OH sites and as a more stable mode through a chemical bond between the acetaldehyde oxygen and the TiO_2 surface Lewis acid sites [239][201]. Part of the weakly and strongly adsorbed acetaldehydes molecules then condensates into 3-hydroxybutanal by β-aldolization [239], which dehydrates into 2-butenal [201][239]. The relative quantities of strongly adsorbed acetaldehyde, 3-hydroxybutanal and 2-butenal depend on the temperature and on other surface conditions. Some authors

reported that only 2-butenal exists at room temperature [239]. In other works, part of acetaldehyde is converted into 2-butenal during both acetaldehyde adsorption and surface flushing [240]. It was also evidenced that acetaldehyde can adsorb as dimers, which both impede the condensation and release one of the acetaldehyde monomers while flushing [241]. Oxidation and reduction reactions can also occur on chemically-bonded acetaldehyde, leading to adsorbed acetate and ethoxy groups [201]. While heating the surface above 400K, benzene is produced from acetaldehyde and 2-butenal [201].

These literature data enable to explain the TPD curve and the presence of the other detected gases. The first peak noticed on Figure 61 can be attributed to the H-bonded adsorption mode. It can be noticed that this peak is already observed close to room temperature. Thus, this weakly bonded mode could be in some extent considered as the continuation of the RTD. The reversibly adsorbed fraction can thus be assigned to the H-bonded mode.

The second desorption peak (Figure 61) could be attributed to the chemically-bonded acetaldehyde molecules. The irreversibly adsorbed quantity which did not desorb as acetaldehyde during the TPD corresponds to i) 2-butenal, ethoxy groups and acetate groups formed during the adsorption and the RTD, which respectively desorb as 2-butenal, ethanol and acetic acid during the TPD, and ii) the thermal conversion of acetaldehyde and 2-butenal into benzene and of the other adsorbed species into CO and CO_2. In this work and regarding the targeted applications, the chemically-bonded acetaldehyde and the 2-butenal molecules can be considered as one apparent mode, since both are strongly-bonded and irreversibly-adsorbed modes.

The significant quantitative difference between both modes could be related to the surface pretreatment under dry air. Indeed, the small fraction of reversibly adsorbed acetaldehyde is due to the low hydroxyl group surface density. When the surface is pretreated at 400°C, Nagao et al [242] evidenced that the hydroxylation rate dramatically decreases. The number of hydroxyl groups per nm² falls from 7.88 (13.1 µmol m^{-2}) for a 25 °C evacuation, to 0.132 (0.219 µmol m^{-2}) for a 600 °C pretreatment. This consideration support a very low reversibly adsorbed amount compared to the irreversibly adsorbed fraction which is not impacted.

Table 34 - Langmuir model parameters of acetaldehyde reversibly adsorbed fraction on P25 TiO_2, under dry condition.

Experimental procedure	$q_{m,rev}$ (µmol/m²)	K ($ppmv^{-1}$)	ΔH (kJ/mol)
reversible isotherm	1.61 ± 0.22	0.0066 ± 0.0012	-61.6 ± 0.5
TPD	1.63 ± 0.17	Ø	-65.3 ± 6.6

ΔH and $q_{m,rev}$ related to the weakly bonded adsorption mode are determined from TPD curve. The remaining adsorbed quantity curve is fitted using the measured temperature and concentration curves (Figure 61). In order to compare values obtained from reversible isotherm and from TPD, both set of data are presented in Table 34. Obtained values do not show any significant differences. This result confirms that the reversible adsorption and the first TPD peak correspond to the same adsorption mode.

Acetaldehyde adsorption in humid air / To assess the influence of humidity on acetaldehyde adsorption on TiO_2, breakthrough and RTD of acetaldehyde have been performed under 50% relative humidity. In this condition, the adsorption has been found to be totally reversible. Water adsorption on TiO_2 is reported [243] to occur as i) dissociative adsorption, which increases the hydroxyl site density on TiO_2 surface and ii) physical adsorption of an H-bonded water molecules ad-layer. Both phenomena increase with relative humidity. Hydroxylation has been reported [244] to be complete above a RH threshold around 20%. Water molecular adsorption is described in literature to be in accordance with the BET model, and to reach complete monolayer coverage for relative humidities of 50%. The total surface hydroxylation could be an explanation to the absence of irreversible adsorption under 50% RH. A similar behavior has been reported [243] for methanol adsorption on anatase as methoxy groups, which only occurs below 10 Torr water vapor pressure. It can be noticed that at 296 K, 50% relative humidity corresponds to 10.5 Torr. Other authors found a lower threshold for water monolayer physisorption. To resume, these works tend to show that the total surface hydroxylation prevents acetaldehyde to adsorb irreversibly.

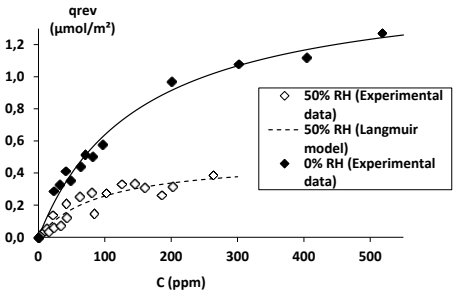

Figure 62 - Acetaldehyde reversible adsorption on P25 TiO_2 isotherm under dry and humid condition, at 23 °C.

At 50% RH, acetaldehyde adsorption on TiO_2 only occurs as reversible physical adsorption. The adsorbed quantities obtained from the breakthrough curves makes possible the plotting of adsorption isotherm for the reversibly adsorbed fraction (Figure 62). This curve has been fitted with a Langmuir model to compare the adsorption parameters of acetaldehyde physical adsorption mode under dry and humid conditions. They are reported in Table 35.

Table 35 - Langmuir model constants for the reversibly adsorbed fraction of acetaldehyde on P25 TiO_2 under dry and humid condition and 23 °C, calculated with the corresponding isotherms.

RH (%)	$q_{m,rev}$ (µmol/m²)	K (ppm^{-1})
0	1.61 ± 0.22	0.0066 ± 0.0012
50	0.49 ± 0.14	0.0109 ± 0.0040

Limitation of classical VOC and water co-adsorption model / The influence of water on acetaldehyde physical adsorption onto TiO_2 hydroxyl groups can be figured out with a Langmuir acetaldehyde-water competitive adsorption model. This can be written as reported in Equation 34.

$$q_{rev} = q_{m,rev}\frac{KC}{1 + KC + K_W C_W} \qquad \textbf{Equation 34}$$

In Equation 34 q_{rev} (µmol m^{-2}) is the amount of physically adsorbed acetaldehyde, $q_{m,rev}$ (µmol m^{-2}) is the maximum adsorbed quantity, K (ppm^{-1}) is the acetaldehyde adsorption constant, C (ppm) is the acetaldehyde gas-phase concentration, K_W (ppm^{-1}) is the water ad-layer molecules adsorption constant and C_W (ppm) the water gas phase concentration. For a given water concentration, this equation can be rewritten as an apparent Langmuir pattern in Equation 35.

$$q = q_{m,rev}\frac{K_H\, C}{1 + K_H C} \qquad \textbf{Equation 35}$$

In Equation 35, the maximum adsorbed quantity is not affected by the water ad-layer presence, and the pseudo adsorption constant K_H (ppm^{-1}) is expected to be lower than the dry adsorption constant, depending on the water vapor concentration, as shown in Equation 36.

$$K_H = \frac{K}{1 + K_W C_W} \qquad \textbf{Equation 36}$$

Thus this model predicts that the $q_{m,rev}$ value should not be effected by the adsorption competition. Since the surface is more hydroxylated at 50% RH than in dry atmosphere, the $q_{m,rev}$ value is expected to be higher in humid condition. The model also predicts that the pseudo adsorption constant should be lower in humid condition than in dry one.

As reported in Table 35, the value of $q_{m,rev}$ is higher in dry condition than in humid one, in spite of the fact that there are more hydroxyl groups in humid condition than in dry one. For VOC physisorption on TiO_2 hydroxyl groups, the $q_{m,rev}$ value depends on the surface of the adsorbed molecule and on the number of available hydroxyl sites. Then, the decrease of the reversible fraction $q_{m,rev}$ can be explained by two hypotheses: (i) part of the hydroxyl sites are not available for acetaldehyde adsorption, and (ii) adsorbed acetaldehyde in humid condition covers a higher surface than in dry condition. Both possibilities could be due to interactions between adsorbed acetaldehyde and water molecules. Surprisingly, the humid condition adsorption constant has been found to be 1.65 times higher than the dry condition value (Table 3). Nevertheless, due to uncertainty

consideration, it is not possible to completely reject the case of equal values. However, the humid condition constant was expected to be significantly lower than the dry one.

The presented model supposes that acetaldehyde and water molecules compete for adsorption onto the same sites, but do not influence one and other. The discrepancy between the model predictions and the experimental results could be due to interactions between adsorbed acetaldehyde and water molecules. Indeed, the presented model supposes that for high acetaldehyde concentration, the surface tends to be covered by acetaldehyde molecules and to retain no more water adsorbed molecules. In case of an interaction between adsorbed acetaldehyde and water molecules, for high acetaldehyde concentration the surface would tend to be covered with both acetaldehyde and water molecules.

New model for acetaldehyde-water co-adsorption / A modified adsorption model has been proposed in the PhD thesis of Frédéric Batault [3] to take into account this behavior and the above hypothesis. In this kinetic model, acetaldehyde adsorption is assumed to occur as clusters of one acetaldehyde molecule in interaction with *n* water molecules. Water is assumed to be adsorbed either as clusters, or as freely adsorbed molecules.

$$\begin{cases} CH_3CHO_{(g)} + nH_2O_{(g)} \underset{\leftarrow}{\rightarrow} CH_3CHO_{(ads)} - - - nH_2O_{(ads)} \\ H_2O_{(g)} \underset{\leftarrow}{\rightarrow} H_2O_{(ads)} \end{cases}$$ **Equation 37**

The adsorbed quantity of clusters is denoted by q_{CLU}. The corresponding adsorption rate is proportional to the gas-phase acetaldehyde concentration *C* and water vapor concentrations C_W, and to the unoccupied surface. The unoccupied surface is the difference between the water monolayer adsorbed quantity q_m' , the quantity of freely adsorbed water q_W and the number of water molecule surface occupied by one cluster. For simplification, this quantity is written as if a cluster occupied the surface on n+1 (for n water molecules and 1 acetaldehyde molecule) adsorbed water molecules. This assumption is not necessarily valid, but the difference can be enclosed into the value of the *n* constant. The cluster desorption rate is proportional to its adsorbed quantity q_{CLU}. The freely water adsorbed quantity kinetic law is also written, following the Langmuir kinetic model. Its adsorption rate is proportional to the water gas-phase concentration and to the unoccupied surface, while its desorption rate is proportional to its adsorbed quantity.

$$\begin{cases} \dot{q_{CLU}} = k_A'.C.C_W[q_m' - (1+n)q_{CLU} - q_W] - k_D'.q_{CLU} \\ \dot{q_W} = k_{AW}.C_W[q_m' - (1+n)q_{CLU} - q_W] - k_{DW}'.q_W \end{cases}$$ **Equation 38**

At equilibrium, the kinetic equations can be rewritten with the equilibrium constants $K' = \frac{k_{A'}}{k_{D'}}$ and $K_W = \frac{k_{AW}}{k_{DW}}$ to get acetaldehyde adsorption isotherm equation. It must be noticed that the adsorption and desorption constants of acetaldehyde as an acetaldehyde-water cluster are likely to be different to the acetaldehyde rate constants without water. For this reason, the adsorption constant of the cluster is written with a prime marker and is different from the adsorption constant of acetaldehyde on hydroxyl groups in dry condition, presented in Table 35.

$$q_{CLU} = \frac{q_m'.K'.C.C_W}{1 + (1+n)K'.C.C_W + K_W.C_W}$$ **Equation 39**

Equation 39 can be rewritten into a Langmuir equation pattern, with apparent Langmuir model parameters $q_{m,revH}$ and K_H, which correspond to the experimentally determined ones (Table 35).

$$q_{CLU} = q_{m,revH}\frac{K_H\,C}{1 + K_H C}$$ **Equation 40**

In this equation, the acetaldehyde maximum adsorbed quantity is:

$$q_{m,revH} = \frac{q_m'}{1+n}$$ **Equation 41**

It can be noticed that the more water molecules acetaldehyde interacts with, the lower is the maximum adsorbed amount. Please note that q_m' is not the dry condition reversibly adsorbed maximum quantity, due to the increased hydroxylation in humid condition. However, q_m' has the same order of magnitude than the dry

condition $q_{m,rev}$, the humid condition $q_{m,revH}$ is likely to be lower than the dry $q_{m,rev}$, as experimentally observed (Table 3). In **Erreur ! Source du renvoi introuvable.**, the apparent adsorption constant can be expressed as follows:

$$K_H = \frac{(1+n)K'.C_W}{1+K_W.C_W} \qquad \textbf{Equation 42}$$

In one hand, adsorption competition tends to make the apparent adsorption constant lower than *K'*. In the other hand, water-acetaldehyde interaction tends to increase the K_H value. The fact that *K'* may have a different value from *K* must be added to these both effects. It is thus difficult to conclude about these three effects. However, K_H and *K* have been found to have close values. By assuming that *K'* and *K* have the same order of magnitude, it can be suggested that the adsorption competition and the interaction between acetaldehyde and water may counterbalance.

Acetic acid adsorption on TiO_2 in dry condition / Multiple breakthrough curves and RTD of acetic acid on TiO_2 have been performed in dry condition to determine the adsorbed quantities for various acetic acid concentrations ranging from 2 to 25 ppm. The RTD evidenced that acetic acid is adsorbed both reversibly and irreversibly in dry condition. The total adsorbed quantity did not show any significant concentration dependency. The reversible fraction is determined with the same procedure than for acetaldehyde.

Figure 63 - Acetic acid adsorption on P25 TiO_2 isotherms under dry condition and 23°C of total (circles) and reversibly (diamonds) adsorbed fraction.

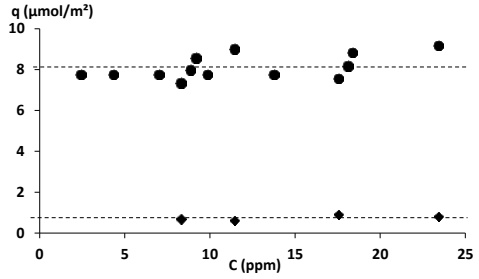

Figure 63 shows the total and reversibly adsorbed quantities versus the gas phase acetic acid concentration. The total and reversibly adsorbed quantities are respectively 8.1 ± 0.6 µmol m^{-2} and 0.8 ± 0.1 µmol m^{-2}. Similarly to the total adsorbed quantity, the reversible and irreversible fractions do not show any significant concentration dependency. It suggests that irrespectively of the input concentration, the reversibly and irreversibly adsorbed fractions always reach their maximum values. Subsequently, all the obtained adsorption equilibriums on the investigated concentration range should correspond to the TiO_2 surface saturation by acetic acid molecules, even for the lowest investigated concentrations. In the Langmuir model framework, reaching high coverage rate for such low concentrations attests a very high adsorption constant and enthalpy. Such a behavior is supposed to be incompatible with a reversible adsorption. However, a reversibly adsorbed fraction is observed for acetic acid. Nevertheless, a strong coverage dependency of the adsorption enthalpy could explain this behavior beyond the Langmuir model. These points, which significantly differ from acetaldehyde, are discussed more in details after the adsorption mode characterization.

Acetic acid adsorption modes on TiO_2 in dry conditions / A TPD has been carried out to identify the adsorption modes of acetic acid on TiO_2. The TPD curve is reported in Figure 64. It shows two peaks: an acetic acid desorption peak between 320 and 650 K, and an acetone peak above 500 K. Other species may have desorbed during the TPD, but have not been detected with the selected SIFT-MS method used. These two peaks correspond either to two adsorption modes, or to one adsorption mode desorbing under different forms, depending on the temperature.

During the TPD of acetic acid, similarly to acetaldehyde TPD, the amount of acetic acid monitored is from far lower than the irreversibly adsorbed amount. Among the acetic acid which adsorbed during the breakthrough, 9 % is desorbed during the RTD, 13 % is desorbed as acetic acid, and 24% as acetone during the TPD. This behavior is due to surface reactions onto TiO_2 while heating despite the use of N_2 as carrier gas during TPD.

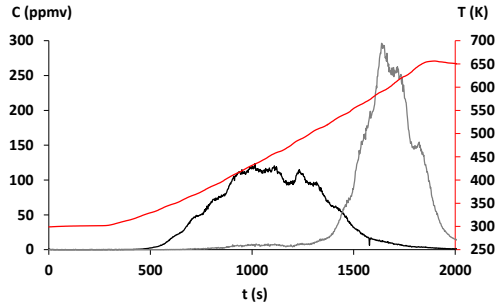

Figure 64 - Reactor outlet acetic acid (black) and acetone (grey) concentrations and reactor temperature (red) versus time during TPD of the irreversibly adsorbed acetic acid on P25 TiO_2 in dry condition, under 100 mL/min dry N_2 flow and 15 K/min heating.

Regarding acetic acid adsorption on TiO_2, three modes are described in the literature: (i) dissociative chemisorption on TiO_2 as acetate groups, (ii) molecular chemisorption by Lewis acid bonding on titanium (IV) sites, and (iii) physisorption by hydrogen interaction on the TiO_2 surface hydroxyl groups or on other adsorbed acetic acid molecules [245][246].

To identify the adsorption modes corresponding to the observed TPD peaks, similar TPDs reported in the literature are compared with this work. Kim et al [247] performed acetic acid TPD from TiO_2 anatase surface. The obtained TPD curves evidenced three desorption peaks. The first one disappeared when authors flushed the adsorption cell during sufficient time. Consequently, it is attributed to a reversible and molecular adsorption mode. During our TPD experiment, acetic acid desorption started only beyond 50°C. Considering this threshold temperature, no reversibly adsorbed acetic acid molecules are present on TiO_2 surface anymore after flushing. The reversible adsorption can be attributed in our study to the physisorbed mode, and this mode is not present after flushing in the irreversible fraction. The two other TPD peaks described by Kim et al [247] are interpreted by the authors as two different desorption pathways of acetate groups: the first one produces acetic acid, while the second one mainly leads to the release of other VOCs including acetone. Some authors reported that acetate groups on TiO_2 surface produce acetone while heating [247]. The temperature range of these peaks is coherent with the observed ones: from 350 to 600 K for the acetic acid peak and above 500 K for the acetone peak. The dissociative adsorption mode thus corresponds to these two peaks.

The molecular adsorption TPD peak could be part of the acetic acid peak. Indeed, this peak covers a wide temperature range. Thus, it could correspond to two overlapped peaks of molecular and dissociative modes. A second hypothesis to explain the peak width is an important coverage dependency of the corresponding mode.

The acetic acid TPD peak has been used to estimate the adsorption enthalpy range for the adsorption mode(s) corresponding to this peak. The acetone peak cannot be used for enthalpy determination because the Langmuir model used for the calculations implies an adsorption-desorption equilibrium. In the case of acetate desorption as acetone, it cannot be ensured that acetone adsorption as acetate groups occurs during the heating. The calculation has been carried out for two different situations.

❶ In the case of a single adsorption mode characterized by a higher coverage dependency, the enthalpies are found to range between -90 ± 21 kJ mol^{-1} (θ = 1) and -114 ± 18 kJ mol^{-1} (θ = 0). The corresponding $q_{m,irr}$ value is estimated to be 1.28 ± 0.19 µmol m^{-2}.

❷ In the case of two overlapped peaks corresponding to two adsorption modes, the enthalpies are found to range between -93 ± 5 kJ mol^{-1} (θ = 1) and -96 ± 6 kJ mol^{-1} (θ = 0) for the first mode and between -108 ± 6 kJ mol^{-1} (θ = 1) and -122 ± 10 kJ mol^{-1} (θ = 0) for the second mode. The corresponding $q_{m,irr}$ values are estimated to be respectively 0.62 ± 0.06 µmol m^{-2} and 0.60 ± 0.05 µmol m^{-2}.

The one-mode hypothesis provides a better fit of the remaining adsorbed quantity curve. Moreover, the concentration curve calculated from these parameters is a wide single peak, while the curve based on the two modes rather leads to two separate thinner peaks. The large coverage-dependency could be due to electronic effects caused by the acetate-titanium chemical bounds. As a result, we can suggest that the TPD denotes a dissociative adsorption mode, leading to the release of acetic acid and acetone while heating.

Acetic acid adsorption under humid air / Breakthrough curves and RTD of acetic acid have been carried out to calculate the adsorbed quantities under seven different acetic acid concentrations ranging from 2 to 53 ppm, and to assess whether acetic acid adsorption leads to reversible and irreversible fractions under 50% RH. Similarly to dry air, acetic acid adsorption has been found to be partly reversible and irreversible under humid

air. Both reversible and irreversible isotherms of acetic acid on TiO_2 are displayed on Figure 65 with their respective Langmuir model fits. The experiments have been performed three times for each concentration. The displayed data correspond to the averaged values. The fit obtained values are given in Table 36.

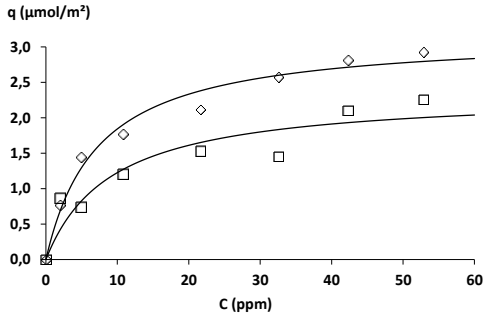

Figure 65 - Acetic acid reversibly (diamonds) and irreversibly (squares) adsorbed quantities on P25 TiO_2 isotherms under 50% RH at 23 °C, with the corresponding Langmuir model fits.

Table 36 - Langmuir parameters for reversible and irreversible fractions of acetic acid adsorption on P25 TiO_2 in humid condition (50% RH), at 23°C.

	reversible fraction	irreversible fraction
q_m (µmol/m²)	3.2 ± 0.3	2.4 ± 0.1
K (ppm^{-1})	0.14 ± 0.04	0.11 ± 0.15

The irreversible adsorption of acetic acid was not expected in humid condition, since TiO_2 surface is totally hydroxylated in this condition. The presence of this fraction can only be explained by some acetic acid removing hydroxyl groups to access the titanium sites. These acetic acid molecules could come from the gas phase, but in that case the adsorption constant of both fractions would probably be more different than experimental values reported in Table 36. They can also come from the reversibly adsorbed molecules on hydroxyl groups. Reaction equilibriums between acetic acid adsorbed as acetate groups and molecularly adsorbed acetic acid have been reported in the presence of water. Water vapor has been evidenced [245] to cause a reaction on TiO_2 surface producing chemisorbed acetate groups from physisorbed acetic acid molecules. Besides, acetate groups can react with water molecules to produce physisorbed acetic acid [246]. Consequently, acetate and H-bonded adsorption modes are in equilibrium under 50% relative humidity. A similar exchange between physically and chemically bonded modes is described in literature [243] for methanol and methoxy groups. This reaction could explain why reversible and irreversible fractions have close apparent *K* values. Indeed, if the irreversible adsorption occurs in two steps via the reversibly adsorbed state, only the first step will depends on the gas-phase concentration. The irreversibly and reversibly adsorbed fractions will thus share the same *K* value. Based on these experimental results, a detailed model has been proposed to explain the observed behaviors regarding the acetic acid-acetate equilibrium by Batault et al [24].

Table 37 gives a general overview of the adsorption experiments achieved with the five selected model VOCs under dry and 50 RH% wet air. Based on quantitative data obtained, this work led to the classification of the VOCs into three different classes as regards of their interaction with TiO_2 surface.

Table 37 - Overview of the VOC adsorption studies on TiO_2 surface. (✓) indicates that experiments are performed and parameters are determined ; (Ø) indicates that experiments are performed but the parameter was not accessible; (✖) indicates non-performed experiments

VOC	q_m		K		ΔH
	0% HR	50% HR	0% HR	50% HR	0% HR
Formaldéhyde	✓	✖	✓	✖	✓
Acétaldéhyde	✓	✓	✓	✓	✓
Acide acétique	✓	✓	Ø	✓	✓
Toluène	✓	Ø	✓	Ø	✓
Décane	✓	Ø	✓	Ø	✓

❶ **Hydrocarbons** (*toluene, decane*): this class of VOC is characterized by the coexistence of a reversibly adsorbed fraction and an irreversibly adsorbed fraction onto TiO_2 surface. These two fractions are characterized by the lowest **ΔH** values determined in this study, indicating a relatively weak interaction with TiO_2 surface. Moreover, this class can be distinguished by a significant sensitivity of **K** and $\mathbf{q_m}$ regarding relative humidity.

❷ **Carbonyls** (*acetaldehyde, formaldehyde*): this class of VOC is characterized as well by the coexistence of a reversibly adsorbed fraction and an irreversibly adsorbed fraction onto TiO_2 surface. However, both fractions differ from the hydrocarbon class by significantly higher values of **ΔH,** attesting of a stronger interaction with TiO_2 surface. This behavior has been correlated to the presence of the carbonyl functional group in the VOC structure. This class evidences no significant sensitivity of **K** and $\mathbf{q_m}$ regarding humidity. This typical behavior probably results from two competitive phenomena. On the one hand water may hinder the direct adsorption of carbonyls onto TiO_2 surface, on the other hand, relative humidities induces the presence of water layers on the photocatalyst surface which may induce favorable interactions. This aspect has been efficiently modeled for acetaldehyde and water interaction on TiO_2 surface. Considering the water solubility of formaldehyde, results may be further extrapolated to this VOC which is of major interest in indoor air.

❸ **Carboxylic acids** (*acetic acid*): this class of VOC is characterized by a major irreversible adsorption onto TiO_2 surface. This behavior can be related to particularly high values of **ΔH** as regards of other investigated VOCs. It attests of a very strong interaction with the photocatalyst surface. The observed interaction is directly correlated with the presence of the carboxylic functional group which favors the direct chemisorption of acetic acid onto TiO_2. Finally, this class is distinguished by a very poor sensitivity of **K** and $\mathbf{q_m}$ regarding relative humidity which suggests that the photocatalytic degradation of such compound should not be dramatically impacted by RH variations.

Results related to the adsorption of acetaldehyde and acetic acid have been published by Batault et al in Chemical Engineering Journal [24]. Results dealing with the three other VOCs are currently under valorization. From an application point of view, these results are highly informative about the interactions between model VOCs and TiO_2 surface. They enlighten the individual VOC behavior when treated as a mixture regarding: (i) priority interactions between TiO_2 and the various VOCs, (ii) potentially deactivating VOCs, (iii) the behavior of the different VOCs as a function of RH level. Subsequently, these quantitative data have been used to interpret phenomena observed during the photocatalytic degradation of the five model VOCs in mixture as exposed in the following.

E-11 UNDERSTANDING MULTIPLE VOC TREATMENT THROUGH ADSORPTION PARAMETERS

Introduction / The five VOCs selected for the adsorption study reported in section E-10 have been submitted to photocatalytic oxidation in the 120 L batch reactor. The purpose of this study is to further assess the mixture effect during photocatalytic treatments in order to correlated observed phenomena with adsorption properties of VOCs on TiO_2. Two sets of experiments have been conducted in the context of the PhD Thesis of F. Batault [3]: one with initial concentrations ca. 200 ppb, another with initial concentrations ca. 1 ppm. In this section, results obtained with the ca. 1 ppm experiments are presented and discussed. First, each VOC has been individually treated in the 120 L batch reactor; second, the 5-VOC mixture has been treated under the same experimental conditions. Further, the kinetic modifications induced by the presence of multiple VOCs are examined, quantified and related to respective VOC sorption parameters.

Individual degradations of VOCs / Figure 66 reported the temporal degradation profiles of acetaldehyde, acetic acid, decane, formaldehyde and toluene when individually treated. Concentrations are measured each hour by SIFT mass spectrometry. As expected, photocatalytic degradations follow a pseudo-first order kinetic. This was determined from the temporal decays linearizations which enabled the determination of the pseudo-first order reaction constant for each VOC. Corresponding values are reported on Figure 67. Kinetic constant determined for toluene and decane have been compared with former values obtained by Debono et al (toluene: 0,31 ± 0,09 h^{-1} [15]; decane0,26 ± 0,13 h^{-1} [17]) and are coherent with expected results. Both studies can be compared since experimental conditions are the same, from relative humidity to irradiation flux.

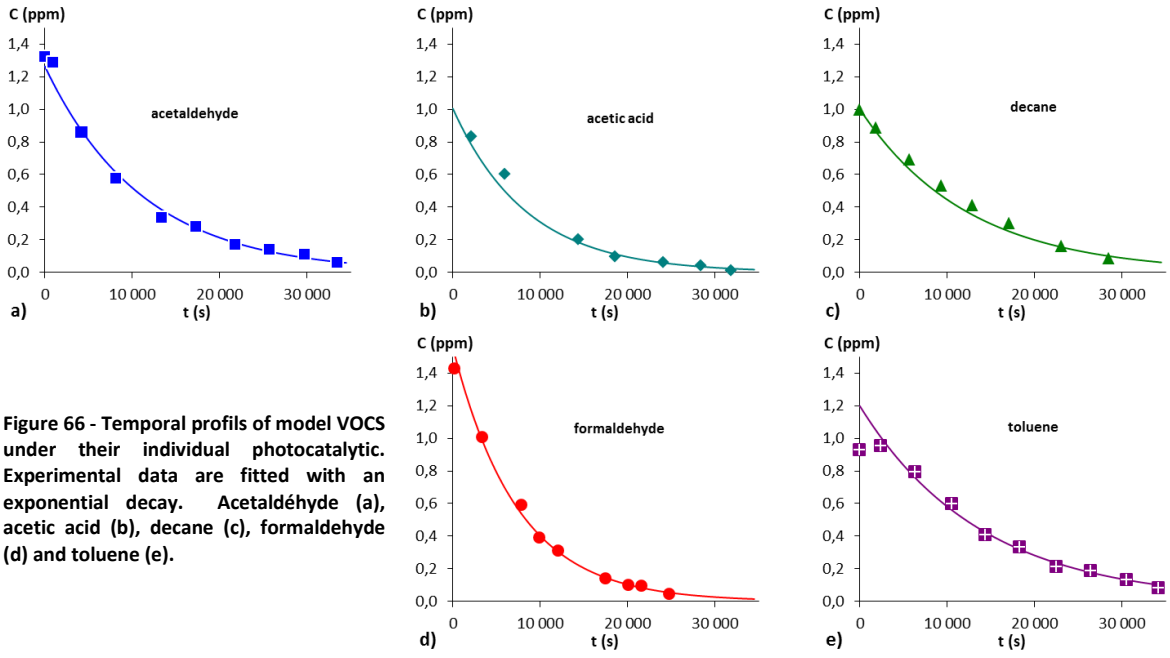

Figure 66 - Temporal profils of model VOCS under their individual photocatalytic. Experimental data are fitted with an exponential decay. Acetaldéhyde (a), acetic acid (b), decane (c), formaldehyde (d) and toluene (e).

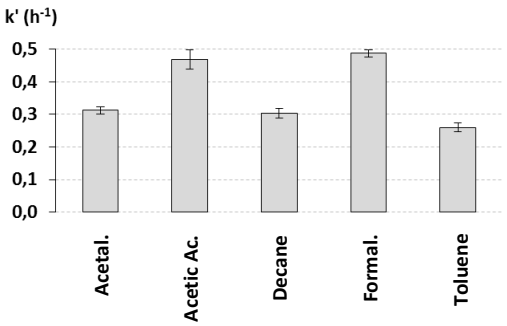

Figure 67 - Pseudo-first order kinetic constants determined during the individual photocatalytic tretament of model VOCs.

5-VOC mixture degradation / The photocatalytic oxidation of the 5-VOC mixture has been achieved with initial VOC concentrations ca. 1 ppm. Temporal profiles obtained for each VOC in the mixture are reported on Figure 68 with color filled symbols. On the same graphs, temporal profiles obtained for individual VOC degradation have been overlaid; they are represented with empty symbols. As an initial approach, temporal profiles on Figure 68 evidence a slowdown of the oxidation kinetic when the 5-VOC mixture is treated.

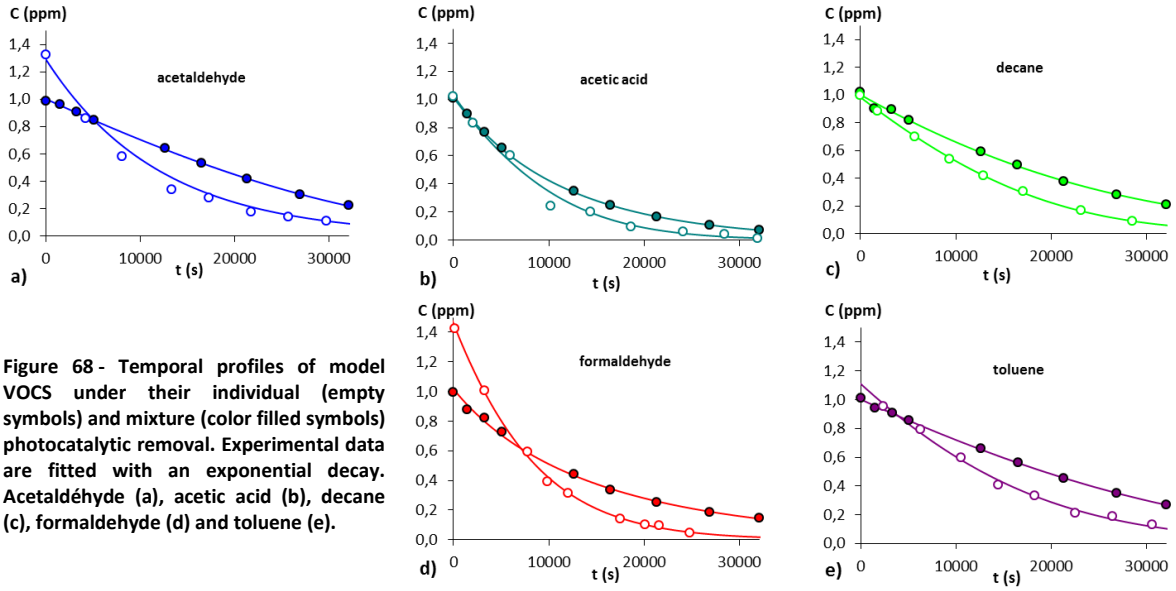

Figure 68 - Temporal profiles of model VOCS under their individual (empty symbols) and mixture (color filled symbols) photocatalytic removal. Experimental data are fitted with an exponential decay. Acetaldéhyde (a), acetic acid (b), decane (c), formaldehyde (d) and toluene (e).

In order to address more precisely the effect of mixture on the removal kinetic, degradation rates have been calculated all along the oxidation reaction for each VOC under both single and mixture conditions. In the case of individual degradation, degradation rates have been determined considering the first-order kinetic. In the case of 5-VOC mixture degradations, corresponding temporal profiles have been fitted with an adapted Langmuir-Hinshelwood equation and the fitting equations have been used to determine degradation rates. Obtained results are reported on Figure 69.

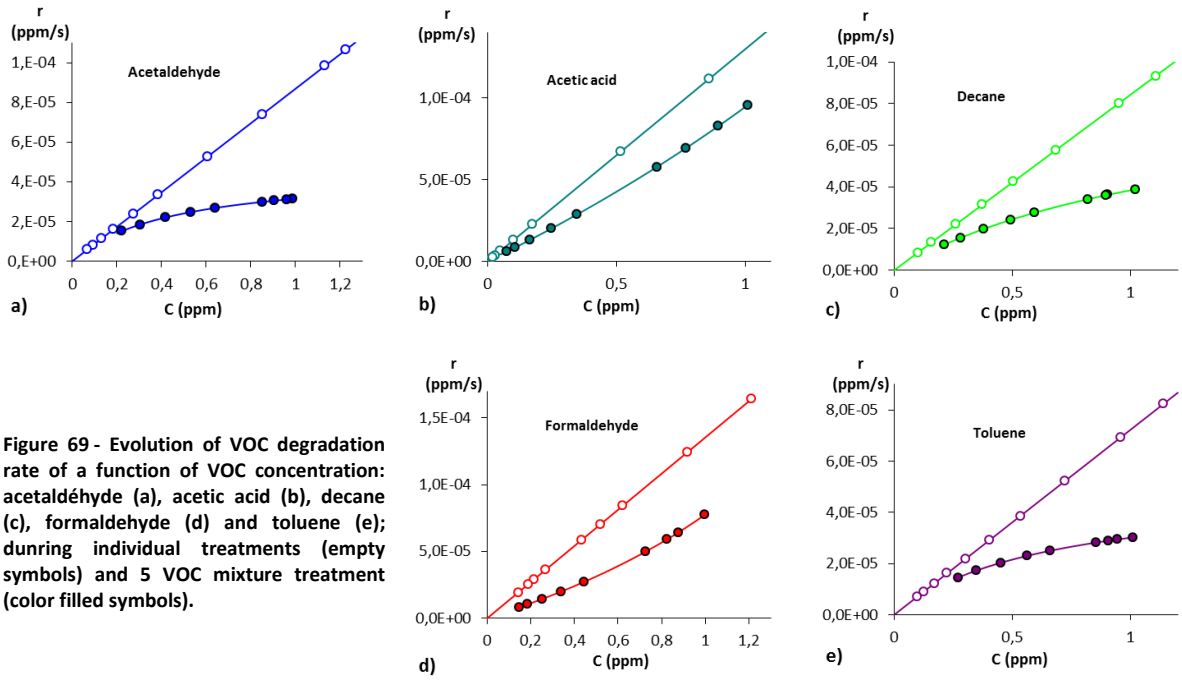

Figure 69 - Evolution of VOC degradation rate of a function of VOC concentration: acetaldéhyde (a), acetic acid (b), decane (c), formaldehyde (d) and toluene (e); dunring individual treatments (empty symbols) and 5 VOC mixture treatment (color filled symbols).

This graphical representation emphasizes the mixture slowdown effect because it compares degradation rates for an equivalent concentration, which is more relevant than an equivalent time as plotted in Figure 68. In the case of individual degradations, the removal rate is directly proportional to the VOC concentration for each investigated VOC as expected from pseudo-first order kinetic. On the contrary, no linear behavior is noticed in the case of VOC mixture. Moreover, for each investigated VOC degradation rates determined in mixture are always lower than in the case of the corresponding individual degradation.

Mixture effect and side-products effect / In the case of acetaldehyde, decane and toluene, rate profiles are characterized by concave shapes. Such a profile is coherent with the expected inhibiting effect of the mixture situation. Indeed, it means that the degradation rate is all the more inhibited by mixture that respective VOC concentrations are higher. On the contrary, formaldehyde and acetic acid are characterized by convex profiles. This shape suggests that another phenomenon is combined to the hindering mixture effect. This secondary effect may probably be attributed to the fact that photocatalytic degradations of toluene and decane generate formaldehyde and acetic acid as reaction intermediates or side-products [15][17]. The side-production of formaldehyde and acetic acid is a secondary source of these two VOCs in the batch reactor; as a result, it contributes to the apparent lowering of formaldehyde and acetic acid removal rates in the mixture conditions. This secondary hindering effect is necessarily characterized by another impact than the simple mixture effect. Indeed, the mixture effect is strongly correlated to VOC concentrations. Considering that the 5 VOCs are simultaneously degraded, their concentrations are simultaneously decreasing and the competition in between VOCs diminishes as well. It means that the mixture effect decreases with time. On the contrary, the production of side-products is a transient phenomenon which may impact the concerned VOCs after few hours of treatment. As a result, these two effects may combine in the case of formaldehyde and acetic acid leading to typical convex profiles.

Behavior at the lowest concentrations / Figure 69 evidences that the difference between individual and mixture degradation rates tends to zero for the lowest concentrations. Indeed, a concentration threshold can be determined for each VOC below which no difference is noticed regarding both sets of degradation rates. For toluene, decane and acetaldehyde, the mixture effect is noticeable till 200 ppb, no difference is visible below. For formaldehyde and acetic acid, the effect is noticeable till 100 ppb. The contribution of competitive adsorption tends to decrease with concentration, whereas the side-product generation effect may still be sensitive at the lowest concentrations since each VOC can contribute and generated side-products are directly formed on the photocatalyst surface. In the context of indoor air, meaning with total VOC concentrations lower than 200 ppb, competitive adsorption will probably poorly impact degradation kinetic. However, in the case of punctual massive release of VOC, the behavior of the compounds on the surface may lead to competitive adsorption and rapidly impact the treatment process.

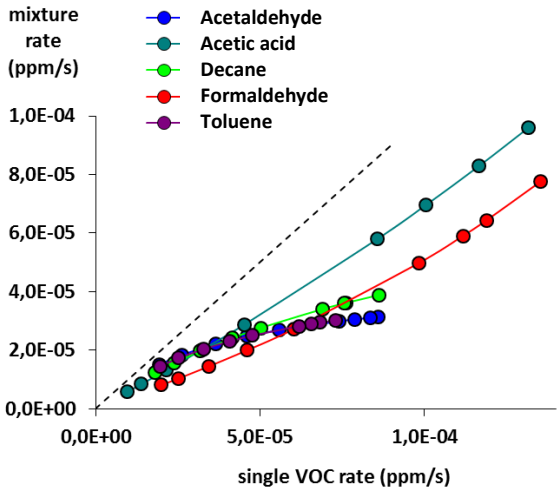

Figure 70 - Evolution of VOC degradation rates determined in mixture experiments as a function of VOC degradation rates determines during individual treatments.

First attempt to quantify the mixture effect / The impact of the mixture effect noticed for concentrations higher than 200 ppb cannot directly be compared from one VOC to another from Figure 69 since VOCs are characterized by different degradation rates. The comparison of VOC sensibility to the mixture effect can be achieved by the plotting of the mixture degradation rates as a function of the single VOC degradation rates for

each VOC. Corresponding results are overlaid on Figure 70. It appears that VOC are not affected to the same extent by the mixture effect. Since the mixture effect is the most prominent at the highest concentrations, an attempt to quantify this effect is proposed on that concentration range. To that end, it is possible to determine the slope of each curve at the highest concentrations on Figure 70 for each VOC and to calculate the difference between the obtained figures and the bisector slope. Obtained values are called VOC sensibility to the mixture effect. Indeed, if the obtained value, i.e. sensibility, is close to 0, then the VOC is not affected by the mixture effect since individual and mixture rates are equivalent; if it is close to 1, then the VOC is extremely affected by the mixture effect and the degradation maybe prevented. Determined sensibilities are contrasted; they range from ca. 0.2 for formaldehyde and acetic acid to ca. 0.8 for toluene and acetaldehyde.

Mixture effect vs. adsorption parameters / As investigated in Section E-10, VOCs interacting with TiO_2 surface lead to the partitioning of compounds between reversible and irreversibly adsorbed fractions. The intense interaction of irreversibly adsorbed fractions with the photocatalyst did not make possible the modeling of obtained isotherm with Langmuir model and the subsequent determination of K_{irr} adsorption constants. However, most of the reversible fraction adsorption constant K_{rev} have been determined under dry and wet conditions. The calculated VOC sensibility values have been plotted for each VOC as a function of the VOC adsorption constants corresponding to the reversible fraction determined under dry (K_{dry}) and wet (K_{wet}), i.e. 50 % RH. Results are reported on Figure 71 for dry air adsorption constants and on Figure 72 for wet air adsorption constants.

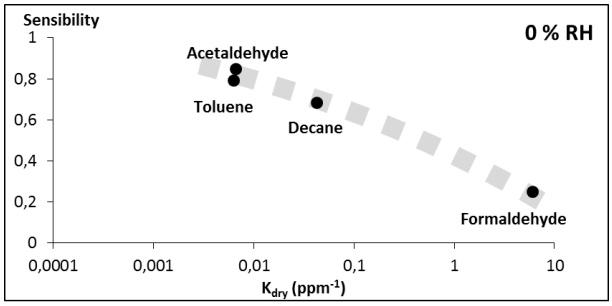

Figure 71 - Evolution of VOC respective sensibility to the mixture effect as a function of the corresponding VOC adsorption constant determined under dry air (0% RH).

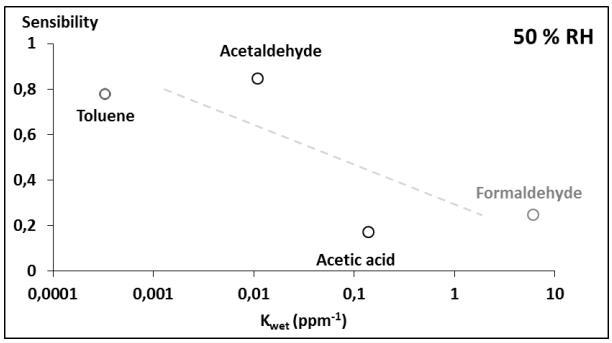

Figure 72 - Evolution of VOC respective sensibility to the mixture effect as a function of the corresponding VOC adsorption constant determined under wet air (50% RH).

Based on Figure 71 a tendency can be perceived between VOC sensibility and their adsorption constant under dry conditions. With a sensibility around 0.8, toluene and acetaldehyde or the most impacted VOCs by the mixture effect; interestingly, determined K_{dry} constant for toluene and acetaldehyde are the lowest and are very close one from another. With a sensibility around 0.65, Decane is less affected by the mixture effect; correspondingly, its adsorption constant is higher by one order of magnitude. Finally, formaldehyde seems to be poorly affected by the mixture effect; this VOC is characterized by the highest adsorption constant. Similarly, acetic acid is weakly impacted by the mixture effect; in spite of the fact that its adsorption constant was not calculated under dry air it can be estimated that it is higher than 10 ppm^{-1}, which is coherent with formerly discussed VOC behavior. **As a result, adsorption constant related to reversibly adsorbed fractions can be considered as a relevant descriptor to evaluate the impact of mixture effect on a VOC.**

Under 50% RH, the adsorption constant of acetaldehyde is close to the value determined under dry condition. However, adsorption constants related to toluene and decane are estimated to be weaker by one order of magnitude at least which is the typical behavior of non-polar hydrocarbons. The gap between acetaldehyde and toluene adsorption constant under wet conditions is mismatching with the fact that both VOCs have close

sensibility values. However, the uncertainty on toluene adsorption constant prevents from any definite conclusion. Under wet condition, acetic acid is characterized by an adsorption constant for the reversible fractions higher than 0.1 ppm^{-1} which is the upper range of determined adsorption constant. In spite of the presence of water vapor, estimated adsorption constant for formaldehyde is close to the value obtained under dry air. As reported on Figure 72, likewise to dry air conditions, VOCs characterized by the lowest adsorption constant are more affected by the mixture effect than VOCs characterized by the highest constants. The correlation between VOC sensibilities and K_{wet} adsorption constants is not as clear as it is on Figure 71 with K_{dry} constants.

Conclusion on adsorption and VOC mixture effect /

The observed decrease in VOC degradation rates has been mainly evidenced as a VOC mixture effect. Contributions of VOCs generated as side-products influence this phenomenon, but no deconvolution of both effects has been achieved yet. A new parameter, so-called sensibility, has been proposed to quantify the impact of the VOC mixture effect on each VOC. Formerly determined adsorption constants related to the reversibly adsorbed fractions have been correlated to the proposed sensibility parameter. In first approach adsorption constants determined under dry and wet air could be used as rough descriptors of the VOC sensibility. Our experimental results show that adsorption constant determined under dry air is a more accurate descriptor of the mixture effect even if the photocatalytic mixture degradation was achieved under wet air. This study is only a first attempt to address VOC mixture effect which is one of the main issues of the photocatalytic indoor air treatment. Concepts and parameters proposed here have to be tested and validated on complementary VOC mixtures to assess the robustness of our approach.

From an applied point of view, the evidence of the mixture effect, even if it is effective for VOC total concentration over 100 or 200 ppb, confirms the relevance of testing photocatalytic air treatment systems as close as possible to real indoor air conditions. Performances obtained on a single VOC, even if reaction intermediates and side-products are evaluated, cannot be extrapolated to any VOC mixture. This study points out the key role of standards to assess the performances of air treatment devices and especially the integration of relevant VOC mixtures in the standard, i.e. VOC mixture corresponding to the environment where the system is supposed to be operated. These aspects are addressed in Part-F as my first research axis perspective.

Part-F RESEARCH PERSPECTIVES

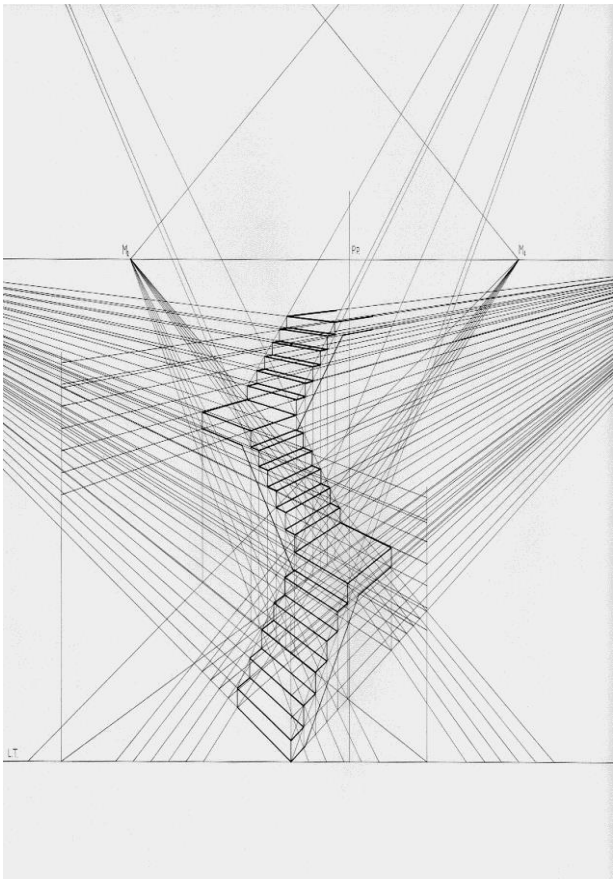

This section aims at outlining the three main research axes I plan to develop at short and mid-terms.

Two of them are related to indoor air treatment; they are the respective prolongations of my research activity and originate from results and achievements presented above on indoor air treatment by photocatalysis and plasma-material coupling.

The first one, related to photocatalysis, recently received a financial support and already began (section F-1). However, no valorization has been achieved so far, it represents my short term research perspectives. The second one, related to plasma-material coupling, is currently under conception (Section F-2).

Finally, I plan to widen my research activities to outdoor air and implement my technical and scientific developments for heterogeneous processes investigations to outdoor air; more precisely mineral dust and VOCs interactions. This research perspective is currently launched in the context of Labex CaPPA (Section F-4). It represents my mid-term research perspectives.

Introduction

As discussed in Section B and presented in Sections D and E, the question of indoor air quality is extensively addressed and the development of operative air purification solutions is highly active. In that context, this work evidenced the potentialities and the initial bases of plasma sorbent coupling applied to air treatment; similarly, it evidenced that photocatalysis is effective for indoor air treatment if preliminary qualifications are performed. These achievements have mainly been performed as close as possible to indoor air conditions and effective analytical techniques have been developed and adapted to this problematic; however it remained at classical, i.e. reduced, laboratory scale regarding the designing of the experiments which necessarily induces bias.

The main future need in indoor air treatment is the accurate assessment and development of air treatment devices at real scale. Such step forward relies on the development of large scale setups, where formerly developed analytical tools are implemented to combine the applicative large and real scale and the analytical accuracy and confidence. Moreover, the development of relevant and more precise standards are required to frame the wild booming of air treatment solutions with highly contrasted variable efficiencies. This new approach is developed in Section F-1 in the context of photocatalysis, and completed in Section F-2 in the context of plasma-material.

In parallel, the development of innovative instruments and protocols to address VOCs interactions with inorganic surface can be applied to the characterization of many other systems than air treatment processes. In section F-3, the role of heterogeneous processes involving VOCs and mineral dusts in the atmosphere in presented through a detailed bibliographic approach. This section aims at drawing the main future outlines of heterogeneous atmospheric chemistry involving VOCs I plan to investigate.

F-1 REAL SCALE ASSESSMENT OF PHOTOCATALYTIC PROCESSES FOR INDOOR AIR TREATMENT

This research perspective is the research project *ETAPE* developed since one year with ADEME and Mines Nantes. Pamela Harb, PhD student at Ecole des Mines, is involved in this research axis since January 2015.

Current photocatalytic treatments in front of indoor air reality / Based on the analysis and synthesis of the market of air treatment devices proposed by Blondeau et al. in 2005 [248], the majority of the commercially available air treatment devices are portable whether they integrate a photocatalytic step or not. Subsequently, the first standards targeted autonomous systems [84][85]. Presently, autonomous air treatment systems are employed in tremendously varied conditions. French companies are leaders on their national market regarding photocatalysis based devices; they display potential applications in many domains as diverse as hospitals, dentistry, hairdressing salon, nail bars, underground parking, smoking room, hotels, industrial working places, schools, dwellings, etc... [249][250]. Environmental conditions reported the above mentioned places are, for the most part, very far from the test conditions defined in the XP B 44-013 standard [84]. Indeed, the mentioned standard requires the generation of a single pollutant matrix comprising only four VOCs, namely acetone, acetaldehyde, heptane and toluene. It is necessary to define and propose test gas matrixes corresponding to typical ambiances to assess the performances and the innocuity of the photocatalytic devices. Moreover, experimental conditions proposed by the standard authorizes experimental chamber as low as 1 m^3. Compared to the treated air flow of photocatalytic autonomous devise ranging from 20 to 200 m^3 h^{-1}, the mismatching between the test conditions and the reality is huge. Finally, the quantitative criterion proposed by the current standards to mark the performance of the tested system, so called CADR (Clean Air Delivery Rate) only comprises the removal of the primary pollutant. Even if the monitoring of some reaction intermediates and side products is required by the standard, they do not interfere in the CADR determination.

Organic side-products generated by photocatalytic reaction / Academic studies initiated since the early 90s about photocatalytic indoor air treatment emphasized the abatement of primary pollutant as the key criterion to qualify the process performance. However, the mineralization of primary organics may be incomplete or even decrease along time, leading to release of secondary organics in the treated air:

Secondary Volatile Organic Compounds

➲ Results obtained by Olivier Debono about the photocatalytic treatment of VOCs under typical indoor air concentrations at ppb levels have clearly shown that the mineralization of toluene and decance is possible, but concomitant with the release a wide diversity of secondary VOCs [15]. In the case of toluene and decane respectively 15 and 18 gas phase reaction intermediates have been evidenced. Beside, formaldehyde is the main side-product.

In order to take this reality into account, standards require the measurement of some secondary organics to test the efficiency of photocatalytic devices [84]. However, the diversity and the concentration of side-products are directly dependent on the composition of the gas matrix to be treated. Subsequently, this aspect should definitely be evaluated through more representative primary pollutant matrixes than the single classical one proposed by XP B 44-013 [84].

Secondary Organic particles

➲ Numerous studies have demonstrated that limonene ozonolysis leads to secondary organic aerosols (SOA) formation with high yields. This homogeneous reaction between ozone and limonene is well described and reported. In indoor atmosphere, the significant occurrence of limonene can make possible the formation of ultrafine particles in the presence of ozone. A recent study has shown SOA formation during the use of a detergent containing limonene [251]. It confirmed that the oxidation of limonene emitted from housecleaning products by ozone is responsible for the SOA formation in real indoor environments meaning with typical indoor air concentrations.

Interestingly, Ourrad et al. [25] have shown the possible heterogeneous production of SOA along photocatalytic oxidation of limonene under typical indoor air conditions. As a consequence, SOA have to be considered as potential harmful side-products of photocatalytic processes.

Inorganic particle release / The most widespread photocatalyst implemented in photocatalytic air treatment devices is TiO_2; this nano-structured material requires a specific anchorage on substrates to be compliant with air treatment process expectations. Thus, the material processing has to combine: (i) strong fixation of photocatalyst, (ii) optimized contact between pollutants and media. Photocatalytic media may consist in (i) the binding of nano-particles or (ii) coating of thin layers on solid substrate as respectively made by *Ahlstrom* and *Saint-Gobain*. Under real operating conditions, the continuous use of photocatalytic media, along with the global ageing of air treatment systems with time, may lead to the release of solid inorganic particles at the system downstream coming from the photocatalyst itself or any other inorganic binder, such as silica or alumina, frequently used in the media processing. This long-term behavior is (i) not addressed at all by air treatment device providers and (ii) not taken into account by any standard yet. However, it may considerably impact (i) long-term performances of the systems and (ii) health of exposed people.

Issues of the research axis / Recent research activities related to photocatalysis and indoor air treatment tend to make experimental conditions closer to real indoor air conditions in terms of pollutant concentrations, pollutant diversity, relative humidity. This research axis aims at going further into this approach through :

- ➲ the development of a large scale (40 m^3) experimental room to reproduce and control indoor air,
- ➲ the generation of complex and humid gas phase matrixes,
- ➲ the implementation of real scale air treatment devices.

Moreover, apart from the abatement of primary pollutants, it is essential to assess the innocuity of air treatment devices, since it is a key point for people's health. This research axis proposes to complement the assessment of innocuity through three criteria related to side-product generation:

- ➲ identification and quantification of gaseous organic reaction intermediates and side products,
- ➲ identification and quantification of secondary organic aerosols,
- ➲ identification and quantification of inorganic particles released by the photocatalytic media.

Objectives of the research axis / The final goal of this research axis is to assess the relevance of the current standard to assess photocatalytic air treatment devices and to propose standard evolutions in order to ensure that, based on this new standard, photocatalytic air treatment devices are effective and safe.

Experimental objective	Scientific objective
➲ This research axis aims at making a significant step forward through the development of an innovative 40 m^3 experimental room characterized by controlled indoor air conditions.	➲ This research axis aims at characterizing the performances, the limitation and the innocuity of real scale air treatment devices under typical indoor air conditions.

Novelty of the research axis / The novelty of this research axis relies on: (i) the challenging development of a 40 m^3 experimental room and (ii) the definition of various and typical indoor air gaseous matrixes to evidence the contrasted behavior of air treatment devices in front of different indoor atmosphere.

Characteristics of the developed 40 m^3 experimental room / Experiments carried out in this research axis are planned in a unique 40 m^3 experimental room developed by our research group. It consists in a 12.5 m^2 and 40 m^3 room. An overview of the experimental room is given on Figure 73. Walls are covered with aluminum to minimize the adsorption and the subsequent desorption of pollutants introduced inside the room. Temperature and humidity are regulated through a looped autonomous air conditioning system. Temperature can be tuned from 15 to 28°C with an accuracy of 1°C, they are homogeneous in the different points of the chamber. Relative humidity typically ranges from 30 to 65 %, depending on the room temperature. Both parameters are constantly monitored by four probes placed in different locations inside the room. The air renewal rate of the room is controlled and regularly monitored through CO_2 injections and decays. Over a span of one year, the air renewal rate inside de room is controlled at 0.20 ± 0.05 h^{-1}.

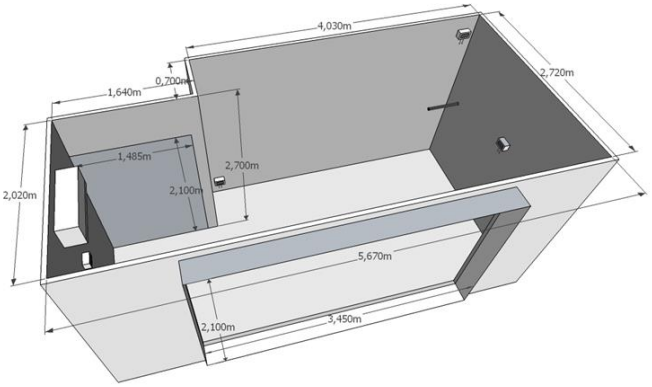

Figure 73 - Overview of the 40 m^3 experimental room developed and validated for real scale indoor air studies.

From the outer part, the room is equipped with a VOC injection system. The developed system relies on the heating and fast pressurized injection of vaporized liquid VOCs. The definition of precise and controlled VOC amounts lead to the generation of gaseous VOCs with individual concentrations ranging from 50 to 1000 ppb. Mixtures of VOCs can be simultaneously injected in the experimental room. From an analytical point of view, the experimental room is equipped with: (i) **Automated sampling ACROSS system:** this device is used for general hydrocarbon sampling on cartridges or more specifically carbonyl compounds sampling through derivatization on DNPH cartridges. Sampled are analyzed of line by GC or HPLC; (ii) **Gas Chromatograph** combined with thermal desorption unit, FID and MS detectors for on line or off analyses of VOCs, this system can also be used on-line by direct sampling inside the experimental room; (iii) **HPLC-UV** for off line analyses of carbonyl compounds sampled on DNPH cartridges; (iv) o**zone analyzer**: to assess the generation of ozone inside the room; (v) **SMPS and DMA analyzer** for counting of particles and the determination of their size distribution.

Typical indoor air matrixes / In the framework of this research axis, five different typical indoor air matrixes have been defined, they comprise from 5 to 6 VOCs which have been determined as specific of one type of indoor air from literature studies:

❶ **Standard** indoor air matrix [*formaldehyde, acetaldehyde, acetone, toluene, decane*];
❷ **Urban** indoor air matrix [*formaldehyde, acetaldehyde, butadiene, benzene, toluene, decane*];
❸ **Hospital** indoor air matrix [*formaldehyde, acetaldehyde, halothane, isopropanol, toluene*];
❹ **Wood-based** buildings indoor air matrix [*formaldehyde, acetaldehyde, acetone, toluene, α-pinene*];
❺**Household products** indoor air matrix [*formaldehyde, acetaldehyde, isopropanol, limonene, α-pinene*].

F-3 PLASMA-TAILORED MATERIAL COUPLING FOR FORMALDEHYDE TREATMENT

This research axis is currently developed in partnership with *Laboratoire de Physique des Plasmas* from *Ecole Polytechnique* (Antoine Rousseau) and *Laboratoire de Chimie de la Matière Condensée de Paris* from *Université Pierre & Marie Curie* and *Collège de France* (Sophie Cassaignon). Based on the studies presented in Section D about plasma-sorbent for indoor air treatment, this research axis aims (i) at going further in that technology and (ii) at solving the specific problem of formaldehyde in indoor air.

Formaldehyde in indoor air

Classification / Among the various VOCs found in indoor air, formaldehyde is a key issue. It is a typical indoor pollutant since its concentration is from 10 to 30 times higher than outdoor. Interestingly, the French observatory of indoor air quality (OQAI) proposed a list of indoor VOCs classified according to their occurrence and toxicity [37]. Three VOCs were classified in the group of "priority pollutants": benzene, acetaldehyde and formaldehyde. Among them, formaldehyde is characterized by the most worrying index.

Sources / Synthetic materials containing foams, resins or glue, and wood based synthetic products, as well as insulation rock wool are the main sources of formaldehyde in indoor air. Emissions are highly dependent on the structure of the emitting material (composition, porosity, surface). They are generally enhanced by temperature and moisture, even if emissions tend to decrease with time. In French dwellings, formaldehyde concentrations range from 1.3 to 86.3 µg/m^3 (1 to 70 ppb), similar concentrations are monitored in schools and offices [38].

Toxicity / Because of (i) high volatility, (ii) excellent water solubility and (iii) high reactivity with organic tissues, formaldehyde is characterized by significant toxicity for short term as well as long term exposition. Subsequently, based on epidemiological studies, formaldehyde was classified as carcinogenic compound of Group 1 in 2004 [34].

Regulations / In order to protect people from formaldehyde exposure, guideline values have been defined. The first guideline was proposed by WHO in 2000 and set as 100µg/m^3. Based on the work of the French AFSSET group (*Agence Française de Sécurité Sanitaire de l'Environnement et du Travail*) French guidelines were set as 50µg/m^3 in 2007 for short term exposure. For indoor air, this value will be reduced to 30 µg/m³ (24 ppb) beyond January 1st 2015, and 10 µg/m³ (8 ppb) beyond January 1st 2023. In parallel regulations on the monitoring of some species in indoor air appeared. From 2015 to 2023 the monitoring of these species will be applied to a wider range of public buildings and the certification of private new buildings regarding indoor air quality is currently under preparation. Considering that the current mean value of formaldehyde in indoor air is 20 µg/m³ (16 ppb) considerable efforts have to be made to reach the guidelines, especially in recent buildings where formaldehyde concentration generally exceeds 50 µg/m³ (40 ppb).

These aspects reveal the urgent situation regarding formaldehyde and indoor air quality. The research axis is located at the key moment when modern buildings have to satisfy antagonist demands. **How is it possible to combine energetic efficiency, modern construction techniques and materials, and indoor air quality in the same building ?**

Plasma regeneration of sorbents / A new approach consists in adsorbing the pollutant on a porous adsorbent which is sequentially regenerated by plasma; the main advantage of the proposed technique is that the plasma is switched on for a limited time reducing significantly the power consumption in comparison to continuous plasma treatments and thermal regeneration of sorbents. As recently shown by Sivachandiran *et al.*, compared to continuous treatment, the sequential regeneration of saturated sorbents by plasma consumes 14 times less energy [26]. Moreover, *in-situ* non-thermal plasma regeneration offers higher mineralization than direct thermal treatment, and better sorbent regeneration compared to *post-situ* (ozonolysis) process [21]. The key point of such process is the pre-concentration step of the targeted pollutants on a sorbent, subsequently:

- ➲ the process is operative for any concentration range, even indoor ppb levels,
- ➲ the discharge is ignited only once the sorbent saturation is achieved to save energy,
- ➲ oxidative species are directly generated in the sorbent surface vicinity to optimize energy
- ➲ surface chemistry of the sorbent can be used to enhance oxidation as synergetic effect,

➲ emission of side-products is prevented not to generate secondary contaminants,
➲ residence time of pollutants is high and mineralization (conversion into CO_2) is enhanced.

So far, only the feasibility of sequential adsorption/non thermal plasma regeneration process was evidenced, and model VOCs have been used (isopropanol, acetone) far from real indoor air conditions. Nevertheless, these preliminary investigations emphasized the crucial role of:

- sorbent surface chemistry (ozone decomposition, redox properties,...),
- sorbent morphology (porosity, specific surface),
- pollutant adsorption parameters on the sorbent (adsorption constant, maximum adsorbed amount)
- water adsorption parameters on the considered sorbent,
- sorbent physical impact on plasma deposited energy.

Plasma-sorbent interaction / The introduction of a material inside the discharge gap implements heterogeneous reactivity into the system. Basically, the presence of the material shortens the discharge gap, modifies the **plasma characteristics** and the discharge behavior. More specifically, the material changes the VOCs decomposition mechanisms owing the VOCs adsorption on its surface. Reactive species such as oxygen radicals and ozone, produced by plasma, can be transported to the material surface. These species may alter and/or take part in the chemical environment of the material surface. Then, they may adsorb and/or react with the adsorbed molecules. As a consequence, coupling a material with a NTP will have mainly two effects:
➲ Modification of the energy transfer to the gas (lowering of breakdown voltage, change of electron energy…),
➲ Gas - surface transfer of plasma produced reactive species and pollutants.

Adsorption and desorption of pollutants from the material surface are key parameters in coupling processes. The **adsorption** of VOCs on catalyst surface changes its retention time and concentration in the discharge zone. In addition, **desorption** of obtained products makes the renewal of pollutants on the surface possible.

Sorbents / Metal oxides appear as the best candidates since they combine (i) good adsorption properties for VOCs, (ii) tuneable surface reactivity compliant with oxidation reactions and hydrophilicity, and (iii) resistance to long-term plasma exposure. Compared to zeolites they can be coated on structured substrates. Compared to activated carbon they promote chemisorption of VOCs rather than physisorption and make possible the characterization of the process carbon mass balance. TiO_2, MnO_2, CeO_2 and their mixtures have to be considered. Commercially available materials do not provide a sufficient and reliable range of (i) specific surfaces, (ii) morphology, (iii) porosity and (iv) crystalline phases. Therefore, the synthesis of the targeted materials with required characteristics is performed in this research axis. Mastering of the synthesis at the LCMCP allows considering a broad comparative study of different metal oxides with perfectly defined characteristics.

In the framework of this research axis, a tailored sorbent / non-thermal plasma coupling process is specifically developed, characterized and validated for formaldehyde removal and oxidation under typical indoor air conditions.

Fundamental and applied objectives of this research axis /

The **operational objective** of this research project is to develop and validate, at real scale, an innovative indoor air treatment process dedicated to the abatement of formaldehyde. This process aims at making indoor air formaldehyde levels compliant with future regulations in modern buildings. The process results in the sustainable removal and mineralization of formaldehyde at low energy and low maintenance costs.

The **scientific objective** of this research axis is to address sorption as well as oxidation of formaldehyde on specially designed and optimized sorbents to be implemented into a large-scale process. Combining material science with heterogeneous physical chemistry and process engineering, the fundamental step forward on *in-situ* monitoring onto mastered surfaces aims at unlocking the process real scale development.

The following operational and fundamental points are more specifically targeted:

- Sorbent surface properties (hydrophilicity related to formaldehyde adsorption, O_3 decomposition).
- Sorbent morphology (porosity, specific surface) related to plasma deposited energy.
- Formaldehyde adsorption parameters.
- Time resolved adsorption and oxidation kinetics and pathways.
- Carbon mass balance determination at ppb levels.
- Impact of indoor air co-pollutants on the process efficiency
- Up scaling to real scale to assess process performances
- Innocuity (side product) and sustainability in large volume chambers

Novelty of the research axis / This is a frontier research axis ranging from controlled material synthesis to heterogeneous reactivity and process validation; it associates three approaches at three different scales.

➲ **Nano-Scale**: Specific metal oxide based sorbents are synthesized, characterized and optimized to achieve the most efficient adsorption of formaldehyde and oxidation under plasma exposure.

➲ **Micro-Scale**: Adsorption and plasma induced oxidation of formaldehyde are investigated in-situ on the sorbent surface in order to screen the various sorbents, to determine the process limitations and to prepare the process optimization.

➲ **Macro-Scale**: A real-scale air treatment unit is developed and implemented on large volume experimental chambers to assess the process performances under typical indoor air conditions (ppb level of HCHO, presence of other VOCs and co-pollutants, high humidity levels), the long term efficiency and the innocuity of the process are more especially determined.

Innovative aspects of the research axis /

Interdisciplinary / So far, research efforts on plasma-material coupling were oriented toward plasma technology development. Thus, only basic and commercially available materials were used. However, understanding the plasma material coupling pointed out (i) the role of sorbent morphology, and (ii) the contrasted behaviors of the different materials. Then, it was necessary to combine aptitudes in material science (LCMCP) and plasma technology (LPP). Moreover, the real scale validation and optimization of the targeted process required competences in analytical chemistry and indoor air monitoring (SAGE).

Controlled synthesis of sorbents / The controlled synthesis and the optimization of dedicated sorbents to be coupled with plasma are both highly novel aspects of this project. The research axis goes far beyond the commercially available materials. As detailed further, sorbent synthesis is achieved in two steps: (i) screening and characterization of selected metal oxides, (ii) synthesis of optimized sorbents.
This approach leads to the formulation of mixed sorbents, optimized regarding their specific surface, porosity and morphology, and dedicated to HCHO sorption and mineralization under NTP.

In-situ reaction monitoring / The surface monitoring of adsorbed pollutants and oxidation intermediates is a key step for the control of indoor air treatment process since it governs (i) performances and (ii) ageing and deactivation. A new surface analyzer, Sorbent-TRACK, is integrated to this project. It makes possible the dynamic and quantitative adsorption and oxidation *in-situ* monitoring of HCHO and side products, directly on sorbents using transmission infrared spectroscopy (FTIR) coupled with quantum cascade lasers diodes. A major advantage is interestingly to operate this highly innovative surface diagnostic: (i) under the direct exposure of sorbents to the plasma, (ii) in the presence of typical indoor air humidity levels.

Real scale process evaluation / In order to step beyond the fundamental understanding of plasma / sorbent coupling the SOFIA project aims at implementing the fundamental achievement to real scale process. The process up-scaling challenge is completely integrated to the project. To that end, process performances are evaluated in large-scale experimental chambers. The largest one, with 40 m^3 in a novel and unique device brought to the project by Armines - SAGE. Moreover, pollutant concentrations generated in the chambers will perfectly mimic the typical pollutant diversity and ppb levels encountered in real indoor air. This approach makes possible the accurate assessment of such plasma - sorbent process performances and innocuity for the first time.

F-3 HETEROGENEOUS REACTIVITY IN ATMOSPHERIC CHEMISTRY: VOC INTERACTION WITH MINERAL DUSTS

This research axis is currently launched in the framework of the French *Labex* (*Laboratoire d'Excellence*) *CaPPA*. A post-doctoral researcher, Manolis Romanias, has been recruited since august 2015 in order to stress our research activity in that interesting domain. A PhD student is recruited in November 2015 on that topic with a dual financial support from *Region Nord-Pas-de-Calais* and *Labex CaPPA*. The *Labex CaPPA* gathers 8 regional laboratories from Ecole des Mines, Dunkirk University and Lille University. Partner labs focus their activities on aerosols and more precisely the origin of aerosols and their impact on climate. It is divided into work-packages combining lab scale studies, field campaigns and theoretical modeling. This project spreads over a 7 years span: 2012 to 2019.

Global atmospheric context / Atmospheric composition has never been constant, interactions between the Earth surface and its gaseous envelope inducing significant modifications with consequences on climate and life. Until the twentieth century, these evolutions occurred on long time scales, likely hundreds of years. However, atmospheric composition changes have been accelerated since the beginning of the industrial era. Human activities led to an increase of anthropogenic emissions of chemical species and particles in the atmosphere, as well as changes in biogenic emissions. These modifications may have a global impact on the Earth system, involving issues of (i) climate change, (ii) air quality, and (iii) deleterious effects on ecosystems. As highlighted by Granier et al. [252], these changes may affect human health, food production, ecosystem equilibriums, and water availability. Since the first world climate conference held in Geneva in 1979, scientific groups, environmental bodies, and policymakers aimed at (i) highlighting the risks of climate change and (ii) defining protocols to promote the limitation of anthropogenic emissions in the atmosphere. Their approach relies on our capabilities of atmospheric composition monitoring and prediction. As a consequence, an improvement of our understanding of atmospheric composition is a prerequisite to (i) design optimal strategies for sustainable development and to (ii) evaluate the impact of sustainable development recommendations.

Earth's atmosphere as a heterogeneous chemical reactor / Atmospheric chemistry is mainly described in models by gas-phase physico-chemical processes. Among them, homogeneous photochemistry is considered as the key process controlling the reactivity of atmospheric trace gases. Considering only homogeneous reactions to describe atmospheric physics and chemistry would be appropriate if the atmosphere were only composed of gaseous species. However, this approach does not correspond to reality. Indeed, the Earth's atmosphere contains more than 1 billion tons of solid particles creating interfaces between the gas and solid phases [253]. These solid particles can either originate from natural phenomena or anthropogenic activities. Both origins lead to the release of soil particles, colloids, and micro-crystallites of minerals or organic aerosols in the atmosphere [254]. An important class of particles is produced by the Earth's crustal erosion, i.e. continental aerosols that are mainly composed of minerals. These mineral particles represent approximately 50% of the total amount of aerosols released in the atmosphere. As a consequence, reactions of trace gases occurring onto mineral particles may have an important impact on atmospheric composition and their inclusion into models of atmospheric chemistry may greatly improve the models' reliability.

Discrepancy between field measurements and models / Interactions between mineral dust particles and atmospheric trace gases may have strong effects on the chemical composition of the atmosphere for both the gaseous and the condensed phases. It has important implications for issues related to air quality and climate change, since such interactions can alter (i) the physical and chemical properties of the particles, (ii) the oxidative capacity of the atmosphere, and (iii) the budget of reactive gases such as volatile organic compounds (VOC) and nitrogen oxides (NO_x) that are key players in the formation of secondary pollutants (such as ozone), and the formation of secondary organic aerosols (SOA).

Volatile Organic Compounds	Secondary Organic Aerosols
➲ Comparisons between field observations and model predictions suggest that taking only gas-phase reactions into account is not sufficient to simulate the atmosphere chemical composition Using both '*chemical box models*' and '*chemistry transport models'*, recent studies investigated the impact of mineral dusts on the concentration of	➲ Similarly to the disagreement reported for OVOCs, modeled concentrations of SOA are usually lower than field observations. Numerical models describing aerosol formation, transport, transformation, and removal in the atmosphere have become available to estimate particulate matter (PM) levels by extrapolating observation

trace gases in the troposphere (SO_2, NO_x, HNO_3, and O_3) [255]. They indicate a significant local influence of mineral dust particles on tropospheric chemistry, but highlight large uncertainties in the modeled results due to inconsistencies in the reported uptake coefficients for the studied trace gases [256]. In addition, large uncertainties are associated to the uptake and ageing of VOCs on mineral dusts due to a lack of understanding of these processes. For example, recent field observations of light oxygenated VOCs (OVOCs) in remote locations have shown discrepancies with model calculations; concentrations of acetaldehyde and propanal measured in the Pacific troposphere were up to ten times higher than modeled concentrations [257], [258], [259]. Similarly, measurements in marine air over the Indian Ocean [260] and in the Northern Atlantic [261] also suggested higher-than-expected concentrations of light OVOCs. There are ongoing discussions to determine whether part of these discrepancies could be assigned to measurement artifacts [262], emissions from the ocean [258], oxidation processes during long range transport of hydrocarbons [261], or an, as yet unidentified, diffuse source of OVOCs. Such a source of OVOCs was recently proposed from the heterogeneous oxidation of organic aerosols in the troposphere [263]. It is interesting to note that long-range transport of mineral dust particles coated with organic compounds could also act as a diffuse source of OVOCs, especially if light-induced chemical processes occurring at the particle surface can enhance the oxidation rate of adsorbed organics.

data [264], [265]. However, the discrepancy between modelled and observed gravimetric measurements remains significant (underestimation of 40-60% for the EMEP model for instance, where SOA and wind-blown re-suspended dust were not taken into account). Besides, when comparing gravimetric measurements with chemical masses derived from particle composition analyses, a full chemical mass closure is rarely achieved, i.e. some compounds remain unidentified after all major constituents have been analysed (e.g. CARBOSOL campaign).

Three possible causes have been proposed to explain these disagreements: (i) measurement artefacts (either during sampling or analysis); (ii) an underestimation of the water content of the particles; (iii) uncertainties related to the organic aerosol composition, especially on the nature and proportion of atoms linked to organic carbon (OC). For example, Tsyro [266] has calculated that when PM measurements are corrected by their water content, only a fraction of the unexplained mass could be resolved (30-80%, depending on the observation site). The organic carbon under-prediction is generally thought to be due to gaps in emission inventories of wood burning.

Similarly to VOCs, the heterogeneous reactivity of SOA precursors on mineral dust particles may explain part of the discrepancies observed between field observations and model calculations of SOA concentrations.

Recent research projects focusing on atmospheric chemistry rarely consider heterogeneous reactions involving mineral materials, except the European *Photopaq* project. The latter investigates heterogeneous reactivity on urban surfaces such as buildings and is therefore more relevant to the local urban scale.

A typical study case, Beirut, Lebanon / Several places around the world are characterized by a high population density, leading to significant anthropogenic emission, and submitted to biogenic VOCs and high levels of mineral dust particle. Among them, Beirut is an interesting study case.

Overlooking the Mediterranean Sea, Beirut is an urban city located at the crossroad of various atmospheric influences. As reported by Kouyoumdjian and Saliba [267], the highest concentrations of PM_{10}, $PM_{10\text{-}2.5}$ and $PM_{2.5}$ recorded in Beirut over a monitoring period of one year were directly correlated to sand storms coming either from the Arabian Desert or the African Saharan Desert. Similar measurements performed by Ganor et al [268] in the Middle East indicate that Arabian and Saharan dust storms contribute to more than 20% of the annual average mass of PM_{10} and $PM_{2.5}$ deposited in the region. Mineralogical and chemical analyses of mineral dust particles collected during dust storms in the Middle East confirm their origins, with silicates, aluminates and various transition metal oxides being the main components of these particles. It has to be noted that Saharan mineral dust particles are especially rich in iron oxides. The study of Saliba et al [269] showed the predominance of crustal elements in PM_{10} during dust storm episodes, such as Si, Ti, Mn and Fe. Apart from their mineralogical compositions, their global chemical compositions were different in that Saharan mineral dusts contain more salts and organic compounds. The authors explained this increase by dust ageing during transport over the Mediterranean Sea (salt) and over urban areas of Egypt and Israel, which had been formerly evidenced by Levin et al [270] and Falkovich et al [271]. This ageing phenomenon confirms that:

➲ mineral dusts are able to **adsorb** various chemical compounds on their surface (salts, VOCs, PAHs, NO_x, etc.)

➲ depending on their composition and atmospheric conditions (solar irradiation, presence of oxidants), heterogeneous **reactivity** may occur at the surface.

Regarding VOCs, anthropogenic emissions are rapidly increasing in the Beirut area because of developing industries, dense traffic, and high population density. Moreover, Beirut is enclosed between the Mediterranean Sea and the Lebanese mountains, which usually leads to intense episodes of pollution by anthropogenic compounds. Emission inventories of gas phase species from this region were performed by Waked et al [272] and Waked and Afif [273]. These measurements have been used to model air pollution in Lebanon, and more especially in Beirut [274]. In terms of abundance, toluene and butane are the two major compounds. Short alkenes, including propene, are also present. These species are measured at significant concentrations over the whole year. In contrast, biogenic VOCs are only observed during the warmest months in Beirut suburbs (April-October). These biogenic VOCs are transported from the close mountains covered by pine trees to the East of Beirut. Isoprene is the most abundant biogenic VOCs, with α-pinene and limonene observed at lower concentrations.

The presence of fresh and aged mineral dusts, combined to the emission of anthropogenic and biogenic VOCs, make Beirut the perfect framework to illustrate this research topic as shown in Figure 74.

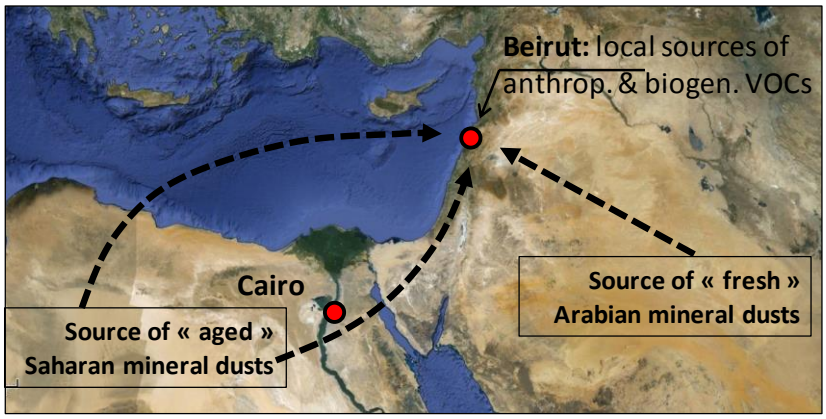

Figure 74 - General situation of Beirut, Lebanon

Mineral dusts as heterogeneous photocatalytically reactive atmospheric platforms / Mineral dust particles may act as efficient platforms for the adsorption and reaction of atmospheric trace gases and organic particles. Two pathways may be considered for VOCs: (i) non-reactive sorption, which would result in long range transport of unmodified species; (ii) reactive sorption, leading to the conversion of primary organics and the formation of secondary compounds, along with the consumption/formation of oxidizing species.

Long range transport of VOCs adsorbed on mineral dust particles / Due to the long lifetime of mineral dust particles in the troposphere [275], up to several days, these aerosols can provide a media to transport atmospheric compounds over long distances. In VOC-rich areas such as urban and forested regions, low vapor pressure VOCs may condense onto the particles. When transported to remote areas that are free of anthropogenic and biogenic emissions, VOCs adsorbed on particles could be released and act as an important diffuse source of gaseous organic carbon. Zamaraev et al [276] reported that a typical continental aerosol has the following composition: montmorillonite (35%), illite (20%), caolinite (20%), calcite (10%), Fe and organics (5%), quartz (5%), KNO_3 (5%). It appears that metal oxides like SiO_2, Al_2O_3, TiO_2 and Fe_2O_3 are among the most represented oxides [277]. Mineral dust particles are constituted of two kinds of metal oxides: insulator metal oxides such as SiO_2, Al_2O_3, MgO and CaO, and semi-conductor metal oxides such as ZnO, TiO_2, SnO_2 and Fe_2O_3. Zakharenko [278] showed that tropospheric conditions are rather favorable to adsorption and photoadsorption of atmospheric VOCs onto both kinds of metal oxides, and suggested that these processes may affect the chemical composition of the Earth's atmosphere. This study was further supported by investigations from Goss and Eisenreich [279] and Goss and Schwarzenbach [280] [281] on the quantification of VOC adsorption onto a wide range of metal oxides, close to tropospheric conditions. Nevertheless, Zakharenko [278] insisted on the need of experimental data – which is still missing – to support this assumption. The average concentration of aerosol particles in the troposphere varies from 1000 $\mu g\, m^{-3}$ in arid areas to 10–100 $\mu g\, m^{-3}$ in ordinary

background conditions. Moreover, for an average particle size of 100 nm, the surface area is ca. 10 $m^2 g^{-1}$. This specific area range is significant because it is similar to values for conventional efficient heterogeneous catalysts.

Heterogeneous oxidation of VOCs adsorbed on mineral dusts / There is much to learn about heterogeneous oxidation processes due to the adsorption of both VOCs and oxidants such as HO° and O_3. Such processes could be described by a Langmuir-Hinshelwood model pathway requiring the preliminary adsorption of organics with oxidizing species. In addition, metal oxides such as Al_2O_3, SiO_2, and TiO_2 that are present in mineral dust particles are well known for their ability to decompose and stabilize oxygenated compounds like O_3, H_2O, and H_2O_2, leading to a significant coverage of their surface by oxidizing chemisorbed species (O_2^-°, HO° and O atoms [282] [283] [284] [285]). These processes may occur on time scales compliant with long range transport. They may lead to significant chemical transformations of adsorbed organic compounds and the subsequent volatilization of secondary organic reaction products during transport.

Photocatalytic oxidation of mineral dusts adsorbed VOCs / Little is known about photocatalytic processes that could occur at the dust particle surface, and yet semi-conductor metal oxides such as ZnO, TiO_2, SnO_2, and Fe_2O_3 are significantly present in the mineral dust particle composition. A photocatalytic oxidation of VOCs requires: (i) the presence of semi-conducting metal oxides, (ii) a large specific surface area to improve adsorption processes, (iii) an appropriate visible or UV irradiation source, and (iv) the presence of oxygen and water molecules. It is worth noting that these four conditions are satisfied in the troposphere. Schoonen et al [286] highlighted that heterogeneous catalysis at the mineral surface, and especially photocatalysis, may help to understand the chemical reactivity in natural systems. Ivanov et al. [277] emphasized this approach describing the Earth as a “global photocatalytic reactor”. Photocatalysts present in mineral dust particles are able to absorb the actinic flux at atmospheric relevant wavelengths. In-situ oxidation processes occurring at the particle surface could enhance the oxidation rate of adsorbed VOCs, leading to a rapid increase of oxygenated functional groups per VOC, which in turn could lead to the fragmentation of organic molecules and the release of OVOCs in the atmosphere [287].

Objectives of the research axis / The description of atmospheric composition and reactivity using gas-phase chemistry models usually shows significant discrepancies when compared to field observations. It is important to note that heterogeneous processes involving mineral dust particles are not taken into account in models although such particles are potentially highly reactive with atmospheric VOCs (based on the concentration of particles, specific area, chemical composition, photocatalytic activation, etc.). The innovative approach of this research axis consists in conducting laboratory scaled experimental studies to quantify the contribution of real and natural mineral dust particle sorption and reactivity to the atmospheric chemistry. The questions this research axis seeks to address are the following:

➲ What are the mechanisms driving the adsorption of VOCs onto mineral dust particles under dark and illuminated conditions ?

➲ Does solar photocatalysis influence the chemical processing of VOCs at the mineral dusts surface ? What are the consequences for the formation of OVOCs and SOA ?

➲ Could oxidation of primary VOCs on mineral dust explain part of the disagreements observed between measured and modeled concentrations of OVOCs and SOA?

The main objective of this research topic is to provide a first database of experimental kinetic parameters to improve simulations of atmospheric composition and evolution. This database will help to develop a novel parameterization in models of atmospheric chemistry to implement heterogeneous processes occurring on mineral dust particles.

The characterization of mineral dust particle emissions and transport is a topic of interest that already led to the creation of international research programs such as SAMUM [275]. Most of these programs aiming at characterizing mineral dust particles from a physical point of view (origin, transport) were very useful to improve the knowledge on mineral dust particles and their

This research topic aims at understanding atmospheric reactivity as a combination of homogeneous and heterogeneous chemical processes to improve our ability to predict the chemical composition of the atmosphere, which in turn will help addressing current issues of atmospheric interest (air quality, climate change…). It is clear that current models are not satisfying.

physical impact on the Earth's radiative budget. The proposed approach is however different since it focuses on the chemistry and atmospheric reactivity of mineral dust particles that are poorly considered in existing research programs, in spite of the strong potential of mineral particles to act as highly reactive platforms for atmospheric VOCs.

An experimental approach is proposed to evaluate the impact of heterogeneous reactions involving mineral dust particles on our understanding of atmospheric chemistry. It is an innovative research axis located at the crossroad between atmospheric chemistry and heterogeneous reactivity.

Short-term operational objectives 2015-2017 /

1. Characterization of the sorption behavior of various selected atmospheric VOCs onto different dusts.
2. Relation between : VOC structure / adsorption modes / dust chemical composition.
3. Experimental evidence of dust photocatalytic activity under typical atmospheric conditions.
4. Experimental evidence of heterogeneous oxidation between sorbed VOC and atmospheric oxidants.

GENERAL CONCLUSION

My main assignment, as I was recruited in 2008 at Ecole des Mines in Dpt SAGE, was to create a novel research activity focused on fundamentals and applications of air treatment process. The development of this new topic was supported by the high academic background of the laboratory in the field of environmental gas phase analyses. In that context, I brought my expertise in the domain of (i) adsorption, (ii) photocatalysis and (iii) non-thermal plasma coupling with catalytic materials. Heterogeneous physical and chemical phenomena are the meeting points of these air treatment technologies, they had to be addressed in details with innovative experimental approaches to be understood and enhanced.

The modern context of indoor air and the dramatic decrease of indoor air quality have been identified as main issues; meanwhile, air treatment technologies could bring effective improvements. An overview of current existing technologies points out the fact that adsorption, photocatalysis and non-thermal plasma are the relevant technologies to face the typical pollution characteristics and the energetic requirements of indoor air. However, none of them were effectively investigated, understood or validated under typical indoor air conditions. The three air treatment techniques share the common characteristics of being heterogeneous processes. To that regard, scientific questions were still open about (i) heterogeneous interactions between pollutants, materials and non-thermal plasma in the plasma-material coupling, (ii) the effectiveness of photocatalytic oxidation at typical ppb in the presence of multi-polluted indoor atmospheres, and (iii) the sustainability these technologies.

The approach I proposed to investigate plasma-material coupling through sequential adsorption of the pollutants and subsequent plasma regeneration of the saturated coupling material offered interesting insights from a fundamental as well as a process point of view. First, it improved the distinction between gas phase and adsorbed phase phenomena. The key role of coupling material surface chemistry has been quantitatively evidenced for (i) pollutant adsorption; (ii) plasma generated oxidizing species consumption and (iii) long term performances and potential deactivation. Second, from a process point of view, it evidenced that the plasma sequential regeneration was a relevant option regarding energy consumption and oxidation reaction advancement. Based on these results, future perspectives in plasma-material coupling are proposed toward material tailored synthesis and tuned surface chemistry.

The detailed investigation of photocatalytic reaction at ppb level was required by the high development of such technologies for indoor air applications whereas its effectiveness was questioned. Based on analytical developments, gas phase and adsorbed phase have been addressed from primary VOC removal to gas phase reaction intermediate, CO_2 and particle matter production. The efficacy of photocatalytic oxidation for VOC abatement under typical indoor air condition was shown. However, the variability of the reaction with the nature and the diversity of VOCs have been clearly evidenced too. Adsorption considerations are relevant to describe and predict the behavior of photocatalysis on multi-polluted indoor air, but deeper investigations have to be carried out. The key point of future developments is the real scale assessment of photocatalytic air treatment devices to propose effective standards and protocols to ensure efficiency and innocuity of such a process.

My research perspectives can be structured according to two main paths. First, at short and mid-term, the development of a large scale experimental room will make possible further investigation of indoor air treatment technologies and more generally indoor air chemistry, from a homogenous to a heterogeneous point of view. This large scale innovative device will be used for the assessment of photocatalytic air treatment device performances and innocuity and for the evaluation of the performances of designed sorbents and catalyst when used for specific VOC adsorption and subsequent plasma regeneration. Second, I plan to widen the scope of my research activities to atmospheric heterogeneous processes investigation. Typically, my involvement in the field of heterogeneous oxidation processes could lead to the development of innovative approaches to tackle the interaction of atmospheric VOCs with mineral dust from arid area and volcanoes and the subsequent air quality impacts.

FIGURE CAPTIONS

TABLE CAPTIONS

REFERENCES

[1] O. Debono, Phd Thesis, *Oxydation photocatalytique de composés organiques volatils et suivi de leurs intermédiaires réactionnels : étude en réacteurs statique et dynamique à des concentrations typiques de l'air intérieur* (2011) UNAM

[2] L. Sivachandiran, PhD Thesis, *Regeneration of inorganic sorbents: investigation of adsorbed VOC oxidation using non-thermal plasma surface discharge* (2013) Ecole Polytechnique.

[3] F. Batault, PhD Thesis, *Influence de l'adsorption et des paramètres opératoires sur le traitement photocatalytique de composés organiques volatils en mélange dans les conditions de l'air intérieur* (2014) Université de Lille.

[4] C. Barakat, PhD Thesis, *VOC abatement by plasma-catalyst coupling: from fundamentals to process engineering* (2015) Ecole Polytechnique.

[5] P. Harb, PhD Thesis, *Etude des performances et de l'innocuité de systèmes de traitement photocatalytiques commerciaux dans une pièce expérimentale reproduisant les conditions de l'air intérieur*, Université de Lille (under progress).

[6] F. Thevenet, G. Panczer, P. Jollivet, B. Champagnon, *Journal of Non-Crystalline Solids,* 351 (2005) 673

[7] F. Thevenet, O. Guaïtella, J.-M. Herrmann, A. Rousseau, C. Guillard, *Applied Catalysis B: Environmental* 61 (2005) 62

[8] A. Rousseau, O. Guaitella, L. Gatilova, F. Thevenet, C. Guillard, J. Roepcke, G. Stancu, *Applied Physics Letters* 87, 221501 (2005)

[9] O. Guaitella, F. Thevenet, C. Guillard, A. Rousseau, *Journal of Physics D: Applied Physics* 39 (2006) 2964

[10] F. Thevenet, O. Guaitella, E. Puzenat, A. Rousseau, C. Guillard, *Catalysis Today* 122 (2007) 186

[11] O. Guaitella, F. Thevenet, E. Puzenat, C. Guillard, A. Rousseau, *Applied Catalysis B: Environmental* 80 (2007) 296

[12] F. Thevenet, O. Guaitella, E. Puzenat, C. Guillard, A. Rousseau, *Applied Catalysis B: Environmental* 84 (2008) 813

[13] J. Thiebaud, F. Thevenet, C. Fittschen, *Journal of Physical Chemistry C,* 114 (2010) 3082

[14] F. Thevenet, J. Couble, M. Brandhorst, J. L. Dubois, E. Puzenat, C. Guillard, D. Bianchi, *Plasma Chemistry Plasma Processing* 30 (2010) 489

[15] O. Debono, F. Thevenet, P. Gravejat, V. Hequet, C. Raillard, L. Lecoq, N. Locoge, *Applied Catalysis B: Environmental* 106 (2011) 600

[16] L. Sivachandiran, F. Thevenet, P. Gravejat, A. Rousseau, *Chemical Engineering Journal,* 214 (2013) 17

[17] O. Debono, F. Thevenet, P. Gravejat, V. Hequet, C. Raillard, L. Le Coq, N. Locoge, *Journal of Photochemistry and Photobiology A Chemistry* 258 (2013) 17

[18] L. Sivachandiran, F. Thevenet, P. Gravejat, A. Rousseau, *Applied Catalysis B: Environmental* 142 (2013) 196

[19] L.Sivachandiran, F. Thevenet, A. Rousseau, *Plasma Chemistry and Plasma Processing* 33 (2013) 855

[20] F. Thevenet, A. Rousseau, C. Guillard, *Chemical Engineering Journal* 244 (2014) 50-58

[21] L. Sivachandiran, F. Thevenet, A. Rousseau, *Chemical Engineering Journal* 246 (2014) 184-195

[22] C. Barakat, O. Guaitella, F. Thevenet, A. Rousseau, *Applied Catalysis B: Environmental* 147 (2014) 302-313

[23] F. Thevenet, L. Sivachandiran, O. Guaitella, C. Barakat, A. Rousseau, *Journal of Physics D: Applied Physics* 47 (2014) 224011

[24] F. Batault, F. Thevenet, V. Hequet, C. Raillard, L. Le Coq, N. Locoge, *Chemical Engineering Journal,* 264 (2015) 197-210

[25] H. Ourrad, F. Thevenet, V. Gaudion, V. Riffault, *Applied Catalysis B: Environmental* 168-169 (2015) 183-194

[26] L. Sivachandiran, F. Thevenet, A. Rousseau, *Chemical Engineering Journal* 270 (2015) 327-335

[27] F. Thevenet, L. Olivier, F. Batault, L. Sivachandiran, N. Locoge, *Chemical Engineering Journal* 264 (2015) 197-210

[28] Patent : Combined treatment of gaseous effluents by cold plasma and photocatalysis, *International patent :* WO 2007/051912

[29] Patent : Method for producing hydrogen peroxide, *International patent :* WO 2010/049634 A1

[30] F. Thevenet, PhD Thesis, *Elimination et mécanismes de degradation de l'acétylène par couplage plasma-froid photocatalyse (2006) Université Lyon-1.*

[31] Michel Lesbats, *Précis de gestion des risques*, 2012 Dunod

[32] Code de l'Environnement, Article L 220-2 modifié par le loi n°2010-788 du 12 juillet 2010 article 179

[33] Indoor Air Facts No. 4, Sick building syndrome. Available from: http://www.epa.gov/iaq/pubs/sbs.

[34] W.H.O. (Wolrd Health Organization) Air quality guidelines for Europe (2000)

[35] P.K. Johnston, G. Hadwen, J. McCarthy, J.R. Girman. US-EPA., (2002) 930–6

[36] L. Mosqueron, V. Nedellec, Revue des enquêtes sur la qualité de l'air intérieur dans les logements en Europe et aux Etats-Unis. Observatoire de la qualité de l'air intérieur, (2004) 1-55

[37] OQAI., http://www.air-interieur.org, (2008)

[38] S. Kirchner, J.F. Arenes, C. Cochet, M. Derbez, C. Duboudin, P. Elias, A. Gregoire, B. Jedor, B., J.P. Lucas, N. Pasquier, M. Pigneret, O. Ramalho, *Rapport Final de l'Observatoire de la Qualité de l'Air Intérieur*, (2007)

[39] World Health Organization. 2014. "Burden of Disease from Household Air Pollution for 2012." http://www.who.int/phe/health_topics/outdoorair/databases/FINAL_HAP_AAP_BoD_24March2014.pdf.

[40] M. Mosqueron, V. Nedellec, *Hiérarchisation sanitaire des paramètres mesurés dans les bâtiments par l'Observatoire de la Qualité de l'Air Intérieur, rapport Final*, (2002)

[41] M.A. Isabell, R.J. Stolzberg, L.K. Duffy, *Science of the Total Environment,* 345 (2005) 31-40

[42] C. Alméras, *Hiérarchisation des polluants dans l'environnement intérieur : mise à jour pour le cas des logements et extrapolation à d'autres environnements intérieurs*, n*ote de synthèse,* (2010).

[43] Booklet ADEME « La démarche HQE » http://www2.ademe.fr/servlet/KBaseShow?sort=-1&cid=96&m=3&catid=16140

[44] Ministère de la Santé, description du « Plan National Santé Environnement », available on line : http://www.sante.gouv.fr/plan-national-sante-environnement-pnse,3480.html

[45] Ministère de l'Ecologie, du Développement Durable et de l'Energie, Commissariat Général au Développement Durable, *Estimation des coûts pour le système de soin français de cinq maladies respiratoires et des hospitalisations attribuables à la pollution de l'air*, Etude et Documents *n°122* avril 2015

[46] S. Brown, M. Sim, M. Abramson, C. Grey, *Indoor Air,* 4 (1994) 123-134

[47] M. Hippelein, *Journal of Environmental Monitoring*, 6 (2004) 745-752

[48] H. Schleibinger, U. Hott, P. Plieninger, P. Marschl, P. Braun, H. Rüden, *Gefahrstoffe Reinhaltung der Luft*, 1 (2001) 28-38

[49] L. Mosqueron, V. Nedellec, *Inventaire des données françaises sur la qualité de l'air à l'intérieur des bâtiments*, (2001) Paris

[50] L. Mosqueron, V. Nedellec, *Inventaire des données françaises sur la qualité de l'air à l'intérieur des bâtiments : actualisation des données sur la période 2001-2004*, (2004) Paris

[51] R.D. Edwards, J. Jurvelin, K. Saarela, M. Jantunen, Atmospheric Environment, 35 (2001) 4531-4543

[52] H. Chikara, S. Iwamoto, T. Yoshimura, Japanese Journal of Hygiene, 1 (2009) 683-688

[53] J. Liu, G. Bai, J. Chen, L. Zhu, W. Guo, X. Shen, Chinese Science Bulletin, 56 (2011) 2683-2689

[54] A.T. Hodgson, H.A.L. Levin, Report from Lawrence Berkley National Laboratory (2003) 1-31

[55] US Environmental Protection Agency, *Report on background Indoor Air Concentrations of Volatile Organic Compounds in North American Residences (1990 - 2005): A Compilation of Statistics for Assessing Vapor Intrusion* (2011) 1-67

[56] Y.P. Zhang, Y. Xu, *International Journal of Heat and Mass Transfers* 46 (2003) 4877-4883

[57] C. Weisel, J. Zhang J, B.J. Turpin, M.T. Morandi, S. Colome, *Health Effect Institute* (2005) 1-144

[58] R. Kostiainen, *Atmospheric Environment* 29 (1995) 693-702

[59] T. Salthammer, *Indoor Air*, 7 (1997) 189-97

[60] ECJRC (European Commission Joint Research Centre), 1997. European Commission, Luxembourg

[61] A. Ahrens, D. Jepsen, H. Lüskow, H.. *Construction Products and Indoor Air Quality* (2007) 1–26 Berlin.

[62] A. Neilson, A. Allard *The handbook of environmental chemistry : Indoor Air Pollution*, Ed. Springer (2002)

[63] B. Seiffert, N. Englert, H. Sagunski, J. Wittert, *Bundesgesundheitsblatt-Gesundheitsforschung-Gesundheitsschutz* 42 (1999) 270-278

[64] World Health Organization guidelines for indoor air quality: selected pollutants (2010) 1-236, Copenhagen

[65] Centre Scientifique et Technique du Bâtiment, (2009) *La certification NF Bâtiments Tertiaires – Démarche HQE® passe les frontières*, available at : http://www.cstb.fr/actualites/webzine/editions/edition-de-mars-2009

[66] Arrêté relatif à l'étiquetage des produits de construction, de revêtement de mur et de sol, et des peintures et vernis, *Journal Officiel de la République Française* n°0111 du 13 mai 2011, texte 15, arrêté du 19 avril 2011

[67] Décret n° 2010-1269 relatif aux caractéristiques thermiques et à la performance énergétique des constructions, *Journal Officiel de la République Française* n°0250 du 27 octobre 2010, texte 2

[68] Décret n° 2012-1530 relatif aux caractéristiques thermiques et à la performance énergétique des constructions de bâtiments *Journal Officiel de la République Française* n°0304 du 30 décembre 2012, texte 64

[69] Arrêté du 10 avril 1974 relatif à l'isolation thermique et au réglage automatique des installations de chauffage dans les bâtiments d'habitation, *Journal Officiel de la République Française* , 10 avril 2014, consolidé au 17 août 2015

[70] http://www.asso-iceb.org/

[71] http://www.lemoniteur.fr/article/qualite-de-l-air-interieur-la-rt-2012-n-autorise-pas-un-renouvellement-d-air-suffisant-selon-l-iceb-24486802

[72] MERMAID project, Caractérisation détaillée de l'air intérieur des bâtiments BBC par couplage entre Mesures Expérimentales Représentatives et Modélisation Air Intérieur Détaillée (2012-2015) ADEME

[73] M. Verriele, PhD Thesis, *Nature et origines des Composés Organiques Volatils et odeurs présents dans un habitacle de véhicule : impact des pièces automobiles sur la qualité de l'air à l'intérieur* (2011) Université Lille-1

[74] B. Ribot, P. Blondeau, A. Ginestet, F. Squinazi, F. De Blay, M. Ott, D. Frochot, *Proposal of a method for measuring performance of portable domestic air cleaners*, Project report (2006)

[75] P. Le Cloirec, *Les composés organiques volatils (COV) dans l'environnement*, Tec & Doc, Edition Lavoisier, Paris

[76] C. Stavrakakis, *Réduction des émissions de Composés Organiques Volatils dans l'industrie* (2010) 1-21

[77] K. Freudenthal, R. Otterpohl, J. Behrendt, *Waste Management* 25 (2005) 975-84

[78] P. Le Cloirec, *Techniques de l'Ingénieur*, 33 (2012) 1-13

[79] M. Schlegelmilch, J. Streese, W. Biedermann, T. Herold, R. Stegmann, *Waste Management* 25 (2005) 917-927

[80] J. Streese, M. Schlegelmilch, K. Heining, R. Stegmann, *Waste Management* 25 (2005), 965-974

[81] M. Schlegelmilch, J. Streese, R. Stegmann, *Waste Management* 25 (2005) 928-939

[82] M. Mohseni, *Chemosphere*, 59 (2005) 335-342

[83] J.M. Herrmann, *Photocatalysis*. Kirk-Othmer Encyclopedia of Chemical Technology (2006)

[84] Norme XP B 44-013, Méthode d'essais et d'analyse pour la mesure d'efficacité de systems photocatalytiques pour l'élimination des composés organiques volatils (COV) /odeurs dans 'air intérieur en recirculation. *AFNOR*, 12-F (2009)

[85] Norme XP B 44-200, Epurateurs d'air autonomes pour applications tertiaires et résidentielles, méthodes d'essais, performances intrinsèques. *AFNOR*, 05-F (2011)

[86] Projet *EPURATEUR3* : LHVP - Marie de Paris, EDF - R&D, CETIAT, Air&Bio, LASIE, TERA-Environnement, Qualification énergétique et sanitaire des systèmes d'épuration intégrés aux réseaux de ventilation.

[87] M.A. Lieberman, A.J. Lichtenberg, *Principles of Plasma Discharges and Materials Processing*. John Wiley and Sons Ltd, (2005)

[88] B. Eliasson, M. Hirth, U. Kogelschatz, *Journal of Physics D: Applied Physics*, 20 (1986) 1421-1437

[89] U. Kogelschatz, *Plasma Chemistry and Plasma Processing*, 23 (2003) 1-46

[90] B.M. Penetrante, S.E. Schultheis, NATO ASI Series - G Series - *Ecological Sciences*, 34 (1993) 1-35

[91] H.H. Kim, A. Ogata, S. Futamura, *Journal of Physics D: Applied Physics*, 38 (2005) 1292-1300

[92] E. Marotta, A. Callea, M. Rea, C. Paradisi, *Environmental Science & Technology,* 41 (2007) 5862-5868

[93] S. Chavadej, K. Saktrakool, P. Rangsunvigit, L.L. Lobban, T. Sreethawong, *Chemical Engineering Journal*, 132 (2007) 345-353

[94] D. Mehandjiev, A. Naidenov, *The Journal of the International Ozone Association*, 14 (1992) 277-282

[95] S. Imamura, M. Ikebata, T. Ito, T. Ogita, *Industrial & Engineering Chemistry Research*, 30 (1991) 217-221

[96] A. Ogata, K. Saito, H.H. Kim, M. Sugasawa, H. Aritani, H. Einaga, *Plasma Chemistry and Plasma Processing*, 30 (2009) 33-42

[97] F. Holzer, U. Roland, F. Kopinke, *Applied Catalysis B: Environmental*, 38 (2002) 163-181

[98] Y.H. Song, S.J. Kim, K.I. Choi, T. Yamamoto, *Journal of Electrostatics*, 55 (2002) 189-201

[99] M. Magureanu, N.B. Mandache, V.I. Parvulescu, C. Subrahmanyam, A. Renken, L. Kiwi-Minsker, *Applied Catalysis B: Environmental*, 74 (2007) 270-277

[100] H.H. Kim, A. Ogata, S. Futamura, *Journal of Physics D: Applied Physics*, 38 (2005) 1292-1300

[101] Y.F. Guo, D.Q. Ye, K.F. Chen, J.C. He, W. Chen, *Journal of Molecular Catalysis A: Chemical*, 245 (2006) 93-100

[102] U. Roland, F. Holzer, F. Kopinke, *Applied Catalysis B: Environmental*, 58 (2005) 217-226

[103] M.A. Henderson, *Surface Science Reports* 66 (2011) 185-297

[104] O. Carp, C.L Huisman, A. Reller, *Progress in Solid State Chemistry*, 32 (2004) 33-177.

[105] J.M. Coronado, M.E. Zorn, I. Tejedor-Tejedor, M.A. Anderson, *Applied Catalysis B Environmental*, 43 (2003) 329-344

[106] I. Langmuir, *Journal of American Chemical Society* (1918) 1361-1403

[107] T. Chafik, O. Dulaurent, J.L. Gass, D. Bianchi, *Journal of Catalysis*, 179 (1998) 503-514

[108] M. Nagao, Y. Suda, *Langmuir*. (1989) 42-47

[109] W. Choi, J.Y. Ko, H. Park, J.S. Chung, *Applied Catalysis B Environmental*, 31 (2001) 209-220

[110] S. Brunauer, P.H. Emmett, E. Teller, *Journal of American Chemical Society*, 60 (1938) 309-319

[111] K. Demeestere, J. Dewulf, H.V. Langenhove, B. Sercu, *Chemical Engineering Journal*, 58 (2003) 13

[112] M.A. Henderson, *Surface Science Reports*, 46 (2002) 1-308

[113] V. Augugliaro, S. Coluccia, V. Loddo, L. Marchese, G. Martra, L. Palmisano, *Applied Catalysis B Environmental*, 20 (1999) 15-27

[114] S.G. Ramalingam, L. Hamon, P. Pré, S. Giraudet, L.L. Coq, P.L. Cloirec, *Journal of Colloids and Interface Science* 377 (2012) 375-378

[115] P.A. Redhead, Thermal desorption of gases, *Vacuum*. 12 (1962) 203-211

[116] J.M. Kanervo, T.J. Keskitalo, R.I. Slioor, A.O.I. Krause, *Journal of Catalysis* 238 (2006) 382-393

[117] I. Langmuir, *Proceedings of the National Academy of Science USA*, 14 (1928) 627-637

[118] M.A. Lieberman, *A mini-course on the principle of plasma discharges*, (2003) available on Austalian National University website http://people.physics.anu.edu.au/

[119] Y.H. Raizer, *Gas Discharge Physics*. J. E. Allen, Ed. (1987) Moscow

[120] U. Kogelschatz, B. Eliasson, W. Egli, *Journal de Physique IV*, 7 (1997) 47-66

[121] W. Siemens, *Poggendorf's Annalen der Physik und Chemie*, 102 (1857) 66-22

[122] A. Fridman, A. Chirokov, A. Gutsol, *Journal of Physics D: Applied Physics*, 38 (2008) 1-24

[123] J. Van Durme, J. Dewulf, C. Leys, H. Van Langenhove, *Applied Catalysis B: Environmental*, 78 (2008) 324-333

[124] R. Barni, P. Esena, C. Riccardi, *Surface and Coatings Technology*, 200 (2005) 924-927

[125] A. Thiemann, Proceedings of the 1st European Conference on advanced Ox & Red Technologies (2004) Göttingen

[126] S.S. Joshi, *Trans. Faraday Soc.* 23 (1927) 227-238

[127] Z. Chen, V. Mathur, *Industrial & Engineering Chemistry Research*, 42 (2002) 2082-2090

[128] F. Fresnet, G. Baravian, L. Magne, S. Pasquiers, C. Postel, V. Puech, A. Rousseau, *Applied Physics Letters*, 77 (2000) 4018-4026

[129] I. Orlandini, U. Riedel, *Catalysis Today*, 89 (2004) 83-91

[130] A. Ogata, K. Yamanouchi, K. Mizuno, S. Kushiyama, T. Yamamoto, *Plasma Chemistry & Plasma Processing*, 19 (1999) 383-394

[131] T. Oda, T. Takahashi, S. Kohsuma, *IAS annual meeting*, Poenix AZ, USA (1999)

[132] H.H. Kim, *Plasma Processes and Polymers*, 1 (2004) 91-110

[133] J. Van Durme, J. Dewulf, C. Leys, H. Van Langenhove, *Applied Catalysis B: Environmental*, 78 (2008) 324-333

[134] E.C. Neyts, A. Bogaerts, Journal of Physics D: Applied Physics, 47 (2014) 224010

[135] A.M. Harling, V. Demidyuk, S.J. Fisher, J.C. Whitehead, *Applied Catalysis B: Environmental*, 82 (2008) 180-189

[136] A.M. Harling, D.G. Glover, J.C. Whitehead, K. Zhang, *Applied Catalysis B: Environmental,* 90 (2009) 157-161

[137] C. Subrahmanyam, A. Renken, L. Kiwi-Minsker, *Chemical Engineering Journal*, 134 (2007) 78-83

[138] T. Hammer, T. Kappes, M. Baldauf, *Catalysis Today*, 89 (2004) 5-13

[139] M.J. Kirkpatrick, W.C. Finney, B.R. Locke, *Catalysis Today*, 89 (2004) 117-125

[140] C. Ayrault, J. Barrault, N. Blin-Simiand, F. Jorand, S. Pasquiers, A. Rousseau, J.M. Tatibouët, *Catalysis Today*, 89 (2004) 75

[141] F. Holzer, U. Roland, F.D. Kopinke, *Applied Catalysis B: Environmental* , 38 (2002) 163

[142] U. Roland, F. Holzer, A. Pöppl, F.D. Kopinke, *Proceedings 4th ISNTP* (2004)

[143] T. Oda, T. Kato, T. Takahashi, K. Shimizu, *IEEE Trans. Ind. Applicat*., 34 (1998) 268

[144] J. Hoard, M.L. Balmer, R. Tonkyn, A. Kim, S. Yoon, D. Jimenez, T. Orlando, S.E. Barlow, SAE Technical Paper no.982511, *International Fall Fuels and Lubricants Meeting and Exposition* (1998)

[145] T. Hammer, S. Bröer, T. Kishimoto, *Journal of Advanced Oxidation Technologies*, 4 (1999) 368-374

[146] M.J. Kirkpatrick, W.C. Finney, B.R. Locke, *Plasmas & Polymers*, 8 (2003) 165-177

[147] D. Li, D. Yakushiji, S. Kanazawa, T. Ohkubo, Y. Nomoto, *Journal of Electrostatics*, 55 (2002) 311-319

[148] C. Liu, J. Wang, K. Yu, B. Eliasson, Q. Xia, B. Xue, Y. Zhang, *Journal of Electrostatics*,, 54 (2002) 149

[149] K. Takaki, J.S. Chang, K.G. Kostov, *IEEE Trans. Dielect. Elect. Insulation*., 11 (2004) 481-490

[150] F. Holzer, F.D. Kopinke, U. Roland, *Plasma Chemistry & Plasma Processing*, 25 (2005) 595-611

[151] A. Ogata, K. Yamanouchi, K. Mizuno, S. Kushiyama, T. Yamamoto, *Plasma Chemistry and Plasma Processing*, 19 (1999) 383-394

[152] U. Roland, F. Holzer, F.D. Kopinke, *Catalysis Today*, 73 (2002) 315-323

[153] T. Ogata, H. Einaga, H. Kabashima, S. Futamura, S. Kushiyama, H.H. Kim, *Applied Catalysis B: Environmental*, 46 (2003) 87-95

[154] H.H.Kim, A. Ogata, M. Schiorlin, E. Marotta, C. Paradisi, *Catalysis Letters*, 141 (2011) 277-282

[155] Y.F. Guoa, D.Q. Yea, K.F. Chenb, J.C. Hea, W.L. Chen, *Journal of Molecular Catalysis A: Chemistry*, 245 (2006) 93–100

[156] A.E. Wallis, J.C. Whitehead, K. Zhang, *Catalysis Letters*, 113 (2007) 29-33

[157] J. Jun, J.C. Kim, J.H. Shin, K.W. Lee Y.S. Baek, *Radiation Physics and Chemistry*, 71 (2004) 1095-1101

[158] M. Kang, B.J. Kim, S.M. Cho, C.H. Chung, B.W. Kim, G.Y. Han, K.J. Yoon, *Journal of Molecular Catalysis. A: Chemistry* 180 (2002) 125-132

[159] D. Li, D. Yakushiji, S. Kanazawa, T. Ohkubo, Y. Nomoto *Journal of Electrostatics*, 55 (2002) 311-319

[160] C.H. Ao, S.C. Lee, *Applied Catalysis B: Environmental*, 44 (2003) 191-286

[161] H.K. Kim , Y.H. Lee , A. Ogata and S. Futamura, Catalysis Communications, 4 (2003) 347-351

[162] H.K. Kim, A. Ogata, S. Futamura, *Journal of Korean Physical Society*, 44 (2004) 1163 -1167

[163] B.Y. Lee , S.H. Park , S.C. Lee ,M. Kang, S.J. Choung, *Catalysis Today*, 93 (2004) 769-776

[164] S. Futamura , H. Einaga , H. Kabashima, L.Y. Hwan, *Catalysis Today*, 89 (2004) 89-95

[165] H.H. Kim, K. Takashima, S. Katsura, A. Mizuno, *Journal of Physics D: Applied Physics*, 34 (2001) 604-613

[166] H.H. Kim, S.M. Oh, A. Ogata, S. Futamura, *Applied Catalysis B: Environmental,* 56 (2005) 213-220

[167] C.H. Ao, S.C. Lee, *Chemical Engineering Science*, 60 (2005) 103-109

[168] C.L. Chang, T.S. Lin, *Plasma Chemistry & Plasma Processing*, 25 (2005) 227-243

[169] B. Ohtani, S. W. Zhang, T. Ogita, S. Nishimoto, T. Kagiya, *Journal of Photochemistry and Photobiology A : Chemistry*,71 (1993) 195-198

[170] J.H. Kim, S.J. Lee, M.B. Kim, J.J. Lee, C.H. Lee, *Industrial & Engineering Chemistry Research*, 46 (2007) 4584–4594

[171] M.A. Sidheswaran, H. Destaillats, D.P. Sullivan, S. Cohn, W.J. Fisk, *Building & Environment*, 47 (2012) 357-367

[172] T. Zhu, Mazzeo Ed., ISBN: 978-953-307-316-3 (2011)

[173] S. Brosillon, M.H. Manero, J.N. Foussard, *Environmental Science & Technology*, 35 (2001) 3571–3575

[174] S.T. Oyama, *Catalysis Review,* 42 (2000) 279-322

[175] J.E. Post, *Proceedings of the National Academy of Science USA*, 96 (1999) 3447-3454.

[176] W. Li, G.V. Gibbs, S.T. Oyama, *Journal of the American Chemical Society*, 120 (1998) 9041–9046.

[177] W. Li, S.T. Oyama, *Journal of the American Chemical Society*, 120 (1998) 9047–9052.

[178] B. Dhandapani, S.T. Oyama, *Applied Catalysis B: Environmental*, 11 (1997) 129–166.

[179] S.T. Oyama, *Catalysis Review*, 42 (2000) 279–322.

[180] F. Arsac, D. Bianchi, J.M. Chovelon, C. Ferronato, J.M. Herrmann, *Journal of Physical Chemistry A*, 110 (2006) 4202–4212.

[181] A. Hu, Y. Fang, J.F. Young, Y.J. Oh, *Journal of the American Ceramic Society*, 82 (1999) 1741-1747.

[182] G. Kai-Uwe, S.J. Eisenreich, *Environmental Science & Technology,* 30 (1996) 2135-2142

[183] Y. Luo, D.F Ollis, *Journal of Catalysis*, 163 (1996) 1-11.

[184] J. Araña, A. P. Alonso, J.M. D. Rodríguez, G. Colón, J.A. Navío, J. P. Peña, *Applied Catalysis B: Environmental,* 89 (2009) 204–213.

[185] J.V. Durme, J. Dewulf, W. Sysmans, C. Leys, H.V. Langenhove, *Applied Catalysis B: Environmental*, 74 (2007) 161-169.

[186] X. Fan, T.L. Zhu, M.Y. Wang, X.M. Li, *Chemosphere*, 75 (2009) 1301-1306.

[187] H.H. Kim, *Plasma Process Polymers*, 1 (2004) 91-110.

[188] C.J. Weschler, A.T. Hodgson, J.D. Wooley, *Environmental Science & Technology*, 28 (1994) 2120-2132

[189] A. Chaloulakou, I. Mavroidis, I. Gavriil, Atmos. Environ, 42 (2008) 454-65.

[190] S. Matsuda, H. Hatano, A. Tsutsumi, *Chemical Engineering Journal*, 82 (2001) 183-188.

[191] F.L. Toma, G. Bertrand, D. Klein, C. Coddet, *Environmental Chemistry Letters*, 2 (2004) 117-121.

[192] C. Morterra, G. Ghiotti, E. Garrone and E. Fisicaro, *J. Chem. Soc. Faraday Trans* 1, 76 (1980) 2102.

[193] J.S. Dalton, P.A. Janes, N.G. Jones, J.A. Nicholson, K.R. Hallam, G.C. Allen, *Environmental Pollution*, 120 (2002) 415-422.

[194] D.C. Sorescu, C.N. Rusu, J.T. Yates, *Journal of Physical Chemistry B*, 104 (2000) 4408-4417.

[195] W.S. Epling, A.Yezerets, N. W. Currier, *Applied Catalysis B: Environmental*, 74 (2007) 117-129.

[196] J. Haubrich, R. G. Quiller, L. Benz, Z. Liu, C. M. Friend, *Langmuir*, 26 (2010) 2445-2451

[197] J.Despres, M. Koebel, O. Kröcher, M. Elsener, A. Wokaun, *Applied Catalysis B: Environmental*, 43 (2003) 389-395.

[198] J. A. Rodriguez, T. Jirsak, G. Liu, J. Hrbek, J. Dvorak, A. Maiti, *Journal of American Chemical Society* 123 (2001) 9597-9605

[199] N. Apostolescu, T. Schröder, S. Kureti, Study, *Applied Catalysis B: Environmental*, 51 (2004) 43-50.

[200] K.I. Hadjiivanov, V. Bushev, M. Kantcheva, D. Klissurski, *Langmuir* 10 (1994) 464-471

[201] J. Raskó, J. Kiss, *Applied Catalysis A: General* 287 (2005) 252-260

[202] J. E. Rekoske, M. A. Barteau, *Industrial and Engineering Chemistry Research* 50 (2010) 41-51

[203] M. Barbeni, E. Pramauro, E. Pelizzetti, E. Borgarelo, N. Seprone, *Chemosphere* 14 (1985) 95

[204] J.M. Herrmann, C. Guillard, P. Pichat, *Catalysis Today*, 17 (1993) 7-20

[205] P. Pichat, J. Disdier, C. Hoang-Van, D.Mas, G. Goutailler, C. Gaysse, *Catalysis Today*, 63 (2000) 363-371

[206] Y. Paz, *Applied Catalysis B: Environmental,* 99 (2010) 446-460

[207] Projet *EPURATEUR3* : LHVP - Marie de Paris, EDF - R&D, CETIAT, Air&Bio, LASIE – La Rochelle, TERA-Environnement, Qualification énergétique et sanitaire des systèmes d'épuration intégrés aux réseaux de ventilation.

[208] C.H. Ao, S.C. Lee, *Applied Catalysis B: Environmental,* 44 (2003) 191-205

[209] C.H. Ao, S.C. Lee, C.L. Mak, L.Y. Chan, *Applied Catalysis B: Environmental,* 42 (2003) 119-219

[210] A.T. Hodgson, H. Destaillats, D.P. Sullivan, W.J. Fisk, Performance of ultraviolet photocatalytic oxidation for indoor air cleaning applications, In*door Air*, 17 (2007) 305-316

[211] M. Sleiman, P. Conchon, C. Ferronato, J.M. Chovelon, *Appl. Catal. B: Env.* 86 (2009) 159-165

[212] A.K. Boulamanti, C.J. Philippopoulos, *Atmospheric Environment*, 43 (2009) 3168-3174

[213] V. Augugliaro, S. Coluccia, V. Loddo, L. Marchese, G. Martra, L. Palmisano, M. Schiavello, *Applied Catalysis B: Environmental*, 20 (1999) 15

[214] T.M. Twesme, D.T. Tompkins, M.A. Anderson, T.W. Root, *Applied Catalysis B: Environmental*, 64 (2006) 153-160

[215] J. Shang, Y. Du, Z. Xu, *Chemosphere*, 46 (2002) 93-99

[216] L. Lin, Y. Chai, B. Zhao, W. Wei, D. He, B. He, Q. Tang, *Open Journal of Inorganic Chemistry*, 2 (2013) 14-25

[217] C. Raillard, V. Hequet, B. Gao, H. Choi, D.D. Dionysiou, A. Marvilliers, B. Illien, Correlation between molecular descriptors from various VOCs and photocatalytic oxidation kinetic constants, International Journal of Chemical Reactor Engineering, 11 (2013) 799-813

[218] R.M. Alberici, W. Jardim, Applied Catalysis B: Environmental, 14 (1997) 57-67

[219] S.B. Kim, S.C. Hong, *Applied Catalysis B: Environmental*, 35 (2002) 305-315

[220] C. Young, T.M. Lim, K. Chiang, J. Scott, R. Amal, *Applied Catalysis B: Environmental*, 78 (2008) 1-10

[221] National Institute of Standards and Technology, *NIST Chemical Kinetics Database [On line],* Available at : http://kinetics.nist.gov/kinetics/index.jsp

[222] H.H. Ou, S.L. Lo, *Journal of Hazardous Materials*, 246 (2007) 302-308

[223] G. Li Puma, I. Salvadó-Estivill, T.N. Obee, S.O. Hay, *Separation and Purification Technology*, 67 (2009) 226-232

[224] P.B. Amama, K. Itoh, M. Murabayashi, *Journal of Molecular Catalysis A: Chemistry*, 217 (2004) 109-115.

[225] M. Mohseni, *Chemosphere*, 59 (2005) 335-342

[226] S. Tissot, A. Pichard, *Seuils de toxicité aigües du phosgène*, Rapport Final, INERIS (2001)

[227] J.M. Coronado, J. Soria, *Catalysis Today* 123 (2007) 37-41

[228] R. Mendez-Roman, N. Cardona-Martinez, *Catalysis Today*, 40 (1998) 353-365

[229] G. Marci, M. Addamo, V. Augugliaro, S. Coluccia, E. Garcia-López, V. Loddo, G. Martra, L. Palmisano, M. Schiavello, *Journal of Photochemistry and photobiology A: Chemistry* 160 (2003) 105-115

[230] S. Poncet-Vincent, PhD Thesis, Université Claude Bernard-Lyon, 1999

[231] A. Calogirou, B. Larsen, D. Kotzias, *Atmospheric Environment*. 33 (1999) 1423-1439

[232] X. Chen, P.K. Hopke, *Indoor Air*. 20 (2010) 320-328

[233] N.L. Ng, J.H. Kroll, M.D. Keywood, R. Bahreini, V. Varutbangkul, R.C. Flagan, J.H. Seinfeld, A. Lee, A.H. Goldstein, *Environmental Science & Technology,* 40 (2006) 2283-2297

[234] R.K. Pathak, C.O. Stanier, N.M. Donahue, S.N. Pandis, *Journal of Geophysical Research: Atmospheres,* 112 (2007) D03201

[235] C. Coeur-Tourneur, A. Tomas, A. Guilloteau, F. Henry, F. Ledoux, N. Visez, V. Riffault, J.C. Wenger, Y. Bedjanian, *Atmospheric Environment,* 43 (2009) 2360-2365

[236] T.N. Obee, R.T. Brown, *Environmental Science and Technology,* 29 (1995) 1223

[237] A. Mills, S. Le Hunte, *Journal of Photochemistry and Photobiology A : Chemistry* 108 (1997) 1-35

[238] M. Kalberer, D. Paulsen, M. Sax, M. Steinbacher, J. Dommen, A. Prevot, R. Fisseha, E. Weingartner, V. Frankevich, R. Zenobi, *Science*, 303 (2004) 1659-1662

[239] M. Singh, N. Zhou, D.K. Paul, K.J. Klabunde, *Journal of Catalysis*, 260 (2008) 371-379

[240] Z. Topalian, B.I. Stefanov, C.G. Granqvist, L. Österlund, *Journal of Catalysis,* 307 (2013) 265-274

[241] B.I. Stefanov, Z. Topalian, C.G. Granqvist, L. Österlund, *Journal of Molecular Catalysis A: Chemistry* 381 (2014) 77-88

[242] M. Nagao, Y. Suda, *Langmuir*. (1989) 42-47

[243] C. Wang, H. Groenzin, M.J. Shultz, *Journal of the American Chemical Society*, 127 (2005) 9736-9744

[244] J.M. Coronado, M.E. Zorn, I. Tejedor-Tejedor, M.A. Anderson, *Applied Catalysis B: Environmental,* 43 (2003) 329–344

[245] M.J. Backes, A.C. Lukaski, D.S. Muggli, *Applied Catalysis B: Environmental* , 61 (2005) 21-35

[246] L.-F. Liao, C.-F. Lien, J.-L. Lin, Physical Chemistry Chemical Physics, 3 (2001) 3831-3837

[247] K.S. Kim, M.A. Barteau, *Langmuir,* 4 (1988) 945-953

[248] P. Blondeau, A. Ginestet, F. De Blay, M. Ott, B. Ribot, D. Frochot, *Mise en place des protocoles de qualification des épurateurs d'air*, Rapport Final (2005)

[249] http://www.biowindgroup.com/

[250] http://www.air-sur.com/

[251] M. Nocolas, L. Chiappini, Household products using and indoor air quality: emission, reactivity and by-products, Rapport Final (2013) projet Primequal

[252] C. Ganier, Y. Rudich, S. Fuzzi, J. Burrows, G. Brasseur, communication in *Planet under Pressure* (2011) London.

[253] B. Breitshneider, I. Kurfurst, *Air Pollution Control Technology*, Elsevier, Amsterdam (1987)

[254] V.N. Parmon, V.S. Zakharenko *Catalysis Technology*, 5 (2001) 96-115

[255] S. Zhu, T. Butler, R. Sander, J. Ma, and M. G. Lawrence, *Atmospheric Chemistry and Physics*, 10 (2010) 3855-3873

[256] C.E. Kolb, R. A. Cox, J. P. D. Abbatt, M. Ammann, E. J. Davis, D. J. Donaldson, B. C. Garrett, C. George, P. T. Griffiths, D. R. Hanson, M. Kulmala, G. McFiggans, U. Pöschl, I. Riipinen, M. J. Rossi, Y. Rudich, P. E. Wagner, P. M. Winkler, D. R. Worsnop, and C. D. O' Dowd, *Atmospheric Chemistry and Physics* 10 (2010) 10561-10605

[257] H. Singh, Y. Chen, A. Staudt, D. Jacob, D. Blake, B. Heikes and J. Snow, *Nature*, 410 (2001) 1078-1081

[258] H. B. Singh, A. Tabazadeh, M. J. Evans, B. D. Field, D. J. Jacob, G. Sachse, J. H. Crawford, R. Shetter, and W. H. Brune, *Geophysical Research Letters*, 30 (2003) 1862

[259] H. B. Singh, L. J. Salas, R. B. Chatfield, E. Czech, A. Fried, J. Walega, M. J. Evans, B. D. Field, D. J. Jacob, D. Blake, B. Heikes, R. Talbot, G. Sachse, J. H. Crawford, M. A. Avery, S. Sandholm, H. Fuelberg, *Journal of Geophysical Research*, 109 (2004) D15S07

[260] A. Wisthaler, A. Hansel, R. R. Dickerson, and P. J. Crutzen, *Journal of Geophysical Research*, 107 (2002) 8024

[261] A.C. Lewis, J. R. Hopkins, L. J. Carpenter, J. Stanton, K. A. Read, and M. J. Pilling, *Atmospheric Chemistry and Physics*, 5 (2005) 1963-1974

[262] M.J. Northway, J.A. de Gouw, D.W. Fahey, R.S. Gao, C. Warneke, J.M. Roberts, F. Flocke, *Atmospheric Environment* 38 (2004) 6017-6028

[263] A. J. Kwan, J. D. Crounse, A. D. Clarke, Y. Shinozuka, B. E. Anderson, J. H. Crawford, M. A. Avery, C. S. McNaughton, W. H. Brune, H. B. Singh, P. O. Wennberg, *Geophysical Research Letters*, 33 (2006) L15815

[264] H. Hass et al. *Proc. EUROTRAC-2 Symposium*, *Garmisch 11-15 March* (2002) 211-217

[265] S.G. Tsyro *EMEP/MSC-W status report 1/2003 Part II*, Norwegian Meteorological Institute, Oslo, Norway (2003)

[266] S.G. Tsyro *Atmospheric Chemistry and Physics*, 5 (2005) 515-532

[267] H. Kouyoumdjian, N.A. Saliba, *Atmospheric Chemistry and Physics* 6 (2006) 1865-1877

[268] E. Ganor, A. Stupp, P. Alpert, *Atmospheric Environment* 43 (2009), 5463-5468

[269] N.A. Saliba, H. Kouyoumdjian, M. Roumié, *Atmospheric Environment* 41 (2007) 6497-6509

[270] Z. Levin, C. Price, E. Ganor, *Atmospheric Environment* 24 (1990) 1143-1151

[271] A. Falkovich, E. Ganor, Y. Rudich, *Journal of Geophysical Research*, 106 (2001) 18029

[272] A. Waked, C. Afif, C. Seigneur, *Atmospheric Environment*, 50 (2012) 88-96

[273] A. Waked, C. Afif, *Atmospheric Environment* 61 (2012) 446-452

[274] A. Waked, C. Seigneur, F. Couvidat, Y. Kim, K. Sartelet, C. Afif, A. Borbon, P. Formenti, S. Sauvage, *Atmospheric Chemistry and Physics Discussions*, 12 (2012) 29571-29606

[275] SAMUM (Saharian Mineral Dust Experiment) research program, *Institute for Tropospheric Research* - Germany

[276] K.I. Zamaraev, M.I. Khramov, V.N. Parmon, *Catalysis Review – Science Engineering*, 36 (1994) 617-644

[277] V.P. Ivanov, D.I. Kochubey, K.P. Kutzenogii, N.S. Bufetov, *Reaction Kinetic and Catalysis Letters*, 64 (1998) 97-102

[278] V.S. Zakharenko, *Catalysis Today* 39 (1997) 243-249

[279] K.U. Goss, S.J. Eisenreich, *Environmental Science and Technology*, 30 (1996) 2135-2142

[280] K.U. Goss, R.P. Schwarzenbach, *Environmental Science and Technology,* 33 (1999) 3390-3393

[281] K.U. Goss, R.P. Schwarzenbach, *Environmental Science and Technology,* 33 (1999) 4073-4078

[282] J.H. Lunsford, *Catalysis Review*, 9 (1973) 135-142

[283] S.H. Chang, *Journal of Vacuum Science and Technology*, 17 (1980) 366-374

[284] P. Pichat, J. Disdier, C. Hoang-Van, D. Mas, G. Goutailler, C. Gaysse, *Catalysis Today*, 63 (2000) 363-369

[285] T. Sano, N. Negishi, E. Sakai, S. Matsuzawa, *Journal of Molecular Catalysis A: Chemistry*, 245 (2006) 235

[286] M.A.A. Schoonen, Y. Xu, D.R. Strongin, *Journal of Geochemical Exploration*, 62 (1998) 201-215

[287] J.D. Smith *Atmospheric Chemistry and Physics*, 9 (2009) 3209-3222